NUMBER	DETAILS OF REVISION
0	Issued to PSC for comment, July 2000

Purpose of Issue	Rev	Date of Issue	Author	Agreed	Approved
Issued to PSC for Comment	0	July 2000	AFD	ML	AFD

This document has been prepared by MSL Engineering Limited for the Participants of the "Joint Industry Project on Assessment Criteria, Reliability and Reserve Strength of Tubular Joints, Phase II - Tubular Joint Non-Linear Modelling Algorithms for Frame Analysis". This document is confidential to the Participants in the Joint Industry Project, under the terms of their contract for participation in the project.

JIP - ASSESSMENT CRITERIA, RELIABILITY AND RESERVE STRENGTH OF TUBULAR JOINTS (PHASE II)

FINAL REPORT

DOC REF C20400R014 Rev 0 **JULY 2000**

MSL Engineering Limited
MSL House
5-7 High Street, Sunninghill,
Ascot, Berkshire SL5 9NQ

Tel: + 44 (0)1344 874424
Fax: + 44 (0)1344 874338
E-mail: MSLCENG@aol.com

FOREWORD

This document has been prepared by MSL Engineering Limited for nine sponsoring organizations:

BP Amoco
Chevron U.K. Limited
ExxonMobil
Elf Exploration UK plc
Health and Safety Executive (HSE)
Maersk Olie Og Gas as
Minerals Management Service (MMS)
Phillips Petroleum Company Norway
Shell U.K. Limited

This document is concerned with the development of algorithms that simulate the behaviour of simple tubular joints under combined axial, in-plane and out-plane moment loads, across the full range of the load-deformation response. The algorithms have been coded up as a module to use with space frame finite element programs. Pushover analysis incorporating proper joint behaviour can now be efficiently conducted with minimal user intervention. The document describes fully the theoretical work undertaken, and the results of module testing and calibration studies against large-scale 2D frame data.

The work described herein builds upon the load-deformation (uncoupled $P\delta$ and $M\theta$) formulations derived in Phase I of the project. The work was performed by MSL with assistance from SINTEF Civil and Environmental Engineering, under the guidance of the Project Steering Committee that included Representatives of the sponsoring organizations. During the life of this phase of the project, the following individuals served on the committee:

Mr P Bailey
Mr R Beck
Mr M Birades
Mr M Birkinshaw
Dr A F Dier
Mr D N Galbraith
Dr Ø Hellan
Dr T M Hsu
Mr M Lalani
Dr C E Smith
Mr J K Smith (Chairman)
Mr R Snell (Chairman)
Mr J P Tychsen
Mr P Zheng

The Project Manager at MSL Engineering was Dr A F Dier who was supported by M Lalani and other MSL Engineering personnel in the execution of the project.

The recommendations presented in this document and the associated software are based upon the knowledge available at the time of publication. However, no responsibility of any kind for injury, death, loss, damage or delay, however caused, resulting from the use of the recommendations or software can be accepted by MSL Engineering, SINTEF or others associated with its preparation.

The participants do not necessarily accept all the recommendations given in this document.

EXECUTIVE SUMMARY

General

The work reported herein concerns the development, testing and calibration of an efficient analysis tool that allows the behaviour of tubular joints within a space frame structure to be appropriately accounted for. Traditional structural analysis of jacket structures assumes that the tubular joints are rigid, not only for elastic analysis but also often for non-linear pushover analysis. Whereas special elements for capturing the buckling behaviour of beam-column members have been in existence for some years, there has been no comparative approach for dealing with tubular joints, that is until this present work. Yet many offshore structures comprise joints which are the weak link, and even in elastic analysis there is increasing recognition that local joint flexibility plays an important role in reducing bending moments at the joint (this has very significant implications for fatigue life estimates).

The development of the joint module was achieved in this Joint Industry Project (JIP), which encompassed two phases. In the earlier Phase I, all test and numerical data on the load behaviour of tubular joints was collated and carefully screened. From the screened database, robust static strength provisions were derived. From those data where full load-deformation ($P\delta$ or $M\theta$) curves were reported, formulations were developed whereby the load-deformation curve (again $P\delta$ or $M\theta$) could be re-created from the joint geometry and material properties. These formulations were developed for the range of simple joints that occur in practice. The load cases considered were uni-directional (ie. compression, tension, in-plane bending or out-of-plane bending) and the $P\delta$ and $M\theta$ formulations were uncoupled.

The success of the load-deformation formulations in predicting the $P\delta$ or $M\theta$ response gave confidence in moving the JIP to the second phase. Phase II is the subject of this report.

Objectives

The main objectives of Phase II of the JIP were:

(i) To develop the Phase I load-deformation formulations to address pertinent influencing factors such as: interaction with chord load, joint classification of axial loads, interaction (coupling) between $P\delta$ and $M\theta$, ductility limits and unloading behaviour. The studies relating to the above resulted in set of mathematical formulations or algorithms.

(ii) To codify the above algorithms in a series of subroutines leading to a joint module that could be used with a suitable frame analysis package.

(iii) To test the module to ensure correct function against individual joint test/numerical data and then to calibrate the module against test data for steel frames.

For the purposes of assisting in achieving objectives ii. and iii. above, it was necessary to select a suitable organization that maintains and develop a non-linear frame package. SINTEF were chosen and their package, USFOS, was the vehicle used to test and calibrate the module. MSL and SINTEF jointly executed the scope of work that was designed to achieve the above objectives.

Algorithm Development

Chord load interaction

The experimental evidence for the effect of chord load on joint behaviour suggests that the capacity of the joint is downgraded but that the initial stiffness is unchanged. This is as expected because the magnitude of chord loading should not affect elastic response. The load-deformation formulations from Phase I were therefore adjusted to ensure that the initial stiffness is not affected by chord loads. Example test data and predictions for the Pδ response of DT joints with chord loading (both axial and moment, which affect the knock down factor Q_f differently) are shown in Figure 1. Similar adjustments were also made to preserve the initial stiffness for varying yield strengths and for a strength level factor (by which the user can elect to use mean, characteristic or some other joint capacity estimate).

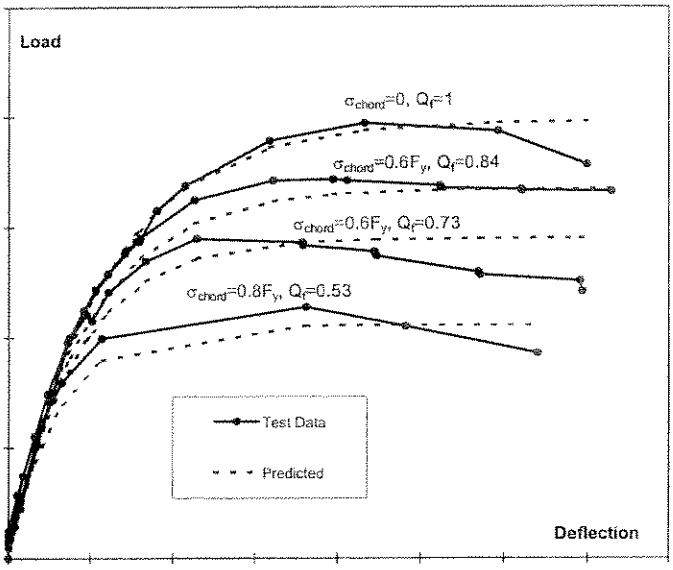

Figure 1: Compression loaded DT joints with various chord stresses

Joint classification

For joint nodes comprising two or more braces, it is usual practice to consider the axial load in a given brace as having components of K, X and Y actions. The classification of the load into these actions is then used to derive a capacity for the joint (for that brace) by taking a weighted average of the simple joint capacities. Inasmuch as joint classification affects joint capacity, it should come as no surprise that the whole Pδ response is also a function of joint classification.

This issue was explored by generating FE data on DK and X joints under various brace axial loads. A typical result for the DK joint is shown in Figure 2. In this figure three FE generated curves are shown (a) K:X = 100:0 (pure K action), (b) K:X = 0:100 (pure X action and (c) K:X = 50:50 (mixed classification). The basic Pδ formulations, adjusted for chord stress effects etc, apply only to simple joints, eg. pure K or pure X action. Studies were therefore undertaken as to how a mixed classification curve could be predicted from the simple joint formulations. An appropriate approach, it was found, is to take weighted averages (according to the classification) of the coefficients in the simple joint Pδ formulations but with an adjustment to correct for a mismatch in initial stiffness that would otherwise result. The approach works well as shown by the closeness of the predicted K:X =50:50 curve to that given by the FE analysis. Other results confirm the approach for different classifications, including those involving a degree of Y action.

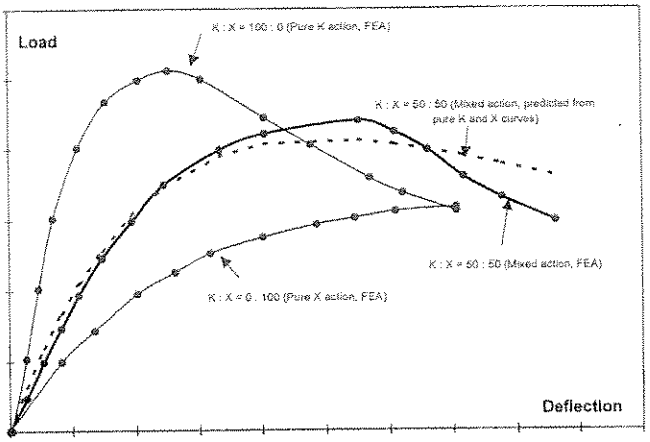

Figure 2: Pδ curves for joints having mixed classifications

In addition to deriving the algorithm for predicting the Pδ response for a joint having a mixed classification, a small study was undertaken on X and K braced frame incorporating elastic local joint flexibilities (LJFs). It should be appreciated that the axial LJFs are functions of axial loads within the frames, but the loads are themselves a function of the LJFs. Therefore, for the first load increment, iterations have to be performed until the loads and LJFs are mutually compatible. It was found that the fewest iterations are required if it is first assumed that all joints are classified as Y joints and thus the LJFs pertaining to Y joints are the initial input values. The study also demonstrated the importance of incorporating LJFs into the analysis to obtain the correct load distribution. It was surmised that fatigue calculations, in particular, are greatly affected by the incorporation of LJFs.

Pδ / Mθ Coupling

A review of a number of possible options for coupling Pδ and Mθ resources indicated that a plasticity algorithm offered the best chance of success and would give a general formulation of wide application. Preliminary studies confirmed that it would work. The mathematics of the plasticity algorithm are quite involved and comprise a yield function, flow rules, hardening rules, etc. However, in principle, the mathematics are no more difficult than those for following the yielding of metals as coded in any general purpose finite element program.

An appreciation of how the plasticity algorithm works can be gained from a perusal of Figure 3. The uniaxial Pδ (adjusted for Q_f and joint classification) and Mθ responses are shown in the top left and bottom right diagrams respectively. The third diagram shows interactions in PM space. Initially the joint response is elastic and Pδ and Mθ are uncoupled. The elastic region is defined by the innermost curve in the PM space (corresponding points on the uniaxial curves are marked) and is taken as a proportion (eg. 60%) of the ultimate interaction curve (outermost curve in PM space). Beyond the elastic region, the instantaneous yielding interaction curve is expanded up to the ultimate curve and then is shrunk for the post peak behaviour (third curve in PM space). During the expansion/shrinking phases, the plasticity routines are invoked.

User options are provided so that the shape of the P-M_{IPB}-M_{OPB} interaction surface can be adjusted.

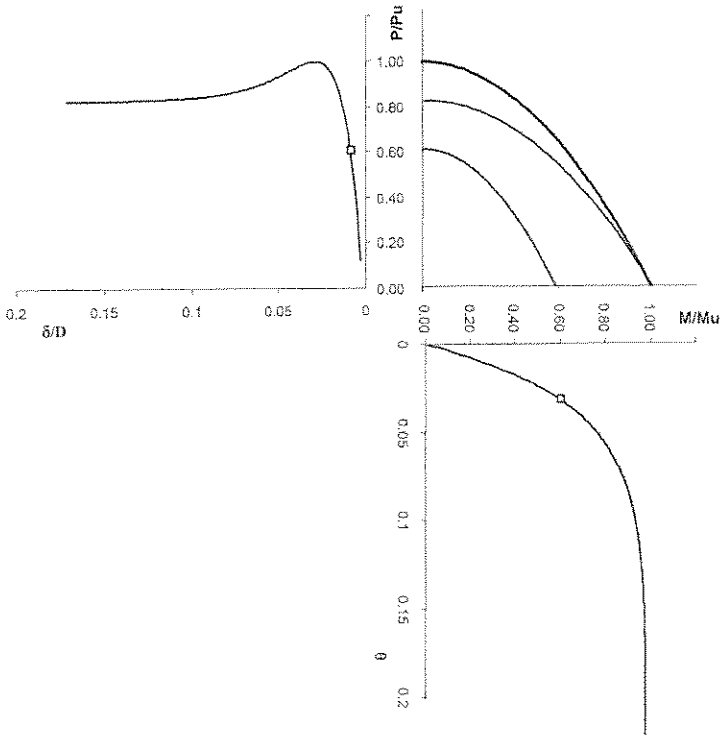

Figure 3: Plasticity model for combined loading

Ductility limits

Joints subjected to tension are potentially subject to fracture. As this has been observed in practice (eg. the K joints of several platforms affected by the passage of Hurricane Andrew were subsequently found to have fractured), it was important to define displacement limits for tension behaviour. The fracture data is rather limited, especially for Y joints of large brace/chord diameter (β) ratios and even more so for K joints. Nevertheless, limits were defined as shown in Figure 4. Furthermore, a study revealed the combinations of K joint classification and β that would predispose shear failure of the chord, rather than brace pull

out, for K joints – see Figure 5. For joints having mixed classification, a linear interpolation of the simple joint limits is recommended.

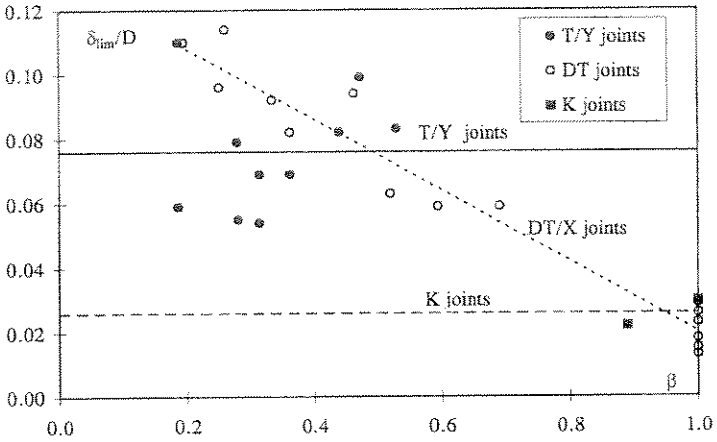

Figure 4: Ductility limits for joints under tension loading

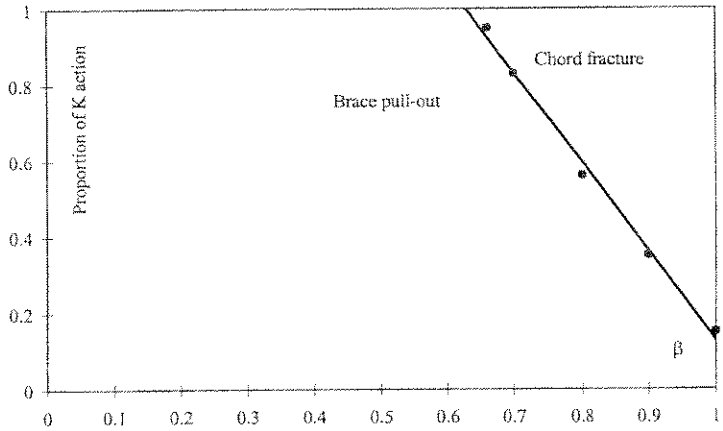

Figure 5: Fracture modes for K joints

Unloading behaviour

It is possible, following member buckling or some other cause for load redistribution, that a joint will unload. Some FE studies were conducted to ascertain the behaviour of joints during unloading. The simple expedient of unloading along a line parallel to the initial loading curve gives an appropriate approximation to the FE data. A typical example is shown in Figure 6.

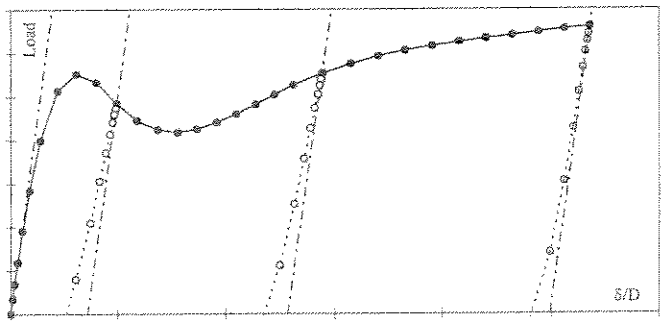

Figure 6: Unloading of DT joint under compression

Testing and Calibration of Module

Coding and testing

The above algorithms were formalized in the manner of a specification and were coded in a joint module comprising several subroutines. The joint module is called MSLJOINT. MSLJOINT was then implemented into a frame analysis package (USFOS) for testing and calibration.

Preliminary testing of MSLJOINT confirmed that the specification requirements were all met, with the joint module producing those aspects of behaviour that formed the basis of the above algorithms. These initial tests were concerned with the behaviour of individual joints.

Calibration to 2D frames

Calibration analyses were performed to compare predictions against test data for five, large scale, 2D steel frames. Two frames were X-braced and three were K-braced. It was found that the calibration exercise was an essential stage of the study and some important observations and conclusions were drawn. Amongst the most important of these concerned the role of the chord stress reduction factor (Qf) for joints in frames (as opposed to individual joint tests).

For X-braced frames, better prediction of frame behaviour were obtained when Qf was maintained at unity rather than when Qf was reduced from unity. For K-braced frames, different Qf factors for the tension brace and for the compression brace were calculated as it was found that the application of these captured K-joint behaviour within frames rather better than if a single Qf value was used. The calibration exercise allowed the setting of appropriate unloading characteristics for joints undergoing fracture.

Figure 7 shows the results of the calibrations against frame data. For each frame, the overall frame PΔ test response is compared to that predicted from an analysis incorporating MSLJOINT and from an analysis assuming rigid joints. Apart from one frame (Frame VI), it can be seen that analyses incorporating the joint module capture elastic behaviour, peak capacity and post-peak response more accurately than do rigid joint analyses. The joint of interest in Frame VI appeared much stronger than expected, possibly due to greater ductility and/or significant strain hardening of the low strength steel employed. Indeed, the frame collapse load was higher than that predicted from the rigid joint analysis. Even so, MSLJOINT could be made to give a very satisfactory result by modifying the steel properties.

Closure

The objectives of the study have been fully met, resulting in a fully specified set of algorithms and the coding of the joint module. Pertinent aspects of joint behaviour have been captured including the driving parameters such as: brace load classification, brace load interaction for axial forces and bending moments, chord load interaction and the modelling of fracture/unloading.

The testing and calibration exercises have demonstrated that in general MSLJOINT is successful, leading to more accurate analyses than the traditional approach of using rigid joint assumption.

As a final observation, in addition to improved predictions for global system response, use of MSLJOINT will lead to increased accuracy of member/joint loads with attendant benefits for component checking, including fatigue life estimation.

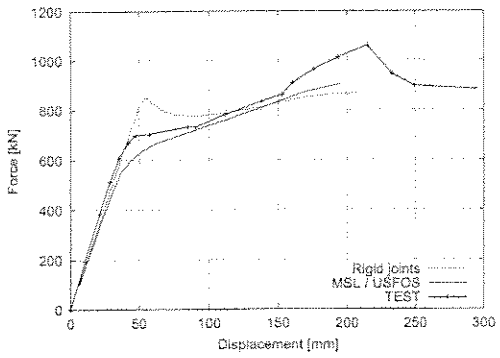

Frame II - X joint in compression

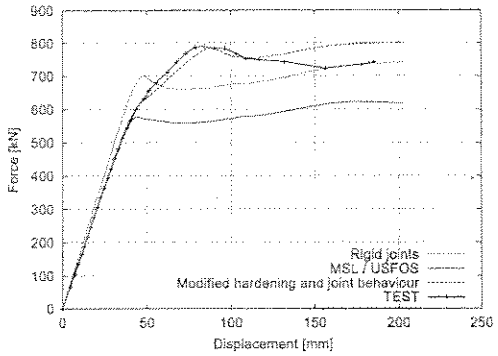

Frame VI - X joint in tension

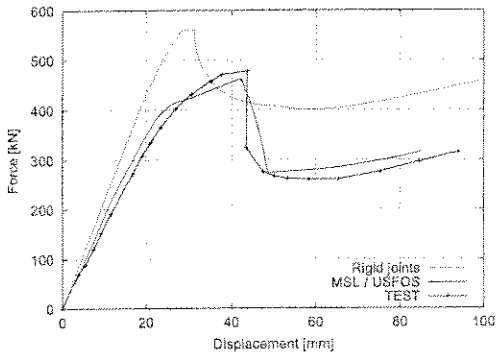

Frame VII - Gap K joint, β = 1.0, g/D=0.1

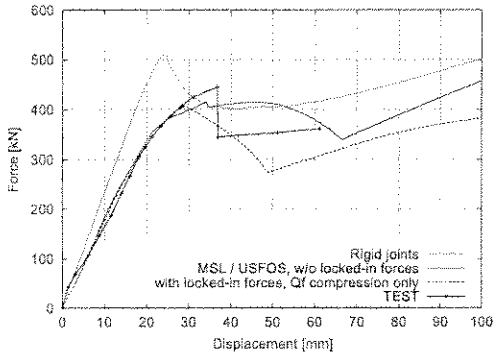

Frame VIII - Gap K joint, β = 0.7, g/D=0.1

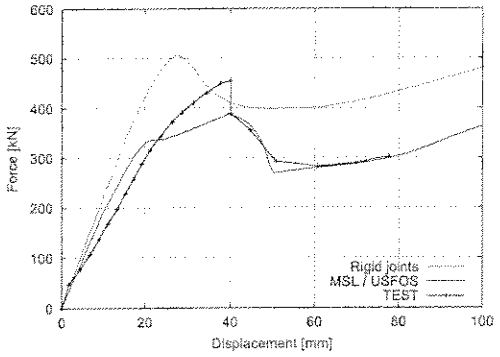

Frame X - Gap K joint, β = 1.0, g/D=0.2

Figure7: Summary of Calibrations Against Frame Data

FINAL REPORT

CONTENTS

Page No

FOREWORD i

EXECUTIVE SUMMARY iii

CONTENTS xi

1. INTRODUCTION 1

1.1 Background 1

1.2 Objectives 2

1.3 Scope of Work 3

1.4 Layout of Report 4

2. SPECIFICATION FOR JOINT MODULE 5

2.1 Introduction 5

2.2 Host Program Requirements 5

2.2.1 General 5
2.2.2 Input Data for Module 6
2.2.3 Output Data from Module 7

2.3 Module Requirements 7

2.3.1 General 7
2.3.2 Details of Subroutines 8

3. DEVELOPMENT OF UNCOUPLED Pδ AND Mθ FORMULATIONS 10

3.1 Summary of Phase I Pδ and Mθ Formulations 10

3.2 Adjustment for Chord Material Strength 11

3.3 Adjustment for Chord Load Effects 12
3.3.1 Screening of Data 12
3.3.2 Assessment of Data 13
3.4 Adjustment for Joint Strength Level 13
3.5 Concluding Remarks 14
4. BRACE LOAD CLASSIFICATION ISSUES 15
4.1 Introduction 15
4.2 Frame Analysis Study 15
4.2.1 Background and Methodology 15
4.2.2 Results of Frame Analyses 18
4.2.3 Implications of Findings 21
4.3 P/δ Curve for Joints of Mixed Classification 22
4.3.1 Statement of Problem 22
4.3.2 Possible Approaches 23
4.3.3 Development of Selected Approach 25
4.3.4 Confirmation of Selected Approach 26
4.4 Concluding Remarks 28
5. DEVELOPMENT OF COUPLED Pδ-Mθ FORMULATION 29
5.1 General 29
5.2 Pδ Springs 29
5.3 Yield Surface Plasticity Formulation 30
5.4 Fibre Modelling 32
5.5 General Finite Element formulation 33
5.6 Elastic Shell Theory 34
5.7 Summary 35
6. FRACTURE CRITERIA FOR JOINTS IN TENSION 36
6.1 Introduction 36

6.2 Methodology 36
6.2.1 General 36
6.2.2 FE Modelling and Analysis of Joints 37
6.2.3 Presentation of Figures 38
6.3 Analyses of T and DT Joints Under Tension 38
6.3.1 Description of Joint Parameters and Selection of Fracture Criteria 38
6.3.2 Discussion of Results 38
6.3.2.1 Load deformation characteristics 38
6.3.2.2 Calculated strain values 39
6.3.2.3 Plastic work done in joints 40
6.3.2.4 Summary 40
6.4 Analysis of K Joints Under Balanced Axial Loading 41
6.4.1 General 41
6.4.2 Boundary Conditions 41
6.4.3 Discussion of Results 42
6.5 Development of Ductility/Failure Criteria 44
6.5.1 Deformation limits 44
6.5.1.1 DT/X joints 44
6.5.1.2 T/Y joints 44
6.5.1.3 K joints 45
6.5.1.4 Joints having mixed classification 45
6.5.2 Failure mode of gapped K joints 46
6.5.3 Implementation issues 47
6.6 Concluding Remarks 48
7. UNLOADING BEHAVIOUR OF JOINTS 50
7.1 Introduction 50
7.2 Description of Analyses 50
7.2.1 FE modelling 50
7.2.2 Joints and load types 50
7.3 Results 51
7.3.1 DT Joint Under Uni-directional Loading 51
7.3.2 DT Joint Under Combined Compression/IPB 51
7.3.3 K Joint Under Balanced Axial Loading 52
7.3.4 DT Joint Undergoing a Change of Classification 52
7.4 Concluding Remarks 53

8. DEVELOPMENT AND TESTING OF MSLJOINT 54

8.1 Introduction 54

8.2 Uni-axial Loading 55

8.3 Mixed Classification 56

8.4 Chord Load Interaction 56

8.5 Combined Loading 57

8.5.1 Initial calibration 57
8.5.2 Shape of (P + IPB) interaction surface 58
8.5.3 Benchmarking analyses 58

8.6 Scaling of Strength Level 60

8.7 Concluding Remarks 61

9. CALIBRATION OF MSLJOINT AGAINST FRAME DATA 62

9.1 Introduction 62

9.2 2D X-Braced Frames 63

9.2.1 Frame II (X joint in compression) 63
9.2.2 Frame VI (X joint in tension) 63

9.3 2D K-Braced Frames 65

9.3.1 Calculation of Q_f for K-joints 65
9.3.2 Calibration of load-shedding behaviour for K-joints in tension 65
9.3.3 Performance of the joint algorithm for K joints 66
9.3.4 Frame VII (Gap K joint, $\beta = 1.0$, g/D=0.1) 67
9.3.5 Frame VIII (Gap K joint, $\beta = 0.7$, g/D=0.1) 67
9.3.6 Frame X (Gap K joint, $\beta = 1.0$, g/D=0.2) 68

9.4 Concluding Remarks 69

10. CLOSURE 70

REFERENCES 1

TABLES

FIGURES

APPENDIX A Non-Dimensional Load-Deformation Formulations for Joints of Mixed Classification

APPENDIX B Plasticity Formulations for Coupled Pδ-Mθ Response

APPENDIX C User Manual Documentation for Joint Module (as Implimented in USFOS)

1. INTRODUCTION

1.1 Background

The continuing need to demonstrate the structural integrity and safety of offshore steel platforms requires that they are subject to periodic structural analysis. Initially, a linear elastic analysis is conducted and component adequacy is checked with reference to recognised codes (eg. API RP2A). Where joint utilisations are indicated to exceed unity, a hierarchy of analysis methods, of increasing complexity, is available to more accurately judge joint adequacy. This hierarchy can be defined as follows:

(a) Elastic analysis with improved code checks for joints.

(b) Elastic analysis with modelling of joint rotation for the joints in question. Code check to API RP2A.

(c) As (b), but with improved code checks for joints.

(d) As (b), but with full modelling of joint non-linear behaviour, uncoupled and coupled.

(e) As (d), but with improved code checks for joints.

(f) System reliability, utilising one of (a) to (e) above for characterising joint and system resistance parameters.

(g) 2-D pushover analysis (non-linear joint and member behaviour).

(h) 3-D pushover analysis.

(i) System reliability, utilising (g) or (h) above for characterisation.

The above hierarchy is nominal, and may be (and often is) adjusted depending on the structure under consideration and the findings from preceding analyses. This is particularly valid for options (f) to (i).

At the outset of this Joint Industry Project (JIP), two specific technical issues became clear from the above analysis methods:

(i) The improved joint code checks noted above, recognise that API RP2A and the HSE Guidance Notes essentially represent 1980 and 1985 technology, respectively, and no fundamental changes have been made since that time. It is also recognised that a number of technological advances have taken place regarding the ultimate limit state of tubular joints from 1980 to date, including the generation of pertinent new data and information. Refined criteria can be established for use in the structural appraisal of existing installations, whereby reliability of capacity algorithms can be increased without compromising safety ("Assessment Criteria").

(ii) Fundamental in the application of analyses (b) to (i) above is the need to understand the behaviour of tubular joints, ie. for jacket structures where a joint or joints represent the weak link, how does the joint behave in the post-

yield and post-peak phase and what are the joint redistribution characteristics? In this respect, the designer is faced with the following issues for a given joint configuration:

- What is the load at which joint 'softening' commences?
- What is the deformation at which joint 'softening' commences?
- What is the deformation at which joint peak load is reached?
- What is the load and deformation at which first crack conditions are reached, for tension loaded joints?

It was against this background that MSL Engineering Limited launched a Joint Industry Project. It was conducted in two phases. This report is concerned with the second phase, the first having been previously reported[1.1]. It is useful, however, to have some appreciation of the Phase I work as this was the foundation for the Phase II studies.

Phase I of the JIP has dealt with two aspects of joint technology. Firstly, it has produced assessment criteria which give more reliable joint strength estimates than any code for joints under uni-directional loading (ie. pure axial or pure moment loading). Implicit in this is the effect of chord loading which is not well captured in any code at present. The results of this part of the work were fed into ISO 13819-2[1.2]. Secondly, Phase I has concentrated on the development of load-deformation formulations for joints under uni-directional loading. The load-deformation characteristics have been captured within the framework of a set of developed equations, the form of which lends itself to the easy creation of the complete $P\delta$ or $M\theta$ curve for T/Y, DT/X and K/YT joints, subjected to axial, IPB or OPB loads. The equation coefficients, for a given joint classification, are simple functions of the non-dimensional joint parameters β, γ, θ, g etc.

The Phase II studies, in summary, have developed the load-deformation equations from Phase I to address brace load interaction and chord load interaction in a set of algorithms. The algorithms were then coded into a joint module (MSLJOINT) for use in frame analysis packages.

1.2 Objectives

In light of the above background, the main objectives of Phase II of the JIP were set as follows:

- To establish yield and ultimate failure envelopes and algorithms encompassing both brace and chord load interaction, through exploitation of Phase I findings and engineering studies of existing and new data (FE or lead-tin alloy tests).
- To develop, test, and benchmark a codified, generic, joint module for use in non-linear frame analysis packages adopted in the offshore industry.

1.3 Scope of Work

The scope of work comprises the extension of the Phase I developed technology to handle brace load and chord load interaction in a robust manner, for both the loading and unloading regime, for the variety of common joint types and loadcases, and to develop, test, and benchmark a codified, generic, joint module for use in non-linear frame analysis packages adopted in the offshore industry. The scope has been developed to fulfil the objectives noted in Section 1.2 and was split into 8 work packages listed below.

Work Package Number	Work Package Title
TJA-1	Management and Co-ordination
TJA-2	Data Capture
TJA-3	Joint Algorithm Approaches
TJA-4	Develop Joint Algorithms
TJA-5	Generation of New Data
TJA-6	Codification of Joint Algorithms
TJA-7	Benchmarking and Sensitivity Studies
TJA-8	Reporting

Because of the nature of the studies, it was necessary for MSL to bring into the project an organization who could provide a host program and software development and coding resources. Following various discussions, SINTEF were selected as having the necessary experience and expertise in preparing non-linear offshore analysis programs (USFOS[1.3] in particular).

A number of interim technical and progress reports were produced during the JIP. The technical reports have now been largely assimilated within this final report, as indicated in Table 1.1.

1.4 Layout of Report

The following sections of this report have been ordered so that, as well as being a logical development of concepts, largely reflect the chronological development of the various studies.

Section 2 has been placed before the other sections as it sets out the requirements of the module. It therefore serves as a road map for the development of the module.

The development of the algorithms on which the module is based is essentially covered in Sections 3, 4 and 5. Section 3 starts with the uncoupled $P\delta$ and $M\theta$ curves from Phase I and continues with their enhancements to account for chord load effects and scaling of strength. Section 4 addresses classification issues in which an axially loaded joint is considered as a mixture of K, X and Y joints. It also examines implementation issues for mixed class joints and reports on a small study showing the effects of local joint flexibility on frame behaviour. Section 5 is where coupling of $P\delta$ and $M\theta$ responses is examined. Appendices A and B contain the detailed mathematical formulations resulting from the developed approaches in Sections 4 and 5.

Sections 6 and 7 contain an assessment of numerical data generated within the project, and some pertinent test data, to set approaches for joint fracture and unloading behaviour.

Section 8 discusses the testing of the module to simulate individual joint behaviour.

Section 9 examines the performance of the module to predict frame behaviour. This important part of the study allowed for some tuning of the module to give robust predictions.

The conclusions are summarized in Section 10.

Finally, Appendix C gives User Manual Documentation for the Module as implemented in SINTEF's analysis package – USFOS.

2. SPECIFICATION FOR JOINT MODULE

2.1 Introduction

This Section 2 represents the specification for the joint module and was used as a basis for coding activities. It also serves as a 'road map' for subsequent sections of this report.

Although USFOS has been selected as the host program in which the module is to be initially incorporated and tested, it has always been the intention that the developed module should be generic, i.e. capable of being used in any suitable frame analysis program. Whilst modifications to a host program (including USFOS) will be inevitable, certain reasonable assumptions of what the host program should be able to provide, by way of input to the joint module, have to be made. There are also issues which are best left to the prerogative of the developers of the host program. These assumptions and issues are discussed in Section 2.2.

Section 2.3 is the main section and defines the requirements of the module. Some thought has been given to the possible eventual use of the module, and it is considered desirable to build in a certain amount of flexibility as to how the module will operate. This is to be achieved by user-defined options, as discussed in Section 2.3.

The joint module is coded using several subroutines, to provide flexibility in implementation and to facilitate coding and checking. The main equations which have been developed for incorporation into the subroutines are presented in various tables and appendices.

2.2 Host Program Requirements

2.2.1 General

This host program clearly has to fulfil the basic requirement of being able to analyse space frame structures and have non-linear capabilities with respect to load incrementation. It is assumed that the model spatial geometry is defined by nodes at the intersection of the centrelines of the tubular elements.

A user-specified option should be implemented as to whether one, some or all tubular joints are to be analysed with the joint module. For those joints which are to be analysed with the module, the host program should insert, either automatically or by user intervention, another node at the chord surface/brace centreline intersection to define a 2-noded 'joint element'.

The host program should call the appropriate subroutine in the module to set initial (elastic) joint stiffnesses before starting load incrementation. It is recommended that these initial stiffnesses should correspond to Y joints, see Section 4 of this report.

The host program, or perhaps rather the user, should decide on iteration requirements with respect to the need for sub-increments and convergence tolerances. In particular, the potential numerical instability resulting from a fractured joint in tension needs careful consideration, as rather large changes in

member loads will occur. Generally equilibrium interactions will be required to provide consistency between the joint element results and the global frame results.

When exercising various options (see below), the host program will be required to be able to read associated input data (e.g. joint capacities or initial joint stiffnesses) and supply them to the joint module.

2.2.2 Input Data for Module

The following data will need to be provided by the host program to the module.

Geometric data

D	chord diameter (or that of can if present)
T	chord thickness (or that of can if present)
d	brace diameter (or that of stub if present)
t	brace thickness (or that of stub if present)
θ	brace angle
g	gap, for K joint (-ve value denotes overlap). Note for KT joint a weighted average value is required.

Load data

P_b	axial load in brace (-ve value denotes compression)
M_{ib}	in-plane moment in brace
M_{ob}	out-of-plane moment in brace
P_c	axial load in chord (-ve value denotes compression)
M_{ic}	in-plane moment in chord
M_{oc}	out-of-plane moment in chord

Load classification data

C_K	proportion of K action in brace
C_X	proportion of X action in brace
C_Y	proportion of Y action in brace

Material data

F_y	yield strength of chord material
F_{yb}	yield strength of brace material (for overlapped K joints)

Optional flags and associated data

FLAG1	= 1 (default value), use MSL mean joint capacities

= 2, use MSL characteristic joint capacities

= 3, use user-specified joint capacities: P_{uK}, P_{uX}, P_{uY}, M_{ui}, M_{uo}

FLAG2 = 1 (default value), use MSL initial joint stiffnesses

= 2, use user-specified initial joint stiffnesses: E_K, E_X, E_Y, E_i, E_o

FLAG3 = 1 (default value), use MSL Q_f functions

= 2, use Q_f (= Q_{fK} = Q_{fX} = Q_{fY}) from host program

FLAG4 = 1 (default value), use MSL Pδ/Mθ formulations

= 2, use idealised elasto-plastic Pδ/Mθ formulations

2.2.3 Output Data from Module

The host program is to react to the following data from the module.

E_{ij}	12 x 12 element tangential stiffness matrix (local system)
P_i	Internal element force matrix (local system)
FRACT	Flag = 1 when the brace has fractured
ERR	Error messages

2.3 Module Requirements

2.3.1 General

The primary objective of the module is to simulate the load-deformation behaviour of a joint, in a phenomenological manner, in both the pre and post-peak regimes. It is to consider pertinent factors which affect joint behaviour such as:

- joint geometry and material strength
- type and magnitude of brace loads and their interaction
- type and magnitude of chord loads
- whether the joint is loading or unloading
- whether the joint has reached some deformation limit (fracture criterion) or not.

The module is to calculate, and return to the host program, the instantaneous tangential stiffness matrix and internal element forces. The module is to contain self-checking routines for detecting potential errors and to output warning/comment messages.

The simulated behaviour is to use the uncoupled Pδ and Mθ formulations developed in Phase 1 of the project and enhanced under the current phase. The instantaneous load-deformation response can be taken as being history (i.e. path) independent.

Various user-defined options are to be built into the module, including the facility to change the capacity of the joint or, indeed, its complete Pδ and Mθ response.

There are a number of steps to be undertaken for deriving the simulated joint response. These have been arranged in a logical sequence in the flowchart shown in Figure 2.1, which also shows the necessary interactions between the host program and the module. The flowchart does not attempt to identify individual subroutines, although it is convenient to treat them as such for the purposes of this specification. Further details of each 'subroutine' are given below.

2.3.2 Details of Subroutines

Each box in the module flowchart, Figure 2.1, has been assigned a number and these are referred to here.

Subroutine 1

The basic joint capacities for axial compression, tension and moments (IPB and OPB) are to be calculated without considering the effects of chord loads; these effects are considered subsequently. The basic capacities need only to be calculated once and stored.

The basic capacities can be given by the mean formulations in Table 2.1 with Q_f set to unity (note the tension formulations are artificially high to produce the appropriate Pδ curve). Alternatively, characteristic capacities may be selected and these are obtained by multiplying the values obtained from Table 2.1 by the corresponding characteristic biases given in Table 2.2. As a third option, the user may wish to supply a separate set of capacities. It is recommended that these are transformed into a set of bias factors with respect to the default mean capacities, along the lines of Table 2.2, as this will simplify subsequent calculations to preserve initial stiffness slopes (see Subroutine 4). Thus, in all cases, the basic capacities are obtained as those from Table 2.1 times the bias factors (default values of unity). The mean capacities and the associated characteristics biases were derived in Phase 1 of the project.

Subroutine 2

The coefficients A and B are to be calculated according to Table 2.3. Note the coefficient B is in units of N/mm^2 and therefore F_y should also be expressed in these units. These coefficients need only be calculated once and therefore this subroutine may usefully be combined with the first, particularly as it relies on the same joint geometry input data. The derivation of the Pδ and Mθ equations is discussed in Section 3 of this report.

Subroutine 3

The MSL Q_f functions from Phase I are presented in Table 2.4. These can be made to conform closely to the API RP2A functions simply by replacing α_1 and α_2 by γ and 1.72γ respectively for all joint and load types.

Subroutine 4

The outputs from Subroutines 1 to 3 are now sufficient to derive the instantaneous Pδ and Mθ curve formulations shown at the bottom of Table 2.3. However, these need adjusting according to the (load) classification of the joint. For joints having mixed classification with respect to axial loads, the three separate curves (one each for K, X and Y action) need combining. This involves the adjustment of elastic stiffness, as discussed in Section 4. Furthermore, to preserve the same elastic stiffness no matter whether mean, characteristic or any other joint capacity is selected (see Subroutine 1), the bias factor can be considered here as well. Guidance on the combination equations to be used is given in Appendix A.

Subroutine 5

Subroutine 5 considers coupling of the Pδ and Mθ responses. This is discussed in Section 5 of this report, where it is recommended that a plasticity formulation is used. A detailed mathematical treatment is supplied in Appendix B.

Subroutine 6

This subroutine applies various checks to determine if the joint has entered into the plastic non-linear region and whether it is continuing to do so or is unloading (see Appendix B). As verified by the FE analyses conducted and reported on in Section 7, the unloading behaviour can be modelled as indicated in Figure 2. That is the slope of the unloading curve is the same as the initial slope. Note, for joints having mixed classifications, the initial Pδ unloading path need not be linear because the classification may change during the unloading process. For tension loaded joints, checks need to be performed to see whether the joint has exceeded ductility limits (see Section 6).

Subroutine 7

Standard matrix operations are to be used to obtain the revised load sets.

3. DEVELOPMENT OF UNCOUPLED Pδ AND Mθ FORMULATIONS

This section briefly summarises the work conducted in Phase I of the project to derive load/deformation formulations for joints subjected to axial load or moment loading separately. It also describes the enhancements made to the Phase I formulations to ensure that:

- the implied elastic local joint flexibilities (LJFs) are independent of the chord material yield strength,
- the effects of chord loads are suitably accounted for,
- the LJFs are preserved if characteristic strengths (or any other strength level for that matter) are specified rather than mean strengths.

3.1 Summary of Phase I Pδ and Mθ Formulations

At the outset of the Phase I studies, it was intended that the Pδ (and Mθ) formulations were to be linear piecemeal functions so that the Pδ curve would be developed as a multilinear approximation. The straight lines would intersect at discrete points such as the point at first softening, the point at peak load and at a post-peak point. However, it soon became apparent that this approach would have led to a considerable amount of work and opens up questions of the required accuracy of the approximation. Therefore attention was directed at the possibility of representing the Pδ curve by a single continuous function with coefficients related to the joint geometric parameters β, γ, τ and material properties. Ideally the mathematical function to describe experimental Pδ curves should:

- be continuous and differentiable over its intended range of application
- be of a simple form with as few coefficients as possible
- be capable of representing the different shapes of Pδ curves observed
- be accurate
- be robust in terms of not being ill-conditioned to avoid difficulties in curve fitting or in application
- have coefficients which do not differ widely in order of magnitude
- have coefficients which have physical meaning.

Following trials with a few mathematical functions, an exponential expression was selected. In its simplest form, this can be written:

$$P = d - a\,(1 - b \,.\, \exp(-c\,\delta))^2 \qquad \ldots 3.1$$

where a, b c and d are constants (or more correctly functions of joint geometry) to be fitted.

Equation 3.1 was found to simulate sample experimental Pδ curves very well, and was subjected to mathematical analysis to learn more about its characteristics. The more important findings from this analysis are noted here:

- So that the Pδ curve passes through the origin, it is found that there are only three independent 'constants' as:

$$b = 1 + (d/a)^{1/2} \quad \ldots 3.2$$

- The constant 'd' is directly associated with P_u, the maximum load.
- The constant 'a' is the magnitude of the drop in load following peak load.
- The initial stiffness of the Pδ curve (at the origin) is given by:

$$K = 2\,a\,b\,c\,(b-1) \quad \ldots 3.3$$

- The displacement of peak load is given by:

$$\delta_u = \ln(b) / c \quad \ldots 3.4$$

Fitting to experimental data was performed with a non-dimensional form of Equation 3.1. Taking into account the dependency of one of the constants on the others (Equation 3.2), the final Pδ and Mθ formulations from Phase I are:

$$P = P_u(1 - A[1 - (1 + 1/\sqrt{A}) \exp(-B\delta/D)]^2) \quad \ldots 3.5a$$

$$M = M_u(1 - A[1 - (1 + 1/\sqrt{A}) \exp(-B\theta)]^2) \quad \ldots 3.5b$$

where P, M = joint load

P_u, M_u = joint mean strength

δ = joint deformation (aligned to an individual brace)

θ = joint rotation (radians)

D = chord diameter

A, B = non-dimensional constants for any given joint geometry and load type.

For completeness, the values of A and B from the Phase I studies are presented in Table 3.1. However, the Pδ and Mθ formulations have since been adjusted as discussed in the next subsection and this has entailed a revision of the constant B.

3.2 Adjustment for Chord Material Strength

It can be shown, through mathematical analysis, that the initial stiffness of the Phase I Pδ formulation (Equation 3.5a) is given by:

$$K = \left[\frac{2(1+\sqrt{A})B}{D}\right] P_u \quad \ldots 3.6$$

with a similar expression holding for the Mθ formulation. The term in the square brackets is a constant, for a given geometry and load type. It can be seen that the Phase I initial joint stiffness is therefore predicted as being directly proportional to the joint capacity (P_u or M_u) and, in turn, to the chord material strength F_y. This is clearly inappropriate as linear elastic behaviour of the joint should be independent of F_y. Rather, the initial stiffness should be given by:

$$K = \left[\frac{2(1+\sqrt{A})B}{D}\right] \frac{P_u}{F_y} \quad \ldots 3.7$$

and this leads to modified formulations as follows:

$$P = P_u (1 - A[1 - (1 + 1/\sqrt{A}) \exp(-B\delta/(F_y D))]^2) \quad \ldots 3.8a$$

$$M = M_u (1 - A[1 - (1 + 1/\sqrt{A}) \exp(-B\theta/(F_y))]^2) \quad \ldots 3.8b$$

Note that the coefficient B in the modified formulations takes on different numerical values and are now dimensionalised (units of F_y) compared to the original (Phase I) formulations. The original values of B have to be multiplied by some weighted average of the F_y values used in the original curve fitting exercise. This was achieved by fitting the products BF_y (one value per test specimen), for each given joint/load type, to the joint geometric parameters rather than just the individual values of B alone as done originally.

The revised B coefficients, along with the A coefficients for completeness, are given in Table 3.2. Comparisons of the modified formulations incorporating the revised coefficients with test data confirm that the modifications are an improvement over the original formulations, albeit only slightly so. This is not unexpected as F_y in the test data varies only over a modest range.

3.3 Adjustment for Chord Load Effects

In general, chord loads degrade joint strength. However, and in a similar appreciation that the chord yield stress does not affect LJF, it can be expected that LJF should also not be affected by chord loads. This subsection reviews the available data and presents further adjustments to the $P\delta$ and $M\theta$ formulations.

3.3.1 Screening of Data

Initially, a preliminary screening of the database was undertaken on the available data. The preliminary screening criteria adopted was to extract only those steel joint test data which contain complete load-deformation curves. Tests on simple T/Y, DT/X and K joints indicate that the presence of compressive stresses in the chord, in addition to those required for equilibrium, can cause a significant reduction in joint strength. Such a reduction is quantified in design codes using the factor Q_f which is nominally defined as the ratio of joint strength in the presence of chord stresses to joint strength in the absence of such stresses. Table 3.3 presents the Q_f factors for different loading conditions derived in Phase I.

The references having relevant steel joint data for joints subjected to chord loading are presented in Table 3.4. It can be seen from Table 3.4 that data are available for T/Y, DT/X and K/YT joints although only in the case of DT/X joints is there data covering a range of chord loading and brace load types, see Table 3.5.

Further screening of the available steel data was undertaken using the screening criteria developed in Phase I (i.e. chord diameters >100mm, F_y measured). It is worth noting for some of the tests, particularly the Japanese data on K joints, that chord diameters of the joints were significantly less than 100mm. In some programmes, limited tests were also performed without chord loading to provide base data for use in quantifying the parameter Q_f associated with tests including chord loading. However, in most of the test programmes, base data are not available or some of the parameters relating to material and/or geometric properties

of the base tests are different to those of the tests with chord loading. In some cases the chord thickness and /or chord yield strength of the reference tests were different to those associated with the interaction tests. In these instances, such discrepancies were overcome by using non-dimensional parameters.

3.3.2 Assessment of Data

To illustrate typical load deformation data available for X joints under brace compression loading, with and without chord loading applied, data from Boone, Yura and Hoadley[3.2] are shown in Figures 3.1 to 3.3. The experimental P-δ and M-θ curves for a single geometry of β=0.67 and γ=25.3, under no chord loading (i.e. tests A1, I7 and O8), under chord axial compression (i.e. tests AP5, AP2, IP12 and OP9) and tests with combined chord axial compression and bending (i.e. tests AM6, IM11 and OM10) are shown. Two different maximum chord stress levels were applied, 0.6 F_y (i.e. tests AP5, AM6, IM11 IP12, OP9 and OM10) and 0.8 F_y (i.e. test AP2). The experimental curves demonstrate that chord stress does not appear to have any significant effect on the initial joint stiffness.

Noting this important observation a further modification to the Pδ and Mθ formulations was undertaken. The modification is similar to that made with respect to the expectation that the yield strength should not affect the initial stiffness, see Section 3.2.

It has been shown that the initial joint stiffness is directly proportional to the joint capacity and therefore also to F_y and to Q_f as both are contained explicitly in the P_u and M_u terms. To account for this, modified formulations are proposed as follows:

$$P = P_u (1 - A[1 - (1 + 1/\sqrt{A}) \exp (-B\delta/(Q_f F_y D))]^2) \quad \ldots 3.9a$$

$$M = M_u (1 - A[1 - (1 + 1/\sqrt{A}) \exp (-B\theta/(Q_f F_y))]^2) \quad \ldots 3.9b$$

Collectively, the results presented in Figures 3.1 - 3.3 indicate that good agreement can be obtained between the results from experimental chord loaded tests and those predicted using the above modified formulations. It can also be observed that the effect of chord stress, which appears to cause the joint stiffness to begin deteriorating at a lower load level and reduces peak load, is captured. However, there is some evidence that as the chord stress level increases, the post-peak unloading characteristic may be more pronounced, depending on joint and load type.

The effect of chord stresses for K Joints under balanced axial loading was studied by de Koning[3.6] for β=0.33 and 1.0. The results are shown in Figures 3.4 and 3.5. Again it can be seen that the predictions capture well the experimental data. Note that it was necessary to take into account equilibrium chord stresses in deriving a base case for zero chord stress.

3.4 Adjustment for Joint Strength Level

So far, the Pδ and Mθ formulations have only considered the mean capacity response curve. It is possible that a user may wish to examine the structural response at the characteristic level or a range of levels if probability/reliability studies were being performed.

It is useful to define the factor ϕ as the ratio of the required strength level to the mean strength. Thus, for an analysis based on the characteristic strength:

$$\phi = P_k / P_u \quad \ldots 3.10$$

Where P_k is the characteristic strength.

Such characteristic factors are defined in Table 2.2.

The required modifications to the Pδ and Mθ formulations are similar to those made for F_y and Q_f adjustments above. The final formulations, which preserve the LJFs, are:

$$P = \phi P_u (1 - A[1 - (1 + 1/\sqrt{A}) \exp(-B\delta/(\phi Q_f F_y D))]^2) \quad \ldots 3.11a$$

$$M = \phi M_u (1 - A[1 - (1 + 1/\sqrt{A}) \exp(-B\theta/(\phi Q_f F_y))]^2) \quad \ldots 3.11b$$

3.5 Concluding Remarks

The Pδ and Mθ formulations from Phase I of the project have been enhanced to account for the observation that neither the chord material strength (F_y) nor chord loads (the Q_f effect) affect initial load-deformation response. The formulations have also been modified to allow the user to select an arbitrary strength level for the joint, again without affecting the elastic LJFs.

There is one further issue to consider for the uncoupled Pδ curves, that is joint classification. The issue of joint classification is addressed in Section 4 and Appendix A.

4. BRACE LOAD CLASSIFICATION ISSUES

4.1 Introduction

The work reported in this section concerns the role of joint classification on joint stiffness, or its reciprocal the local joint flexibility (LJF). Properly, LJFs have to be implemented into the frame structure analysis in order to obtain more realistic results. They can be incorporated by using spring elements in the FE Model. The values of the spring stiffnesses for each joint are determined by LJFs which, in general, are functions of:

- joint geometry
- brace load combination (axial, IPB and OPB)
- chord load effects
- joint classification.

Since the LJF for a given joint will change during a complete pushover analysis, e.g. due to load redistribution following non-linear behaviour, it will be necessary to apply platform loads incrementally. For the initial increment or increments, the structure will be elastic, and member loads generally small. During this phase the LJFs for axial, IPB and OPB behaviour will be uncoupled and the effects of chord load will be negligible. The uncoupled joint spring stiffnesses can be calculated from the Pδ and Mθ formulations derived in Section 3. However, there is a difficulty with the selection of the axial LJFs for the first load increment. This is because the axial LJF for each brace is dependent on the joint classification which, in turn, is dependent on the loads in all braces at the joint, which are unknown at the outset of the analysis. The difficulty does not arise with the moment LJFs as, in common with the moment capacity, these are not dependent on joint classification.

It is the primary objective of the studies reported in this section to establish an appropriate methodology which addresses the above difficulty in a robust manner.

It may be noted that the present-day design practice is to assume rigid joints for jacket structure analysis. Thus with the appropriate LJF information at hand, the second objective of this investigation is to demonstrate the importance of establishing a technology which permits LJFs and joint response characteristics to be adequately captured.

A third objective is to develop a methodology that can generate the complete Pδ curve (i.e. both in the linear and non-linear regions) for joints with mixed classifications.

4.2 Frame Analysis Study

4.2.1 Background and Methodology

As noted in the introduction in Section 4.1, the axial spring stiffness of a joint is a complex function of several variables, including joint geometry. As an example, the non-dimensional Pδ curves for K, X and Y joints having $\beta = 0.3$, $\gamma = 25$, $\theta =$

45° (and g = 2T for the K joint) are plotted together in Figure 4.1. It can be seen that for these particular joint geometry parameters, the initial stiffness of the Y joint is intermediate between those of the K and X joints. (With increasing levels of joint deformation, but not necessarily of load, the K joint stiffness becomes the softest as its capacity is reached the soonest.)

In a structural frame, it is not only the joint stiffness which affects the response - the stiffness of the brace members also have a role to play. It is the ratio of joint and member stiffnesses that determines their relative importance to frame response. Again, the member axial stiffness is a function of its geometry, i.e. member area and its length. The total stiffness, K_T, can be calculated as follows:

$$K_T = \frac{P}{\Delta_t} = \frac{P}{\Delta_j + \Delta_m} = \left(\frac{1}{K_j} + \frac{1}{K_m} \right)^{-1} \qquad \text{.....4.1}$$

where P is load and Δ_t is total displacement including joint displacement Δ_j and member displacement Δ_m. K_j and K_m are the stiffnesses for tubular joint and associated member respectively. K_j can be $K_{j,y}$, $K_{j,x}$, $K_{j,k}$ (i.e. stiffness of Y, X or K joint respectively) or some weighted combination of these.

It is possible to define K* for a reference case where all tubular joints are assumed as Y joints as follows:

$$K^* = \left(\frac{1}{K_{j,y}} + \frac{1}{K_m} \right)^{-1} \qquad \text{.....4.2}$$

K^*/K_T is a function of ratio of brace length(l) and brace diameter (d). The K^*/K_T against l/d curves are presented in Figure 4.2 for joints with the following parameters.

Parameter	Range
β	0.3, 0.7, 1.0
γ	10, 25
τ	1
θ	45°

When l/d = 0, the stiffness of the joint/member combination is just that of the joint alone and therefore the ratio K^*/K_T is simply the LJF of the joint compared to the Y joint. It can also be seen in Figure 4.2 that as l/d increases, the three curves in each diagram converge and that the rate of convergence is more rapid for the lower γ value. This is because increasing l/d values lead to a more dominant role of the member on total stiffness, and that this effect is more noticeable for stiffer (lower γ) joints.

One aspect not yet considered is that for Y joints, though not X and K joints under balanced axial loading, additional flexibility arises due to chord bending. This flexibility is a function of the chord cross-sectional properties and the effective length over which chord bending occurs. For long chord effective lengths, it may be supposed that the Y joint LJF has only a minor effect on the total flexibility of the joint/member/chord system. In other words, the actual value of the Y joint LJF would not have much of an impact on the axial load result from a frame analysis.

In general, the loads in the members at a given nodal joint may be such that a mixed joint classification (load-based) is applicable for each brace/joint at the node. Two questions therefore arise. Firstly, given a mixed classification, how should the relevant spring stiffness be calculated? This question is addressed in Section 4.3 of this report, but for now and in the following subsections it is assumed that the weighted average (weighted according to the proportions of the K, X and Y actions in the classification) of the individual joint stiffnesses applies. Secondly, given that joint spring stiffnesses are affected by joint classification and hence the loads arising from the input spring stiffnesses, how accurate do the input spring stiffness have to be?

Because of the interplay between joint and member stiffnesses, and possibly chord bending stiffness, the latter question can only be addressed by reference to frame analysis results. Therefore, a small study involving frame analysis was conducted.

The study involves linear elastic FE analyses of two simple frames with and without LJF. The first model consists of a one bay X-braced 2D frame shown in Figure 4.3. The geometry of the members and joints has been deliberately selected to maximise the differences between the LJFs of certain joints assuming each to be classified as 100% K or 100% X. Thus, the upper and lower horizontal members, and the diagonal braces of the DT joint, have a diameter of 0.3 that of other members; the ratio of (l/d) is 10 for the central X joint; all joints have thickness ratio(τ) of unity and the K joints have a narrow gap (2T). Axial and (in-plane) rotational springs attach each brace member to the joint node.

Each node and element has been assigned a number, as have the ends of the elements, see Figure 4.3. A horizontal point load is applied at the top left hand corner (node 4). Pinned conditions are assumed at the bottom of the legs.

The second model consists of a one bay K-braced 2D frame shown in Figure 4.4. Again, the geometry has been selected to maximise LJF differences; achieved by making the diameter of the diagonal and upper horizontal members 0.3 times the diameter of other members.

Four different sets of initial axial stiffnesses for the joint springs were assumed and analysed:

1. a model with all springs given an arbitrarily high value. This model thus represents rigid joints and provides a present-day design reference case for comparison.

2. a model in which spring stiffnesses have been assigned values considering a geometric classification scheme (i.e. a joint which looks like a K joint has been assigned K joint spring stiffnesses).

3. a model in which the axial spring stiffnesses have been assigned values corresponding to the average value of the relevant X and K joints, i.e.:

$$Kj = \frac{Kj,x + Kj,k}{2}$$

The above stiffness does not include a contribution from the Y joint on the basis that this was expected to not be so relevant due to chord bending effects (see discussion above).

4. a model with all axial joint stiffnesses set to those of the corresponding Y joints.

It was hoped that the stiffnesses in Models 2 or 3 above would provide reasonably accurate results (as compared to "correct" results following iterations to find correct load classification and spring stiffness input values). In the event this did not prove to be the case and these models are only included for completeness.

4.2.2 Results of Frame Analyses

4.2.2.1 Load Classification

It was clear on inspecting early results that the initially assumed load classifications, and the associated joint axial stiffnesses, were not compatible with the resulting load distributions obtained with those stiffnesses. It was therefore necessary to conduct iterations such that the input classification, and associated input spring stiffnesses, lead to a load distribution in the frame giving the same classification:

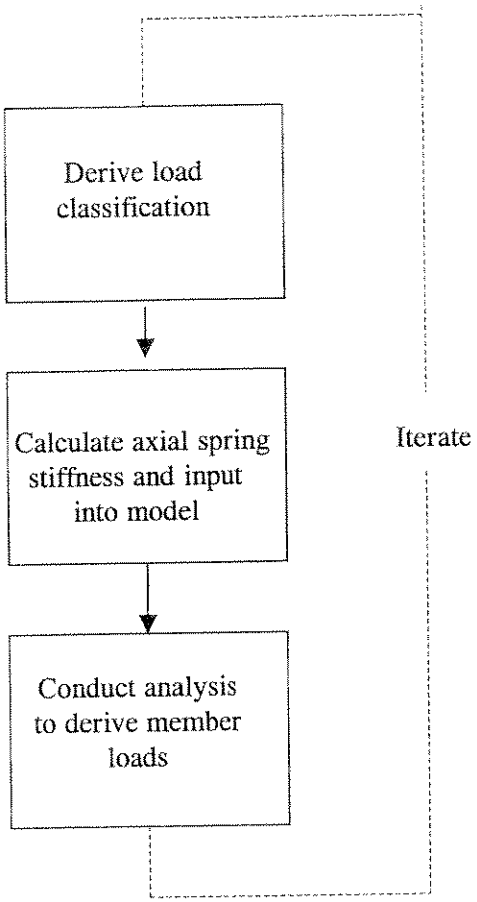

The results of a comparison of the load classification convergent rate for three different starting assumptions are tabulated in Table 4.1 for the X-braced frame. The stippled cells in the table indicate where convergence has not yet been obtained.

It can be seen that the same final load classification is reached no matter what starting assumptions are made. However, the starting assumptions do affect how many iterations are required to obtain convergence, this being most for the rigid joint assumption and least for when the joints are initially assumed to be all Y joints. Rapid convergence is also obtained for the K-braced frame with Y joint assumptions, see Table 4.2.

The final joint classifications for the X-braced and K-braced frames are indicated in Figures 4.5 and 4.6 respectively. These figures demonstrate that a load classification scheme based on geometry is inadequate, especially for the X-braced frame.

After each iteration, the load distribution within the frame changes, even for members for which the joint load classification does not alter. It may be remarked that load classification is largely a step function (i.e. most joints would have 100% Y, K or X) whereas loads can be of any value. Figure 4.7 shows the axial load distributions after successive iterations for the X-braced frame with the joint

stiffnesses initially taken as the average of K and X joints. It can be seen that there are significant differences in the load distribution between successive iterations. These results confirm the need to conduct iterations to derive correct spring stiffnesses and hence load distributions.

4.2.2.2 Effect of LJFs

Figure 4.8 shows the axial forces in the members of X-braced frame resulting from the rigid joint model and a converged model considering LJFs. As may be seen, there are significant differences between these two sets of results, particularly for the diagonal members, the upper portions of the legs and the lower horizontal member. Overall, the introduction of LJF into the system tends to increase the axial forces in the members. This is because there is more truss action, and less portal action, compared to the rigid joint frame.

The LJF frame is about 4.2 times more flexible than the rigid joint frame, as inferred from the horizontal deflections at node 4. This has an impact on the natural frequency of the structure, and hence on dynamic behaviour.

The results from the two models for the X-braced frame are compared in Figure 4.9 in terms of ratios. For each member end, ratios are given for the value in the frame with flexible joints to the value in the frame with rigid joints. The ratios are:

- P_{LJF}/P_{Rigid} - axial force ratio
- M_{LJF}/M_{Rigid} - bending moment ratio
- $\sigma_{LJF}/\sigma_{Rigid}$ - maximum combined stress ($|P/A| + |M/Ze|$) ratio
- $\sigma_{LJF}/\sigma_{max}$ - ratio of member combined stress for the frame with flexible joints to the maximum value for either frame
- $\sigma_{Rigid}/\sigma_{max}$ - ratio of member combined stress for the frame with rigid joints to the maximum value for either frame.

Inspection of the results in Figure 4.9 reveals the following observations:

(i) In relative terms, estimates of member loads (P and M) may be widely in error when rigid joints are assumed, as in present-day practice. This is particularly so for moment loads. Undoubtedly some of the more gross errors, manifested by high load ratios, are due to low absolute values of the loads resulting from the rigid joint analysis.

(ii) For some member ends, loads are of opposite senses in the two models.

(iii) As a result of item (i), the maximum combined stress ratio varies about unity, from 0.16 to 2.79. In other words, calculated utilisations for individual members on the basis of rigid joints assumptions will generally be incorrect.

Perhaps of most interest is the factored utilisation ratio given in the last two columns of Figure 4.9. These have been obtained by factoring all the member end combined stresses such that the maximum result anywhere is unity (node 2 of member 1 for the LJF frame). The values are only indicative of member utilisations because strictly a proper code check would be required as axial force and moment are weighted differently.

It can be seen that the two analysis models identify the same member end, mentioned above, as being the critical element. However, the present-day design practice of assuming rigid joints underestimates the utilisation of the critical element in this frame by 11%. It can be expected that this value may well be larger in the case of frame with increased structural redundancy (LJFs play no role in member loads of statically determinate structures).

In the consideration of fatigue behaviour, the error in underestimating utilisations become even more important as the error is raised to the index in the SN equations (generally m=3). Thus the fatigue lives of members and joints could be an order or more in error, and fatigue life ranking will not be accurate. It is known that the incidence of fatigue cracking does not follow the ranking established on the basis of a rigid joint analysis. It would be instructive to learn whether better correspondence could be obtained from a ranking based on an analysis with LJFs included.

The member effective length factor (k) used to determine the axial capacity of a member is dependent on the degree of end fixity and hence the LJFs of the connection between the member and the structure. It may therefore be inferred that the assumption of rigid joints could lead to an over-estimation of member capacity.

Finally, Table 4.1 gives the resulting joint classification based on the loads resulting from the two analyses. (That for the rigid frame are those obtained after the first iteration.) It can be seen that the joints at either end of member 10 (the lower horizontal) are classified completely differently in the two analyses, and significant differences exist for the braces at node 12 (the DT joint) and for the diagonal brace (member 5) at its lower end (node 2). Therefore, the present-day design practice of assuming rigid joints not only give incorrect load distributions, but also may give rise to an inappropriate selection of joint resistances.

Similar results and inferences to the above can be made with respect to the K-braced frame, see Figures 4.10 and 4.11.

4.2.3 Implications of Findings

It is clear that appropriate joint stiffnesses have to be used in a frame analysis to obtain accurate results. Because of the interrelationship of joint classification, joint spring stiffnesses and frame load distribution, it has been found necessary to conduct iterations at the outset of an analysis to obtain a compatible set of spring stiffnesses with the load distribution. It is recommended that for the first iteration, spring stiffnesses based on 100% Y classification should be used.

For the next load step in the analysis, assuming it to be sufficiently small that the frame responds elastically, there will be no change in the relative proportions of the

member loads and hence the joint classifications. Therefore, the spring stiffness are still appropriate and no iterations would be required.

With subsequent load steps, as members/joints start and continue to exhibit non-linearity, including member/joint fracture, the relative load proportions and joint classification will change. It therefore becomes possible that the spring stiffnesses assumed at the beginning of the load step are not appropriate to the loads obtained at the end of the step. It is difficult to say whether the resulting inaccuracy is significant at present: only a few joints would be affected and, if the load step is small, by not a large amount. A short study is required to establish whether iterations would be required in the non-linear response regime. Alternatively, it may be possible from the response history to predict the load distribution at the end of the current load step and use this predicted load distribution to predict the joint classifications and hence the appropriate spring stiffnesses for use in the load step. This alternative will probably prove more efficient computationally than carrying out iterations. Nevertheless, in the case of member/joint fracture, very rapid changes in joint classification would result and this may necessitate iterations.

4.3 P/δ Curve for Joints of Mixed Classification

4.3.1 Statement of Problem

In Section 3, Pδ formulations were developed for simple Y, X and K joints. In general, however, multiple-braced joints are subjected to load combinations such that individual braces at a joint are (load) classified as a mixture of the three simple joint types. There is, therefore, a question of how to predict the joint Pδ behaviour for joints having mixed joint classifications from the Pδ behaviour of simple joints (e.g. what is the Pδ response of a K:X = 50:50 classed joint given the K joint and X joint individual responses).

To answer this question with a degree of confidence, recourse to data must be made. Although there are no pertinent steel model data, some FE studies were performed in Phase I on DK joints which are very useful. The studies involved a DK joint (of β = 0.6, various γ, θ = 45 and g/D = 0.15 - to give zero secondary moment effects) that was subjected to the following load combinations:

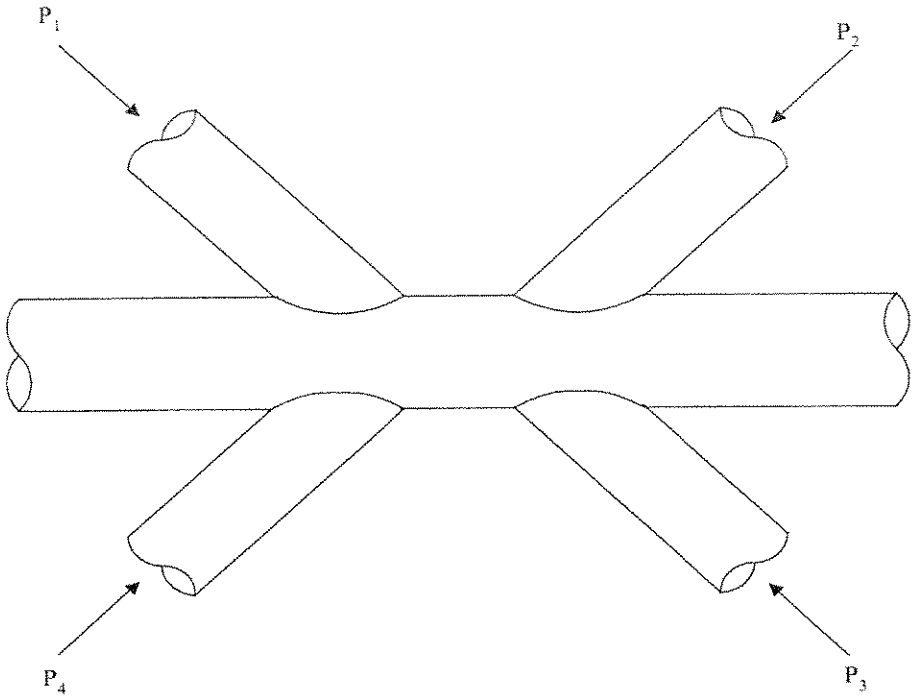

a.	P_1	=	P_3	=	P	
	P_2	=	P_4	=	-P	(i.e. pure K action)
b.	P_1	=	P_3	=	P	
	P_2	=	P_4	=	0	(i.e. pure X action)
c.	P_1	=	P_3	=	P	
	P_2	=	P_4	=	-0.5P	(i.e. 50:50 share of K and X action)
d.	P_1	=	P_3	=	P	
	P_2	=	P_4	=	-0.65P	(i.e. 65:35 share of K and X action)
e.	P_1	=	P_3	=	P	
	P_2	=	P_4	=	-0.85P	(i.e. 85:15 share of K and X action)

The most complete set of results relate to $\gamma = 30$ and the $P\delta$ plots are shown in Figure 4.12. The problem is to simulate the three mixed classed curves from the pure K and pure X action curves.

4.3.2 Possible Approaches

In this subsection, attention is directed towards classifications involving two joint types (K and X, not Y). Furthermore, only the K:X = 50:50 case for mixed classifications is addressed as this clarifies the issues involved. It should be appreciated that there is no obvious a priori reason to favour one of the following

approaches over the others; the acid test is to examine how well each performs against the available data.

Three approaches are discussed here:

(i) Average Force Approach

In this approach the load P is taken as the weighted average (i.e. the simple average for K:X = 50:50) of the loads for K and X joints at the same level of deformation. In the linear elastic region, this approach is identical to taking a weighted average of the initial K and X joint stiffnesses:

$$K_{mixed} = C_K K_K + C_X K_X \quad \text{... 4.3}$$

in which K_{mixed} = initial stiffness of the joint of mixed classification

K_K = initial stiffness of K joint

K_X = initial stiffness of X joint

C_K = proportion of K joint action

C_X = proportion of X joint action

($C_X = C_K = 0.5$ in the present case).

The resulting prediction is compared to the FE data in Figure 4.13. It can be seen that the initial stiffness is not predicted well and that the predicted curve is always necessarily bounded by the K and X curves, this being at variance with the FE curve for the 50:50 case.

(ii) Average Displacement Approach

This approach is similar to the previous one except that a weighted average of the displacements of the K and X joints at the same load is taken. In the linear elastic region, this approach is equivalent to taking a weighted average of the LJFs:

$$K_{mixed} = \left[\frac{C_K}{K_K} + \frac{C_X}{K_X} \right]^{-1} \quad \text{... 4.4}$$

The prediction is compared to the FE data in Figure 4.14. The initial slope of the predicted curve is a fair approximation to that of the FE data but the curve eventually falls away, significantly underestimating the joint capacity. Furthermore, only a limited displacement range can be calculated with this approach.

(iii) Average Coefficients Approach

The K joint curve and X joint curve can both be described by the analytical function:

$$P = d - a(1 - b.\exp(-c\delta))^2 \quad \text{... 4.5}$$

in which there are three independent coefficients a, c and d ($b = 1 + (d/a)^{1/2}$ so that the function passes through the origin). A predicted response can be made from taking weighted averages of the coefficients, viz:

$$a_{mixed} = C_K a_K + C_X a_X$$

$$c_{mixed} = C_K c_K + C_X c_X$$

$$d_{mixed} = C_K d_K + C_X d_X \quad \ldots 4.6$$

in which the subscripts K and X refer to the K and X joints respectively.

The resulting prediction is compared to the FE data in Figure 4.15. Overall, the predicted curve displays the general features of the FE data, e.g. it penetrates the envelope of the pure K and the pure X curves and has a similar peak value. However, the initial stiffness of the predicted curve is too great compared to the FE data.

No doubt other approaches can be proposed and explored but, with the further development described below, the third approach provides a useful basis for estimating the Pδ behaviour of mixed classed joints.

4.3.3 Development of Selected Approach

The average coefficient approach described in the previous subsection has much to recommend it, not least of which is that the same Pδ formulation is used as for singly-classed joints, though of course with adjusted coefficients. One major drawback, however, is that the initial stiffness is too great. It was noted above that the second approach, the average displacement approach, gave an acceptable initial stiffness and use is made of this observation to 'correct' the average coefficient approach.

The initial stiffness implicit in the Pδ formulation (Equation 4.5) can be written:

$$K = 2abc(b - 1) \quad \ldots 4.7$$

The above equation is now modified by the introduction of a new coefficient, ψ, which is the ratio of Equation 4.4 to Equation 4.7 (the latter evaluated with the weighted coefficients in Equation 4.6), to give:

$$K = 2abc(b - 1)\,\psi \quad \ldots 4.8$$

$$\psi = \frac{\text{Equation 4.4}}{2a_{mixed}\, b_{mixed}\, c_{mixed}\, (b_{mixed} - 1)} \quad \ldots 4.9$$

To preserve the form of Equation 4.5, ψ has to be assigned to one of the three coefficients a, b or c in Equation 4.8 and thence in Equation 4.5. Clearly, assignment to either a or c in Equation 4.8 is easier. Physically, the coefficient 'a' controls the degree of the post-peak fall off in load and the coefficient 'c' has a scaling effect on displacements. It was therefore considered more appropriate to assign ψ to the coefficient 'c', i.e.:

$$c^* = \psi\, c_{mixed} \qquad \ldots 4.10$$

where c* is the adjusted coefficient c to use in Equation 4.5.

The resulting predicted curve using the adjusted coefficient c* is compared to the FE data in Figure 4.16. This is much improved compared to the unadjusted curve of Figure 4.15, and the revised curve performs most satisfactorily over almost its entire extent only diverging from the FE data at the end.

One further improvement may therefore be implemented, that is to increase the coefficient 'a' to bring the predicted curve and the FE data closer together at the end. This can be effected by redefining the weighted 'a' as:

$$a_{mixed} = \left(C_K\,(a_K)^2 + C_X\,(a_X)^2\right)^{\frac{1}{2}} \qquad \ldots 4.11$$

The improvement in the predicted curve with this redefined coefficient can be seen by comparing Figures 4.16 and 4.17. Although only a small improvement is indicated, it is at no additional complexity or computational expense and therefore is worth doing.

The above approach was applied to different mixed classifications, and these are shown in Figures 4.18 and 4.19. These show the approach to be robust. It is worth noting that the predicted curve will degenerate to the pure K joint or the pure X joint responses as appropriate.

It is considered that the match of the predicted curves and the FE data in Figures 4.17 to 4.19 is a most excellent result, particularly bearing in mind other approximations elsewhere (e.g. fitting to original, variable, steel data) and that the post peak FE results appears to fall faster than steel model data.

4.3.4 Confirmation of Selected Approach

The above approach has been developed on the basis of mixed K and X action. Following recommendations to the Project Steering Committee, it was considered prudent to check that the approach also works for joints having a degree of Y action. For this purpose, the following joint and load combinations were analysed.

DT joint

β = d/D = 0.67

γ = D/(2T) = 21.4

τ = t/T = 1.0

α = 2L/D = 12.0

D = 406.4 mm

F_y = 358N/mm^2

Load in brace 1	Load in brace 2	Comment
P	P	Pure X action
P	3P/4	X:Y = 75:25
P	P/2	X:Y = 50:50
P	P/4	X:Y = 25:75
P	0	Pure Y action

The geometry of the joint was designed such that true joint failure, as opposed to premature yielding of the chord or the brace, determines the capacity of the joint.

The analyses were conducted using ABAQUS, an industry-accepted general purpose FE program. The mesh used is as indicated in Figure 4.20. Only a quarter model needed to be analysed because of symmetry considerations. The elements were 20-noded solid elements with reduced integration.

The results from the FE analyses are presented, in a non-dimensional format, in Figure 4.21. The parameter δ in this figure relates to the local joint deformation of a single brace and excludes the elastically calculated brace contraction and any deflection due to chord bending. The FE results were further analysed, and predictions made, as follows:

- All Pδ curves were extracted.
- Curve fitting was carried out for the 100%X and 100%Y cases to establish the base coefficients, see Figure 4.22.
- The coefficients for mixed class joints were predicted using the methodology set out in Section 4.3.3.
- Create comparative plots of the FE data and predicted responses for the mixed class joints, Figures 4.23 to 4.25.

An inspection of Figures 4.23 to 4.25 reveals that the initial slopes and the general shapes of the Pδ curves have been well predicted. There is a tendency for the predicted peak load to lie slightly below the FE data for the mixed class joints. It can be seen in Figure 4.21 that even when the joint classification has X action as high as 50%, little reduction in capacity from the Y joint strength occurs. It is this aspect of behaviour which leads to relatively low predicted strengths for the mixed class joints. It does not indicate a fundamental shortcoming in the approach for establishing mixed class Pδ curves. Furthermore, the discrepancies are considered to be of only a minor nature (10% difference on load at worst).

The above analyses have confirmed that the methodology developed in section 4.3.3 for establishing the Pδ response of a joint having mixed K and X actions can also be applied to joints having mixed X and Y actions. A key assumption made during the development of the methodology is that the K and X 'springs' (representing joint flexibilities) act as though they were in series. The work presented in this subsection confirms that the 'Y' spring also acts in series, and therefore the methodology is robust for joints under any combination of K, X and Y action.

4.4 Concluding Remarks

The studies reported in this Section 4 have clarified the issues with respect to the role of joint classification on the conduct of frame analysis. All perceived difficulties have been addressed and satisfactorily resolved.

The main findings are that:

- Joint stiffness plays an important role in analysis, from a static, dynamic or fatigue point of view.
- At the outset of an analysis, iterations will be required to ensure appropriate spring stiffnesses are used. The initial stiffnesses, before iteration, should be assumed as those relating to Y joints.
- It is possible to derive, in a robust manner, the complete load-deformation response for a joint subjected to loads of mixed classification (various degrees of K, X and Y action) from the responses of similar joints under singly-classed loads.

The methodology for dealing with joints having mixed classification, as set out in Section 4.3, has been applied to the non-dimensional forms of the Pδ equations. The resulting formulations are set out in detail in Appendix A, and these also include the adjustments discussed in Section 3.

5. DEVELOPMENT OF COUPLED Pδ-Mθ FORMULATION

5.1 General

This Section describes the work performed by SINTEF in the evaluation of five approaches for modelling joint behaviour:

(i) Pδ springs

(ii) Yield surface plasticity formulation

(iii) Fibre modelling

(iv) General finite element modelling

(v) Modelling based on elastic shell theory.

The general FE modelling approach is included for the sake of completeness as is the approach based on shell theory. The latter formulation has been developed at NTH/SINTEF for elastic analysis but could be enhanced to take account of plastic behaviour.

The evaluation of each of the above five approaches has been made against a list of various criteria. This allows for a rational comparison between the approaches as summarised in Section 5.7.

For the first three approaches listed above, joint behaviour is modelled in the frame analysis by introducing additional two-node elements between the original chord centre node and new nodes at the chord surface (Figure 5.1). The properties of these 'joint elements' are determined by the Pδ and Mθ formulations with suitable adjustments to account for brace load interaction effects.

5.2 Pδ Springs

Generality of Application	Can only be applied to the joint configurations covered by the original database.
Joint Classification	The formulation itself does not recognise joint geometries or joint force classification. Joint classification has to be done external to the joint formulation.
Numerical Calibration	The Pδ springs are based on extensive screening of available data, and careful calibration to make the curves fit the data. No additional calibration is required to get an accurate representation within a joint module.
Single Brace Loading	Again, the Pδ springs can be carefully calibrated to available data, and can give a good representation of single brace loading.

Brace Load Interaction	To represent brace load interaction by means of Pδ springs, separate formulae have to be developed for different interaction scenarios. This is deemed to be very time consuming, and may not in the end lead to a very general formulation.
Chord Load Effects	Chord load effects have already been assessed, and appropriate modifications to the Pδ curves developed.
Failure Modes	A fracture/failure criterion can be defined as a function of deformation or rotation, and a subsequent unloading slope or de-coupling mechanism introduced. However, the failure criterion cannot be formulated in terms of maximum strains, and the formulation is not suited to represent gradual "un-zipping" of the joint.
Data Input Requirements	Joint geometry and joint classification.
Numerical Stability	Pδ springs are numerically very robust in the uncoupled cases. For interaction situations the stability of the formulation is uncertain (transition from curve to curve as the load path changes).
Ease of Coding	Easy to implement once all required Pδ curves are available.

5.3 Yield Surface Plasticity Formulation

Generality of Application	Same as the Pδ springs, but offers easy generalisation to additional load cases (e.g. brace load interaction).
Joint Classification	Same as for Pδ springs: the formulation itself does not recognise joint geometries or joint force classification. Joint classification has to be done external to the joint formulation.
Numerical Calibration	The plasticity parameters can be calculated directly from the Pδ curves. No additional calibration is required.
Single Brace Loading	Same accuracy as the Pδ springs (see below).

Brace Load Interaction	Better than the Pδ springs: Brace load interaction is captured by plastic interaction curves (e.g. the API capacity formula or the HSE capacity formula), describing the interaction between the single brace loading degrees of freedom.
Chord Load Effects	Same accuracy as the Pδ springs.
Failure Modes	Same as for Pδ springs: a fracture/failure criterion can be defined as function of deformation or rotation, and a subsequent unloading slope or de-coupling mechanism introduced. However, the failure criterion cannot be formulated in terms of maximum strains, and the formulation is not suited to represent gradual "un-zipping" of the joint.
Data Input Requirements	Joint geometry and joint classification, interaction formula.
Numerical Stability	The plasticity formulation is less robust than the Pδ springs in the uncoupled case. Some interaction formulae have singular points at the vertices of the curve, and special procedures are required to traverse these singularities. The formulation should however be good enough for all practical purposes.
Ease of Coding	Easy to implement once the uncoupled Pδ curves are available.

Preliminary studies with plasticity model

Figures 5.2 and 5.3 show the Pδ curves generated according to MSL's equations, and the resulting behaviour from a plasticity formulation. The left-hand curve is the original Pδ curve. This curve is used as input to the plasticity formulation, and plasticity parameters are calculated directly from the curve. The resulting plasticity parameters are then assigned to an element in USFOS, and the element loaded in axial compression and bending. The resulting force/deformation curves are shown with the three right-hand curves.

The results from the plasticity formulation are shifted along the x-axis to make it possible to distinguish the individual curves. The simulations are done with different step sizes to assess the numerical stability of the formulation. In the present simulations, the step size has no influence on the accuracy obtained with the plasticity model.

The simulations apply to a T joint with D/T=508/20 mm, d/t=203/10 mm and f_y=350 MPa.

These results are obtained from a simpler plasticity formulation than the one eventually used for the joint modelling (un-coupled degrees of freedom, implemented for a one-node finite element).

To illustrate the ability to model brace load interaction, the existing general plasticity model in USFOS (for beam-columns) is used. This model cannot trace individual Pδ or Mθ curves. Instead, the plasticity parameters have been calibrated to give an approximate fit to the MSL curves, see Figures 5.4a and 5.4b. These parameters are then used to analyse a T-joint loaded in tension and out-of-plane bending ($\beta = 0.4$, $\tau = 0.5$, $\gamma = 12.7$). Two beam elements are used to represent the chord, one beam element to represent the brace, and one element with nodal behaviour according to the plasticity model.

The chord ends are fixed, and the brace end is loaded by a transverse force. This produces out-of-plane bending in the joint, initially. But as the transverse displacement increases, the load is carried more and more by membrane forces in the brace. Hence, joint loads are redistributed from high out-of-plane bending (and low tension load) to high tension (and small out-of-plane bending moment). Figure 5.4c illustrates the load versus deflection of the brace end. The membrane force effect is clearly observed. The analysis results corresponds well to a detailed shell FE analysis[5.1]. Figure 5.4d shows the redistribution of forces in the joint, from initial loading in opb to a loading state dominated by axial force. Clearly, it is a very non-proportional history. The development of bending moment and axial tension are plotted in Figures 5.4e and 5.4f, respectively, as a function the brace end deformations.

This preliminary study demonstrates that brace load interaction can be taken into account by a plasticity model.

5.4 Fibre Modelling

Generality of Application	Same as the Pδ springs, and can be generalised to additional load cases (e.g. brace load interaction).
Joint Classification	Same as for Pδ springs and plasticity formulation: the formulation itself does not recognise joint geometries or joint force classification. Joint classification has to be done external to the joint formulation.
Numerical Calibration	Requires one additional step of numeric calibration compared to the Pδ springs and the plasticity model: the fibre model requires σ-ε curves for each fibre. These curves must be calibrated from the original Pδ curves, and calibrated such that the integrated effect of the σ-ε curves produces the required Pδ and Mθ behaviour.

Single Brace Loading	Once a proper calibration is achieved, the fibre model should give the same accuracy as the Pδ springs and the plasticity model.
Brace Load Interaction	Not as general as the plasticity formulation: once the σ-ε curves are calibrated to produce the required Pδ and Mθ behaviour, the interaction behaviour is fixed. As the fibres all are connected by the "rigid" footprint of the joint, the combined axial deformation and rotation of the joint will give deformations in the individual fibres that do not comply with the original calibration for single brace loading. An alternative model might be envisaged where fibres calibrated to carry axial load could be uncoupled from fibres calibrated to carry bending moment. However, as the axial load capacity is affected by bending moment, and vice versa, the ultimate capacity for each load component then has to be reduced according to some interaction rule.
Chord Load Effects	Same accuracy as the Pδ springs and plasticity formulation.
Failure Modes	Better than the Pδ springs and plasticity formulation: a fracture/failure criterion can be formulated in terms of maximum strains, and the formulation can represent gradual "un-zipping" of the joint to a certain extent.
Data Input Requirements	Joint geometry and joint classification.
Numerical Stability	Numerically quite robust: better than the plasticity formulation, but not as good as the Pδ springs.
Ease of Coding	Easy to implement once the required σ-ε curves are calibrated.

5.5 General Finite Element formulation

Generality of Application	Can be applied to all joint configurations.
Joint Classification	Recognises joint geometries and joint force paths (ie. no need to classify).

Numerical Calibration	None, assuming a suitable modelling methodology is available.
Single Brace Loading	Implicitly accounted for.
Brace Load Interaction	Implicitly accounted for.
Chord Load Effects	Implicitly accounted for.
Failure Modes	A fracture / failure criterion can be formulated in terms of maximum strains, and fracture / "un-zipping" of the joint can in principle be modelled. However, this is a demanding task, and is usually not done.
Data Input Requirements	Extensive: full FE model of the joint.
Numerical Stability	Usually quite robust.
Ease of Coding	Not Applicable.

5.6 Elastic Shell Theory

Generality of Application	Can be applied to most joint geometries. ($\beta < 0.95$ and $\theta > 25$ deg.) Covers single brace and multi brace joints, uni-planar and multi-planar. It also includes brace-to-brace interaction effects.
Joint Classification	Recognises joint geometries and joint force paths (ie. no need to classify).
Numerical Calibration	None.
Single Brace Loading	OK (elastic flexibility).
Brace Load Interaction	OK (elastic flexibility). Also includes brace-to-brace interaction.
Chord Load Effects	Not included.
Failure Modes	N.A.
Data Input Requirements	Joint geometry, only.
Numerical Stability	Robust.

Ease of Coding Already implemented for elastic behaviour.

Further details of this approach is given by Holmås (5.2) and Hellan (5.3).

5.7 Summary

This Section gives an overall comparison of the different joint algorithms. Five modelling approaches have been discussed in the context of various criteria. The performance of each approach against these criteria are summarised in a qualitative manner in the table below.

Pδ springs, yield hinge plasticity formulations and fibre models all seem to satisfy the functionality requirements of a generic joint module. Pδ springs and a plasticity formulation would be able to use the generated Pδ and Mθ curves directly; a fibre model would require back-calculation and calibration of individual σ-ε curves to represent the integrated Pδ curves. A plasticity formulation would seem better suited to model brace load interaction effects, whereas a fibre model would give better representation of joint cracking and fracture. Overall, it is felt that a plasticity formulation would be better suited for further development and implementation, due to the direct representation of the generated Pδ and Mθ curves, and the greater versatility in the modelling of brace load interaction effects.

The development and the theoretical basis of the plasticity formulation is described in Appendix B.

Overview of Joint Modelling Approaches

	Pδ springs	Plasticity form.	Fibre model	General FE	Elastic shell theory
Generality of application	0	0	0	+	+
Joint classification	0	0	0	+	+
Numerical calibration*)	+	+	0	+	+
Single brace loading	+	+	+	+	+
Brace load interaction*)	0	+	0	+	+
Chord load effects	+	+	+	+	N.A.
Failure modes	0	0	+	0	N.A.
Data input requirements	+	+	+	-	+
Numerical stability	0	0	+	+	+
Ease of coding	+	+	0	+	+

*) Items receiving particular emphasis

Key: + = good rating, 0 = average rating, - = poor rating

6. FRACTURE CRITERIA FOR JOINTS IN TENSION

6.1 Introduction

The work reported in this Section concerns the studies carried out to develop ductility (fracture) criteria for tension loaded joints. The work was undertaken as part of Work Package TJA-5 (new data generation) and builds upon the Phase I studies into deformation limits for tension loaded T and DT joints.

In Phase I of the project, axial deformation limits were investigated and this resulted in the following equations:

For T joints: $$\frac{\delta_{lim}}{D} = 0.21\beta \quad \ldots 6.1$$

For DT joints: $$\frac{\delta_{lim}}{D} = 0.13 - 0.11\beta \quad \ldots 6.2$$

An inspection of these equations reveals that the limiting deformation is a function of β, but with differences even with regard to the sign of the slope for the two joint types. The equations however do not address deformation limits for K joints or joints with mixed classification.

During the passage of Hurricane Andrew, a number of GoM platforms suffered damage and, in some instances, K joints failed by chord shear in the gap region[6.1]. This observation indicates that K joints, too, require some ductility criterion which is perhaps not surprising considering that one of the braces would normally be subject to applied tension. No such criterion was developed in Phase I. Indeed, tests have not indicated this mode of failure, possibly because deformations have always been lower than limiting values or because of different boundary conditions used in test specimens compared to K joints within frames. Nevertheless, some criterion needs to be developed for K joints.

Following recommendations made by MSL, it was agreed by the Project Steering Committee that ductility limits should be studied further and that finite element analysis should be undertaken.

6.2 Methodology

6.2.1 General

It has been recognised that ductility criteria are best developed with reference to steel data, and that there is some risk in attempting to use FE data for these purposes. There is no industry-wide accepted methodology for using FE data to address deformation limits for joints in tension, although a limiting plastic strain value is often used as a criterion to obtain the limiting capacities of joints made of an isotropic, ductile steel. It was therefore initially proposed that whatever approach was selected, the criterion should be calibrated against the FE analyses at the deformation limits given by the Equations 6.1 and 6.2. However, as discussed in Section 6.3.2, it was found necessary to amend the T/Y joint deformation limit.

Equations 6.1 and 6.2 intersect at a β ratio of 0.4. It was decided that T and DT joints having $\beta = 0.4$ should be analysed to develop a consistent criterion for T and DT joints and which therefore hopefully applies to K joints as well. To enable a robust criterion to be developed, at least one other β value needs to be encompassed and a value of $\beta = 0.8$ was selected.

A single FE analysis of a K joint with $\beta = 0.4$ was undertaken to provide some data for comparison.

6.2.2 FE Modelling and Analysis of Joints

The analyses were carried out using the non-linear general-purpose ABAQUS FE program. The analyses were executed by means of 20 node brick elements with reduced integration (C3D20R). The use of reduced integration elements overcomes the problem of overestimating strength caused by incompressibility of brick elements with full integration. Since the reduced integration brick element uses only two Gauss integration points through the thickness, two layers of elements were used through the thickness of the chord for $\beta = 0.4$ joints, because of significant local bending of the chord wall. For $\beta = 0.8$ joints, only one layer of elements through the chord thickness was used, as much of the load transfer at the brace-chord intersection is by membrane action. A sample FE analysis for a $\beta = 0.8$ DT joint using two elements through the chord wall produced the same load deformation curve as that using one element through the thickness. For all analyses only a single layer of elements was used in the brace.

Both geometric and material non-linearities were included in the analyses. The plasticity of the material was followed using the von-Mises criterion. The joint material used for the analyses was assumed to have a yield strength of 350 MPa with no hardening, an elastic modulus of 2×10^5 MPa and a Poisson's ratio of 0.3. Although actual material properties used for fabricating offshore structures show hardening beyond first yield, analyses (eg. Reference 6.2) show that the difference between the load deformation patterns obtained with perfectly elastic-plastic and hardening material properties are small. Beyond the first peak load, where material non-linearities could lead to an unstable equilibrium path, the RIKS algorithm was used to trace the complete load-deformation history.

For the axially loaded T and DT joints, uniformly distributed loads were applied at the ends of the brace. For the K joint, a concentrated load was applied to the braces, via thick end plates. In all cases, symmetry was employed to reduce the size of the models. Weld modelling was ignored since a previous parametric study[6.3] on axially loaded T joints had shown good correlation between experimental and numerical results ignoring the welds. In all models, the chords had stiff end plates, which were suitably restrained to simulate the end conditions. The end plates were modelled by means of thick shell elements (S8R), using the multi-point constraint facility available in ABAQUS to enforce compatibility between the different degrees of freedom between brick and shell elements.

6.2.3 Presentation of Figures

A number of figures are presented in the following Sections which share some common terms. For convenience these are defined here:

- Non-dimensional (N.D.) load $= \dfrac{P \sin\theta}{F_y T^2}$
- Non-dimensional (N.D.) deformation $= \delta / D$
- First crack load is the mean load at which cracking was first observed in tests.
- Ultimate load is the mean load used to define capacity equations, and is generally based on the load at the Yura deformation limit.
- Limiting δ/D (or δ_{lim} / D) is when separation of the brace from the chord, or when chord shear failure in K joints, occurs. It represents the end point for predicted $P\delta$ curves.

6.3 Analyses of T and DT Joints Under Tension

6.3.1 Description of Joint Parameters and Selection of Fracture Criteria

Analyses have been carried out for T and DT joints with $\beta = 0.4$ and 0.8, to examine the suitability of a limiting plastic strain value or other criterion. A γ value of 25 was used for the joints. The chord had an outer diameter of 1020.4 mm with a chord wall thickness of 20.4 mm. The chord lengths were chosen to have an α value of about 16 for all joints. This value of α was chosen to prevent the possibility of chord length effects affecting the joint response. These joints have a τ value of 0.81. The boundary conditions applied to the FE models were designed to reduce the chord moment. All rotational degrees of freedom were restrained at the centre of the end plate, with the chord free to translate along its length. Finite element meshes are shown in Figures 6.1 to 6.4.

Three failure parameters were identified at the commencement of these studies that may form a suitable criterion to define a deformation limit. These are:

- Limiting plastic strain
- Plastic work done in the joint
- Maximum principal strain.

6.3.2 Discussion of Results

6.3.2.1 Load deformation characteristics

Figures 6.5 to 6.8 show the load-displacement curves obtained from the analyses as they compare with the predicted load deformation curves using the formulations in Section 3. These figures also contain the predicted joint capacities according to the equations obtained from Phase I. It can be seen that for the $\beta = 0.4$ joints (Figures

6.5 and 6.6), there is excellent agreement in the initial joint stiffness obtained from the FE analyses and the predicted joint stiffness. There is also very good agreement in terms of overall response. However, for the $\beta = 0.8$ joints, the FE results show apparently stiffer response, when compared to the predicted joint response. In developing the formulation for predicting the Pδ curves of DT/X joints in tension in Phase I of this project, most of the DT joints were low and medium β joints, with a few at $\beta = 1.0$ and having low to medium γ. Thus, there is likely to be a bias in the parameters used for obtaining the Pδ curves, with a tendency towards more accurate prediction for low and medium β joints. However, there is fair agreement between the FE analyses and predicted responses overall for the $\beta = 0.8$ joints.

In Figure 6.7, the $\beta = 0.8$ T joint exhibits unloading behaviour before the predicted peak load. This observation from the FE analysis was found to be contrary to the reported Pδ plots reported in the literature for T joints of similar joint parameters. The FE element analysis revealed that this loss in load carrying capacity was due to local buckling of the chord wall in compression around the brace-chord intersection (Figure 6.9). This prompted a review of the original literature containing the joints with high β. A critical re-appraisal of the source references revealed that deformations that were recorded as joint deformations actually included chord bending deformations. (Whereas figures in the source references would suggest chord bending was excluded, the texts describing measuring techniques indicates that some chord bending would have been picked up.) Further examination of these joints also showed that at the ultimate load values obtained from the tests, the chord plastic moment capacity would have been severely exceeded. The joints were apparently reported as having failed by chord bending yield or chord shell bending yielding, although the reported load-deformation curves did not show the apparent loss in strength usually associated with local buckling. An estimate of the plastic moment capacity of the $\beta = 0.8$ T joint used in the present FE studies assuming fixed boundary restraints, showed that the joint will exceed its plastic moment capacity at a non-dimensional load (Q_u) of 49. This is consistent with the FE result which shows local buckling of the chord shell below the predicted ultimate load capacity (see Figure 6.7). This finding with respect to the $\beta = 0.8$ T joint threw into doubt the validity of the T joint limiting δ/D equation (based on previous experimental results) for predicting the deformation limit of tension loaded T joints. The implication of this is discussed further in Section 6.5.

6.3.2.2 Calculated strain values

One of the objectives of these studies was to examine the possibility of using the plastic strain limit as an appropriate criterion for determining the deformation limits of joints loaded in tension. While it is recognised that the magnitude of the strains are influenced by the degree of mesh refinement and local notch effects at the weld toe which are not accounted for in the FE model, nevertheless by making comparisons at the same locations under the same loading regimes for different joint types, the relative influence of the joint types can be seen.

Figures 6.10 and Figure 6.11 respectively show the variation of the equivalent plastic strain and maximum principal strain values (tensile) in the saddle region obtained from the FE analyses, against the non-dimensional joint deformations.

There is an almost linear relationship between the strain and the non-dimensional deformation, before chord plastification becomes pronounced. It is evident from the figures that at the proposed deformation limit for T and DT joints with $\beta = 0.4$, the magnitude of the strains for the T joint is about 70 % greater than that of the corresponding DT joint (also see Table 6.1).

Figures 6.12 to 6.15 show the load versus equivalent plastic and maximum principal strains at the chord saddle region. It can be observed from the figures that the equivalent plastic strains and maximum principal strains are of about the same magnitude. This is to be expected as the strains in this region are dominated by hoop and chord axial strains. The loads at first crack and at ultimate as inferred from Phase I are also shown in the figures. A summary of the strains corresponding to the first crack and predicted ultimate loads are contained in Table 6.1. The FE results tend to indicate that cracking would occur at an equivalent plastic strain of about 5 - 8 % for the DT joints and for the T joint at $\beta = 0.8$. However for the T joint with $\beta = 0.4$, predicted first crack load occurs at a strain of about 14%. It is possible that residual stresses from the welding and fabrication processes, and local notch effects could play a significant role in the crack initiation of test joints.

Figures 6.12 to 6.15 clearly show that for the same β, cracking occurs in the T joint at a load about 50 % greater than the equivalent DT joint. This ratio is about the same as the ratio of the strains at which failure occurs (Table 6.1). However, these values of predicted cracking strains are well below the values of strains measured at which tensile test coupons show necking.

6.3.2.3 Plastic work done in joints

The plastic work done in the joints was also examined as a possible criterion for establishing a deformation limit. Figure 6.16 shows the variation of the plastic work done with the non-dimensional deformation further normalised with respect to the proposed deformation limit (Equation 6.1 or 6.2 as applicable). The figure shows that apart from the $\beta = 0.8$ T joint which exhibited local buckling of the chord wall, the plastic work done in the joints up to the proposed deformation limits are of about the same magnitude. The slight discrepancy between these calculated values of plastic work may be attributed to the fact that the proposed deformation limits are based on an empirical formula derived from test results.

6.3.2.4 Summary

It is concluded that a limiting strain value is not an appropriate criterion for establishing a ductility/fracture criteria for tension loaded joints of dissimilar geometry. The calculated plastic work done obtained from the FE element analyses may form a better basis for the establishment of failure/ductility limit for tension loaded joints.

In addition, the finding that some of the data used for establishing the Phase I deformation limits for T joints under tension loading contained test specimens which failed due to severe chord wall plastification, means that a new ductility/fracture criteria needs to be developed for tension loaded T/Y joints. This is discussed in Section 6.5.1.2.

6.4 Analysis of K Joints Under Balanced Axial Loading

6.4.1 General

In Phase I of the project, no ductility/fracture criteria was developed for K joints under axial loads. Nevertheless, a ductility/fracture criterion needs to be developed for K joints.

A review of Figures 6.5 to 6.8 for the T and DT joints, showed that at the predicted ultimate loads using the equations obtained from Phase I of the project, the non-dimensional deformation of the joint was generally about 0.03 (except for the β = 0.8 T joint which failed by local chord wall buckling). Although the FE analyses results for the T and DT joints had shown that the strain values are not reasonably constant for T and DT joints for the range of β selected, there was an indication that the plastic work done may serve as an alternative criterion to define a suitable deformation limit.

A single FE analysis of a K joint (β = 0.4, γ =15, τ = 0.81, θ = 60°) under balanced axial load was therefore undertaken. This was intended:

- To see if the amount of plastic work done as obtained from the T and DT joints can be applied to K joints.
- To provide additional data for calibration of the simplified design model that will be developed for K joints.
- To see where the Yura deformation limit lies with respect to K joints.

6.4.2 Boundary Conditions

For K joints, the test boundary conditions are many and varied in open literature. Previous work and subsequent analyses [6.4] have shown that the test boundary restraints can strongly influence the capacity and mode of failure. Tests of K joints have 'typical' conditions of chord support with one end free. Loads are frequently applied to one brace, with the other brace supported to put it tension. These boundary conditions are deemed to be unable to replicate the shearing action across the gap region as the braces act in opposition on the chord, to replicate the kind of failure mode observed in some high β K joints as noted during the passage of Hurricane Andrew.

A test has been carried out for a K joint (β = 1.0, g/D = 0.1) under the boundary conditions identical to that shown in Figure 6.17 (a) and the results compared with that of a test of a K-braced frame [6.4]. Evidence from the test programme showed the physical response to be limited by cracking in the gap region. Similar FE studies [6.5] have also confirmed the sensitivity of K joint responses to the support conditions. In particular for K joints, it has been shown to be important to provide support to both chord ends and to load both braces in opposition if the conditions at the joint in the frame are to be accurately replicated.

In order therefore to account for all likely modes of failure in a K joint, the joint was analysed using the matrix of boundary conditions shown in Figure 6.17 (a - e). A typical finite element mesh is shown in Figure 6.18.

6.4.3 Discussion of Results

Figure 6.19 shows the load-deformation plots for the tension and compression braces of the K joints analysed. It can be observed from the figure that there is no noticeable difference in the compression Pδ curves in the pre-peak loading regime, and very minor differences in the post-peak regime. A common feature of the Pδ curves is that there is a reduction in compressive strength after the first peak load and then a subsequent increase in load.

With reference to the displacements at the tension intersection, an enlarged scale is shown in Figure 6.20, it can be seen that the initial stretching is apparently reversed at high loads. This is a result of the deformation of the chord due to the interaction between the tension and compression braces. In particular, the results of the analyses using Models 1, 2 and 3, show that the tension brace may exhibit significant reversal of displacement after the peak load of the joint has been attained. However Models with loads applied only to the compression brace and both braces supported are not able to capture this behaviour. It can also be observed that Model 5 produces a slightly stiffer response in the tension brace. These differences in responses support the need for loads to be applied to both braces, if the conditions at a joint in a frame are to be accurately simulated. Besides these differences, there is in general a similarity in the overall behaviour of the models.

The Yura deformation limit of about 0.04 D, when applied to the compression brace, occurs in the K joints beyond the joint first peak load. This deformation limit generally corresponds to a maximum strain in the gap region of about 30% (Figure 6.21). Although this value of strain is less than observed fracture strain of about 40% for tensile coupons, it would be reasonable to infer that cracking may have occurred on the basis of T and DT joint behaviour, see Table 6.1. However, there may still be some residual deformation capacity. Indeed, test results of individual K joints suggests that cracking occurs in the load minima following peak loads, corresponding to a N.D. deformation of about 0.05 to 0.08 for the compression brace.

The results from the analyses of the T and DT joints have shown that the plastic work done per unit chord area is reasonably constant at the proposed deformation limits (Equations 6.1 and 6.2), except for the β =0.8 T joint. It is therefore of interest to see how the plastic work done in the K joint varies with the joint deformation. Figure 6.22 shows the variation of the plastic work (per chord area) done in the K joints with the compression brace non-dimensional deformation as compared to T and DT joints of β = 0.4. It is apparent from the figure that the plastic work done is practically the same for the K joints using Models 1, 2 and 3, which is also in agreement with the observation of identical Pδ curves obtained from the FE analyses for the three boundary constraints considered. Figure 6.22 tends to suggest that at a deformation of about 0.08 in the compression brace, the plastic work done in the K joint is about the same as for the T and DT joints. It is

interesting to note that this deformation is in close agreement with the proposed deformation limit (0.084) for $\beta = 0.4$ T and DT joints. A further examination of Figure 6.19 indicates that this value of deformation corresponds to the point of joint stiffening beyond the initial drop in load following the first peak load. It may therefore be conjectured that this value of limiting deformation in the compression brace may provide an appropriate point for establishing a deformation limit for K joints.

At a deformation of 0.08, the maximum equivalent principal strain in the gap region (chord crown) is about 55% (Figure 6.21). Although this absolute value of strain should be treated with caution since the joint is well past its peak load, which occurs at a strain of about 15% (Figure 6.23), and greater than the 40% maximum elongation of coupons of steel under uniaxial tension, this value compares very well with maximum plastic strain value obtained in the chord saddle region for the $\beta = 0.4$ T joint at its deformation limit. Figure 6.24 shows the contour plot of the equivalent plastic strains in the joint corresponding to the last load steps shown in Figures 6.19 and 6.20. The concentration of strain in the vicinity of the gap region between the tensile and compression braces reflects the likelihood of cracking of the chord wall at this location. However, because of the lack of a tensile failure criterion in FE models, it is impossible to say whether subsequent joint failure will be by brace pull-out or chord shear in the gap region.

For K joints, results of tests and the experience from Hurricane Andrew have shown that gapped K joints can fail either by tension brace pull-out or chord shear in the gap region. The deformation plots obtained from these analyses for a $\beta = 0.4$ gapped K joint are quite different from those obtained from a previous FE and test study for $\beta = 1.0$, $g/D = 0.1$ [6.4], in which failure occurred by tearing of the chord wall, due to the shearing action in the chord along the plane of the compression brace. The K joints that also failed by shearing action in the chord wall during the passage of Hurricane Andrew were generally $\beta = 1.0$ K joints, and the failure modes were similar to that observed in tests described in Reference 6.4. Thus while the present study reveals the tendency for cracking of the chord wall in the gap region, the lack of an appropriate tensile failure criterion makes it impossible to determine whether ultimate failure will finally occur by brace pull-out or chord shear. The present FE study however confirms that for gapped K joints, the post-peak response and final failure will be determined by an initial crack in the joint in the gapped region near the tension brace footprint. The isolated test conditions do not restrain the joint sufficiently for these high strains to develop, hence failure of K joints has been mainly ascribed to severe chord wall deformations at the compression brace intersection.

6.5 Development of Ductility/Failure Criteria

6.5.1 Deformation limits

6.5.1.1 DT/X joints

Of all the joint types, the deformation limit for DT joints is considered to be the most robust. This is because there is relatively a large amount of data which indicate a consistent trend. The mean equation, derived in Phase I of the project, is given by:

$$\frac{\delta_{X,m}}{D} = 0.13 - 0.11\beta \qquad \ldots 6.3$$

This relationship is shown with measured data in Figure 6.25. A characteristic line is also identified on the figure and its equation is:

$$\frac{\delta_{X,ch}}{D} = 0.089 - 0.075\beta \qquad \ldots 6.4$$

6.5.1.2 T/Y joints

It was highlighted in Section 6.3.2.1 that as a result of the analyses carried out in this study, it was found that some of the joints that were included in the data for deriving the empirical formula for tension-loaded T joints in Phase I of this study were actually invalid. These were high β joints (β greater than 0.7). These joints had apparently failed by chord wall yielding or chord shell bending (local buckling), and the values that were quoted as joint deformation actually included some chord bending deformation. The inclusion of these data points led to the apparent increase of limiting deformation with β. It was therefore concluded that for an accurate deformation limit for T joints, these data points at high β should be eliminated. Figure 6.26 shows the distribution of the remaining data points with β, with two data points relating to K joints discussed below.

The T/Y joint data show considerable scatter, with no well-defined trend. Because chord bending failure and associated bending deformation will generally occur before rupture for high β T joints, it is not too important to obtain great accuracy in predicting limiting deformations for such joints. It was decided to base the prediction equation on a constant value. The selected mean and characteristic equations therefore respectively become:

$$\frac{\delta_{Y,m}}{D} = 0.076 \qquad \ldots 6.5$$

$$\frac{\delta_{Y,ch}}{D} = 0.044 \qquad \ldots 6.6$$

The characteristic equation above takes into account the number of data points in the sample.

6.5.1.3K joints

The FE analyses discussed in the last section suggests that fracture might occur when the deformation in the compression brace is about $\delta/D = 0.8$, ie. in the dip following peak load in that brace. The specification of a deformation limit for K joints, however, should ideally apply to the tension brace and not to the compression brace. On a pragmatic level, this is because the development of the joint algorithm in this project has proceeded along the lines of describing joint behaviour on a brace-by-brace basis. It would be awkward indeed to introduce a tensile brace failure criterion based on compressive brace behaviour.

When the deformation in the compressive brace is $\delta/D = 0.8$, the FE tension brace results indicate little deformation and in fact are undergoing a reversal, see Figure 6.19. This does not agree with observed K joint behaviour in frames, where no such reversal takes place. It was therefore decided to examine the experimental evidence to establish a tension brace ductility criterion.

Only two experimental data points are available to this project and these have been extracted from References 6.4 and 6.6. Both points relate to high β values, as shown in Figure 6.26. The mean equation has been taken as the simple average of the two points:

$$\frac{\delta_{K,m}}{D} = 0.026 \qquad \ldots 6.7$$

Other, confidential, data for a further two K joints supports the above mean equation. It will be observed that the K joint deformation limit is about 70% of that for Y joints. It is to be expected that the K joint limit should be lower than the Y joint limit because of the additional restraint offered by the compression brace. A valid argument can be made that the K joint limit should converge to the Y joint limit for large gaps (when the K joint behaves as two independent Y joints). In other words, the K joints limit should properly be a function of the gap parameter. However, there are clearly insufficient data to pursue this further.

There are insufficient data, too, for establishing a K joint characteristic limit. It is therefore assumed that the characteristic bias pertaining to T/Y joints also applies to K joints. On this basis the characteristic K joint equation is:

$$\frac{\delta_{K,ch}}{D} = 0.015 \qquad \ldots 6.8$$

6.5.1.4Joints having mixed classification

For tension loaded joints with mixed classification (i.e. with proportion of Y, X and K action), there is no available analytical or experimental data to obtain a deformation limit. A predicted deformation limit has been formulated based on a simplified linear interpolation based on the formulations for T/Y, K and DT/X joints. The equation is of the form:

$$\delta/D = (k\,\delta_k + y\,\delta_y + x\,\delta_x) / D \qquad \ldots 6.9$$

where k, y, x are the proportions of K,Y and X action in the brace, respectively (note $k + y + x = 1.0$)

$\delta_k, \delta_y, \delta_x$ are the limiting values obtained from Equations 6.3 to 6.8, using the mean or characteristic values as appropriate.

D is the chord diameter.

Figure 6.27 shows a combined plot of deformations for T/Y, K and DT joints, and the respective lines representing the predicted deformation limits. The proximity of the prediction lines for T/Y, K and DT joints would indicate that any error that may result from using the linear interpolation proposed above for joints with mixed classification would be minimal.

6.5.2 Failure mode of gapped K joints

It was noted above (Section 6.4.3) that K joints in an actual frame condition may fail either by brace pull-out or by shearing action of the chord in the gap region. It is reasonable to expect that at low β, K joints will be more likely to fail by brace pull-out rather than chord shear failure. With increasing β, the propensity may be towards chord shear failure, with brace pull-out becoming increasingly less likely. But, there is no indication as to the likely value of β at which this change-over in failure mode occurs.

Although tests are normally carried out for balance axial loading, in a real Offshore Jacket structure, there is more likely to mixed K and Y-actions. As the degree of K-action increases, shearing should increase in the gap region due to the opposing action of the brace loads, leading to failure precipitated by rupture of the chord. As the percentage of Y action increases, whilst K-action decreases, brace pull-out may become more onerous than shear of the chord. However, irrespective of the degree of K or Y-action, the propensity for either mode of failure will be dependent on the β value of the joint.

In order to establish the limits of β and degree of K-action at which either brace pull-out or chord shear failure would occur, recourse was made to engineering mechanics principles. A parametric study was carried out to establish the limits of β and the degree of K and Y action for a low gapped K joint ($g/D = 0.1$). In estimating the transverse shear through the chord and the brace pull-out shear:

- The area of the shear plane in the chord was assumed to be parallel to the compression brace in line with the results of tests reported in Reference 6.4 and evidence available from failure observed during the passage of Hurricane Andrew [6.1]. The shear area of the chord is assumed to be the cross-sectional area multiplied by $2/\pi$.
- The brace pull-out area was taken as the footprint perimeter times the chord thickness.

The length of the curve of intersection of the brace footprint with the chord (L) is obtained from:

$$L = a + b + 3\left(a^2 + b^2\right)^{\frac{1}{2}} \quad \ldots 6.10$$

where:

$a = \frac{1}{2} d \operatorname{cosec} \theta$

$b = (d/3)\left(3 - \beta^2\right)/\left(2 - \beta^2\right)$

$\beta = d/D$

d and D are the brace and chord diameters respectively.

θ is the angle of the joint.

The relative magnitudes of the shear value in the chord and brace will determine the likely mode of failure. Figure 6.28 shows the result of the parametric study. An empirical equation has been developed based on these results. The equation gives the K-action utilisation in a low gapped K joint above which fracture of the chord due the shearing action in the gapped region is likely to occur. Below this value of K action utilisation, the mode of failure is likely to be governed by tension brace pull-out. A closer examination of Figure 6.28 will indicate that chord fracture is only likely to occur at β values greater than about 0.65, irrespective of the degree of K-action. As would be expected, for high β K joints, chord fracture becomes increasingly more likely with increasing K-action utilisation. A smaller amount of K action would be required to cause chord shear with increasing β. The area below the equation line in Figure 6.28 represents brace pull-out whilst the region above represents chord fracture.

That is brace pull-out should be assumed unless:

$$k > 2.47 - 2.35\,\beta \quad \ldots 6.11$$

when chord shear failure may occur.

6.5.3 Implementation issues

Four other issues deserve mentioning and these concern the numerical implementation of the above guidance.

i. Member fracture represents a most severe, sudden, change of loads within the structure and the loss of load in the failed member needs to be redistributed in an orderly manner. This may require additional iterations by the host program.

ii. It is possible that two or more members may fracture in the same load increment, particularly if the redistributed load from the first member precipitates failure in adjacent members. Provision needs to be made in the host program to handle this scenario.

iii. It is conceivable that simultaneous fracture could be indicated for both braces in a X joint (assuming a small tolerance on loads is permitted). In these instances, it would be useful for a message to be displayed and, if deemed

necessary, to permit the user to adjust the input data such that fracture is predisposed to occur in a selected brace.

iv. At present, the Pδ formulations for the tension and compression braces of a K joint under balanced axial loading are similar except that the peak capacity of the tension brace is set to be 10% higher than that of the compression brace. This was done to replicate observed behaviour of tests on individual K joints. The compression brace deforms and the tension brace behaviour reflects that of the compression brace at low to moderate loads, but at higher loads the observed tension brace behaviour tends towards a low limiting deformation value. Inspection of Figure 6.19, for example, then indicates that the limiting value above (mean $\delta/D = 0.026$) would never actually be attained for balanced axial loading and, in turn, the joint will never be predicted to fracture under pure balanced axial load conditions.

This may not be a problem as in reality there will always be some Y action and this may trigger the fracture criterion. This issue was examined further during the benchmarking and sensitivity exercises, Section 9.

6.6 Concluding Remarks

The following conclusions were inferred from the results of the FE analyses and studies.

- The use of a limiting or maximum plastic strain value as frequently adopted in FE analyses to determine the ultimate capacities of joints, does not provide a reasonable and consistent basis for determining the ductility limits of tension-loaded joints. The results of the FE analyses show the limiting strains to be joint geometry dependent.
- The criterion of plastic work (analogous to the fracture toughness) done at the joint of about 5 Joules per mm^2 of chord area provides a better basis for determining the ductility limits of tension loaded joints. However, it does not work with high β T joints.
- The application of the plastic work criterion to a K joint produced a seemingly reasonable deformation limit, but there was no means of checking it.
- The previously derived DT joint deformation limit was confirmed as being robust, see Section 6.5.1.1.
- The FE result for the high β T joint led to a review of the basis of the deformation limit previously derived for T/Y joints. A revised limit was formulated, see Section 6.5.1.2.
- A new K joint deformation limit was derived on the basis of the few test data available to this project, see Section 6.5.1.3.

- It was proposed that for joints having mixed classifications, a simple linear interpolation function should suffice to determine an overall limit from the limits for individual joint types, see Section 6.5.1.4.
- For all joint types, both mean and characteristic deformation limits were given, see Section 6.5.1.
- For joints having a degree of K action, two modes of failure were considered: brace pull-out and chord shear failure. A study of this aspect led to a simple formulation to determine which mode is more likely, see Section 6.5.2.

The above observations and conclusions are appropriately incorporated into MSLJOINT, to allow the host program to address the possibility of joint fracture occurring.

7. UNLOADING BEHAVIOUR OF JOINTS

7.1 Introduction

This section reports on Finite Element studies which examine the stiffness response of joints undergoing unloading. It also encompasses the effect of joints in which the load in the subject brace remains constant but other braces unload. This is therefore an issue of the behaviour of a joint (for a subject brace) undergoing a change of classification.

7.2 Description of Analyses

7.2.1 FE modelling

All analyses were carried out using the non-linear general-purpose ABAQUS FE program. The models were created using 20 node brick elements with reduced integration. Two layers of elements were used in the chord, only one was used in the brace.

Both geometric and material non-linearities were accounted for in the analyses. An ideal elasto-plastic material obeying the von Mises yield criterion was selected.

Loads were applied at the ends of braces by distributing the load over the cross-section area. Reaction forces, at the ends of the chord, were taken out through diaphragm plates modelled with thick shell elements.

7.2.2 Joints and load types

In this study, both DT and K joints were considered. The models were adapted from those used in Section 6 on ductility criteria. The non-dimensional geometric properties were as follows:

DT joint: $\beta = 0.4,\ \gamma = 25,\ \gamma = 0.81$

K joint: $\beta = 0.4,\ \gamma = 15,\ \gamma = 0.81.$

The meshes used for axial loading are shown in Figures 7.1 and 7.2 respectively. For those DT joint analyses requiring applied bending moments, the mesh shown in Figure 7.1 was reflected to produce a ¼ model.

The following analyses were performed:

(1) DT joint

- axial compression loading, and unloading from three positions
- axial tension loading, and unloading from four positions
- in-plane bending, and unloading from two positions
- combined axial compression and in-plane bending, and unloading from one position. Three unloading paths were studied; unloading P alone, M alone or both P and M together

- axial compression loading, and unloading the non-subject or the subject brace from one position. These analyses explore the role of changing the joint classification.

(2) K joint

- balanced axial loading, and unloading from three positions.

7.3 Results

Results are generally presented as non-dimensional load/deformation plots. The non-dimensional loads are defined as $P/(F_yT^2)$ and $M/(F_ydT^2)$ for axial loads and moments respectively, and the corresponding non-dimensional deformations are δ/D and θ.

In all figures that follow, 'theoretical' unloading lines are also shown. These have been constructed by drawing lines parallel to the initial loading response and passing through the points where unloading commenced.

7.3.1 DT Joint Under Uni-directional Loading

The loading and unloading responses of the DT joint under compression, tension and in-plane bending are shown in Figures 7.3 to 7.5 respectively.

Compared to the slope of the elastic loading response drawn through the origin, the unloading response of the compression case is less steep. However for the tension and IPB cases, the unloading curves are steeper.

The initial elastic loading line gives a good approximation to the slope of the compression and IPB unloading curves and a fair approximation for the tension case in the region of interest (ie. δ/D up to about 0.8 – the validity range before fracture would be expected to occur). It is to be noted that the onset of cracking for the tension loaded joint is not modelled, and therefore the FE result may not give a good representation of real joint behaviour, either during loading or unloading, once cracking has been initiated.

7.3.2 DT Joint Under Combined Compression/IPB

The DT joint was proportionally loaded with compression and IPB, and then unloaded along different paths:

- unloading compression only
- unloading moment only
- unloading compression and moment proportionally.

The results are summarised in Figures 7.6 and 7.7.

The maximum compression load, in the combined case, was found to be 0.39 that of the unidirectional case (Figure 7.3). Similarly, the moment ratio was found to be 0.83. These values, when substituted in the interaction equation $P/P_u + (M/M_u)^2$,

give a joint utilisation of 1.08 which supports the validity of the interaction equation.

When unloading the compression load alone, the Pδ response is well approximated by a line drawn parallel to the initial loading slope, see Figure 7.6. Note that the initial loading slope is independent of any co-existing moment as P and M are uncoupled when the behaviour is essentially elastic. When the moment alone is unloaded, with P remaining constant, there is a small decrease in axial deformation, see Figure 7.6. This indicates that there is a coupling effect between M and δ but it is not large. When both P and M are proportionally unloaded, the Pδ path follows the diagonal of a parallelogram, two sides of which are formed by unloading individual load components.

The Mθ responses are shown in Figure 7.7. In this case, only a very little Pθ coupling effect is noted. The unloading response is well approximated by a line drawn parallel to the initial loading slope.

7.3.3 K Joint Under Balanced Axial Loading

The loading and unloading responses of the K joint subjected to balanced axial loading are presented in Figures 7.8 and 7.9 for the compression and tension braces respectively. The compression brace unloading behaviour is well captured by a line drawn parallel to the initial loading responses, Figure 7.8. The tension brace unloading response is also well captured when unloading occurs before peak load is attained. Thereafter the loading curve doubles back on itself (due to unloading in the compression brace) before deformations pick up again. In this regime, the match between the FE results and the constructed unloading curves is only fair. It is noted, however, that the tension brace deformations are small and therefore the mismatch is also small in absolute terms.

7.3.4 DT Joint Undergoing a Change of Classification

The DT joint was loaded with the load on the subject brace being twice that on the non-subject brace. This leads to a joint classification for the subject brace of X : Y = 50 : 50 and that for the non-subject brace of X : Y = 100 : 0.

Two unloading scenarios, starting from the peak load position, were then explored:

- unloading the non-subject brace to zero. During unloading, the joint classification X : Y of the subject brace changes from 50 : 50 to 0 : 100.
- unloading the subject brace to zero. During unloading the joint classification X : Y of the subject brace progressively changes from 50 : 50 to 100 : 0, until the loads in the braces become equal, and remains at 100 : 0 whilst the subject brace is fully unloaded.

The responses are presented in Figure 7.10. Because of the evident interest in 100 : 0, 0 : 100 and the 50 : 50 classifications, the loading curves for all three are shown.

When the non-subject brace is unloaded, with the load in the subject brace remaining constant, there is a relaxation of the deformation for the subject brace. This, ostensibly, indicates a coupling effect of the other brace on the subject brace deformation.

When the subject brace is unloaded, with the load in the non-subject brace remaining constant, the deformation eventually becomes negative. This can be explained by ovalisation effects caused by the load in the non-subject brace, ie. coupling between subject brace deformations with the load in the other brace is observed. The net result of this coupling is that the unloading curve obtained from the FE result is less stiff than either the elastic slopes assuming pure Y or X action.

7.4 Concluding Remarks

The finite element method has been used to explore the unloading behaviour of DT and K joints. Based on the results the following observations and conclusions have been made:

- Unloading response can be predicted by assuming linear elastic behaviour with a joint stiffness given by the response to initial loading. This applies even for unloading well beyond peak load.
- There is a small amount of coupling between in-plane bending moment and axial deformation (Mδ coupling), but negligible Pθ coupling, for combined compression/IPB.
- There is a moderate coupling between loads in one brace and the deformation in the other brace for axially loaded DT joints.

Despite the above noted coupling effects, it is nevertheless recommended that unloading behaviour is modelled as linear elastic behaviour using stiffnesses obtained from the initial response to loading.

8. DEVELOPMENT AND TESTING OF MSLJOINT

8.1 Introduction

This section reports on work conducted by SINTEF that demonstrates the performance of the codified joint algorithm to simulate various aspects of joint behaviour, including verification against relevant test data. The comparisons are largely, although not exclusively, made against individual joint tests.

The various aspects of joint behaviour studied in the following subsections include:

- Uni-axial loading

  This includes the ability of MSLJOINT to follow the intended load-deformation curve, even with large load steps, and encompass rapid unloading due to rupture of the joint.

- Pδ response of joints having mixed classification

  This is to confirm that the mixed class Pδ curve can be ascertained from the Pδ curves for pure K, X or Y action.

- Chord load interaction

  This is to show that MSLJOINT gives reduced joint capacity, whilst still maintaining the elastic LJF, for joints subjected to chord loading.

- Combined brace loading

  A number of aspects are examined in this subsection including the influence of the shape of the interaction curve and the general ability of MSLJOINT to capture combined load data.

- Scaling of strength level

  This is to confirm that scaling of joint capacity (eg. from mean to characteristic values) does not affect the elastic LJF.

It is helpful for the ensuing comparisons and discussions to be reminded of the central theme of the joint algorithm.

Essentially, each force component follows its uncoupled Pδ or Mθ curve. The interaction between individual force components is captured by a requirement that the combined force state is limited by the generic interaction function given in Equation 8.1. The API and HSE interaction functions are listed for reference.

$$\Gamma = \begin{cases} \cos\left(\frac{\pi}{2}\frac{N}{N_U}\right) - \sqrt{\left(\frac{M_{ipb}}{M_{U,ipb}}\right)^2 + \left(\frac{M_{opb}}{M_{U,opb}}\right)^2} & \text{, API} \\ \left|\frac{N}{N_U}\right| - \left(\frac{M_{ipb}}{M_{U,ipb}}\right)^2 + \left|\frac{M_{opb}}{M_{U,opb}}\right| - 1 & \text{, HSE} \\ \left(\frac{N}{N_U}\right)^{\alpha 1} - \left(\left(\frac{M_{ipb}}{M_{U,ipb}}\right)^{\alpha 3} + \left(\frac{M_{opb}}{M_{U,opb}}\right)^{\alpha 4}\right)^{\alpha 5} - 1 & \text{, Generic} \end{cases} \quad \ldots 8.1$$

In the current formulation, the joint capacities are described by pre-defined proportionality limits N_0, $M_{0,ipb}$ and $M_{0,opb}$ multiplied by hardening terms R_N, R_{ipb} and R_{opb} that represent the remaining inelastic part of the curve, as functions of δ/D or θ. That is:

$$\Gamma = \left(\frac{N}{R_N N_0}\right)^{\alpha 1} - \left(\left(\frac{M_{ipb}}{R_{ipb} M_{0,ipb}}\right)^{\alpha 3} + \left(\frac{M_{opb}}{R_{opb} M_{0,opb}}\right)^{\alpha 4}\right)^{\alpha 5} - 1 \quad \ldots 8.2$$

During analysis, the intersection point between the interaction surface and the N- and M- axes moves as the each force component hardens or softens. The interaction surface not only expands or contracts, as seen for conventional hardening models, but may also change shape when the individual force components change. This is illustrated in Figure 8.1. The latter ability is especially relevant for modelling of ductility limits and reduction of capacity at certain deformation levels.

The shape of the interaction surface is plotted in Figure 8.2 and Figure 8.3 for different combinations of α's.

- $[\alpha_N = 1,\ \alpha_M = 2]$ represents the HSE joint capacity function for combined axial and in-plane bending
- $[\alpha_N = 1,\ \alpha_M = 1.75]$ closely resembles the API cosine joint capacity function (see Figure 8.3).

The role of α_{IPB} and α_{OPB} is explored in subsection 8.5.

8.2 Uni-axial Loading

Figure 8.4 and Figure 8.5 show typical uni-axial predictions from MSLJOINT. They overlay the analytical (input) curves closely. (The original $P\delta$ and $M\theta$ curves are shown as dotted lines in Figure 8.13 and Figure 8.14 respectively). These, and other tests, show that MSLJOINT reproduces the original uni-axial load-deformation curves.

MSLJOINT was also prepared for implementation of ductility limits. This is shown in Figure 8.6, where a ductility limit $\delta_{max}/D = 20\%$ has been defined, followed by rapid unloading to simulate rupture. As shown, the algorithm is able to capture rather extreme reductions in capacity.

Figure 8.7 shows the same analysis executed with extremely large load steps (step size = $0.6 \times N_U$). MSLJOINT is still able to converge to the Pδ curve, and return the correct element forces for the deformation level given by the host program.

This indicates that the joint algorithm is robust, and should produce reasonable results even if the specified step sizes are excessive. (It is of course not recommended to apply such load steps in any non-linear analysis.) Initial step sizes exceeding the proportionality limit of one of the force components will result in an error message from MSLJOINT.

8.3 Mixed Classification

Uni-axial Pδ curves for joints of mixed classification have been implemented according to the procedure described in Section 4 and Appendix A.

Figure 8.8 and Figure 8.9 show resulting Pδ curves for a joint varying in classification from 100%K to 100%Y, and from 100% Y to 100% X. These results demonstrate that MSLJOINT can generate a family of Pδ curves with a smooth transition from 100% of one joint classification to 100% of another.

In some applications, it is possible for a classification to have all three joint types represented. The bold lines in Figure 8.10 and Figure 8.11 shows Pδ curves for a combination of 30% Y, 20% X and 50% K. Pδ curves for 100%K, 100%Y and 100%X are included for reference.

These tests demonstrate that the algorithm for handling mixed classed joints works well.

8.4 Chord Load Interaction

Chord load effects have been included in the joint algorithm according to the procedure set out in Section 3.3. The resulting numerical predictions are compared to test results in Figure 8.12. The diagrams in the figure are arranged as follows:

Pδ test	Pδ simulation
$M_i\theta_i$ test	$M_i\theta_i$ simulation
$M_o\theta_o$ test	$M_o\theta_o$ simulation

The performance of MSLJOINT is compared to test data from Boone et.al.[8.1] for axial, IPB and OPB loading.

Superimposed on the test data (left-hand plots) are numerical predictions with the joint equations fitted to each particular test curve. Numerical predictions from MSLJOINT (right-hand plots) represent the generic joint formulae, i.e. with the joint equations fitted to the complete database.

There is some difference between the test results and the uni-axial Pδ curve for compression loading, both with and without chord load. It is emphasized that this is not a failing within the module, but rather reflects that the Boone data differs from the mean of other test series. However, the reduction in capacity due to chord

stresses is captured, and also the different effect of chord bending stresses as compared to chord compression stresses. This is also reflected in Table 8.1, which compares the Q_f factors predicted by MSLJOINT to the Q_f factors reported by Boone.

Tests (Reference 8.1)					MSLJOINT				
σ_{Ax}/f_y	σ_{Ben}/f_y	Q_f axial	Q_f IPB	Q_f OPB	P/P_U	M/M_P	Q_f axial	Q_f IPB	Q_f OPB
.0	.0	1	1	1	0	0	1	1	1
-.32	.28	0.84	0.75	0.88	-.32	.28	0.82	0.73	0.81
-.6	0	0.73	0.57	0.81	-.6	0	0.73	0.60	0.81
-.8	0	0.53	-	-	-.8	0	0.52	0.28	0.66

Table 8.1: Test[8.1] and predicted Q_f factors

8.5 Combined Loading

8.5.1 Initial calibration

The performance of the joint algorithm under combined loading is evaluated against relevant test data. Initial calibration is based on test data from Stol et.al.[8.2, 8.3 and 8.4], for combined Axial and IPB loading of tubular T-joints with $\beta=0.36$ and $\gamma=15$ (test specimens 1, 6, 7 and 8).

$P\delta$ characteristics and $M\theta$ characteristics from the tests are shown in Figure 8.13 and Figure 8.14. These figures also show the analytical predictions for uni-axial loading.

The T joint geometry was modelled in USFOS (5 nodes, 3 beam elements, 1 "joint" element), and eccentric compression loading applied to the brace end. This is illustrated in Figure 8.15. The resulting numerical predictions are shown in Figures 8.16 to 8.19.

The initial analyses (Figure 8.16 and Figure 8.17) showed little resemblance with the test results. The analyses predicted significant interaction between bending moment and axial load, but overestimate the reduction in axial capacity caused by the presence of bending moments. Also, the post-peak load shedding is overestimated.

It could, however, be reasonably assumed that the numerical model would overestimate the P-Δ effects of the eccentric compression load. In the FE model, the brace end is free, with no lateral restraint whatsoever. In the tests the brace end would be connected to the hydraulic actuators, which would provide some (possibly significant) lateral restraint.

To evaluate the impact of the P-Δ effects, the analyses were repeated with the loads moved from the brace tip to the brace/chord intersection. Thus, the loads were acting directly on the "joint element" and the P-Δ effects were eliminated. The resulting numerical predictions are shown in Figure 8.18 and Figure 8.19.

These analyses show better agreement with the test results. Since it seems reasonable to assume that the actuator system imposes noticeable lateral restraints at the brace tip, the remaining analyses presented in this Section 8 have been performed with the loads moved from the brace tip to the brace/chord intersection. Thus, the following analysis results refer to loads acting directly on the "joint element", with P-Δ effects eliminated.

8.5.2 Shape of (P + IPB) interaction surface

Different shapes of the interaction surface are evaluated herein (see the discussion in Section 8.1) for the case of combined compression and IPB. Combinations involving OPB are addressed in Section 8.5.3.

Figure 8.20 and Figure 8.21 show analysis results for different combinations of α's. The results should be compared to Figure 8.13 and Figure 8.14. The results show significant impact of interaction surface shape. Linear interaction [$\alpha_N=1$, $\alpha_M=1$] (full line, + marks) underestimates the resulting capacity both for axial force and bending. Spherical interaction [$\alpha_N=2$, $\alpha_M=2$] (dashed line, × marks) seems to overestimate the resulting capacity.

Both [$\alpha_N=2$, $\alpha_M=1$] and [$\alpha_N=1$, $\alpha_M=2$] seem to give reasonable agreement with the test data. Since [$\alpha_N=1$, $\alpha_M=2$] is reasonably close to the API and HSE (and ISO) joint interaction functions, this combination is to be preferred.

8.5.3 Benchmarking analyses

Selected test results from Stol have again been analysed. It is assumed, initially, that $\alpha_N = 1$ and that $\alpha_{IPB} = \alpha_{OPB} = 2$ applies. The interactions studied are:

- **Combined Axial and IPB loading**: Stol specimens 1, 6, 7 and 8. Proportional loading at different combinations of axial force and in-plane bending. Test results and simulations are compared in Figure 8.22, with the diagrams arranged as follows:

Pδ test	Pδ simulation
Mθ test	Mθ simulation
MP test	MP simulation
δθ test	δθ simulations

- **Combined Axial and OPB loading**: Stol specimens 2, 6, 21 and 22. Proportional loading at different combinations of axial force and out-of-plane bending. Test results and simulations are compared in Figure 8.23 as follows:

Pδ test	Pδ simulation
Mθ test	Mθ simulation
MP test	MP simulation
δθ test	δθ simulations

- **Combined Axial, IPB and OPB loading**: Stol specimens 1, 2, 6, 50, 51 and 52. Proportional loading (specimen 50) and non-proportional loading (specimens 51 and 52) at roughly the same combinations of axial force, in-plane bending and out-of-plane bending. Test results and simulations are compared in Figures 8.24 to 8.26 showing the following data:

Figure 8.24

Pδ test	Pδ simulation
$M\theta_i$ test	$M_i\theta$ simulation
$M\theta_o$ test	$M_i\theta_o$ simulation

Figure 8.25

MP test	M_iP simulation
MP test	M_oP simulation
MM_o test	M_iM_o simulation

Figure 8.26

$\theta_i\delta$ test	$\theta_i\delta$ simulation
$\theta_o\delta$ test	$\theta_o\delta$ simulation
$\theta_i\theta_o$ test	$\theta_i\theta_o$ simulation

Superimposed on the test data (left-hand plots) are numerical predictions with the joint equations for uni-axial loading. There is some difference between the test results and the uni-axial Pδ formulae, both for axial and bending loads. As mentioned previously, this reflects a divergence of Stol's data from the mean of all data rather than a shortcoming in the module.

Barring these initial differences between the uni-axial test data and the corresponding uncoupled load-deformation curves, the joint algorithm gives excellent agreement with the test results on combined loading. The agreement is equally good for proportional and non-proportional loading.

The above comparisons have been made with the assumption that $\alpha_{OPB} = 2$ in the interaction equation. However, codified guidance tends to use $\alpha_{OPB} = 1$ in capacity checks and therefore it was necessary to investigate the role of α_{OPB} further before a final set of α factors could be recommended. For this purpose, some of the above comparisons have been revisited, assuming now that $\alpha_N = 1$, $\alpha_{OPB} = 2$ and $\alpha_{OPB} = 1$.

- **Combined Axial and OPB loading**: Stol specimens 2, 6, 21 and 22. Proportional loading at different combinations of axial force and out-of-plane bending. Test results and simulations are compared in Figure 8.27 and Figure 8.28, showing the following data:

Pδ test	Pδ simulation
Mθ test	Mθ simulation

Figure 8.27 shows results for $\alpha_N=1$, $\alpha_{IPB}=2$, $\alpha_{OPB}=2$.

Figure 8.28 shows results for $\alpha_N=1$, $\alpha_{IPB}=2$, $\alpha_{OPB}=1$.

- **Combined Axial, IPB and OPB loading**: Stol specimens 1, 2, 6, 50, 51 and 52. Proportional loading (specimen 50) and non-proportional loading (specimens 51 and 52) at roughly the same combinations of axial force, in-plane bending and out-of-plane bending. Test results and simulations are compared in Figure 8.29 and Figure 8.30, showing the following data:

Pδ test	Pδ simulation
$M_i\theta_i$ test	$M_i\theta_i$ simulation
$M_i\theta_o$ test	$M_i\theta_o$ simulation

Figure 8.29 shows results for $\alpha_N=1$, $\alpha_{IPB}=2$, $\alpha_{OPB}=2$.

Figure 8.30 shows results for $\alpha_N=1$, $\alpha_{IPB}=2$, $\alpha_{OPB}=1$.

Superimposed on the test data (left-hand plots) are numerical predictions with the joint equations for uni-axial loading. There is some difference between the test results and the uni-axial Pδ formulae, both for axial and bending loads.

Barring these initial differences between the uni-axial test data and the corresponding uncoupled Pδ curves, there is a marked difference between analyses performed with $\alpha_N=1$, $\alpha_{IPB}=2$, $\alpha_{OPB}=2$ and analyses performed with $\alpha_N=1$, $\alpha_{IPB}=2$, $\alpha_{OPB}=1$.

An inspection of the figures suggest that using $\alpha_N=1$, $\alpha_{IPB}=2$ and $\alpha_{OPB}=2$ gives a better fit to the test results than $\alpha_N = 1$, $\alpha_{IPB} = 2$, $\alpha_{OPB} = 1$.

8.6 Scaling of Strength Level

The joint algorithm is codified such that the user can specify characteristic joint strength, mean joint strength, or mean strength factored by some user-defined value. However, it is a requirement that this scaling of strength should not affect the initial joint flexibility. This subsection contains the results of a small sensitivity study to confirm that MSLJOINT meets the above requirements.

The X frame analyses reported in Section 9 has been repeated with capacity level set to "mean", "characteristic" and mean×1.25. The resulting Frame PΔ curves are shown in Figure 8.31, and the joint behaviour is shown in Figure 8.32.

The analyses show that joint strength can be scaled without affecting the initial joint stiffness. The analyses also show very good fits to the test results.

8.7 Concluding Remarks

On a conceptual level, the joint algorithm is based on:

- Uni-axial Pδ and Mθ curves, including
  - mixed-mode classification (for Pδ only)
  - chord load interaction
- A force interaction function, Equation 8.2, defined by:
  - the shape of the interaction function (choice of α's)
  - the extent of the elastic area (definition of the proportionality limits N_0, $M_{0,ipb}$ and $M_{0,opb}$)

The present simulations have been done with the proportionality limit for all loading directions set to 60% of the capacity. Although different proportionality limits will produce slightly different results (there will be no difference for uni-axial loading), the results indicate that this level for the proportionality limit gives sufficiently accurate simulations.

The present simulations show that the joint algorithm accurately reproduces the original Pδ curve for uni-axial loading, including mixed classification and chord load interaction effects.

The joint algorithm is robust with respect to size of the load steps.

MSLJOINT is implemented with ductility limits and handles unloading to simulate rupture.

The joint algorithm simulates brace load interaction in an efficient manner. The joint algorithm gives excellent agreement with the test results on combined loading, being equally good for proportional and non-proportional loading. It is recommended that in the interaction equation, the α factors should be taken as follows:

α_N = 1

α_{IPB} = 2

α_{OPB} = 2, and

$\alpha 5$ = 1.0.

Local joint flexibility is preserved for scaling of strength level, including changes in chord yield strength and chord loads.

9. CALIBRATION OF MSLJOINT AGAINST FRAME DATA

9.1 Introduction

The basic performance of MSLJOINT to simulate individual joint behaviour was addressed in Section 8 where it was found that it performed well, meeting all specified requirements. This Section 9 presents the benchmarking results and calibration studies related to predicting the behaviour of frames. These studies were performed by SINTEF.

There are a number of issues that can be examined within the context of frame analysis, as opposed to analysis of individual joints. These are:

(i) General ability of MSLJOINT's performance to improve predictions of frame behaviour.

(ii) How accurately do the uncoupled load-deformation curves for joints need to be represented (eg. does rigid-plastic behaviour give an appropriate approximation for use in frame analysis)?

(iii) How is the performance of MSLJOINT affected, if at all, when there are several sources of non-linearity in the frame (eg. due to a number of members and/or joints failing)?

(iv) The boundary conditions for joints within frames tend to be different to those used in individual joint tests.

(v) How does the implementation of ductility limits and subsequent unloading behaviour affect frame behaviour? In particular, this applies to X-braced frames where the X brace in tension and to K-braced frames with K joints of large β.

To investigate these issues, the results of tests on five large scale 2D steel frames tested in the Frames Project, Phases I[9.1] and II[9.2], were used in the benchmarking and calibration studies. Both X-braced and K-braced 2D frames were examined.

For predicting frame behaviour, MSLJOINT must necessarily be used in conjunction with a frame analysis package. MSLJOINT was implemented in USFOS for the purposes of this project. The frames are modelled by beam-column elements, generally one element per member. Only the joint of interest in each frame is analysed with MSLJOINT, the remaining joints are treated as rigid. The analyses are performed with very little strain hardening for the tubulars, using the default strain hardening parameters of the program, i.e. 0.2%.

Despite the good performance of MSLJOINT in capturing individual joint behaviour, in order that more accurate simulations of frame behaviour can be made it was deemed appropriate to make certain adjustments to the module. These adjustments were mainly concerned with the value of the chord stress factor (Q_f), and are discussed in the following subsections. It may be noted here that the Q_f factor is one of the least researched areas in tubular joint technology, and therefore such adjustments do not generally conflict with known joint behaviour.

9.2 2D X-Braced Frames

9.2.1 Frame II (X joint in compression)

Frame dimensions and properties for Frame II are shown in Figure 9.1. Brace and chord yield strengths for the X joint were measured as 290 and 325 MPa respectively.

Figure 9.2 shows predicted frame behaviour, compared with test results. The simulations give good agreement with the test results. The analysis captures the dominant frame mechanisms and gives good agreement with observed frame behaviour in the elastic range and during joint yielding. It can be observed that rigid joint assumptions gives an optimistic first peak.

The X joint formulation is limited to joint deformations $\delta \leq D/2$, and does not account for force build-up when the brace ends make contact after joint flattening (this occurs at a frame displacement of about 150mm). The X joint behaviour is shown in Figure 9.3.

Figure 9.4 shows resulting frame deformations (including member utilisation) at 200 mm frame displacement.

9.2.2 Frame VI (X joint in tension)

Frame VI is nominally identical to Frame II, except that for this frame the braces at the X-joint act in tension instead of compression. The joint material properties were significantly different from the material used in the joint in Frame II. Brace and chord yield strengths in Frame VI were measured to 234-260 MPa, compared to 290-325 MPa in Frame II. Whether strain-hardening properties differed is not known.

The Frame VI test was done as test number two on the same frame, with the joint being retro-fitted after the first test. This imposed locked-in forces in the frame, both axially and in bending. Only the axial forces were recorded from the test. The simulations are performed with locked-in forces imposed though a separate temperature loadcase prior to the mechanical loading.

The initial analysis results diverged from the test data: whilst the elastic response was satisfactory, neither the peak load nor the post peak response was adequate. Further analyses were therefore conducted with variations in Q_f and suppressing the ductility limit for the X joint in tension. The analyses conducted are listed below and the results are presented in Figures 9.5 and 9.6.

- MSL Q_f with ductility limit (initial analysis)
- MSL Q_f, no ductility limit
- Q_f based on chord compression load only, no ductility limit
- Q_f set to unity, no ductility limit
- Rigid joint.

Best agreement with MSLJOINT is achieved with Q_f set to unity. Alternative calculations with the MSL Q_f formula, or Q_f calculated from chord axial forces only, give less good agreement. Figure 9.7 compares predicted X brace tension forces and X brace compression forces (joint chord forces) to the measured forces (Q_f = 1 in the simulations). The measured tension joint behaviour is shown in the full line with "×" marks. Figure 9.8, frame deformations, shows frame failure is precipitated by buckling of the compression brace.

During testing the tension joint showed nonlinear response even in the early stages of loading, and as the joint continued to yield in tension the loads were being shed into the stiffer compression load path. Significant ovalisation of the joint chord was reported before compression brace buckling. The test records show that the tension joint yields, but instead of rupturing and shedding load, it picks up more load until the whole brace yields in tension. In the simulations the joint yields at a slightly lower load level, and does not pick up more force after yielding. (Given the remarkable ductility in the test joint, this led to the MSL joint ductility limit being turned off in the simulations.)

Figure 9.9 shows the variation of the Q_f factor during the analyses and these are seen to drive the joint response (compare Figures 9.6 and 9.9). The dashed line shows Q_f based on axial forces only, with a curve that closely reflects the buckling load in the compression brace (joint chord). The dotted line shows Q_f calculated according to the MSL formula, which includes both compression and bending terms. This curve shows the same reduction in Q_f as the compression brace is loaded, but shows an even further reduction as the post-buckling leads to yielding in bending in the chord.

The measured chord forces (compression X brace) is shown with dashed line and "∗" marks in Figure 9.6. This shows significantly higher buckling capacity than the simulations, and a more "ductile" buckling mode. Both the observed tension joint behaviour and the observed buckling behaviour may be consistent with a very ductile material with significant strain hardening.

Additional analyses are therefore performed with a different post-yield behaviour specified for the tension joint, and with significant strain hardening on the compression X brace (joint chord). Figure 9.10 shows the alternative tension joint behaviour: instead of a yield plateau, the joint regains stiffness and picks up more load until it reaches a loadlevel of 1.5 times the initial joint capacity. Figure 9.11 shows the compression brace buckling characteristics with 10% strain hardening.

With these modifications to the model, the simulations give good agreement with the test results. The analysis captures the dominant frame mechanisms; the X joint formulation gives good agreement with observed frame behaviour in the elastic range and during joint yielding. The resulting frame behaviour is shown in Figures 9.12 to 9.14.

9.3 2D K-Braced Frames

9.3.1 Calculation of Q_f for K-joints

The results presented in following are based on the assumption that Q_f for the tension joint is calculated from the stresses in the compression chord, while Q_f for the compression joint is calculated form the stresses in the tension chord (ref. Figure 9.15). In other words: the Q_f's will lead to a greater knockdown effect on the tension strength than on the compression strength.

This provides the means to reproduce the observed behaviour of K joints in frames while still using the K joint characteristics derived from isolated tests and simulations. With 10% higher tension capacity than compression capacity, all plastic deformations would be concentrated in the compression joint if the same Q_f were to be used on both the compression and tension side. This would contradict observed frame behaviour which is an initial softening of the compression joint followed by tension joint failure (rupture).

Alternatively, the tension joint capacity could be reduced below that of the compression joint. This would, however, concentrate all plastic deformations in the tension joint, and would not produce the desired effect. Figure 9.16 shows frame analyses (Frame VII) with different ways to calculate Q_f, i.e. setting $Q_f^{Tens} = Q_f^{Comp}$, using different Q_f for tension and compression as outlined above, and reducing the tension joint capacity to concentrate yielding in the tension part of the joint. It can be seen that $Q_f^{Tens} = Q_f^{Comp}$ fails to predict the peak load and global unloading of the frame, since the joint failure mechanism is ductile yielding of the compression joint. Reducing the tension joint capacity captures the peak load and global unloading of the frame, but underestimates the frame capacity and ductility. Using different Q_f for tension and compression gives the most accurate results, i.e. a reasonable representation of the dominating joint and frame failure mechanisms.

9.3.2 Calibration of load-shedding behaviour for K-joints in tension

The elastic joint flexibility and the joint yield behaviour is uniquely defined by the MSL Pδ curves. The joint behaviour after the ductility limit is passed is not addressed by the MSL formulae and has been calibrated to produce a reasonable fit to observed frame behaviour.

The "post rupture" part of the curve can be described by a residual force, P_{Res}, the associated deformation, δ_{Res}, and a final slope, θ, as illustrated in Figure 9.17. Systematic parameter variations have been run for Frame VII (Section 9.3.4) to come up with a combination of parameters that gives good agreement with the joint and frame load-shedding behaviour. The combinations that were explored are listed in Table 9.1.

		$(\delta_{Res}-\delta_{Frac}) / \delta_{Frac}$			
		1	2	3	4
P_{Res}/P_{ult}	0.75	x	x	x	x
	0.50	x	x	x	x
	0.33	x	x	x	x
	0.25	x	x	x	x

Table 9.1: Matrix of parameter variations

Best agreement with the test data set was obtained with $P_{Res} = 0.33 \cdot P_{Ult}$, $\delta_{Res} = 4 \cdot \delta_{Frac}$ and a continuing load-shedding (downward slope) after P_{Res}. The analyses reported in the following are all done with this set of parameters; no additional calibration was required for Frame VIII or X.

9.3.3 Performance of the joint algorithm for K joints

Figure 9.18 and Figure 9.19 illustrate the performance the joint algorithm during pushover analysis of Frame VII (Section9.3.4). Figure 9.18 shows the tension joint behaviour, and Figure 9.19 shows the compression joint behaviour. The dashed lines show the uni-axial Pδ curves as they are re-calculated at every step during the analysis (or re-calculated at selected intervals).

1. At the initial load step, all joints are classified as "100% Y (compression)", as the force state is not yet known to the program. (See Section 4.2.3).

2. In load step 2, all joints are re-classified; in the current case the capacities are increased from "100% Y" to "100% K".

3. In subsequent steps, both the Q_f factors and hence the Pδ curves are continuously updated. Initially, the tension K capacity is 10% higher than the compression K capacity, which will typically produce yielding / softening of the compression joint before tension joint yielding. But since Q_f for the tension joint is calculated from the stresses in the compression chord, the Q_f will lead to a degradation of the tension capacity (ref. Section 9.3.1). If Q_f is reduced beyond 0.91, the tension capacity will become lower than the compression capacity, and plastic deformation will start to accumulate in the tension joint instead of the compression joint. (The compression joint will experience elastic unloading with some permanent deformations.) Plastic deformations will continue to accumulate in the tension brace until the ductility limit is reached and the joint has "failed".

4. The tension joint will then unload along the downward slope of the Pδ curve, and the compression joint will have to follow to maintain static equilibrium over the K joint (save for shear forces in the chord).

5. After failure in the tension joint, the joint no longer acts as a "classical truss-work K", but will develop larger shear and bending stresses. This will knock down the Q_f factor even further, since chord bending stresses have a more onerous effect than axial stresses. This is what leads to the large reduction in the P-δ capacity curves towards the latter part of the analysis (see Figure 9.18 and Figure 9.19).

9.3.4 Frame VII (Gap K joint, $\beta = 1.0$, g/D=0.1)

Dimensions and steel types for Frame VII are shown in Figure 9.20.

Figure 9.21 shows predicted frame behaviour, compared with test results. The simulation gives good agreement with the test results, and captures the dominant frame mechanisms. The K joint formulation gives good agreement with observed frame behaviour in the elastic range and during joint yielding.

The joint yields initially in compression, with inelastic deformation of the compression part of the joint. During the subsequent loading the build-up of chord forces decreases Q_f for the tension brace and reduces the tension joint capacity below that of the compression joint. From this stage the compression brace unloads elastically with some permanent deformations imposed. Further deformations concentrate in the tension brace until the ductility limit is reached. The tension joint then starts to shed loads (at increasing plastic deformations), which leads to a global unloading of the frame. This joint behaviour is shown in Figure 9.22, and is compared to the measured behaviour in Figure 9.23.

Figure 9.24 shows the frame deformations (including member utilisation) at 40 mm frame displacement.

The elastic joint flexibility and joint yielding is uniquely determined by the MSL Pδ curves. The joint behaviour after the ductility limit is passed is not addressed by the MSL formulae, and has been calibrated to produce a reasonable fit to the observed frame behaviour. Frame VII has been used for this calibration. The following cases (Frames VIII and X) are analysed with the same data as used for Frame VII; without any additional calibration being conducted for these frames.

9.3.5 Frame VIII (Gap K joint, $\beta = 0.7$, g/D=0.1)

Frame VIII is nominally identical to Frame VII, except that for this frame the chord diameter is increased, leading to a joint $\beta = 0.7$.

Frame VIII was tested as test number two on the same frame (Frame VII being the first), with the joint being retro-fitted after the Frame VII test. This imposed significant locked-in forces in the frame, both axially and in bending. Only the axial forces are however recorded from the test.

Figure 9.25 compares the predicted frame behaviour with test measurements. The simulations are performed with and without locked-in forces which, when present, were imposed though a separate temperature loadcase prior to the mechanical loading. The application of locked-in forces though temperature contraction/ elongation (particularly in the braces) leads to such high bending moments in the

bottom horizontal (joint chord) that this member is close to yielding in bending before the mechanical loading is applied. This again leads to very much reduced Q_f's due to chord bending effects ($Q_f \approx 0.25$), and a joint and frame capacity far below the tested capacity.

The full line in Figure 9.25 represents the frame behaviour without locked-in forces. The dotted line represents the frame behaviour with locked-in forces and chord bending effects included in the Q_f, and the dashed line represents the frame behaviour with locked-in forces but without chord bending effects included in the Q_f. Figure 9.26 compares the calculated Q_f factors with and without chord bending effects.

The simulations with MSLJOINT give good agreement with observed frame behaviour in the elastic range and also during joint yielding if chord bending effects are taken out of the Q_f. (It should again be noted that only axial locked-in forces are recorded from the test. On the other hand, such high K-brace forces cannot be sustained without significant bending in the chord of the K.) The simulations give a fair representation of the peak load, slightly on the conservative side.

Figure 9.27 compares predicted brace (tension and compression) forces to the measured forces. The measured tension joint behaviour is shown in the full line with "×" marks.

Due to locked-in tension forces both in the compression and tension brace, all inelastic deformations are concentrated in the tension brace, as shown in Figure 9.28. Thus, the peak load is uniquely defined by the ductility limit imposed in the tension K behaviour.

Figure 9.29 shows the resulting frame behaviour with the ductility limit increased to twice the deformations in the MSL formula. This time the simulation gives good agreement with observed frame behaviour in the elastic range and during joint yielding, and also at the peak load. Figure 9.30 compares predicted alternative brace tension forces and compression forces to the measured forces.

The global deformations of the frame are illustrated in Figure 9.31.

9.3.6 Frame X (Gap K joint, $\beta = 1.0$, $g/D=0.2$)

Frame X is nominally identical to Frame VII, except that for this frame the K joint gap is larger at $g/D = 0.2$.

Frame X was tested as test number four on the same frame, with the joint being retro-fitted after the previous tests. This imposed significant locked-in forces in the frame, both axially and in bending. Only the axial forces are however recorded from the test.

Figure 9.32 compares the predicted frame behaviour with test measurements. The simulations are performed with locked-in forces imposed though a separate temperature loadcase prior to the mechanical loading. For this frame the locked-in forces in the braces were negligible, i.e. not imposing any bending moments in the bottom horizontal (joint chord). Locked-in forces in the horizontals are however

included in the analysis. Thus, for the present frame the analyses have been performed with both the axial and bending contribution in the Q_f calculation.

The USFOS simulation with MSLJOINT gives slightly stiffer response in the elastic range and a more pronounced stiffness reduction upon joint yielding compared to the test data. The peak load is underestimated, whereas the frame ductility and post-collapse behaviour show good agreement.

The joint yields initially in compression, with inelastic deformation of the compression part of the joint. During the subsequent loading the build-up of chord forces increases Q_f for the tension brace and reduces the tension joint capacity below that of the compression joint. (The variation in Q_f during the analysis is shown in Figure 9.34.) From this stage the compression brace unloads elastically with some permanent deformations imposed. Further deformations concentrate in the tension brace until the ductility limit is reached. The tension joint then starts to shed loads (at increasing plastic deformations), which leads to a global unloading of the frame. The joint behaviour is shown in Figure 9.34, and is compared to the measured behaviour in Figure 9.35.

The global deformations of the frame are illustrated in Figure 9.36.

9.4 Concluding Remarks

The present investigations show that the joint algorithm gives good agreement with results from 2D frame testing, as long as the joint behaviour is within the validity limits of the formulation.

The performance of the joint algorithm as implemented in USFOS is summarised in Figures 9.37 to 9.41. The joint formulation gives good agreement with observed frame behaviour in the elastic range and during joint yielding. Compared to the present tests, the formulation is slightly conservative. Overall, it certainly gives better predictions than the analyses based on rigid joints.

The X joint formulation is limited to joint deformations $\delta \leq D/2$, and will not account for force build-up when the brace ends make contact after joint flattening.

The K joint formulation gives good agreement with observed frame behaviour in the elastic range and during joint yielding. The use of different Q_f for tension and compression produces initial compression joint softening followed by tension joint failure (rupture), as observed in the frame tests.

The load-shedding characteristics for K-joints in tension, which was calibrated from the Frame VII test, also give good agreement for the Frame VIII and Frame X data.

10. CLOSURE

Much work has been conducted in this phase of the project to derive analysis tools which exploit the tubular joint load-deformation curves formulated in Phase I. The uncoupled Pδ and Mθ curves have been enhanced in four respects:

(i) Incorporation of the chord load factor (Q_f) in the formulation in such a way as to preserve elastic LJF.

(ii) Incorporation of chord yield stress, again preserving elastic LJF.

(iii) Optional use of mean, characteristic or user-defined joint capacity, yet again preserving elastic LJF.

(iv) For axial loading when the joint brace has a mixed classification (ie. various proportions of K, X and Y actions), a weighting procedure has been developed for simulating the Pδ response.

Coupling of the Pδ and Mθ responses has been accomplished through plasticity routines. These include hardening rules, to model the expansion of the yield envelope up to the ultimate interaction surface, and subsequent contraction of the surface for following post-peak response.

Other aspects of joint behaviour have also been studied to allow a comprehensive set of algorithms to be developed. These include unloading behaviour following redistribution of frame loads, unloading behaviour of tension joints undergoing rupture and ductility limits when such rupturing may occur.

The above works and developed algorithms lead, in principle, to the complete definition of the Pδ and Mθ response curves given certain input parameters (eg. joint geometry, brace loads). As such, the primary objective of the project, ie. the development of suitable algorithms, has been met.

The second objective concerns the coding, testing and calibration of the algorithms. USFOS, an industry-accepted non-linear frame analysis package, was used during the testing and calibration stages. Testing involved confirmation that the joint module (MSLJOINT) gave the results expected for individual joint-behaviour. Calibration was concerned with simulating frame response and comparing against large scale test data. The results of the calibration demonstrate that MSLJOINT gives better predictions than alternative joint modeling approaches, ie. the traditional rigid joint approach or invoking rigid-plastic approximations. It is therefore considered the second objective also has been successfully achieved.

Nevertheless, the studies have highlighted areas of ignorance in tubular joint technology. The foremost, perhaps, is the role of chord loads (ie. the Q_f factor) on joint strength. The calibration studies, in particular, suggest that adjustments in Q_f can lead to better correlation between experiment and simulations. However, there is comparatively little work done in this field, although current studies at EWI can be expected to shed some light on this in some particular instances.

Another area concerns multi-planar joint technology. The Pδ and Mθ formulations in Phase I were derived from tests on uni-planar joints. As such, the algorithms are

essentially based on 2D behaviour. For primary joints in face frames, 2D or uni-planar behaviour is considered sufficient.

It is intended to address these and other areas of ignorance, and thereby improve MSLJOINT, by means of a "MSLJOINT users group". Sponsors of the project have free access to this group, and will be kept informed of developments. The group is expected to run for 12 months.

Users of MSLJOINT are encouraged to feedback their experience through the group, as this can be used for the benefit for all.

REFERENCES

1.1 MSL Engineering Limited. "JIP on Assessment Criteria, Reliability and Reserve Strength of Tubular Joints. (Final Report for Phase I)". MSL Doc. Ref. C14200R018 Rev 0, March 1996.

1.2 International Standards Organisation. "ISO 13819-2 (Committee Draft): Petroleum and Natural Gas Industries, Offshore Structures. Part 2: Fixed Steel Structures".

3.1 Dept. of Energy, "Static Strength of Large Scale Tubular Joints", OTI 89-543.

3.2 Boone TJ et al "Chord Stress Effects on the UTS of Tubular Joints" Texas Univ. Report PMFSEL N°82-1, Dec 1982.

3.3 Sanders DH et al "Strength of Tubular Double Tee Tubular Joints in Tension" OTC 5437, 1987.

3.4 Weinstein RM et al "The Effect of Chord Stresses on the Static Strength of DT Tubular Connections" PMFSEL N°85-1, Jan 1985.

3.5 Togo T "Experimental Study on Mechanical Behaviour of Tubular Joints" PhD Thesis, Osaka University, Japan, January 1967. (in Japanese)

3.6 de Koning C et al "The Static Strength of Welded CHS K-joints" Stevin Report 6-81-13, Delft Univ.

3.7 Makino Y & Kurobane Y "Strength & Deformation Capacity of Circular Tubular Joints" Kumamoto Univ. Japan.

3.8 Nakajima T et al, "Experimental Study on the Strength of Thin-wall Welded Tubular Joints" (1st & 2nd Report), IIW Doc XV-312-71, London 1971.

5.1 Skallerud, B. (1994): Ultimate capacity of cracked tubular joints. Int. conf. on Behaviour of Offshore Structures (BOSS), Boston.

5.2 Holmås, T. (1987) Implementation of Tubular Joint Flexibility in Global Frame Analysis, Division of Structural Mechanics Report No. 87-1, The Norwegian Institute of Technology, Trondheim.

5.3 Hellan, Ø. (1995) Nonlinear Pushover and Cyclic Analyses in Ultimate Limit State Design and Reassessment of Tubular Steel Offshore Structures. MTA report 1995:108, Division of Marine Structures, The Norwegian Institute of Technology, Trondheim.

6.1 Health and safety Executive, "Hurricane Andrew Effects on Offshore Platforms". Offshore technology Report - OTN 92 243, PEN/U/2959, 1993.

6.2 Hyde, T.H., et al, "A critical assessment of the finite element method for predicting the static strength of tubular T and YT-joints". Tubular Structures VIII, Choo and van der Vegte, Balkema, Rotterdam, 1998.

6.3 van de Valk C A C, "Factors controlling the static strength of Tubular Joints". Behaviour of Offshore Structures Conference, BOSS '88, Trondheim, 1988.

6.4 "Joint Industry Tubular Frames Project - Phase IIA". 1996.

6.5 Connelly L M and Zettlemoyer N, "Frame behaviour effects on Tubular Joint Capacity". Paper P2.03, International Symposium on Tubular Structures, Finland 1989.

6.6 Amoco UK Exploration Company, "Final Reports for the Testing of K joints". ST102/83A & ST125/83A, Wimpey Laboratories Limited, 1983.

8.1 Boone, T.J., et-al.: "Chord Stress Effects on the UTS of Tubular Joints", Texas University Report PMFSEL No. 82-1, December 1982

8.2 Stol, H.G., Puthli, R.S. and Bijlaard, F.F.: "Static Strength of Welded Tubular T-joints under Combined Loading", Part I TNO Report No. B-84-561/63.6.0829, March 1985

8.3 Stol, H.G., Puthli, R.S. and Bijlaard, F.F.: "Static Strength of Welded Tubular T-joints under Combined Loading", Part II TNO Report No. B-84-561/63.6.0829, March 1985

8.4 Stol, H.G., Puthli, R.S. and Bijlaard, F.F.: "Static Strength of Welded Tubular T-joints under Combined Loading", Part III TNO Report No. B-84-561/63.6.0829, March 1985

9.1 "Joint Industry Tubular Frames Project – Phase I", The Steel Construction Institute, 1987-1990.

9.2 "Joint Industry Tubular Frames Project – Phase II", 1990-1996.

Title	Work Pack N°	MSL Identification Number	Issue Date	PSC Meeting		Assimilated in Section
				N°	Date	
TECHNICAL REPORT N° 1 Data Capture	2	C20400R001 Rev 0	September 1997	1	18 September 1997	-
TECHNICAL REPORT N° 2 Adjustments to Load/Deformation Curves to Account for F_y and Q_r	3	C20400R002 Rev 0	February 1998	2	11 March 1998	3
TECHNICAL REPORT N° 3 Joint Classification Issues	3	C20400R003 Rev 0	February 1998	2	11 March 1998	4
TECHNICAL REPORT N° 4 Specification for Joint Module	4	C20400R004 Rev 0	February 1998	2	11 March 1998	2
TECHNICAL REPORT N° 5 Recommendations for Generating New Data	5	C20400R005 Rev 0	March 1998	2	11 March 1998	-
TECHNICAL REPORT N° 6 SINTEF Report on Brace Load Interaction Approaches	3	C20400R006 Rev 0	March 1998	2	11 March 1998	5
TECHNICAL REPORT N° 7 Confirmation of Methodology for Establishing Pδ Curve for Joints of Mixed Classification	5	C20400R007 Rev 0	July 1998	3	29 July 1998	4
TECHNICAL REPORT N° 8 Development of Ductility (Fracture) Criteria for Tension Loaded Joints	5	C20400R008 Rev 0	June 1999	4	10 June 1999	6
TECHNICAL REPORT N° 9 Unloading Behaviour of Joints	5	C20400R009	June 1999	4	10 June 1999	7
TECHNICAL REPORT N° 10 SINTEF Report on Development of Module	6	C20400R010 Rev 0	June 1999	4	10 June 1999	8
TECHNICAL REPORT N° 11 SINTEF Report on Benchmarking and Sensitivity Studies for 2D Frames	7	C20400R011 Rev 0	November 1999	5	12 November 1999	9
TECHNICAL REPORT N° 12 SINTEF Report on Impact of α OPB in Interaction Eq.	7	C20400R012 Rev 0	November 1999	5	12 November 1999	8
TECHNICAL REPORT N° 13 SINTEF Report on Joint Module Scaling of Strength Level	7	C20400R013 Rev 0	November 1999	5	12 November 1999	8
INTERNAL REPORT Data on Brace Load Interaction	2	C20405R003 Rev 0	December 1997	-	"	-
INTERNAL REPORT Chord Load Effects	2	C20405R004 Rev 0	December 1997	-	"	-

Table 1.1: Document Register

Joint Type	Load Type	P_u or M_u
T/Y	Comp.	$1.27\,(1.9 + 19\beta)\,Q_\beta^{0.5}\,Q_f\,F_y\,T^2 / \sin\theta$
	Tension	$(42.3\,\beta + 17.6)\,Q_f\,F_y\,T^2 / \sin\theta$
	IPB	$5.5\,\beta\,\gamma^{0.5}\,Q_f\,F_y\,T^2\,d / \sin\theta$
	OPB	$4.2\,\gamma^{(0.5\beta^2)}\,Q_f\,F_y\,T^2\,d / \sin\theta$
DT/X	Comp.	$1.16\,(2.8 + 14\beta)\,Q_\beta\,Q_f\,F_y\,T^2 / \sin\theta$
	Tension[4]	$(37.3\beta + 6.6)\,Q_f\,F_y\,T^2 / \sin\theta$ for $\beta \le 0.9$ $[40 + (\beta - 0.9)\,(37.6\gamma - 364)]\,Q_f\,F_y\,T^2 / \sin\theta$ for $\beta > 0.9$
	IPB	$5.5\,\beta\,\gamma^{0.5}\,Q_f\,F_y\,T^2\,d / \sin\theta$
	OPB	$4.2\,\gamma^{(0.5\beta^2)}\,Q_f\,F_y\,T^2\,d / \sin\theta$
K	Balanced Axial[5]	$1.30\,(1.9 + 19\beta)\,Q_\beta^{0.5}\,Q_g\,Q_{yy}\,Q_f\,F_y\,T^2 / \sin\theta$
	IPB	$5.5\,\beta\,\gamma^{0.5}\,Q_f\,F_y\,T^2\,d / \sin\theta$
	OPB	$4.2\,\gamma^{(0.5\beta^2)}\,Q_f\,F_y\,T^2\,d / \sin\theta$

Notes:

1. Q_β = $0.3 / (\beta(1-0.833\beta))$ for $\beta > 0.6$
   = 1.0 for $\beta \le 0.6$

2. Q_g = $1.9 - (g/D)^{0.5}$ for $g/T \ge 2.0$
   but ≤ 1.0
   = $0.13 + 0.65\,\phi\,\gamma^{0.5}$ for $g/T \le -2.0$
   where $\phi = t\,F_{yb}/(TF_y)$
   = linear interpolated value between the limiting values of the above two expressions for $-2.0 < g/T < 2.0$

3. Q_{yy} = 1.0 when $\theta_t \le 4\theta_c - 90°$
   = $(110° + 4\,\theta_c - \theta_t)/200°$ when $\theta_t > 4\theta_c - 90°$

4. The expression for tension loaded X joints when $\beta > 0.9$ should only be applied when the braces are reasonably co-linear (say $e/D \le 0.2$). If the braces are not reasonably co-linear the expression for $\beta \le 0.9$ should be invoked.

5. The expression for a K joint under balanced axial loading relates to the compression brace. For the tension brace, increase the calculated value of P_u by 10%.

Table 2.1: Mean joint capacities for use in Pδ and Mθ Equations

Brace Loading	Joint Classification			
	Y	K		X
		Gapped	Overlapped	
Axial compression	0.791	0.769	0.867	0.864
Axial tension	0.554	0.769	0.867	0.878
In-plane bending	0.824	0.804	0.804	0.810
Out-of-plane bending	0.789	0.822	0.822	0.878

Table 2.2: Characteristic bias factors, ϕ

Joint Type	Load Type	Coefficient	
		A	B
T/Y	Comp.	$((\ -\ 4)\ \sin^3\ )\ /\ 62$	$B = 600 + 13500$
	Tension	0.001	$B = 12000 + 1200$
	IPB	0.001	$B = 9700 + 6700$
	OPB	0.001	$B = 8600 + 1200$
DT/X	Comp.	$(\ +\ 10)\ /\ 100$	$B = 90000\beta\gamma^{-0.4}$
	Tension	0.001	$B = 3900 + 5000$ when $\beta \le 0.9$ $B = 8510 + (\beta - 0.9)\left(\frac{6000000}{\gamma} - 80000\right)$ when $0.9 < \beta \le 1.0$
	IPB	0.001	$B = 9700 + 6700$
	OPB	0.001	$B = 8600 + 1200$
K	Balanced Axial	$(\ -\ 7)\ /\ 18$ where $=\ -0.1$ but $0.025 <\ <\ 0.25$	$(13 + 4\gamma)\psi$ where $\psi = 320 - 450\zeta$ but $170 \le \psi \le 320$
	IPB	0.001	$B = 9700 + 6700$
	OPB	0.001	$B = 8600 + 1200$

Table 2.3: Summary Of New Coefficients For Use In Prediction Equations

$$P = \phi P_u (1 - A[1 - (1 + 1/A) \exp(-B\delta/(\phi Q_f F_y D))]^2)$$

or

$$M = \phi M_u (1 - A[1 - (1 + 1/A) \exp(-B\theta/(\phi Q_f F_y))]^2)$$

where P, M = joint load

P_u, M_u = predicted mean strength

ϕ = strength scaling factor

δ = joint deformation (aligned to an individual brace)

θ = joint rotation (radians)

D = chord diameter

A = constant for any given joint geometry and load type

B = dimensional constant in units of N/mm^2 for any given joint geometry and load type.

ζ = (g/D), (Gap between brace toes/Chord diameter)

γ = (R/T), (Chord radius/Chord wall thickness)

$$Q_f = 1.0 - \lambda U^2$$

where

λ = 0.030 for brace axial load
= 0.045 for brace in-plane bending moment
= 0.021 for brace out-of-plane bending moment

$$U = \frac{1}{\Gamma_q}\left[\alpha_1\left(\frac{P_{dc}}{P_y}\right)^2 + \alpha_2\left(\frac{M_{dc}}{M_p}\right)^2_{ipb} + \alpha_2\left(\frac{M_{dc}}{M_p}\right)^2_{opb}\right]^{0.5}$$

Joint Type	α_1	α_2
T/Y joints under brace axial loading	25	11
K joints under balanced axial loading	14	43
T/Y and K joints under brace moment loading or DT/X joints under any brace loading	25	43

Notes:

1. P_{dc} and M_{dc} (ipb and opb) are the factored axial load and bending moments in the chord member, respectively.

2. P_y and M_p are respectively the yield axial and plastic moment resistances of the chord member, or of the joint can if present.

3. Γ_q is an assessment factor of safety, not to be taken as greater than unity.

4. Two values of U should be calculated, corresponding to each side of the joint, and the maximum one selected.

5. Apart from DT/X joints with $\beta > 0.9$, Q_f may be set to unity if the magnitude of the chord axial tension stress is greater than the maximum combined stress due to chord moments.

Table 2.4: Chord load Factor Q_f

Joint Type	Load Type	Coefficient	
		A	B
T/Y	Comp.	$((\gamma - 4) \sin^3 \theta) / 62$	$15\beta + 27$
	Tension	0.001	$29\beta + 5$
	IPB	0.001	$42\beta + 13$
	OPB	0.001	$30\beta + 4$
DT/X	Comp	$(\gamma + 10) / 100$	$250\beta / \sqrt{\gamma}$
	Tension	0.001	$12\beta + 11$ for $\beta \leq 0.9$ $21.8 + (\beta - 0.9)(19400/\gamma - 218)$ for $0.9 < \beta \leq 1.0$
	IPB	0.001	$42\beta + 13$
	OPB	0.001	$30\beta + 4$
K	Balanced Axial	$\varphi (\gamma - 7) / 18$ where $\varphi = \zeta - 0.1$ but $0.025 < \varphi < 0.25$	$(3 + 0.3\gamma) \psi$ where $\psi = 10 - 15\zeta$ but $5 \leq \psi \leq 10$
	IPB	0.001	$42\beta + 13$
	OPB	0.001	$30\beta + 4$

Table 3.1: Summary of Phase I Coefficients for use in Equation 3.5

Joint Type	Load Type	Coefficient	
		A	B
T/Y	Comp.	$((\gamma - 4)\sin^3\theta) / 62$	$B = 600\beta + 13500$
	Tension	0.001	$B = 12000\beta + 1200$
	IPB	0.001	$B = 9700\beta + 6700$
	OPB	0.001	$B = 8600\beta + 1200$
DT/X	Comp.	$(\gamma + 10) / 100$	$B = 90000\beta\gamma^{-0.4}$
	Tension	0.001	$B = 3900\beta + 5000$ when $\beta \le 0.9$ $B = 8510 + (\beta - 0.9)\left(\frac{6000000}{\gamma} - 80000\right)$ when $0.9 < \beta \le 1.0$
	IPB	0.001	$B = 9700\beta + 6700$
	OPB	0.001	$B = 8600\beta + 1200$
K	Balanced Axial	$\phi(\gamma - 7) / 18$ where $\phi = \zeta - 0.1$ but $0.025 < \phi < 0.25$	$(13 + 4\gamma)\psi$ where $\psi = 320 - 450\zeta$ but $170 \le \psi \le 320$
	IPB	0.001	$B = 9700\beta + 6700$
	OPB	0.001	$B = 8600\beta + 1200$

Table 3.2: Summary Of New Coefficients For Use In Prediction Equations

$$P = P_u (1 - A[1 - (1 + 1/\sqrt{A}) \exp(-B\delta/(Q_f F_y D))]^2)$$

or

$$M = M_u (1 - A[1 - (1 + 1/\sqrt{A}) \exp(-B\theta/(Q_f F_y))]^2)$$

where P, M = joint load

P_u, M_u = predicted mean strength

δ = joint deformation (aligned to an individual brace)

θ = joint rotation (radians)

D = chord diameter

A = constant for any given joint geometry and load type

B = dimensional constant in units of N/mm^2 for any given joint geometry and load type.

ζ = (g/D), (Gap between brace toes/Chord diameter)

γ = (R/T), (Chord radius/Chord wall thickness)

$$Q_f = 1.0 - \lambda U^2$$

where

λ = 0.030 for brace axial load
= 0.045 for brace in-plane bending moment
= 0.021 for brace out-of-plane bending moment

$$U = \frac{1}{\Gamma_q}\left[\alpha_1\left(\frac{P_{dc}}{P_y}\right)^2 + \alpha_2\left(\frac{M_{dc}}{M_p}\right)^2_{ipb} + \alpha_2\left(\frac{M_{dc}}{M_p}\right)^2_{opb}\right]^{0.5}$$

Joint Type	α_1	α_2
T/Y joints under brace axial loading	25	11
K joints under balanced axial loading	14	43
T/Y and K joints under brace moment loading or DT/X joints under any brace loading	25	43

Notes:

1. P_{dc} and M_{dc} (ipb and opb) are the factored axial load and bending moments in the chord member, respectively.
2. P_y and M_p are respectively the yield axial and plastic moment resistances of the chord member, or of the joint can if present.
3. Γ_q is an assessment factor of safety, not to be taken as greater than unity.
4. Two values of U should be calculated, corresponding to each side of the joint, and the maximum one selected.
5. Apart from DT/X joints with $b > 0.9$, Q_f may be set to unity if the magnitude of the chord axial tension stress is greater than the maximum combined stress due to chord moments.

Table 3.3: Chord load Factor Q_f

Joints Types	Chord Load Case	Brace Load Case						
		Comp	Ten	IPB	OPB	Balanced Axial	Unbalanced Axial	Ref.
T/Y	Comp	1		1	1			3.1
	Comp+IPB	1		1	1			3.1
DT/X	Comp	1						3.1
	Comp	2		1	1			3.2
	Comp		1					3.3
	Comp	2		1	1			3.4
	Comp	9						3.5
	Ten	9						3.5
	Comp+IPB	1		1	1			3.2
	Comp+IPB	1		1				3.4
K	Comp					9		3.6
	IPB						10	3.7
YT	Comp					22		3.8

Table 3.4: Steel Tubular Joint Database with Full Pδ and/or Mθ Information for Chord Stress Effect

Reference	β	γ	Brace Load	Chord Load	Chord Stress
Boone et al (3.2)	0.67	25	Compression Compression IPB IPB OPB OPB	Compression Comp + IPB Compression Comp + IPB Compression Comp + IPB	0.6 F_y 0.8 F_y 0.6 F_y 0.6 F_y 0.6 F_y 0.6 F_y 0.6 F_y
Weinstein/ Yura (3.4)	0.35 1.0	25 25	Compression Compression Compression IPB IPB OPB	Compression Comp + IPB Compression Compression Comp + IPB Compression	0.65 F_y 0.65 F_y 0.65 F_y 0.6 F_y 0.6 F_y 0.6 F_y
Sanders/Yura (3.3)	1.0	25	Tension	Compression	0.6 F_y
Togo (3.5)	0.48	16.0	Compression	Compression Tension	0.32 F_y, 0.65 F_y, 0.97 F_y 0.32 F_y, 0.65 F_y, 0.97 F_y
Frames Phase I (Frame II)	1.0	16.5	Compression	Tension	(Varied during frame test)
Frames Phase I (Isolated Test II)	1.0	18.7	Compression	Tension	(Varied during test to simulate frame chord loading)
Frames Phase II (Frame V & Frame VI)	1.0 1.0	18.7 18.7	Compression Tension	Tension Compression	(Varied during test) (Varied during test)
Frames Phase II (Isolated Test VI)	1.0	18.7	Tension	Compression	(Varied during tests to simulate frame chord loading)

Table 3.5: Screened Steel Tubular Joint DT/X Database with Full Pδ and/or Mθ Information for Chord Stress Effect

Model: Frame X		Initial Classification			Class. after Iter. 1			Class. after Iter. 2			Class. after Iter. 3			Class. after Iter. 4			Class. after Iter. 5		
Node	Member	K	X	Y	K	X	Y	K	X	Y	K	X	Y	K	X	Y	K	X	Y
4	7	Rigid Joints Assumed			0%	0%	100%	0%	0%	100%	0%	0%	100%	0%	0%	100%	0%	0%	100%
	6				0%	0%	100%	0%	0%	100%	0%	0%	100%	0%	0%	100%	0%	0%	100%
2	5				0%	0%	100%	22%	0%	78%	24%	0%	76%	24%	0%	76%	24%	0%	76%
	10				0%	0%	100%	100%	0%	0%	100%	0%	0%	100%	0%	0%	100%	0%	0%
12	6				0%	100%	0%	0%	86%	14%	0%	63%	37%	0%	57%	43%	0%	56%	44%
	9				0%	69%	31%	0%	100%	0%	0%	100%	0%	0%	100%	0%	0%	100%	0%
9	7				100%	0%	0%	100%	0%	0%	100%	0%	0%	100%	0%	0%	100%	0%	0%
	8				76%	0%	24%	74%	0%	26%	73%	0%	27%	72%	0%	28%	72%	0%	28%
7	9				5%	0%	95%	0%	0%	100%	0%	0%	100%	0%	0%	100%	0%	0%	100%
	10				100%	0%	0%	0%	0%	100%	0%	0%	100%	0%	0%	100%	0%	0%	100%

Model: Frame X		Initial Classification			Class. after Iter. 1			Class. after Iter. 2			Class. after Iter. 3			Class. after Iter. 4		
Node	Member	K	X	Y	K	X	Y	K	X	Y	K	X	Y	K	X	Y
4	7	50%	50%	0%	0%	0%	100%	0%	0%	100%	0%	0%	100%	0%	0%	100%
	6	50%	50%	0%	0%	0%	100%	0%	0%	100%	0%	0%	100%	0%	0%	100%
2	5	50%	50%	0%	21%	0%	79%	24%	0%	76%	24%	0%	76%	24%	0%	76%
	10	50%	50%	0%	100%	0%	0%	100%	0%	0%	100%	0%	0%	100%	0%	0%
12	6	50%	50%	0%	0%	77%	23%	0%	61%	39%	0%	57%	43%	0%	56%	44%
	9	50%	50%	0%	0%	100%	0%	0%	100%	0%	0%	100%	0%	0%	100%	0%
9	7	50%	50%	0%	100%	0%	0%	100%	0%	0%	100%	0%	0%	100%	0%	0%
	8	50%	50%	0%	68%	0%	32%	72%	0%	28%	72%	0%	28%	72%	0%	28%
7	9	50%	50%	0%	0%	0%	100%	0%	0%	100%	0%	0%	100%	0%	0%	100%
	10	50%	50%	0%	0%	0%	100%	0%	0%	100%	0%	0%	100%	0%	0%	100%

Model: Frame X		Initial Classification			Class. after Iter. 1			Class. after Iter. 2			Class. after Iter. 3		
Node	Member	K	X	Y	K	X	Y	K	X	Y	K	X	Y
4	7	0%	0%	100%	0%	0%	100%	0%	0%	100%	0%	0%	100%
	6	0%	0%	100%	0%	0%	100%	0%	0%	100%	0%	0%	100%
2	5	0%	0%	100%	18%	0%	82%	24%	0%	76%	24%	0%	76%
	10	0%	0%	100%	100%	0%	0%	100%	0%	0%	100%	0%	0%
12	6	0%	0%	100%	0%	69%	31%	0%	59%	41%	0%	56%	44%
	9	0%	0%	100%	0%	100%	0%	0%	100%	0%	0%	100%	0%
9	7	0%	0%	100%	100%	0%	0%	100%	0%	0%	100%	0%	0%
	8	0%	0%	100%	64%	0%	36%	72%	0%	28%	72%	0%	28%
7	9	0%	0%	100%	0%	0%	100%	0%	0%	100%	0%	0%	100%
	10	0%	0%	100%	0%	0%	100%	0%	0%	100%	0%	0%	100%

= Convergence not reached

Table 4.1: Comparison of Load Classification Convergence Rate using 3 Different Initial Assumptions for X-Braced Frame

Model: Frame K		Initial Classification			Class. after Iter. 1			Class. after Iter. 2			Class. after Iter. 3			Class. after Iter. 4		
Node	Member	K	X	Y	K	X	Y	K	X	Y	K	X	Y	K	X	Y
4	5	0%	0%	100%	0%	0%	100%	0%	0%	100%	0%	0%	100%	0%	0%	100%
	6	0%	0%	100%	0%	0%	100%	0%	0%	100%	0%	0%	100%	0%	0%	100%
2	7	0%	0%	100%	0%	0%	100%	0%	0%	100%	0%	0%	100%	0%	0%	100%
18	6	0%	0%	100%	57%	0%	43%	100%	0%	0%	95%	0%	5%	96%	0%	4%
	9	0%	0%	100%	100%	0%	0%	98%	0%	2%	100%	0%	0%	100%	0%	0%
9	5	0%	0%	100%	71%	0%	29%	100%	0%	0%	100%	0%	0%	100%	0%	0%
	9	0%	0%	100%	100%	0%	0%	95%	0%	5%	96%	0%	4%	96%	0%	4%
7	8	0%	0%	100%	0%	0%	100%	0%	0%	100%	0%	0%	100%	0%	0%	100%

Note: [ ] = Convergence not reached

Table 4.2: Load Classification Convergence Results using Initial Y Joint Assumption for K-Braced Frame

β	Ultimate		Cracking	
	T	DT	T	DT
0.4	53.57	30.74	13.79	5.69
0.8	-	19.34	7.41	4.72

Table 6.1: Equivalent Plastic Strains (%) at Cracking Load and Deformation Load

stresses is captured, and also the different effect of chord bending stresses as compared to chord compression stresses. This is also reflected in Table 8.1, which compares the Q_f factors predicted by MSLJOINT to the Q_f factors reported by Boone.

Tests (Reference 8.1)					MSLJOINT				
σ_{Ax}/f_y	σ_{Beu}/f_y	Q_f axial	Q_f IPB	Q_f OPB	P/Pu	M/Mp	Q_f axial	Q_f IPB	Q_f OPB
.0	.0	1	1	1	0	0	1	1	1
-.32	.28	0.84	0.75	0.88	-.32	.28	0.82	0.73	0.81
-.6	0	0.73	0.57	0.81	-.6	0	0.73	0.60	0.81
-.8	0	0.53	-	-	-.8	0	0.52	0.28	0.66

Table 8.1: Test[8.1] and predicted Q_f factors

8.5 Combined Loading

8.5.1 Initial calibration

The performance of the joint algorithm under combined loading is evaluated against relevant test data. Initial calibration is based on test data from Stol et.al.[8.2, 8.3 and 8.4], for combined Axial and IPB loading of tubular T-joints with $\beta=0.36$ and $\gamma=15$ (test specimens 1, 6, 7 and 8).

Pδ characteristics and Mθ characteristics from the tests are shown in Figure 8.13 and Figure 8.14. These figures also show the analytical predictions for uni-axial loading.

The T joint geometry was modelled in USFOS (5 nodes, 3 beam elements, 1 "joint" element), and eccentric compression loading applied to the brace end. This is illustrated in Figure 8.15. The resulting numerical predictions are shown in Figures 8.16 to 8.19.

The initial analyses (Figure 8.16 and Figure 8.17) showed little resemblance with the test results. The analyses predicted significant interaction between bending moment and axial load, but overestimate the reduction in axial capacity caused by the presence of bending moments. Also, the post-peak load shedding is overestimated.

It could, however, be reasonably assumed that the numerical model would overestimate the P-Δ effects of the eccentric compression load. In the FE model, the brace end is free, with no lateral restraint whatsoever. In the tests the brace end would be connected to the hydraulic actuators, which would provide some (possibly significant) lateral restraint.

To evaluate the impact of the P-Δ effects, the analyses were repeated with the loads moved from the brace tip to the brace/chord intersection. Thus, the loads were acting directly on the "joint element" and the P-Δ effects were eliminated. The resulting numerical predictions are shown in Figure 8.18 and Figure 8.19.

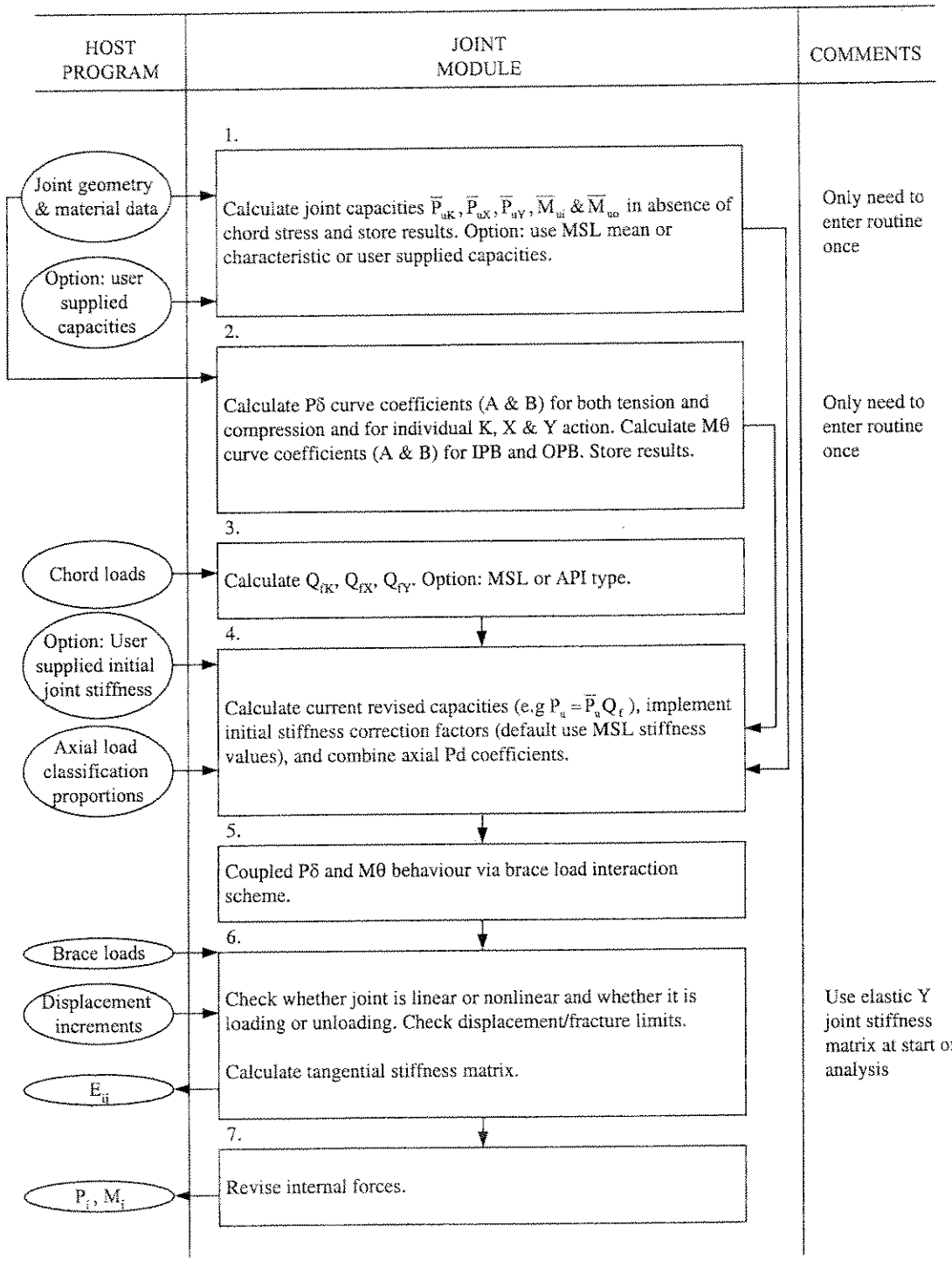

Figure 2.1: Flowchart

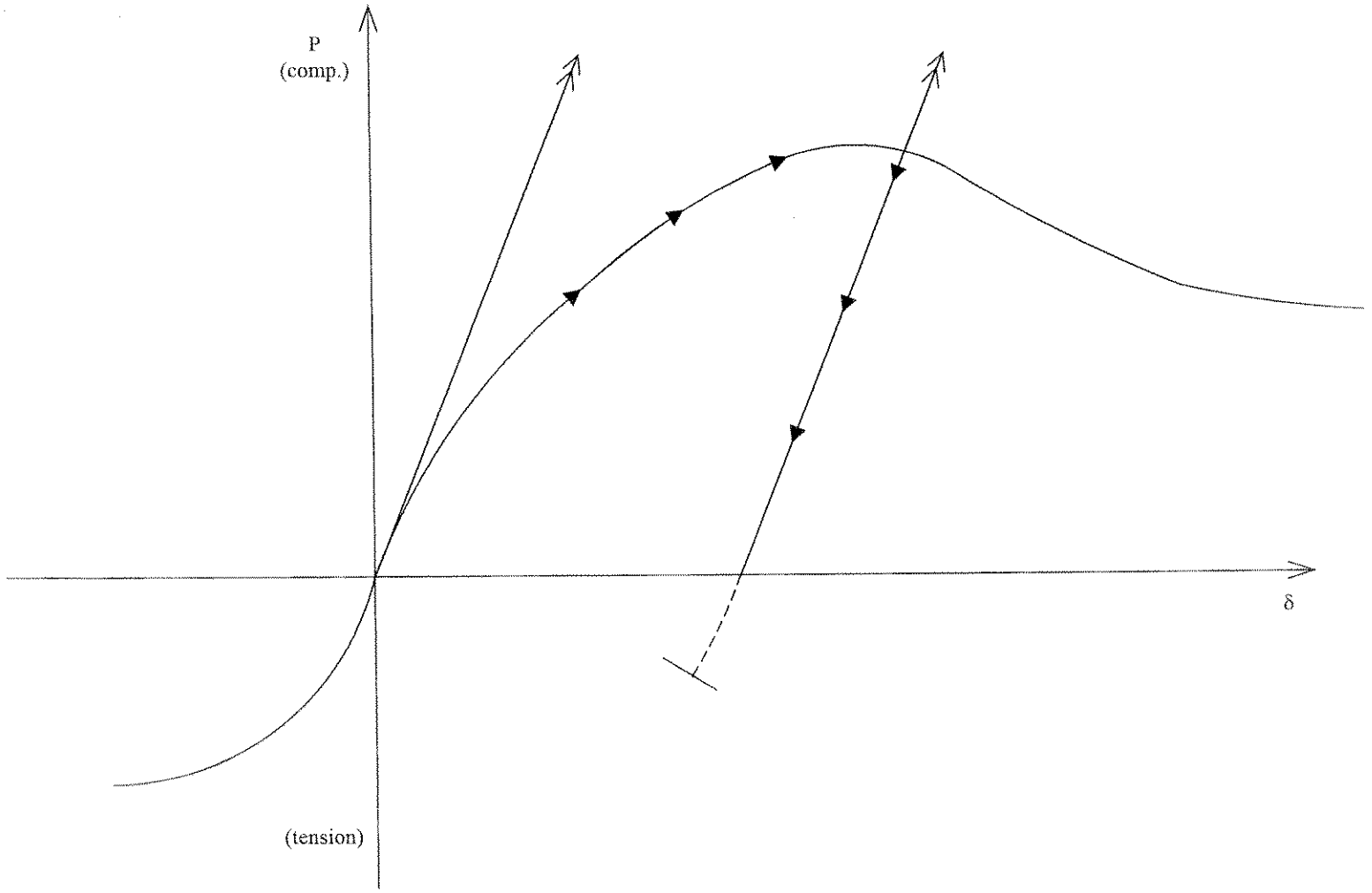

Figure 2.2: Unloading Behaviour

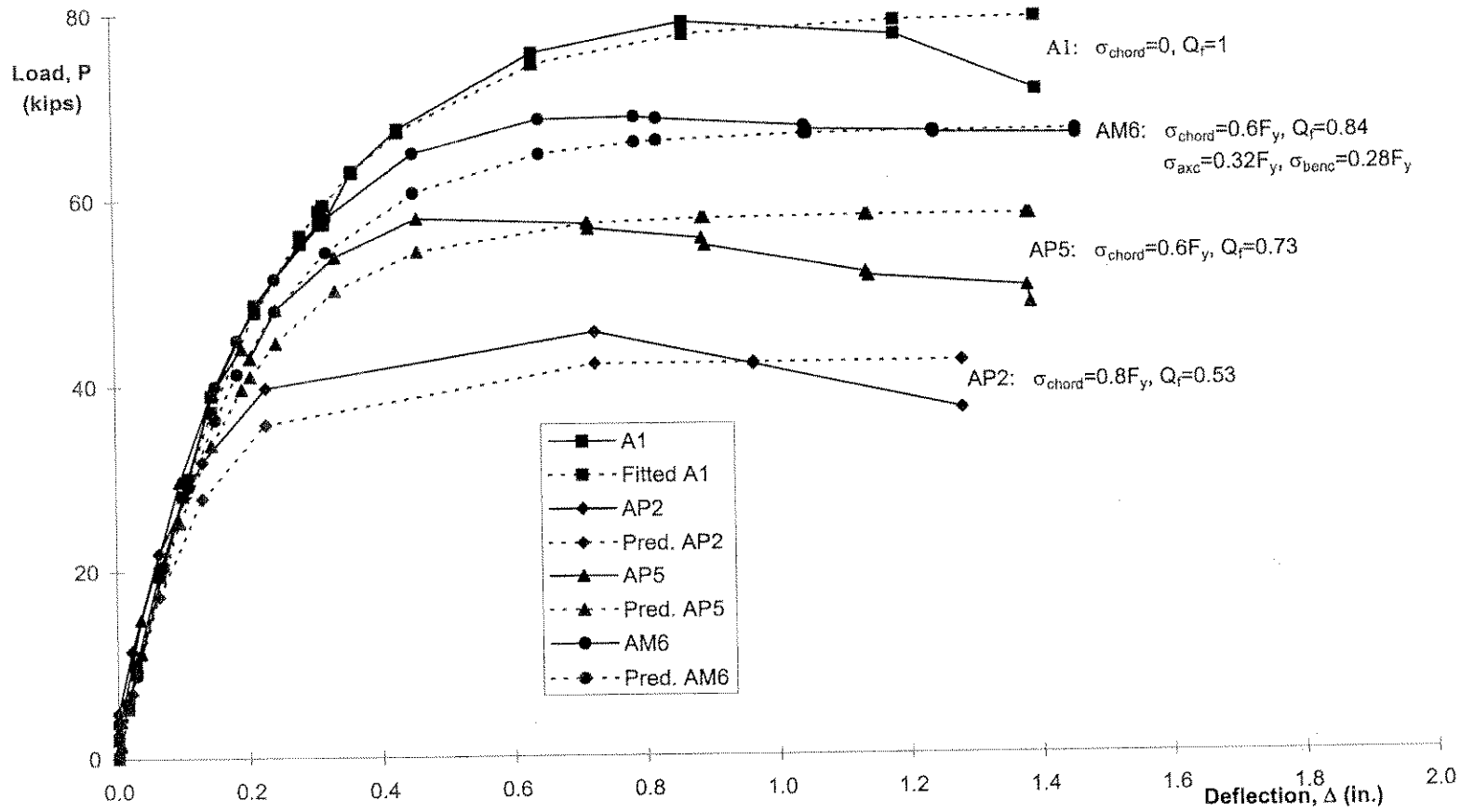

Figure 3.1: Compression Loaded DT (β = 0.67) Joints subjected to Varying Chord Compression Stress (Ref. 3.2)

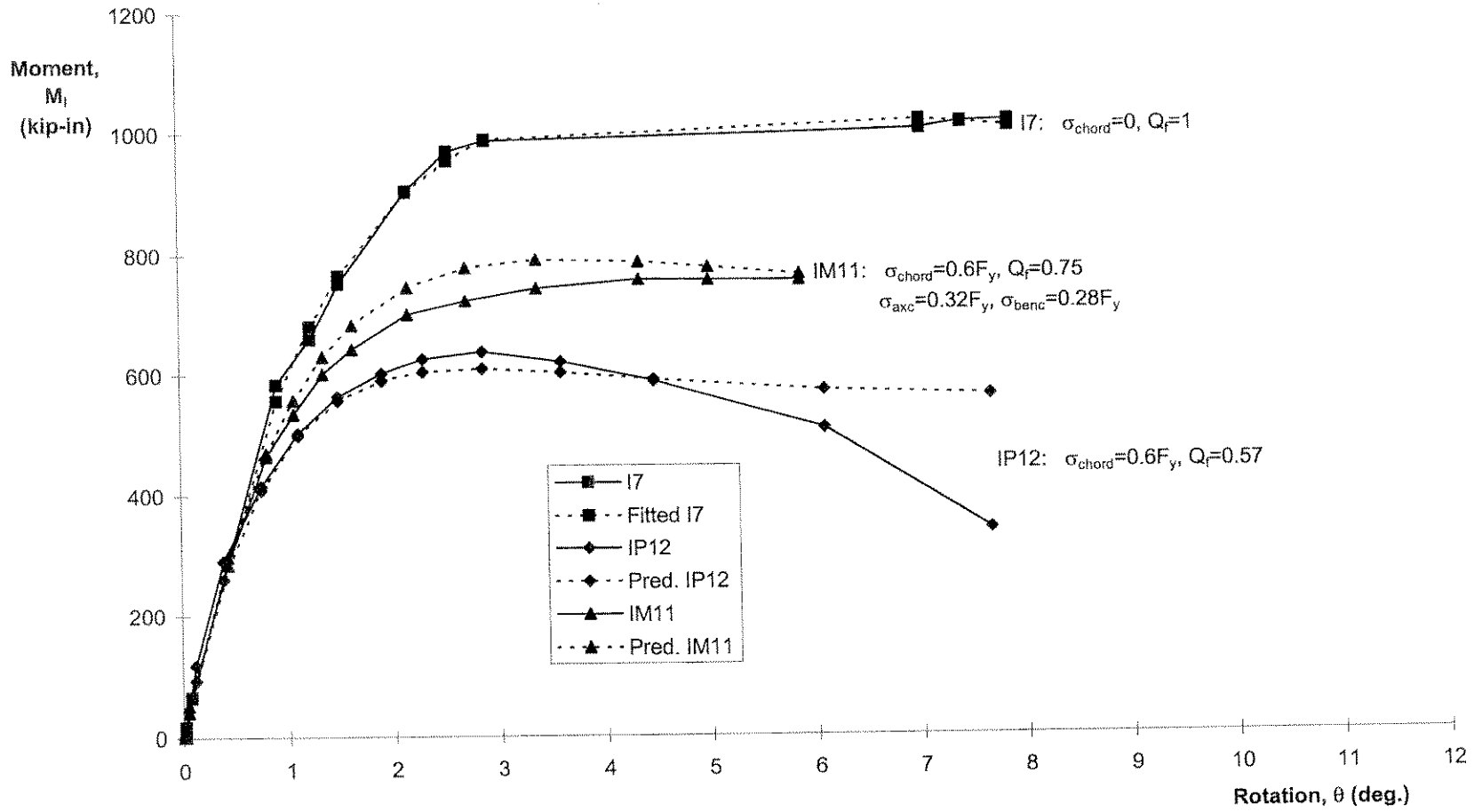

Figure 3.2: In-Plane Bending Loaded DT (β = 0.67) Joints subjected to Varying Chord Compression Stress (Ref. 3.2)

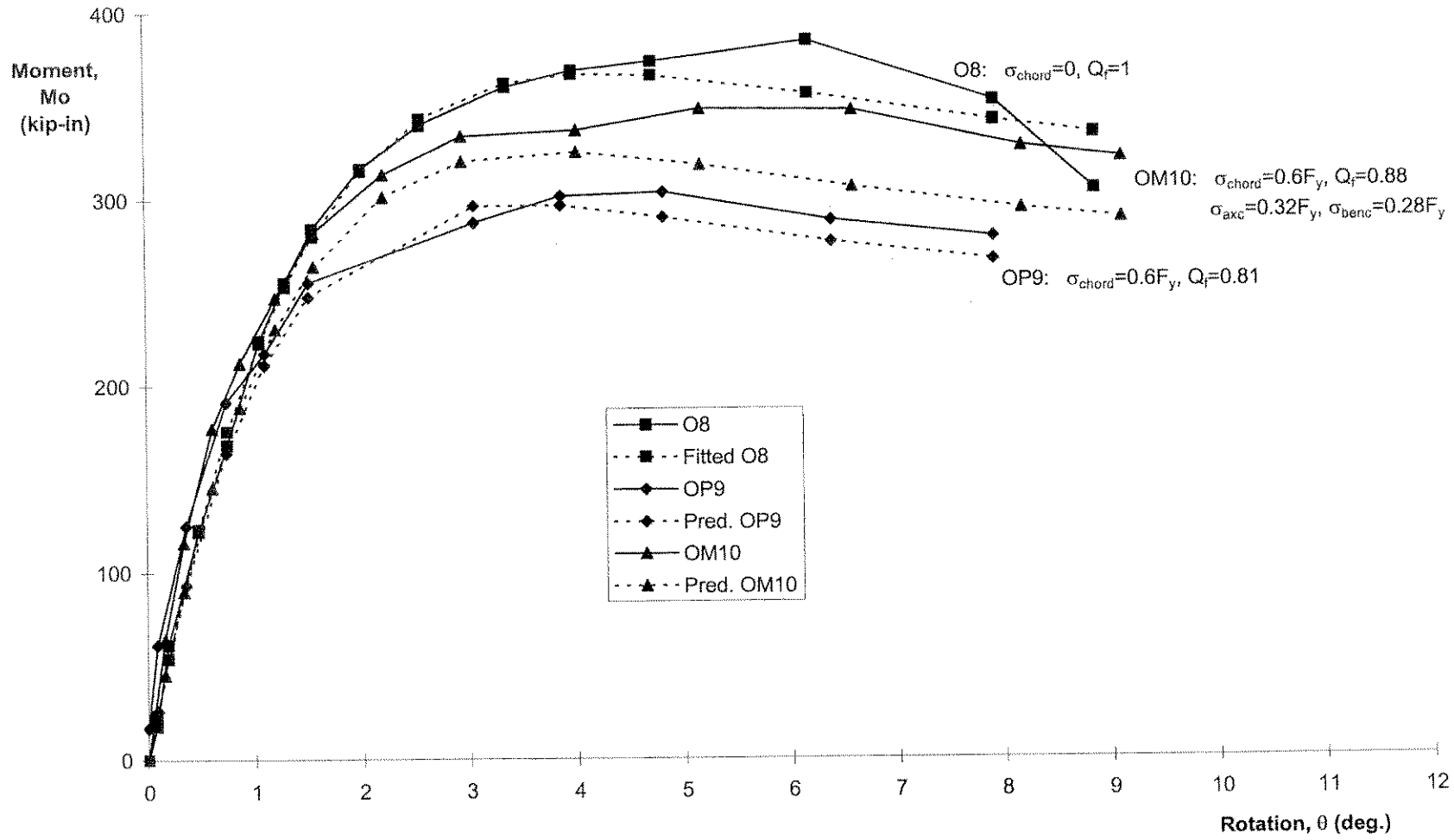

Figure 3.3: Out-of-Plane Bending Loaded DT (β = 0.67) Joints subjected to Varying Chord Compression Stress (Ref. 3.2)

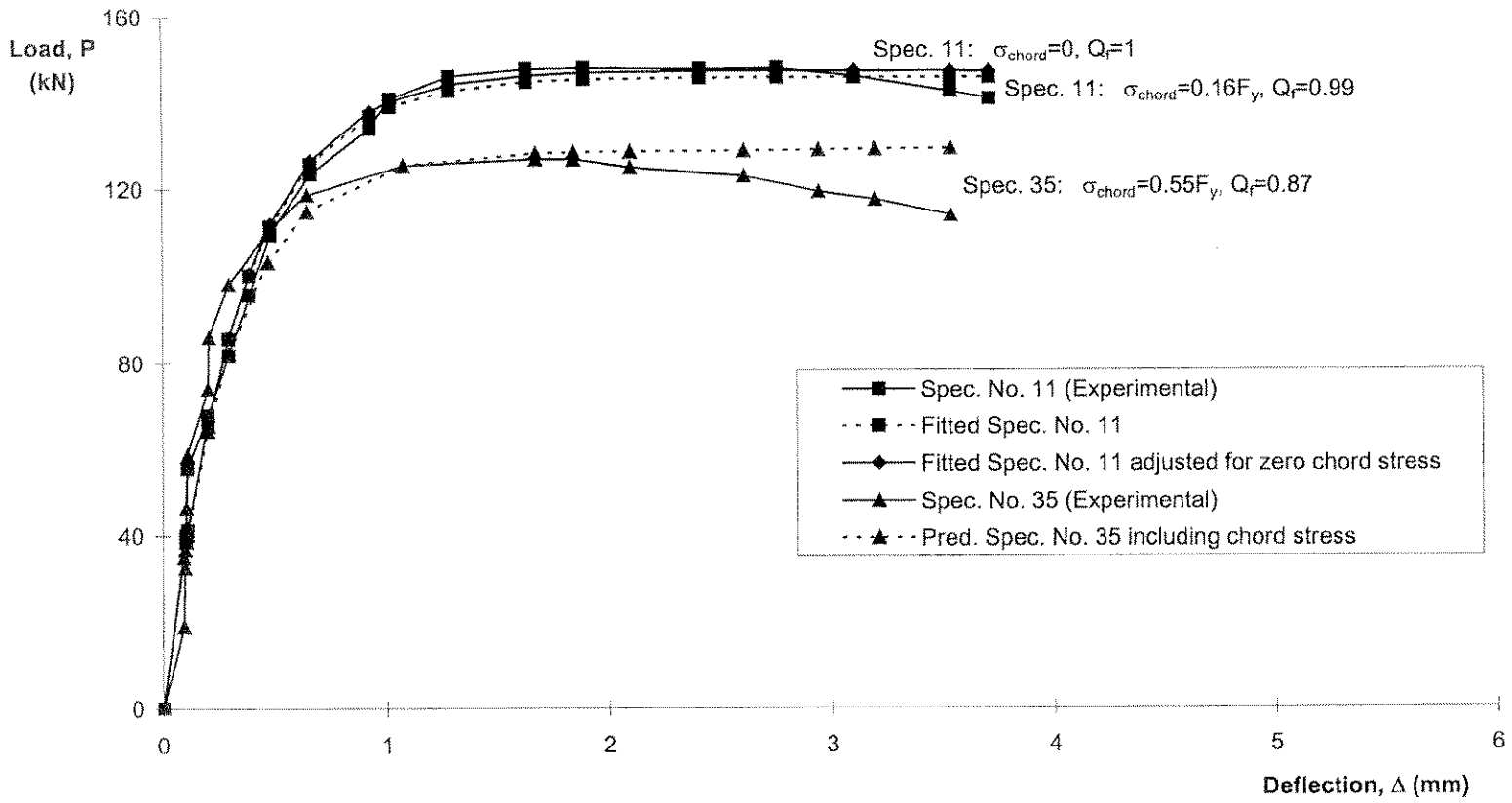

Figure 3.4: Compression Loaded Brace of K ($\beta = 0.33$) Joints subjected to Varying Chord Compression Stress (Ref. 3.6)

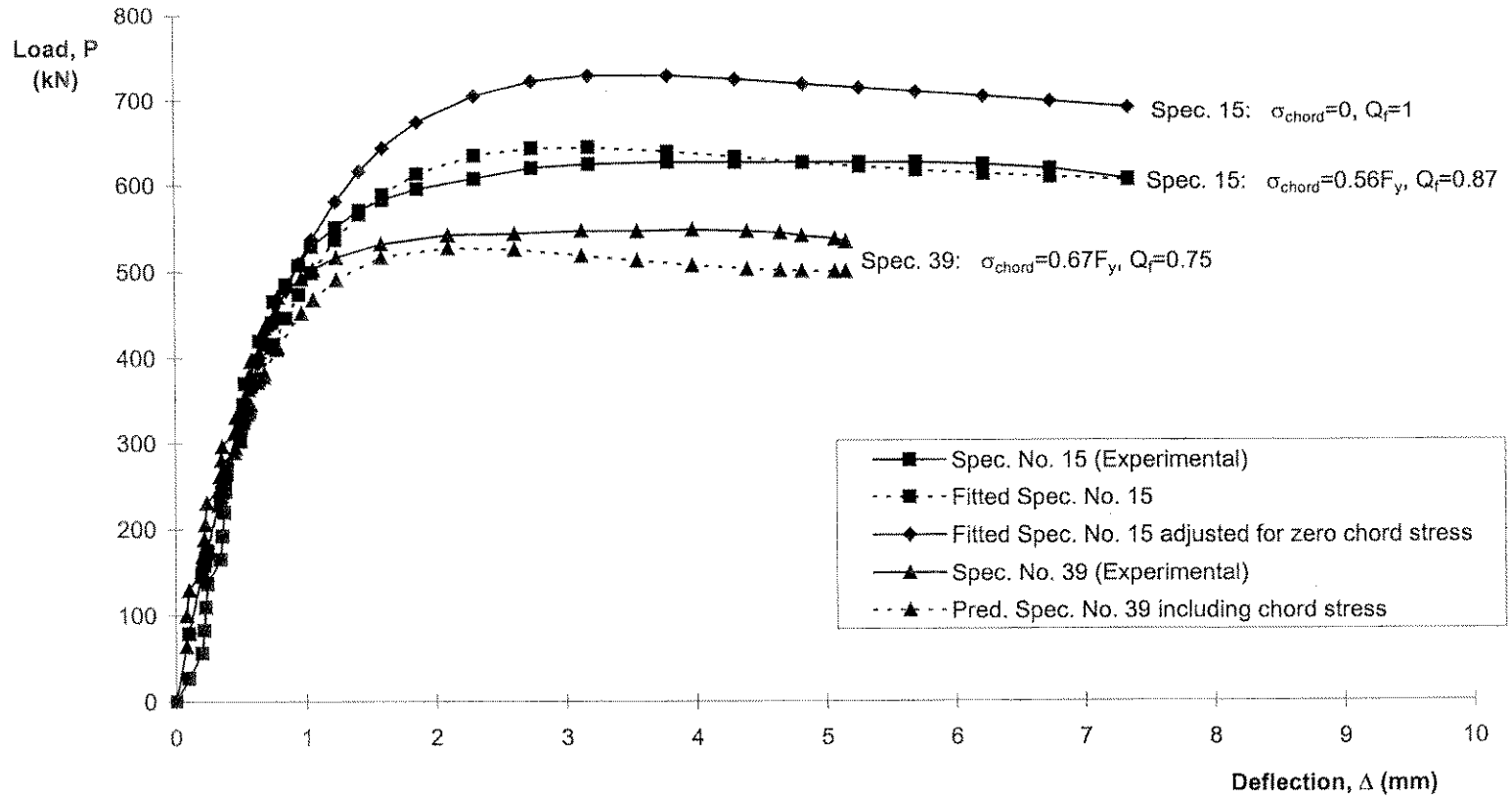

Figure 3.5: Compression Loaded Brace of K (β = 1) Joints subjected to Varying Chord Compression Stress (Ref. 3.6)

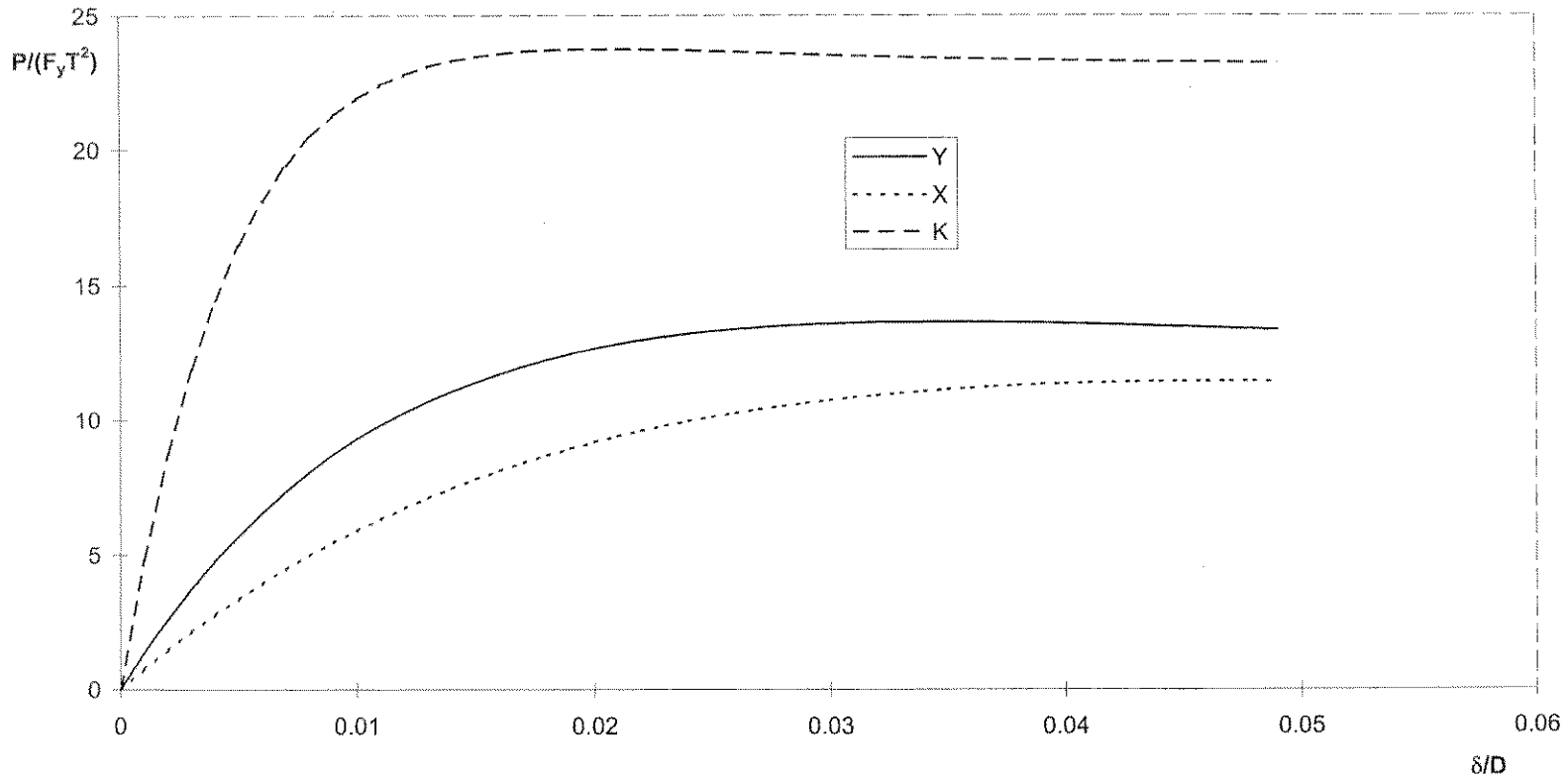

Figure 4.1: Comparison of Non-Dimensional Load Deformation Curves for Different Joint Types ($\beta = 0.3$, $\gamma = 25$ and $\theta = 45°$)

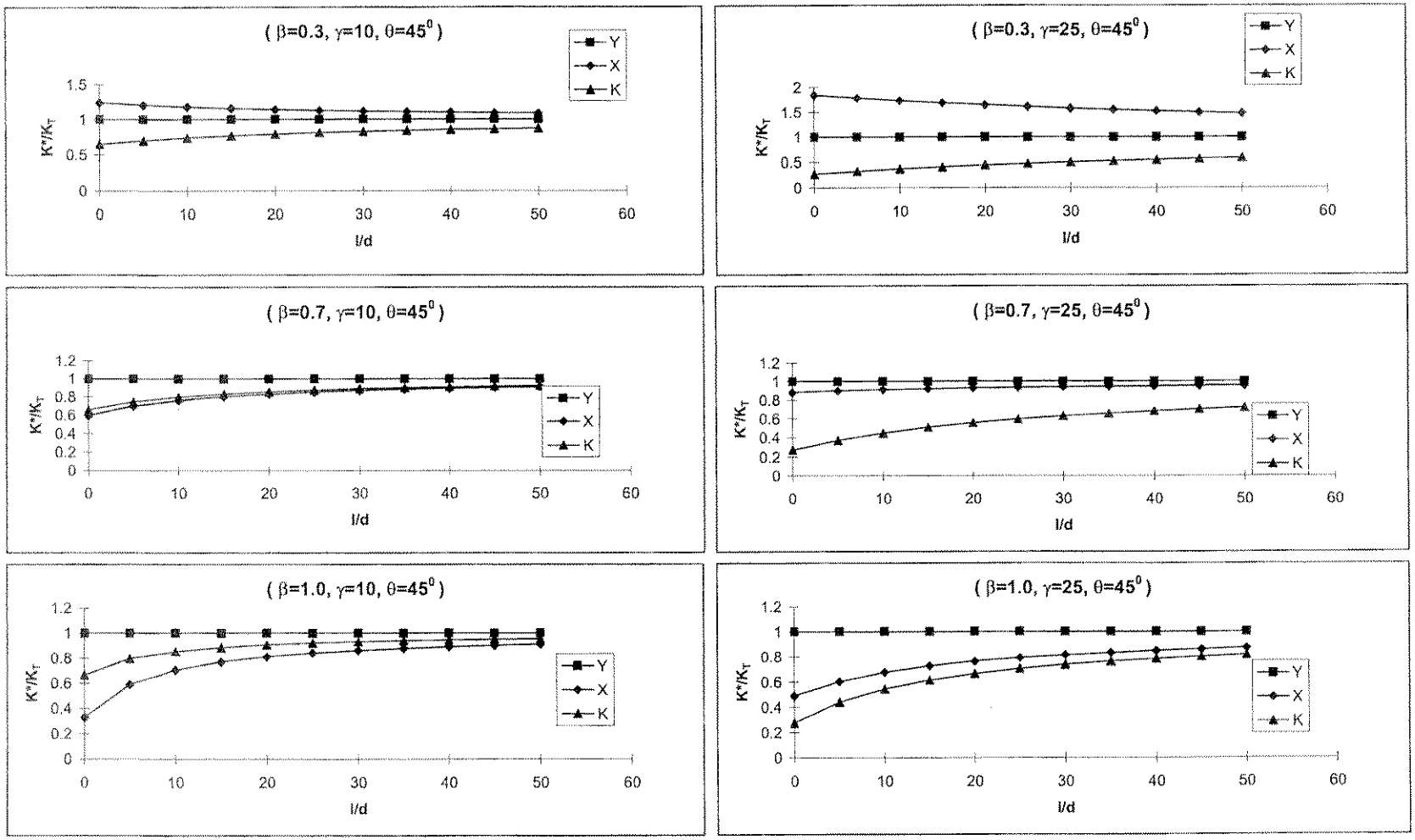

Figure 4.2: Comparison of Stiffness of Joint Plus Associated Brace for Different Joint Types

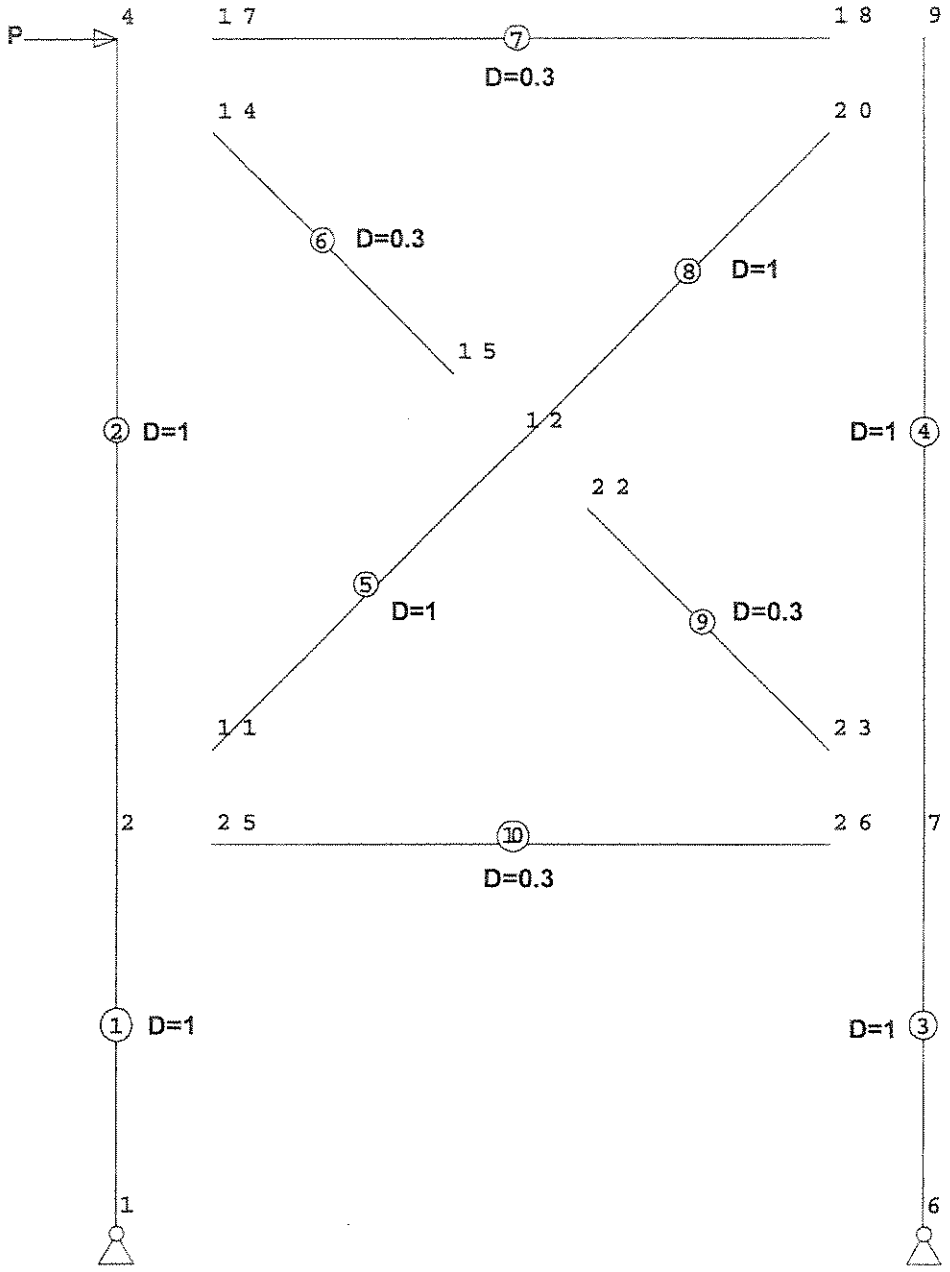

Figure 4.3: Node and Element Numbers of X-Braced Frame

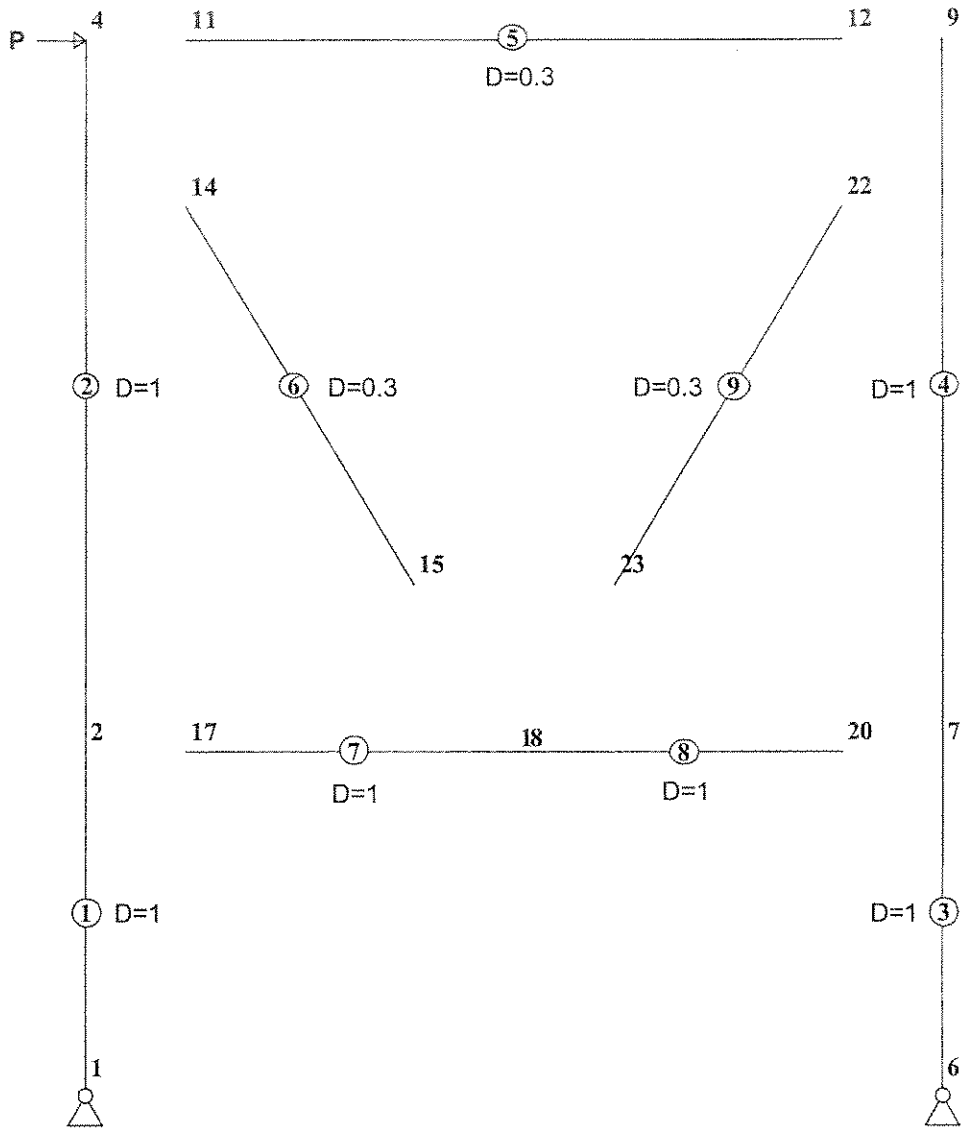

Figure 4.4: Node and Element Numbers of K-Braced Frame

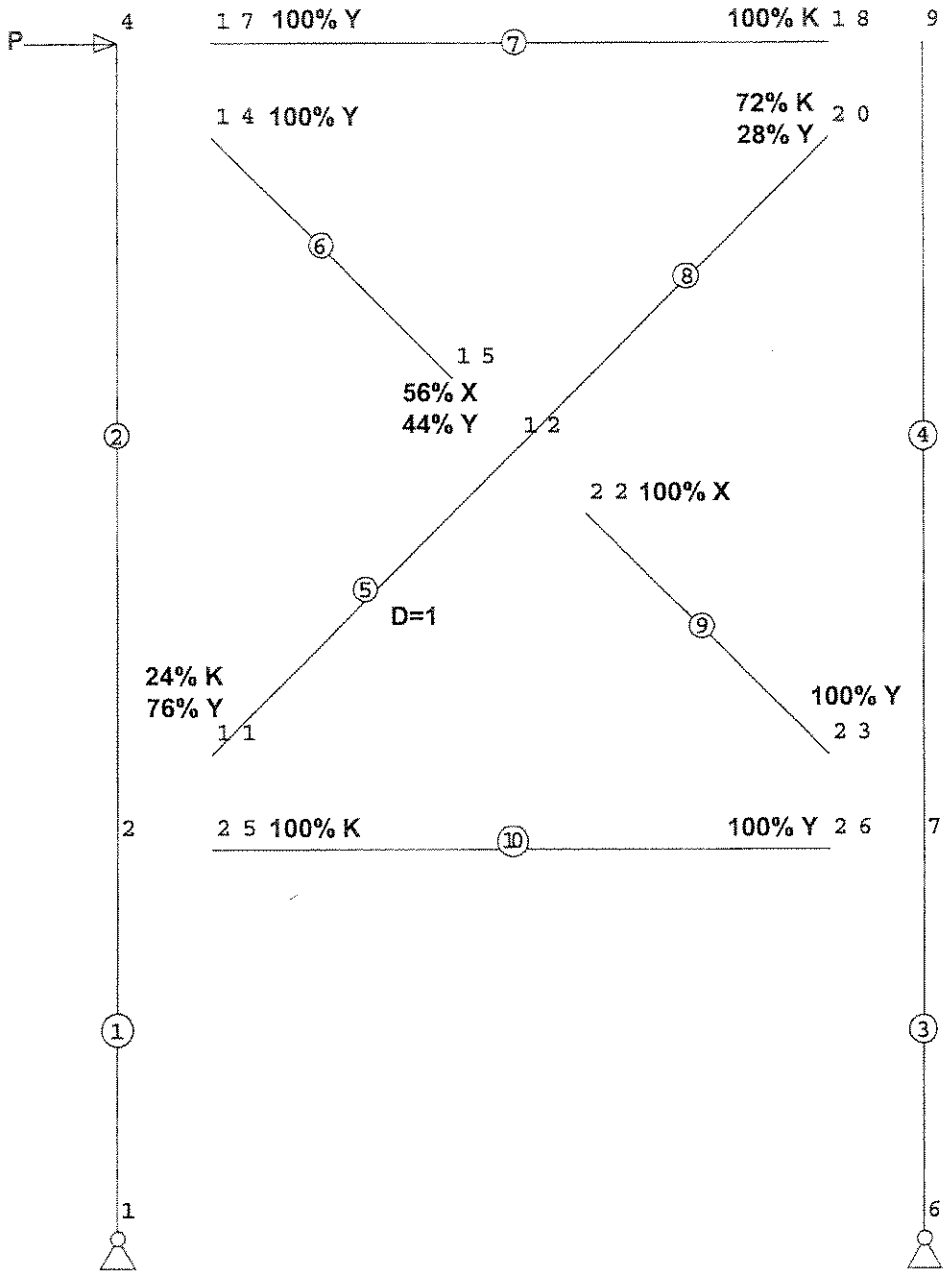

Figure 4.5: Final Joint Classifications for X-Braced Frame

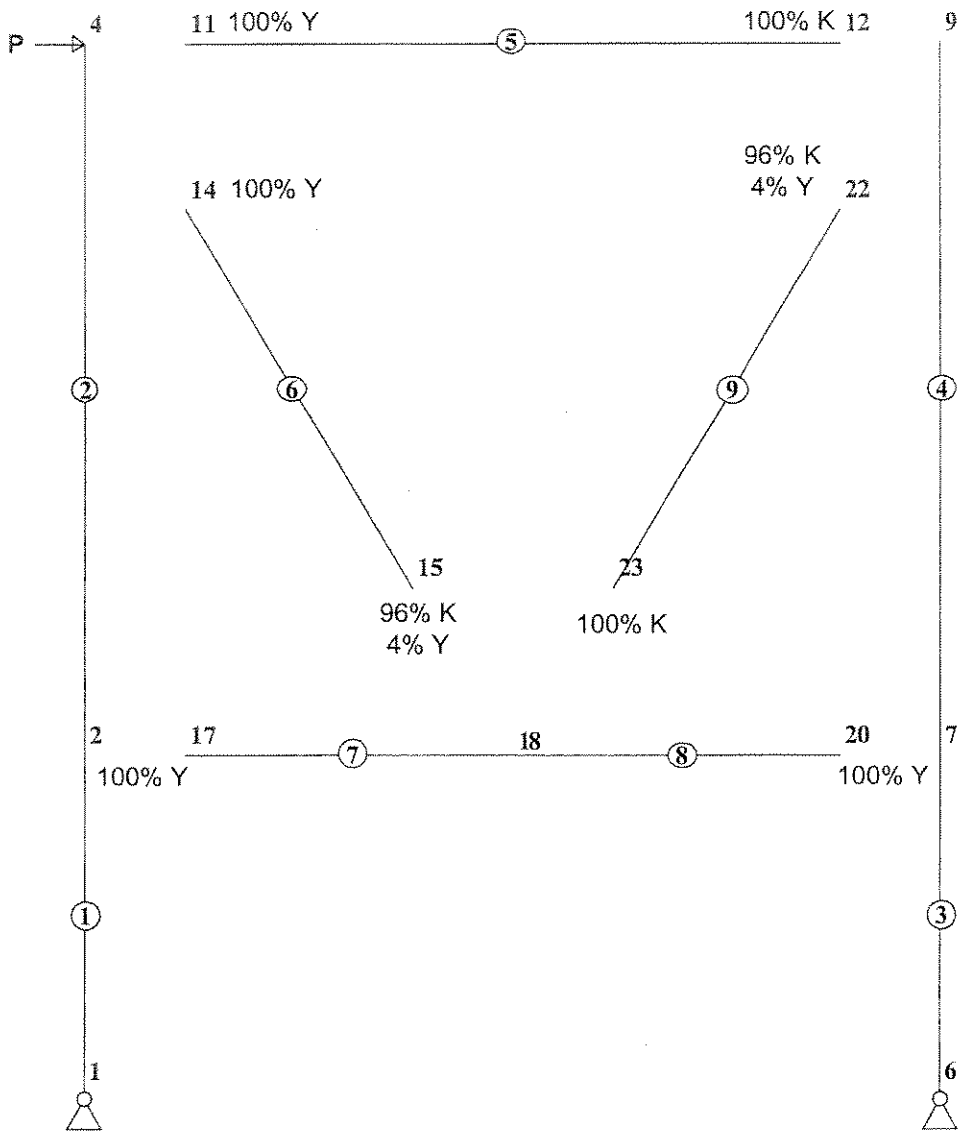

Figure 4.6: Final Joint Classifications for K-Braced Frame

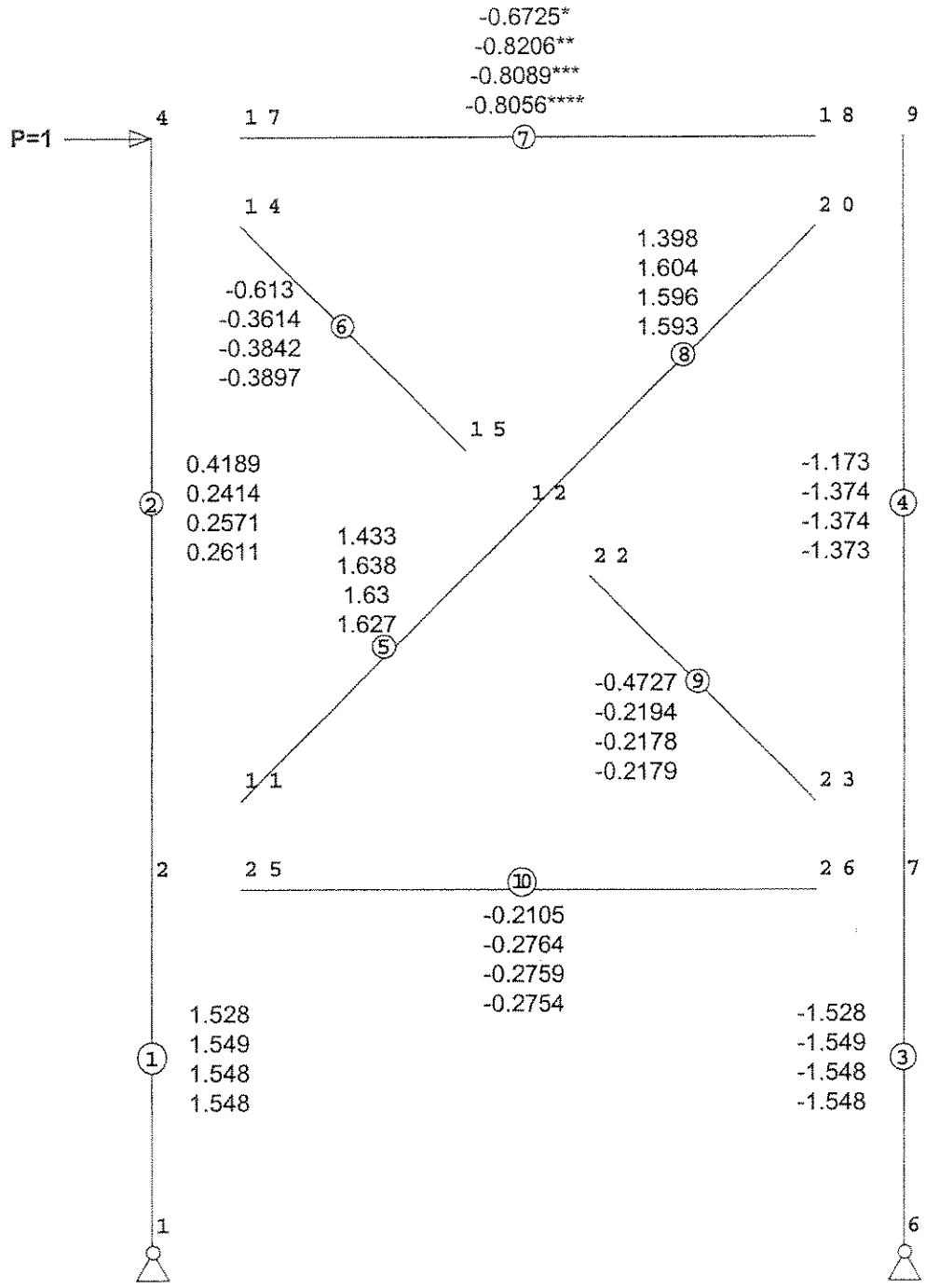

Note: Number of * represents the iteration number.

Figure 4.7: Comparison of the Axial Load in Members in X-Braced Frame During the Iteration Process with Joint Stiffnesses Initially Taken as Average of K and X Joints

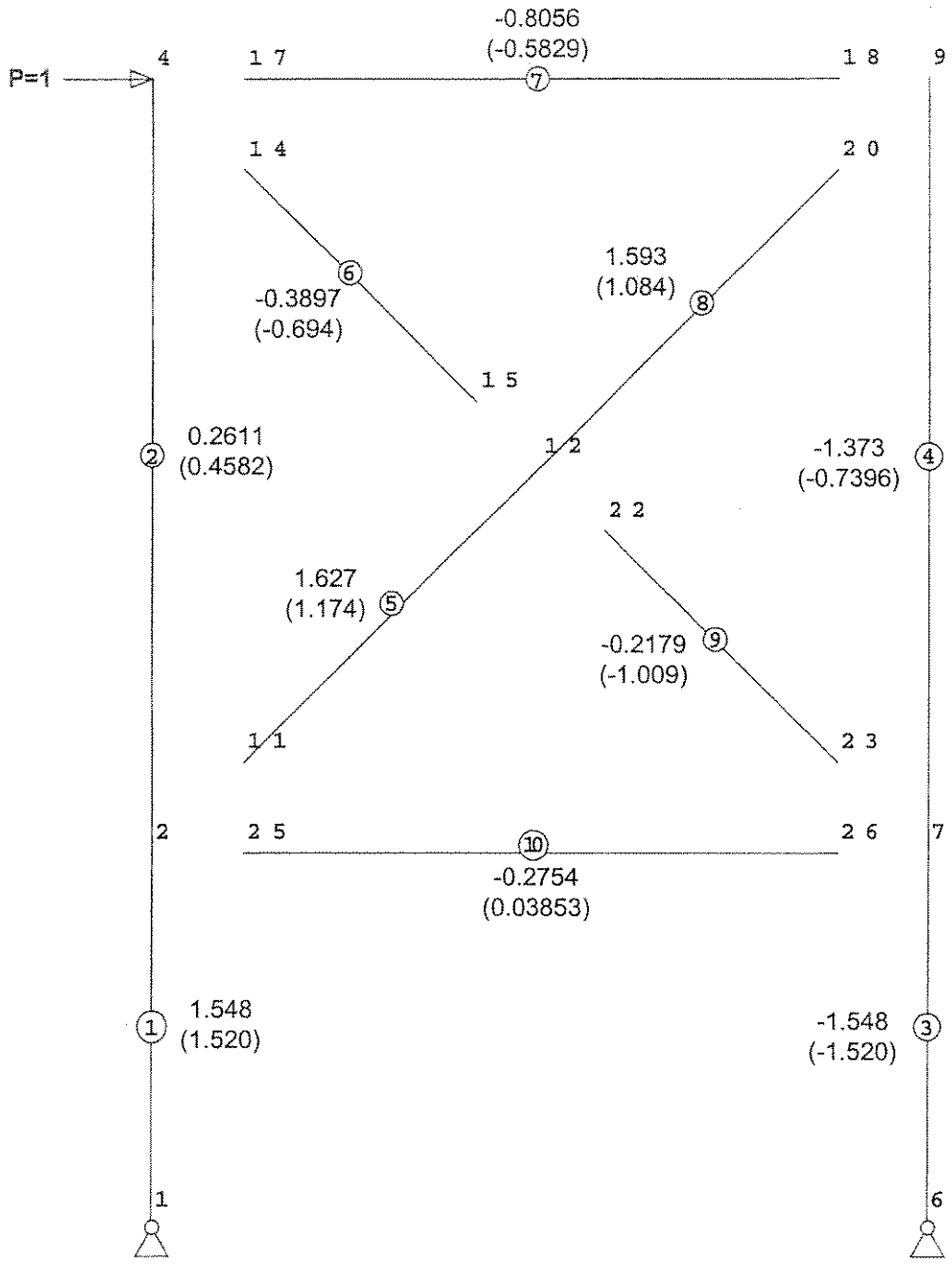

Note: Upper and lower numbers relate the frames with the appropriate LJFs and Rigid joints respectively.

Figure 4.8: Axial Forces in Members for X-Braced Frame

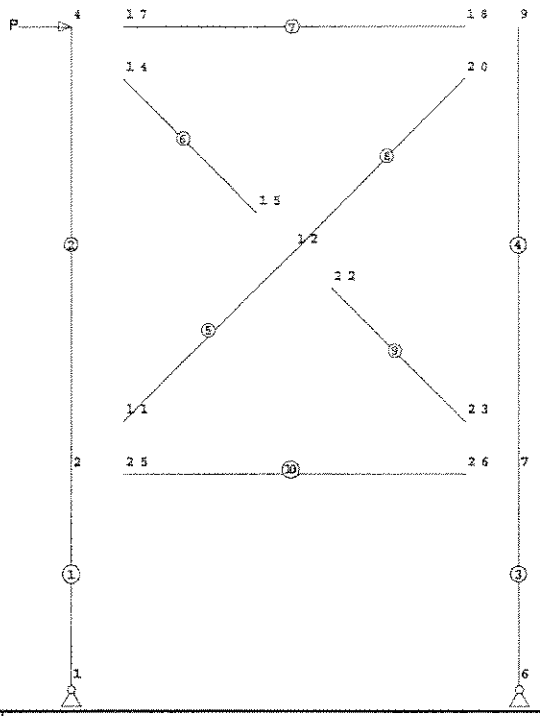

Model: Frame X		Force, Moment and Stress Ratios			Utilisation Ratio	
Member	Node	P_{LJF}/P_{Rigid}	M_{LJF}/M_{Rigid}	$\sigma_{LJF}/\sigma_{Rigid}$	$\sigma_{LJF}/\sigma_{max}$	$\sigma_{Rigid}/\sigma_{max}$
1	1	1.02	1.0	1.02	0.23	0.22
	2	1.02	1.15	1.12	1.00	0.89
2	2	0.57	1.17	1.04	0.32	0.31
	4	0.57	-0.10	0.45	0.04	0.09
3	6	1.02	1.0	1.02	0.23	0.22
	7	1.02	0.80	0.87	0.64	0.74
4	7	1.86	0.87	1.06	0.59	0.55
	9	1.86	-2.03	1.93	0.36	0.19
5	11	1.39	1.17	1.24	0.71	0.57
	12	1.39	12.88	2.56	0.49	0.19
6	14	0.56	0.72	0.63	0.38	0.60
	15	0.56	1.15	0.82	0.50	0.61
7	17	1.38	263.06	2.12	0.61	0.29
	18	1.38	-4.23	1.61	0.50	0.31
8	12	1.47	10.11	2.79	0.53	0.19
	20	1.47	-1.97	1.63	0.39	0.24
9	22	0.22	-0.71	0.34	0.22	0.66
	23	0.22	0.08	0.16	0.14	0.88
10	25	-7.15	0.85	1.17	0.43	0.37
	26	-7.15	0.62	0.93	0.37	0.40

Note: LJF data refer to the converged results.

Figure 4.9: Summary of Results Expressed as Ratios for X-Braced Frame

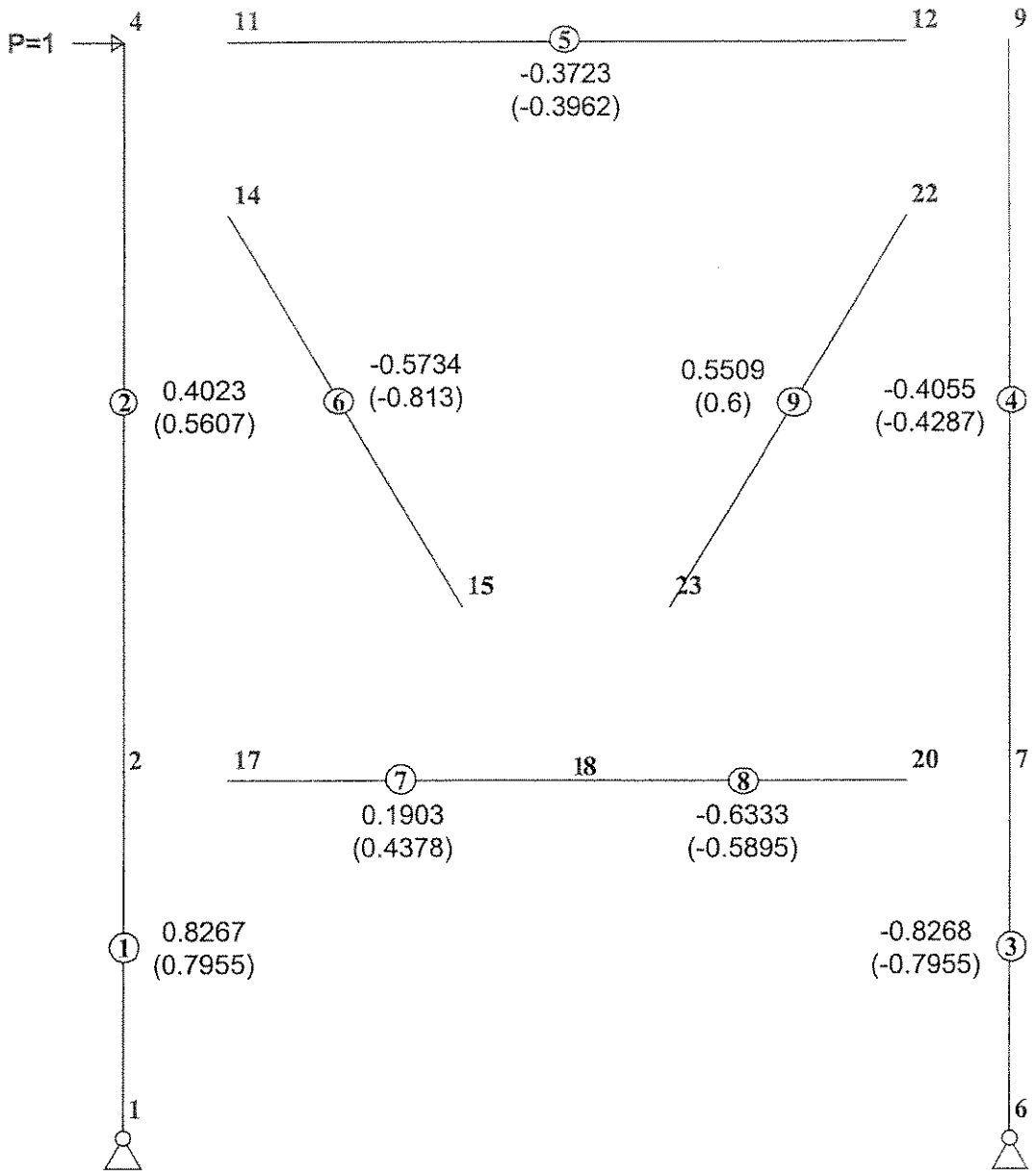

Note: Upper and lower numbers relate the frames with the appropriate LJFs and Rigid joints respectively.

Figure 4.10: Axial Forces in Members for K-Braced Frame

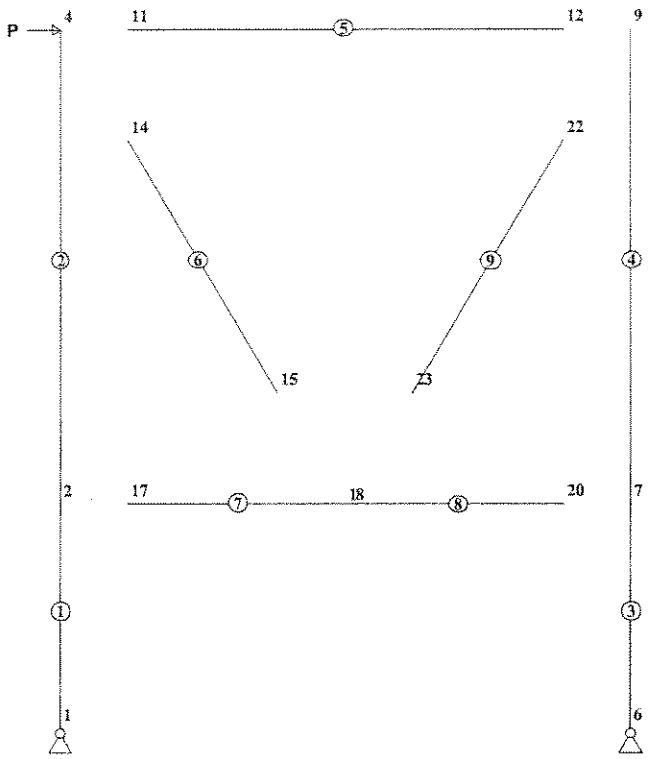

Model: Frame K		Force, Moment and Stress Ratios			Utilisation Ratio	
Member	Node	P_{LJF}/P_{Rigid}	M_{LJF}/M_{Rigid}	$\sigma_{LJF}/\sigma_{Rigid}$	$\sigma_{LJF}/\sigma_{max}$	$\sigma_{Rigid}/\sigma_{max}$
1	1	1.04	1.00	0.96	0.20	0.19
	2	1.04	0.88	1.08	0.56	0.61
2	2	0.72	28.54	0.32	0.46	0.15
	4	0.72	-26.57	1.02	0.13	0.13
3	6	1.04	1.00	0.96	0.20	0.19
	7	1.04	1.10	0.92	0.78	0.72
4	7	0.95	1.02	1.02	0.17	0.18
	9	0.95	3.30	0.86	0.13	0.11
5	11	0.94	2.36	0.69	0.72	0.49
	12	0.94	2.09	0.78	0.58	0.45
6	14	0.71	0.09	1.78	0.47	0.84
	15	0.71	1.53	1.00	1.00	1.00
7	17	0.43	1.69	0.69	0.78	0.54
	18	0.43	1.09	1.43	0.12	0.18
8	18	1.07	1.30	0.85	0.30	0.25
	20	1.07	1.11	0.91	0.65	0.59
9	22	0.92	-4.28	0.94	0.53	0.50
	23	0.92	2.27	0.88	0.64	0.57

Note: LJF data refer to the converged results.

Figure 4.11: Summary of Results Expressed as Ratios for K-Braced Frame

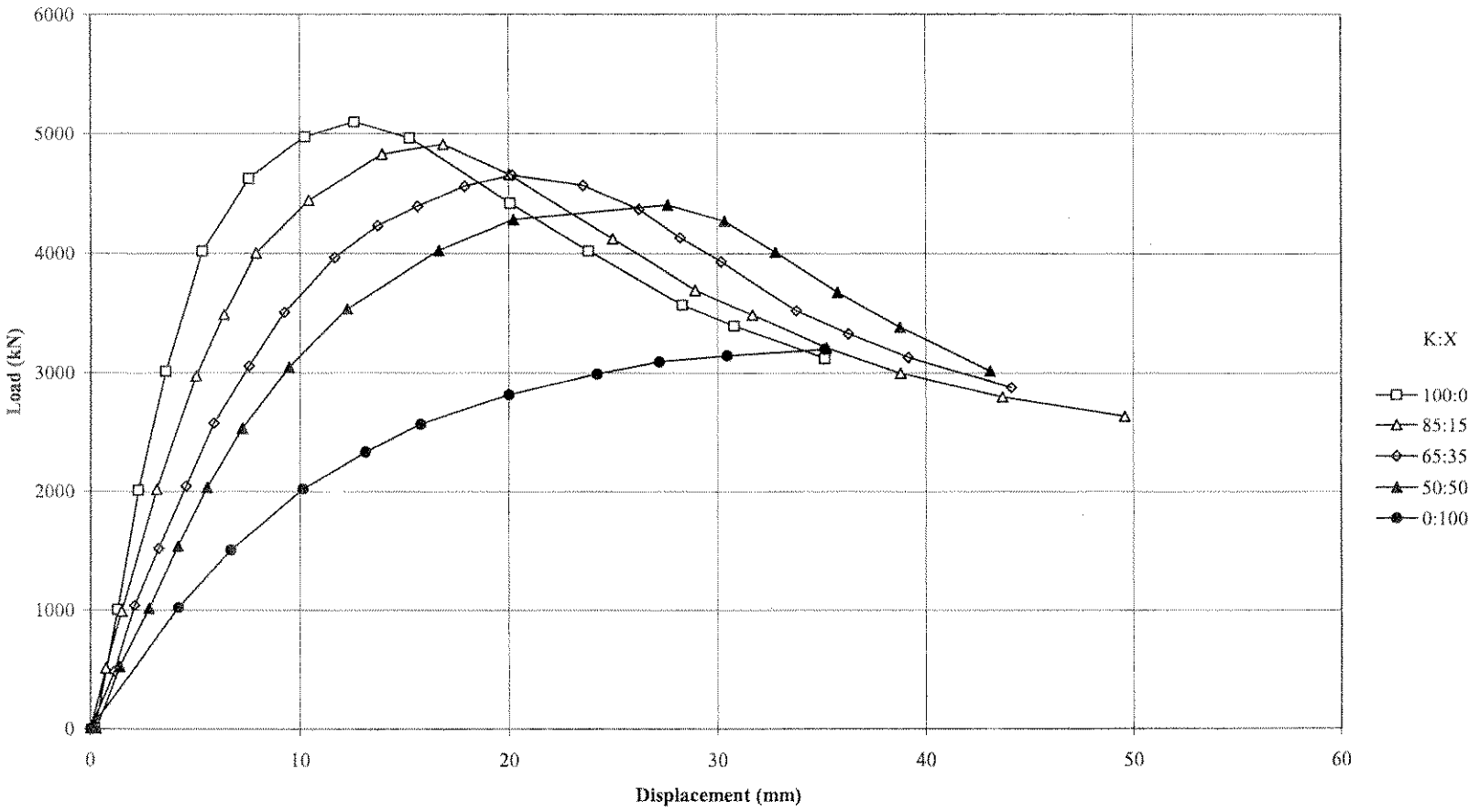

Figure 4.12: Load Displacement Curves for DK Joints, $\gamma = 30$

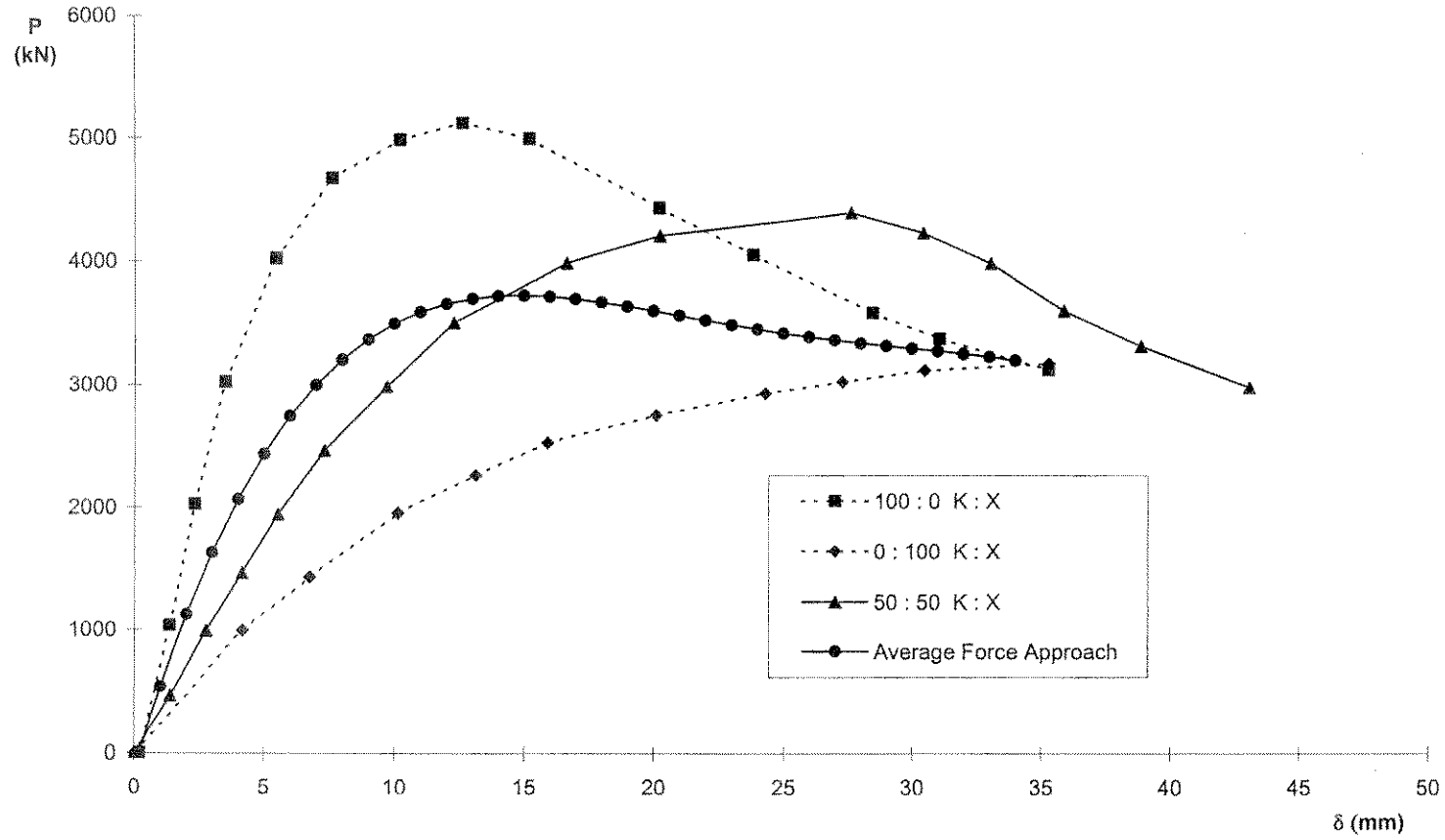

Figure 4.13: Average Force Approach

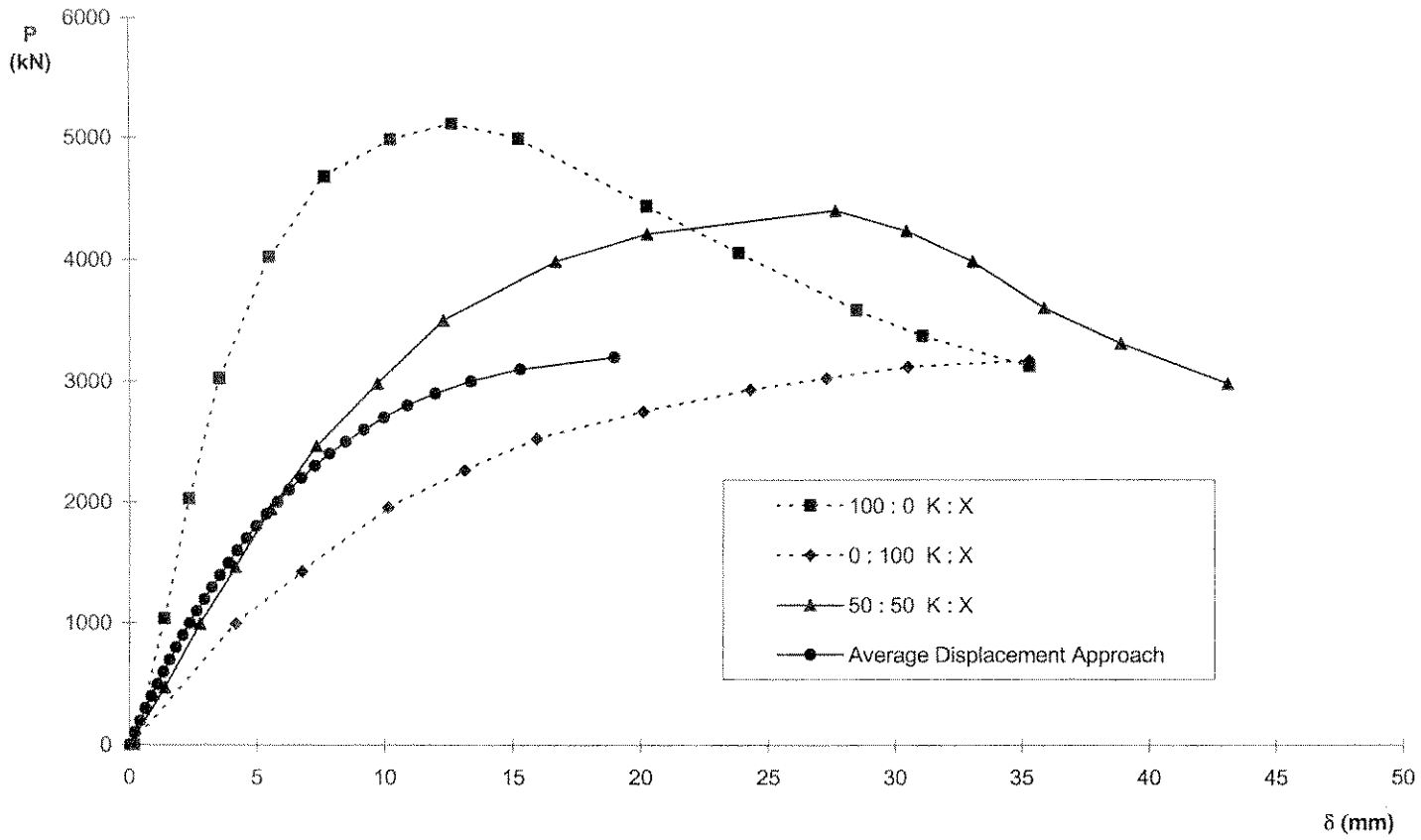

Figure 4.14: Average Displacement Approach

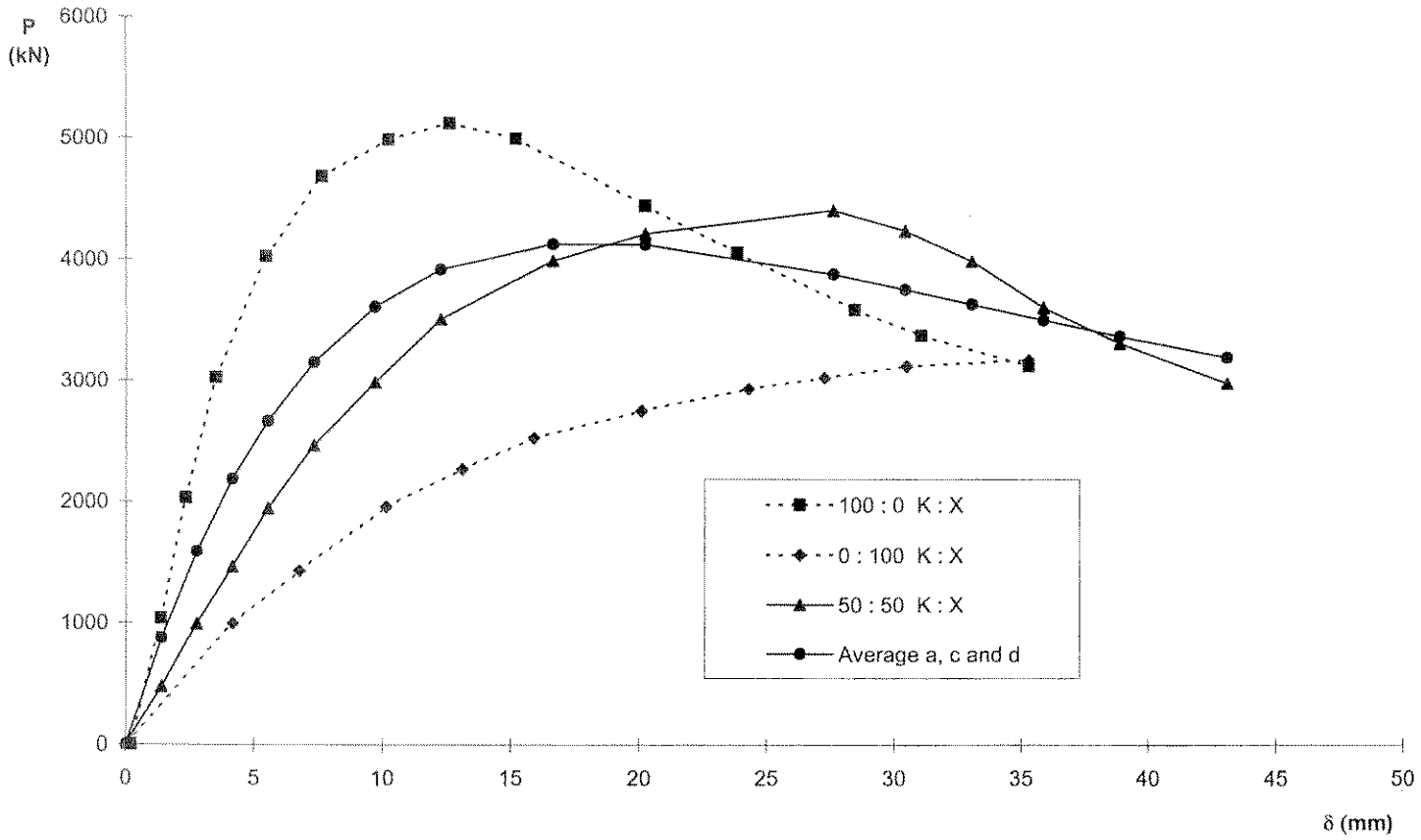

Figure 4.15: Average Coefficients Approach

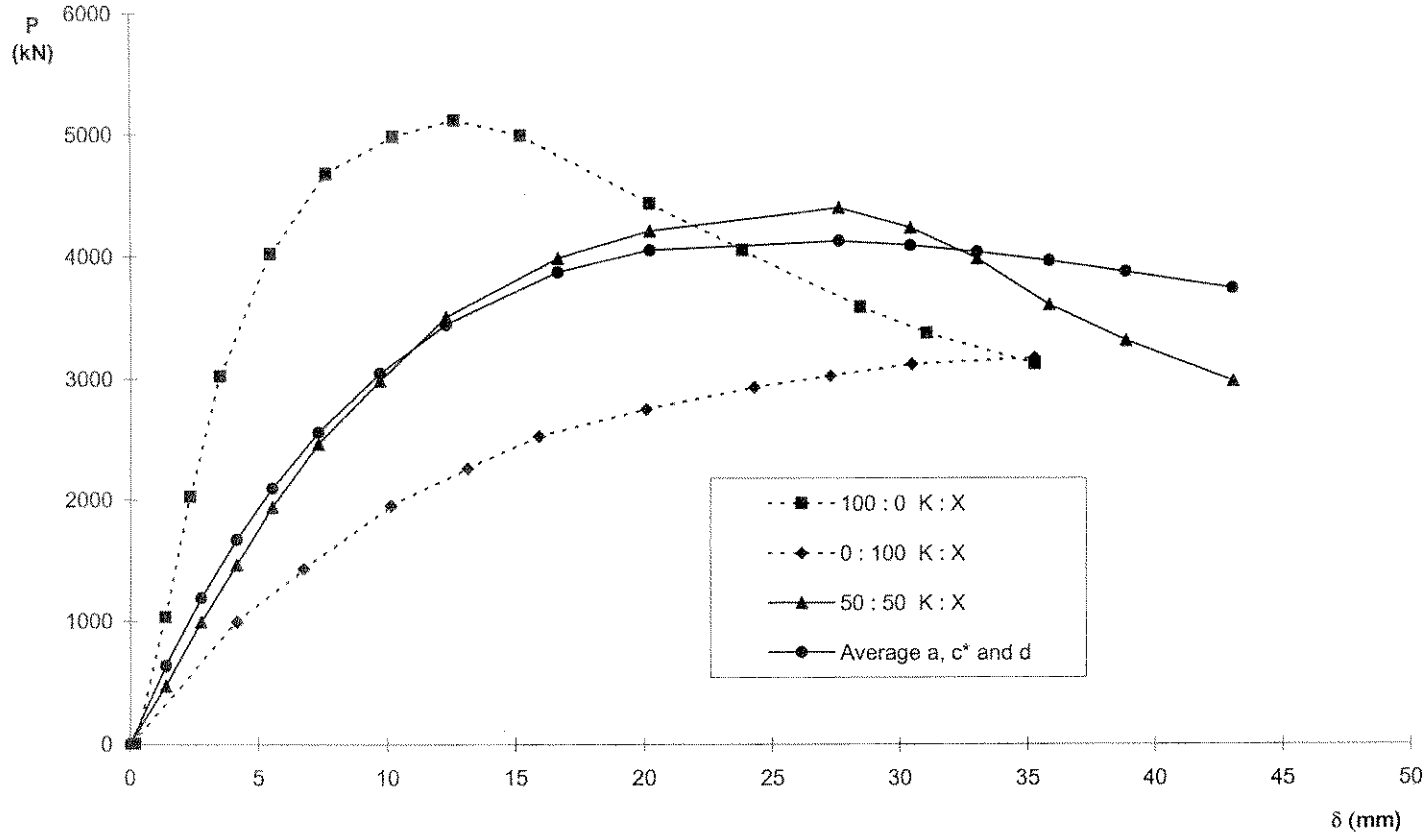

Figure 4.16: Average Coefficients Approach with Adjustments to Coefficient 'c'

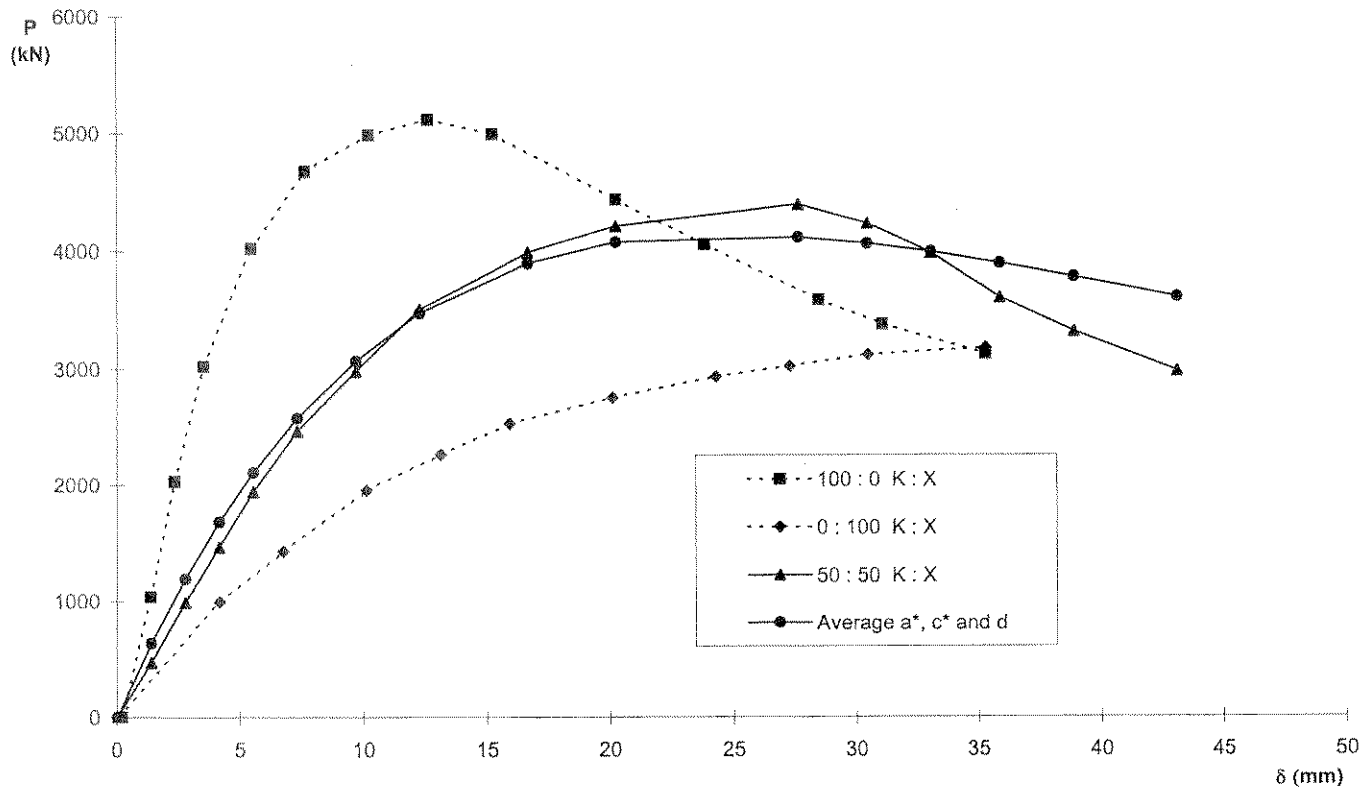

Figure 4.17: Average Coefficients Approach with Adjustments to Coefficients 'a' and 'c' for the K : X = 50 : 50 case

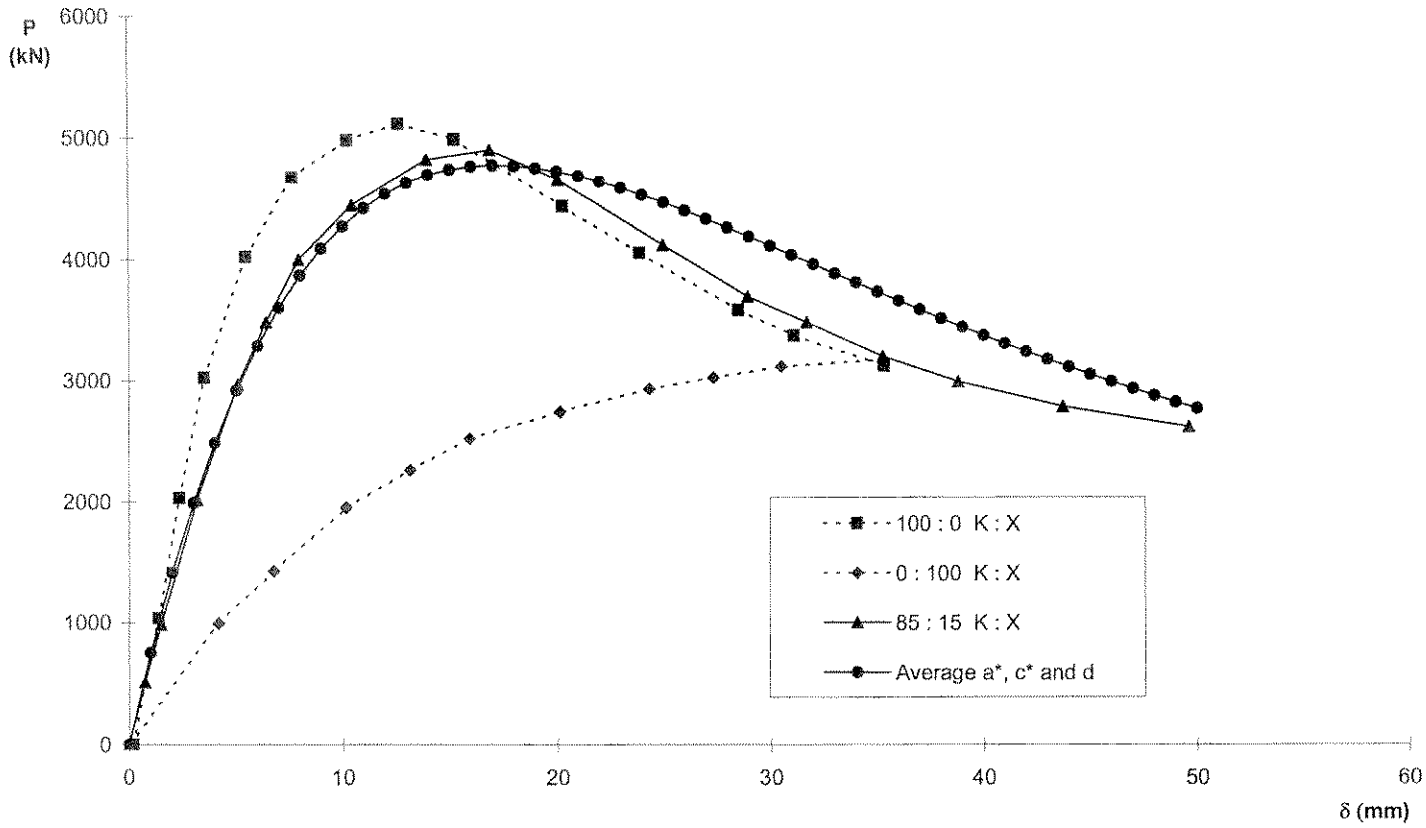

Figure 4.18: Average Coefficients Approach with Adjustments to Coefficients 'a' and 'c' for the K : X = 85 : 15 case

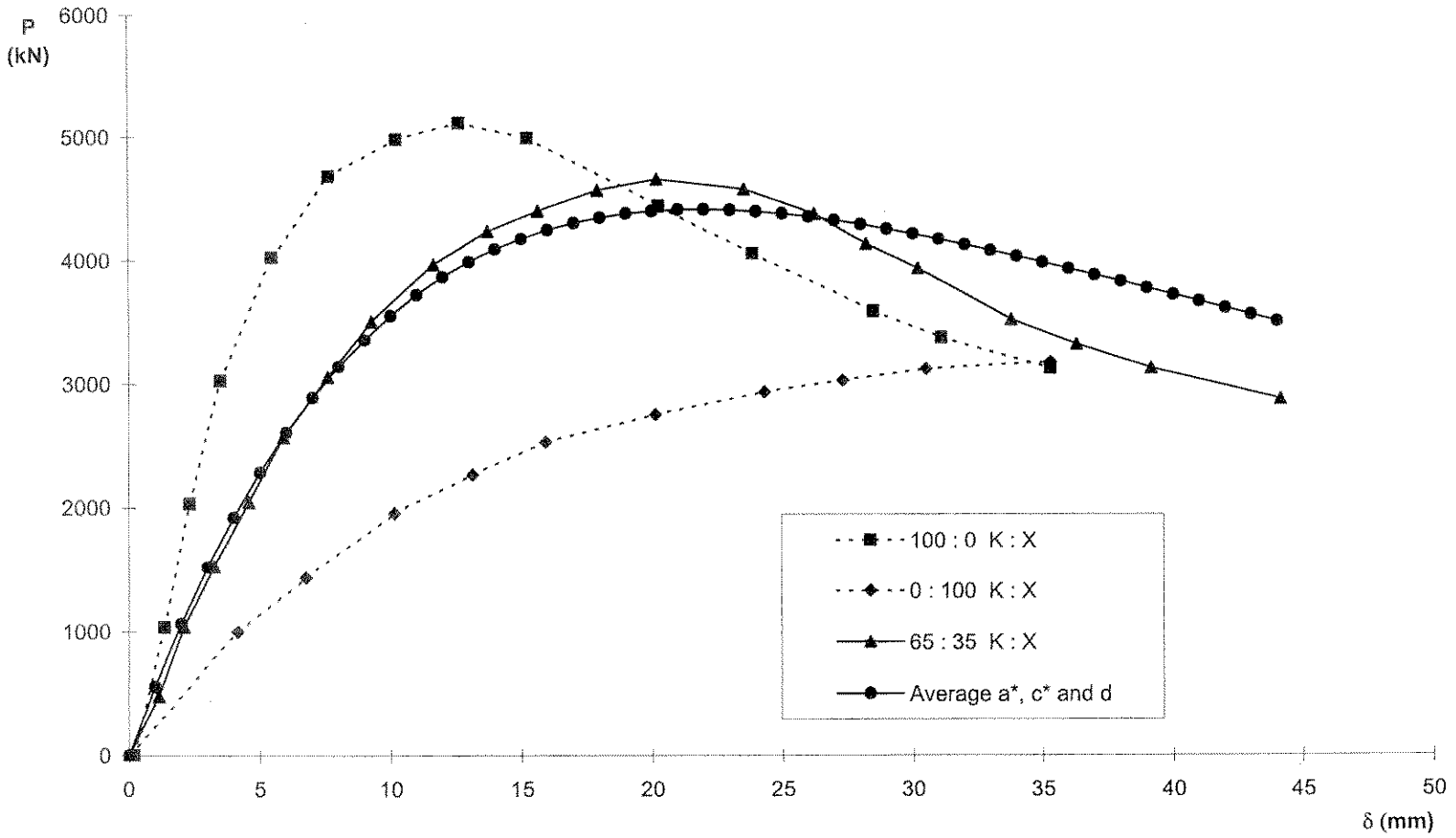

Figure 4.19: Average Coefficients Approach with Adjustments to Coefficients 'a' and 'c' for the K : X = 65 : 35 case

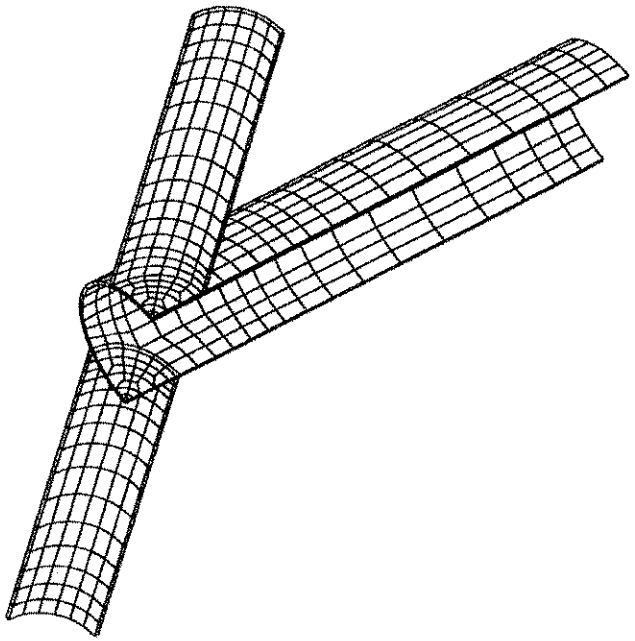

Figure 4.20: FE Mesh (quarter model)

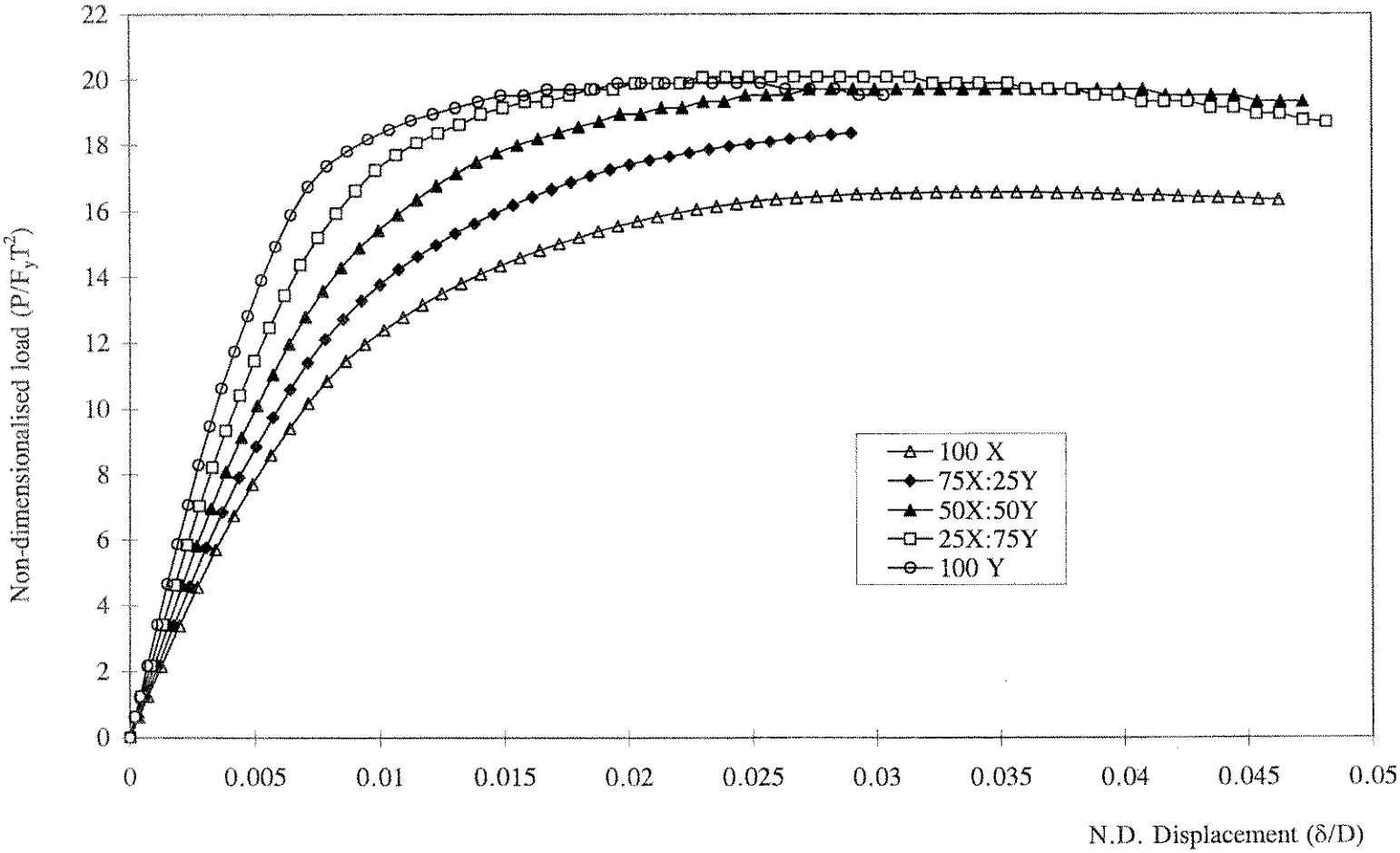

Figure 4.21: FE Non-Dimensionalised Load-Displacement Plots for DT Joint Under Compression

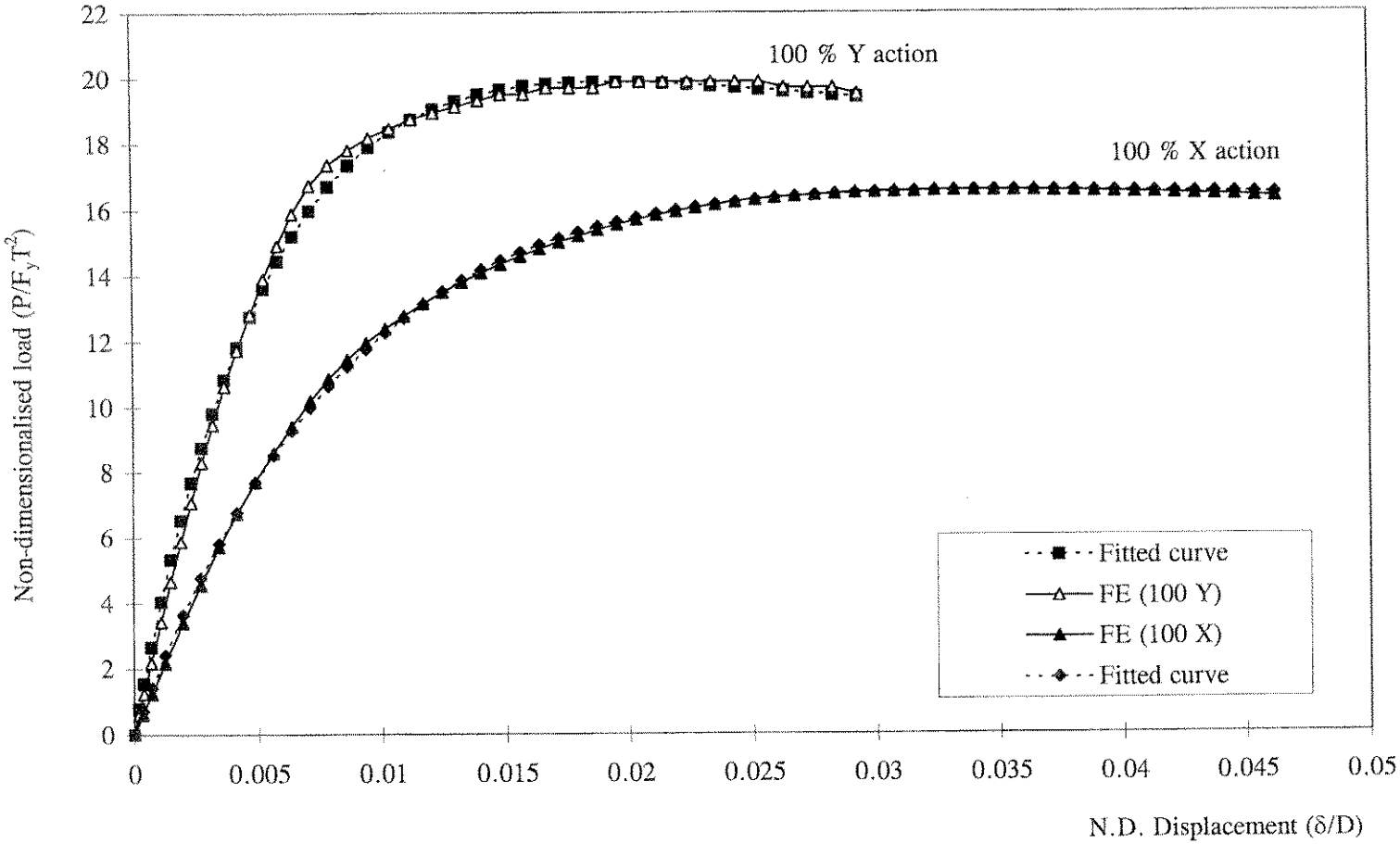

Figure 4.22: Curve Fitting to 100% Y and 100% X FE Curves

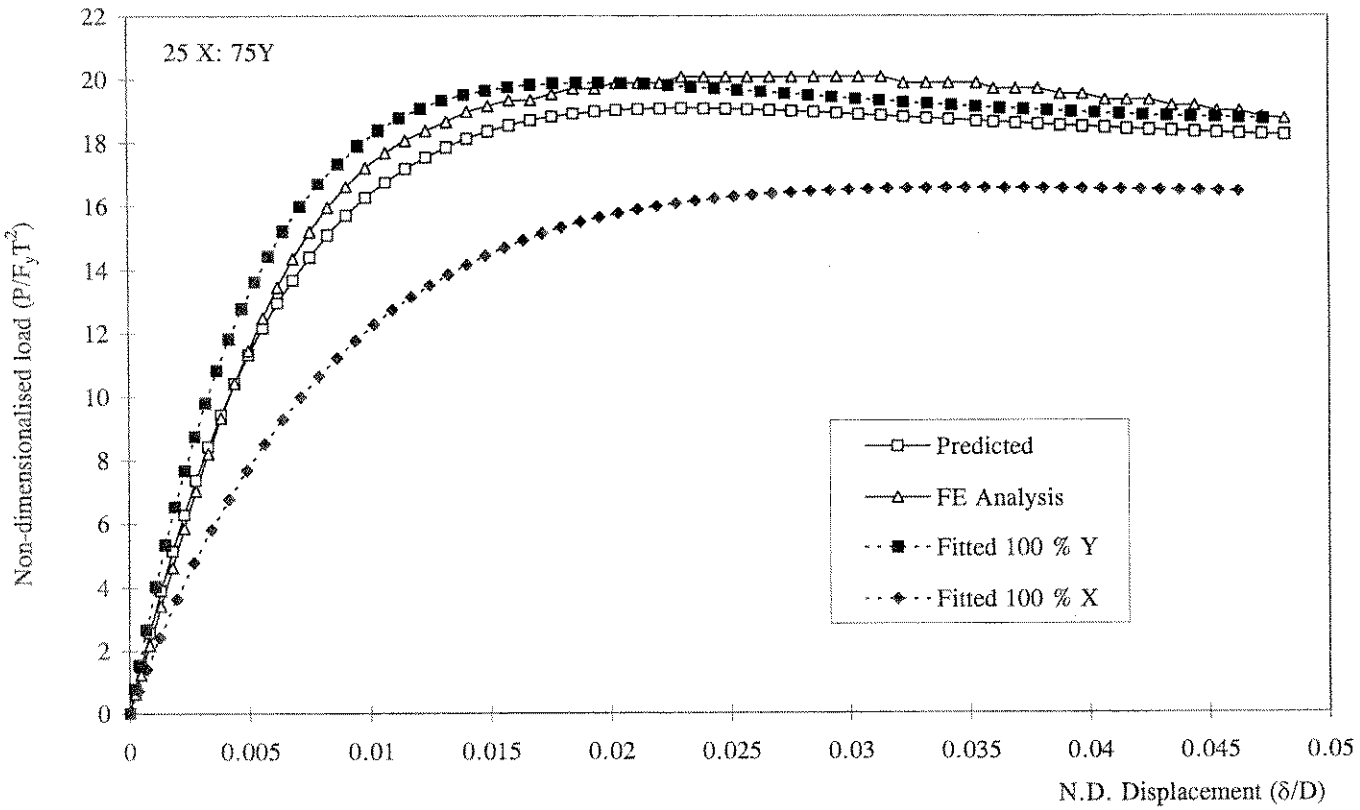

Figure 4.23: Predicted Non-Dimensionalised Load-Displacement Plots for DT Joint Under Compression for X : Y = 25 : 75 Case

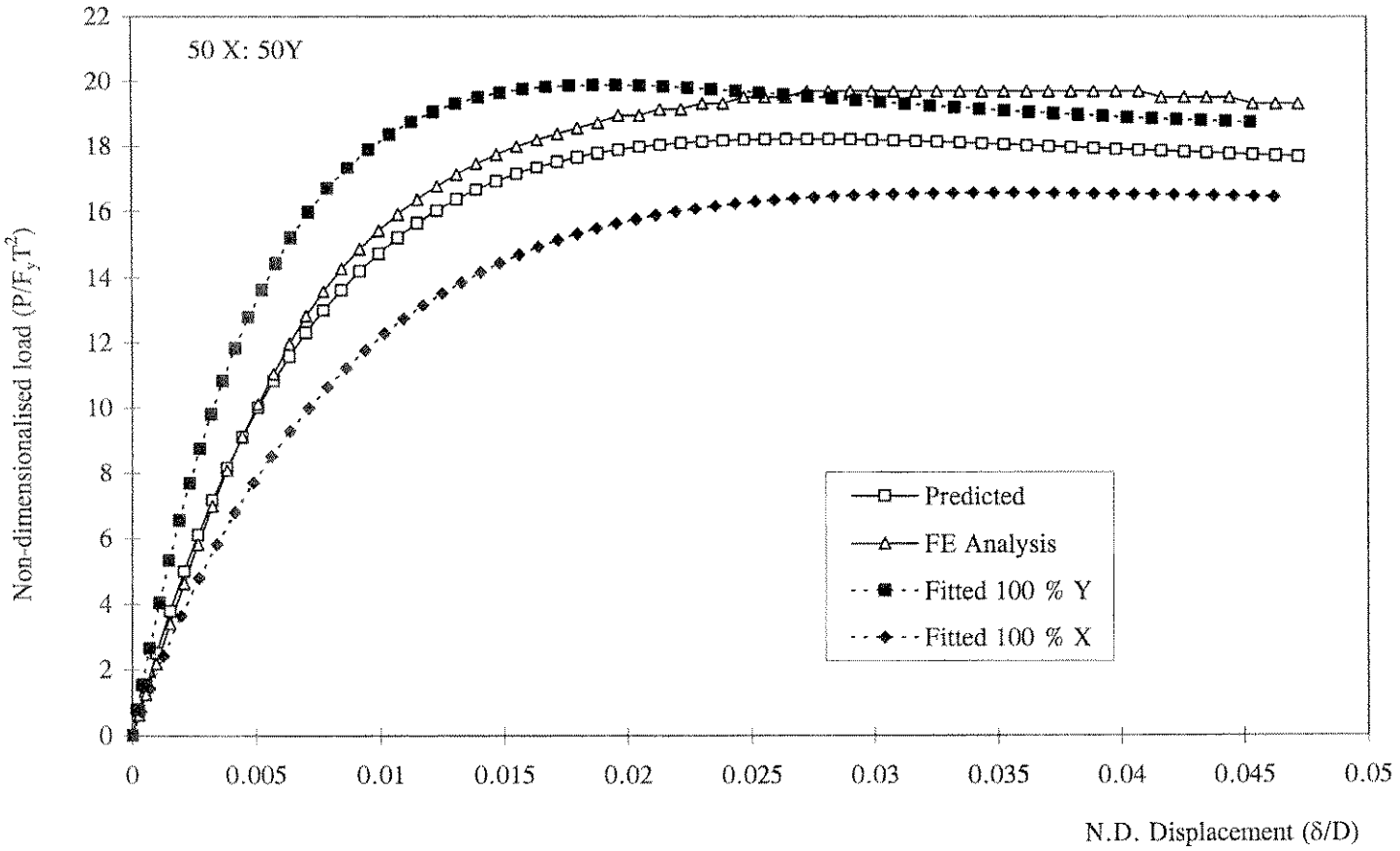

Figure 4.24: Predicted Non-Dimensionalised Load-Displacement Plots for DT Joint Under Compression for X : Y = 50 : 50 Case

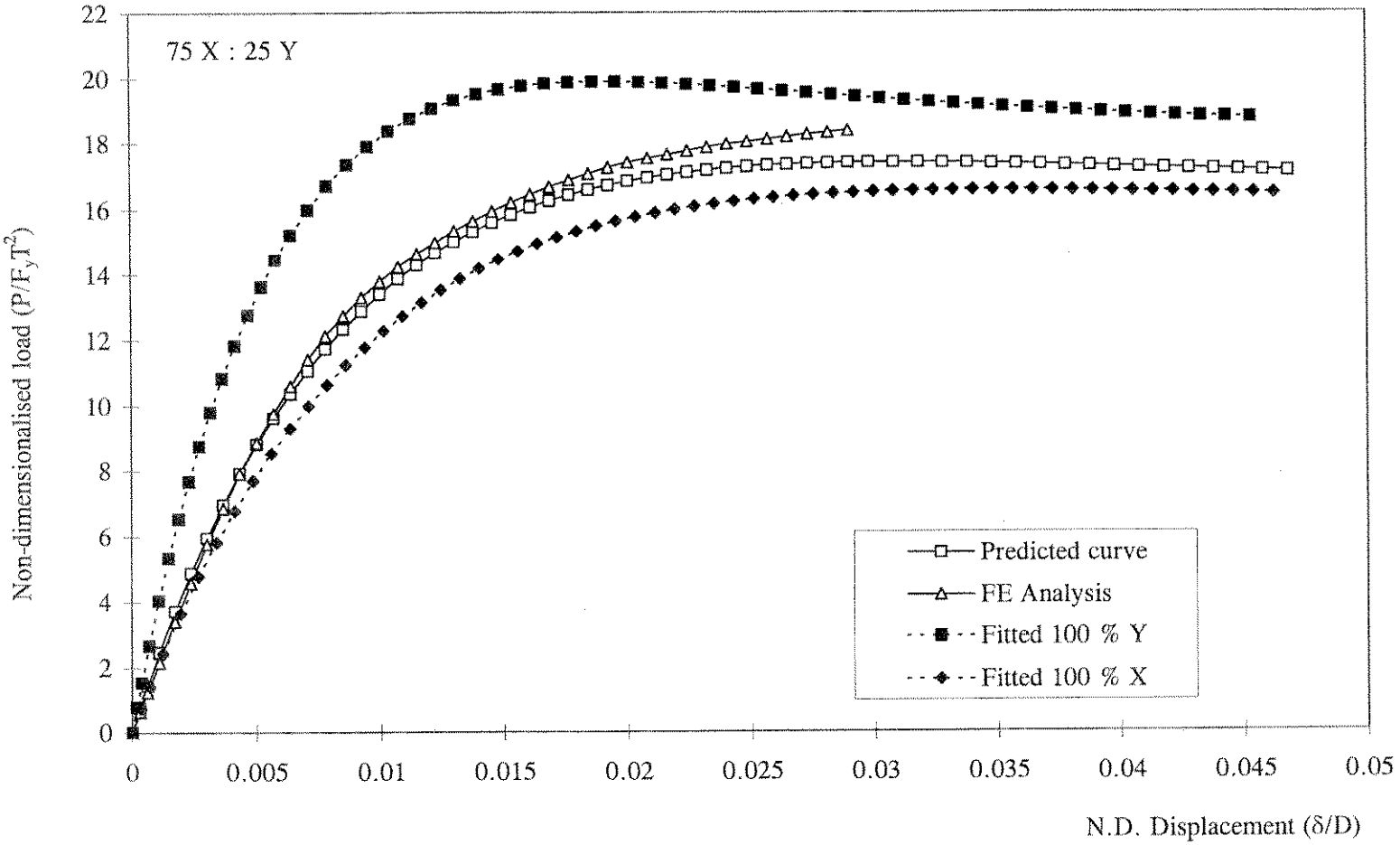

Figure 4.25: Predicted Non-Dimensionalised Load-Displacement Plots for DT Joints Under Compression for X : Y = 75 : 25 Case

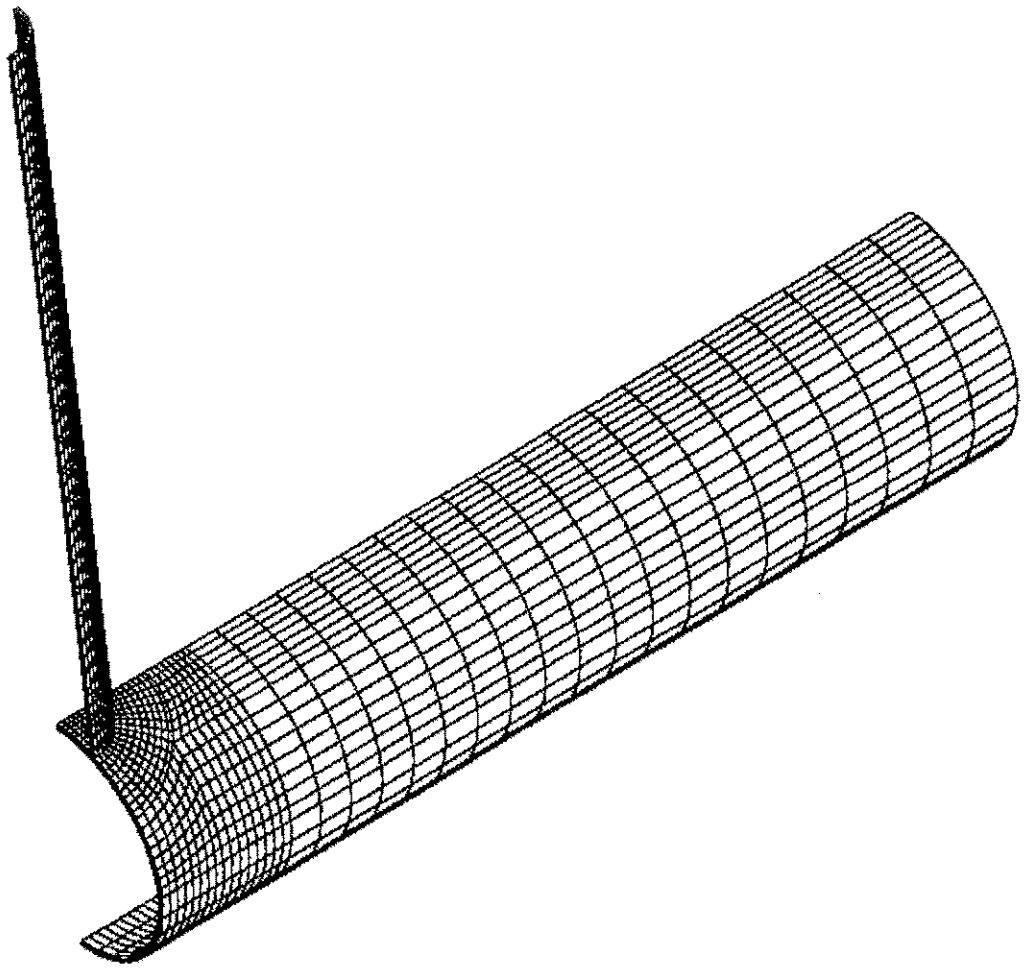

Figure 6.1: FE Mesh for T Joint, $\beta = 0.4$

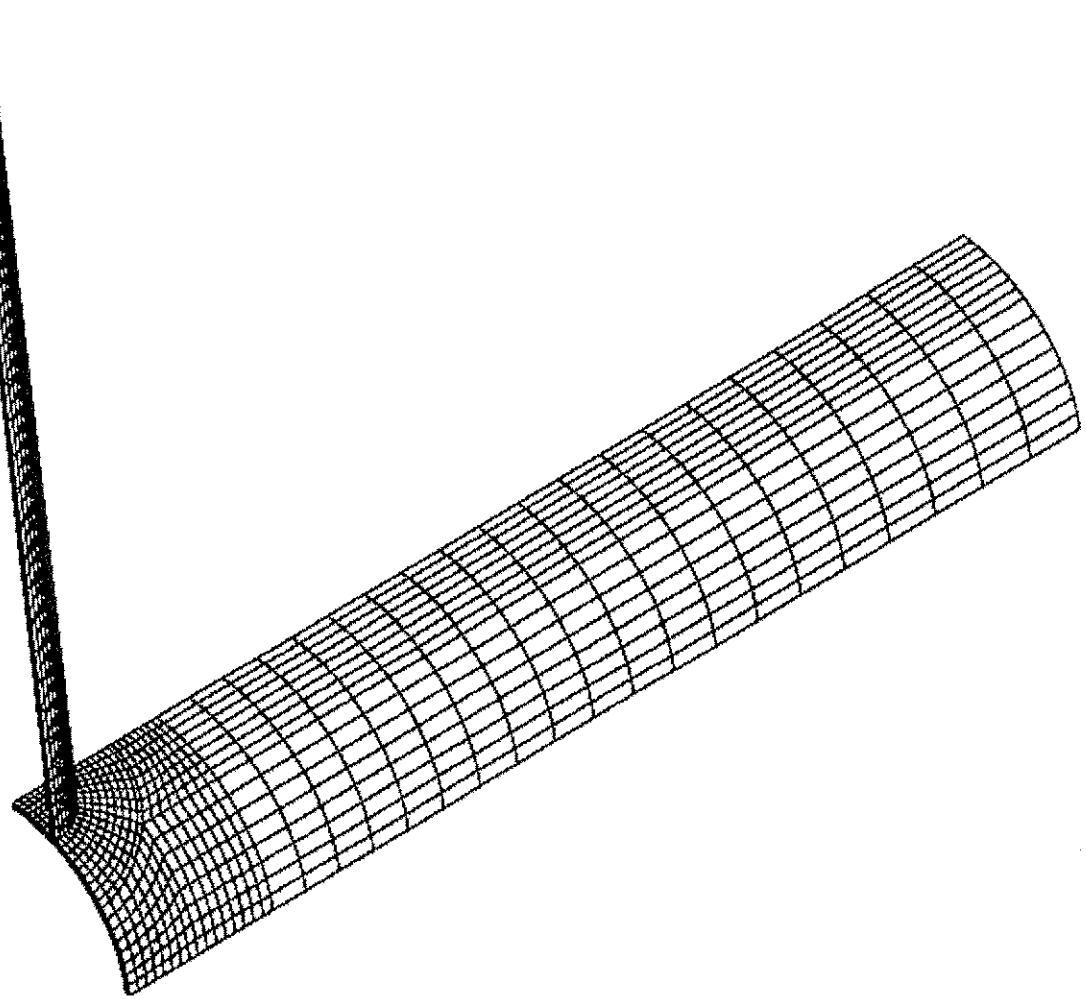

Figure 6.2: FE Mesh for DT Joint, $\beta = 0.4$

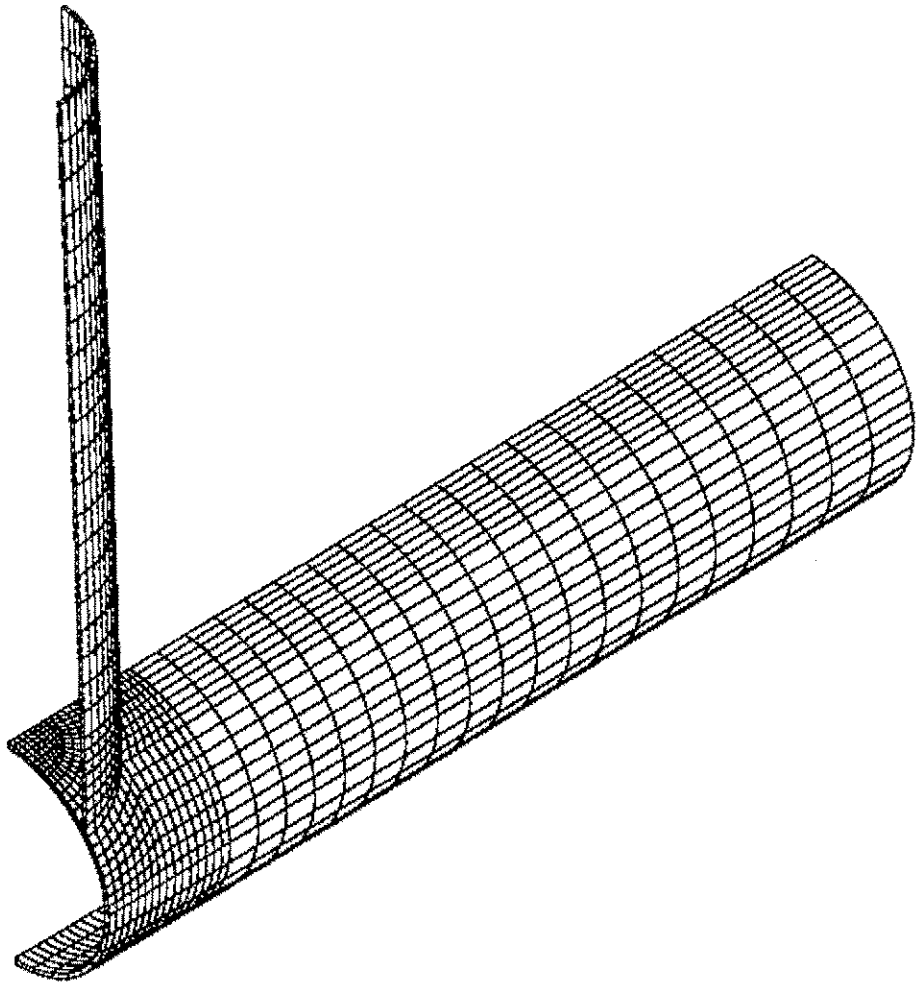

Figure 6.3: FM Mesh for T Joint, $\beta = 0.8$

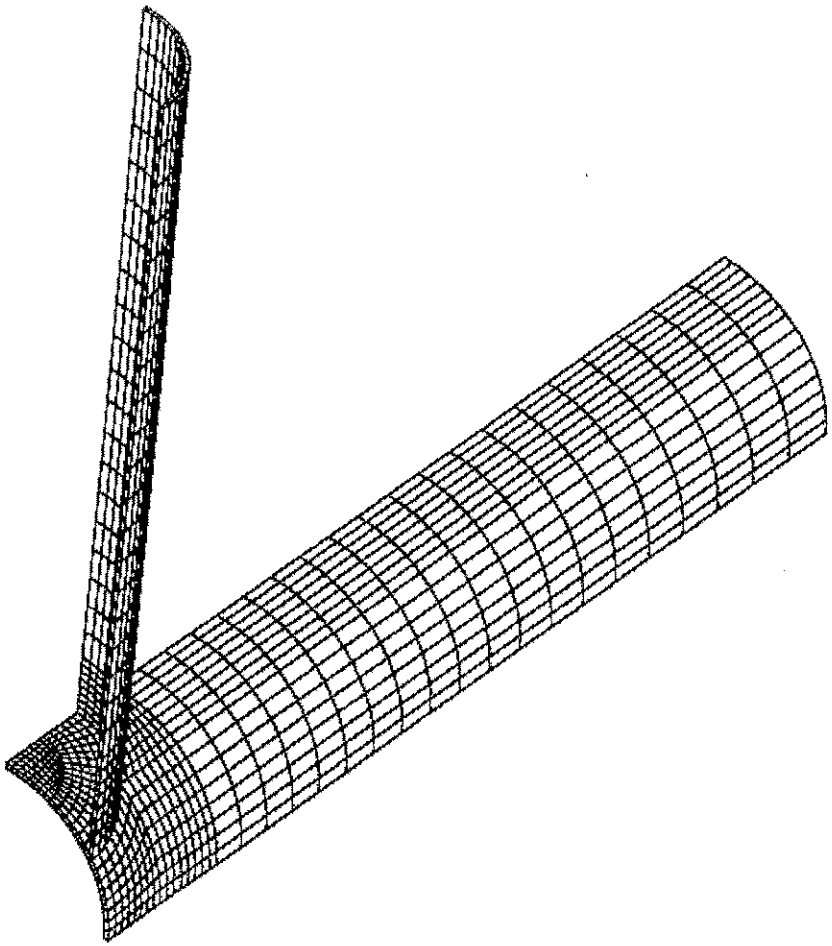

Figure 6.4: FE Mesh for DT Joint, $\beta = 0.8$

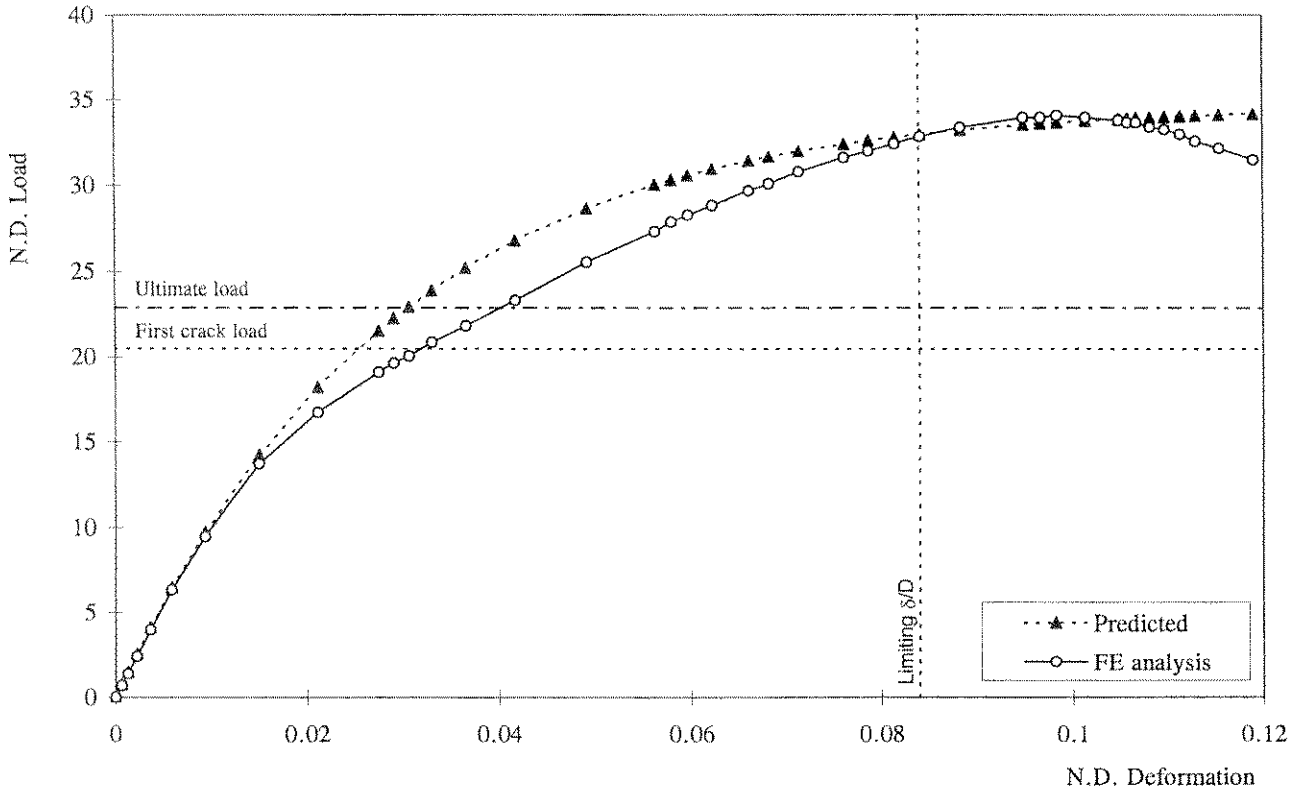

Figure 6.5: P-δ Plot for T Joint Under Tension Loading, $\beta = 0.4$, $\gamma = 25$, $\tau = 0.81$

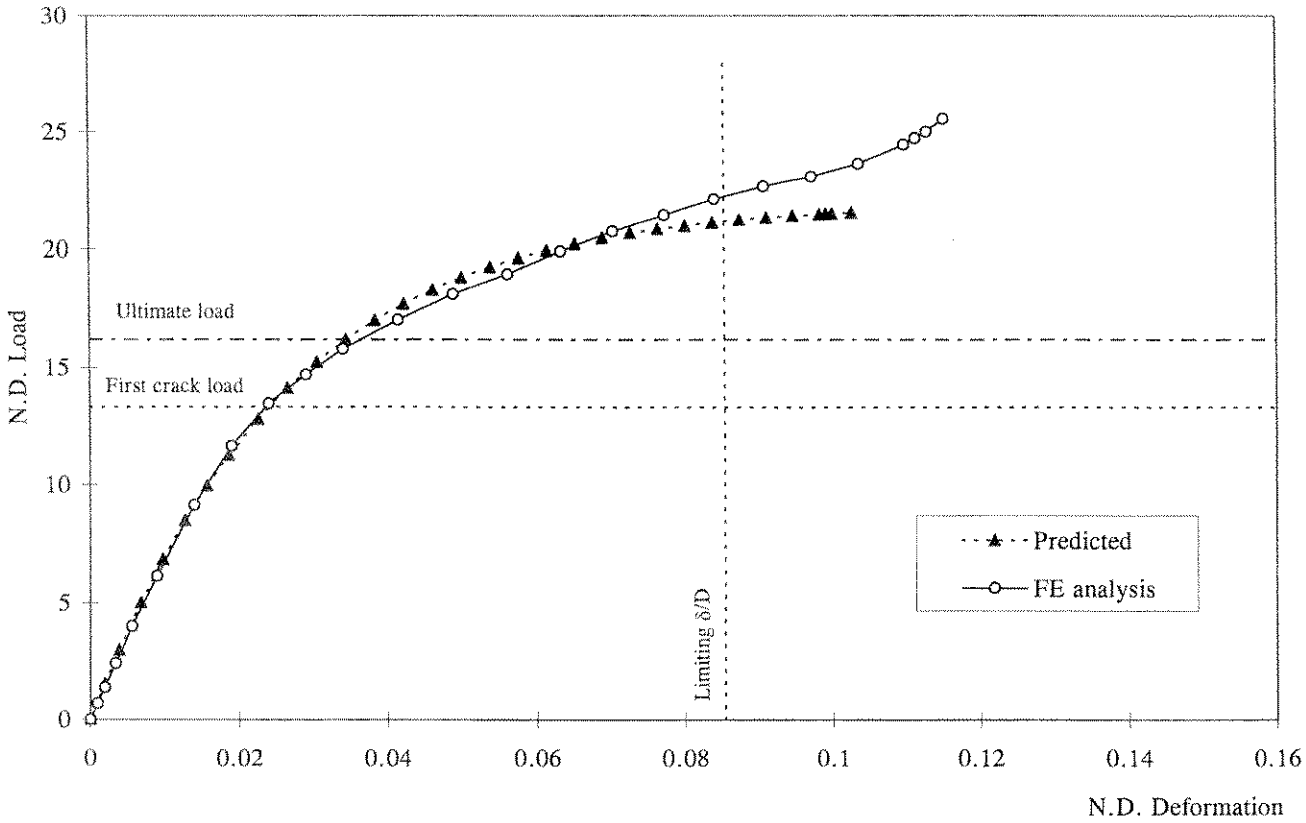

Figure 6.6: P-δ Plot for DT Joint Under Tension Loading, $\beta = 0.4$, $\gamma = 25$, $\tau = 0.81$

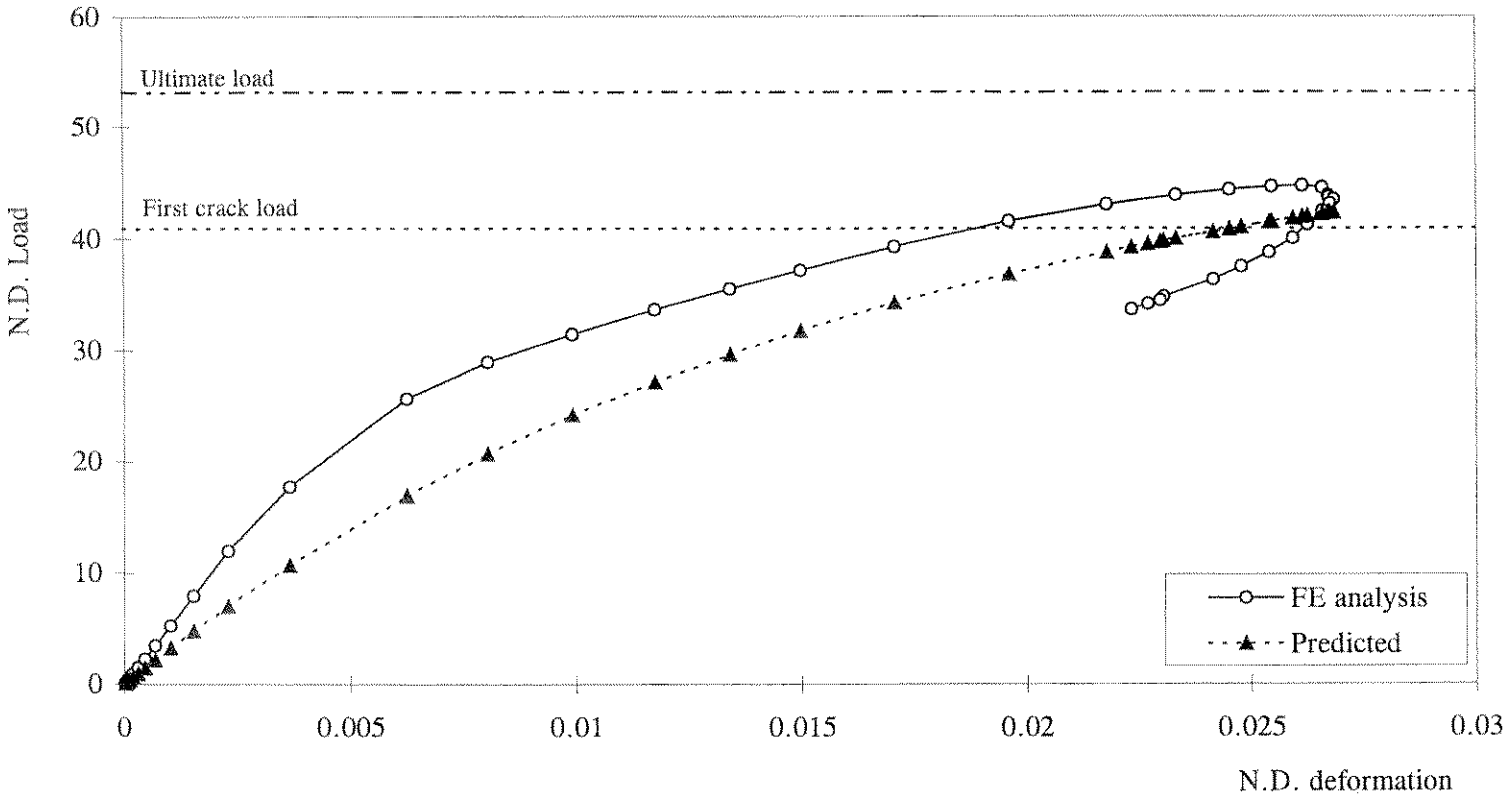

Figure 6.7: P-δ plot for T joint under tension loading, β = 0.8, γ = 25, τ =0.81

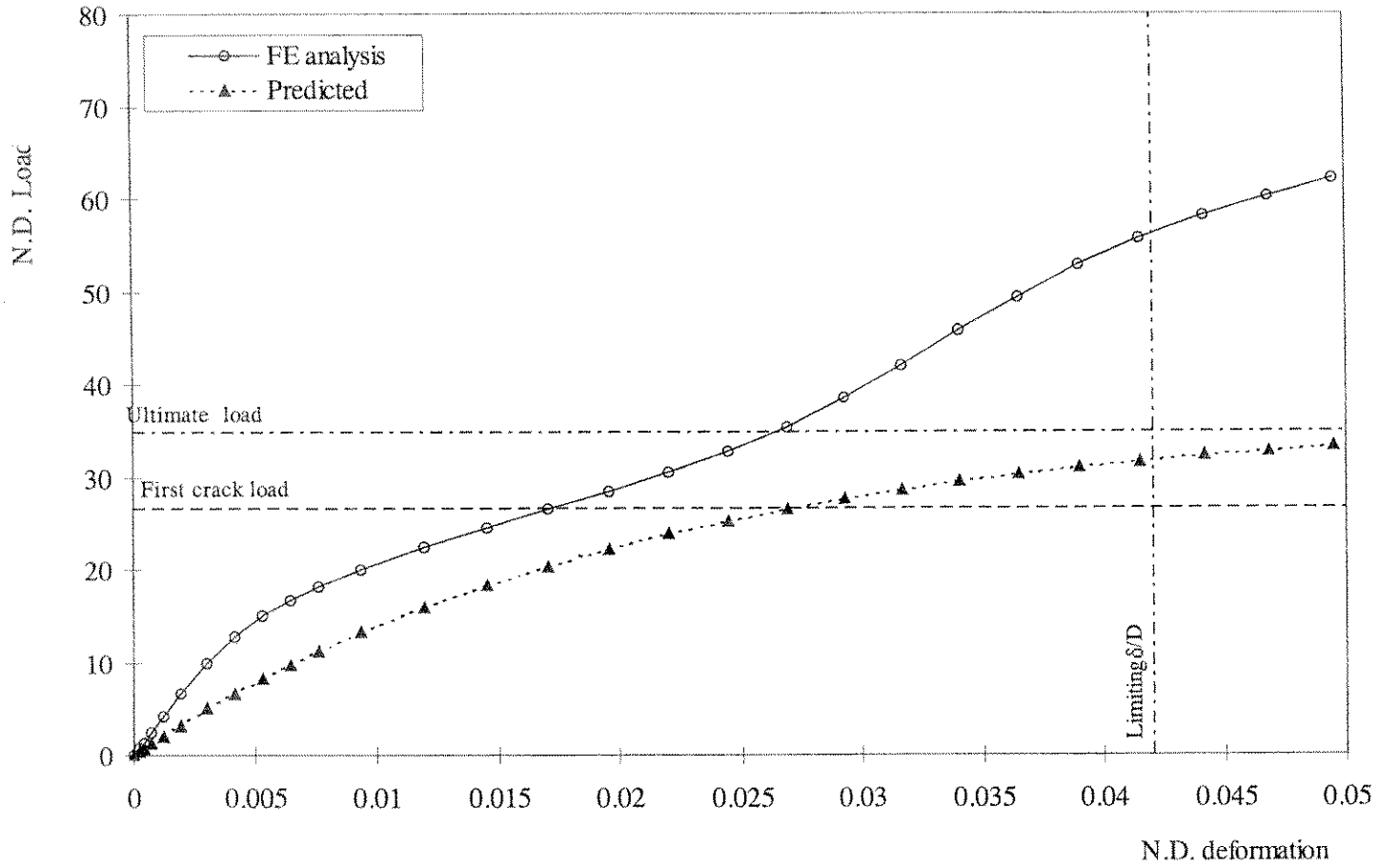

Figure 6.8: P-δ plot for DT joint under tension loading, β =0.8, γ =25, τ =0.81

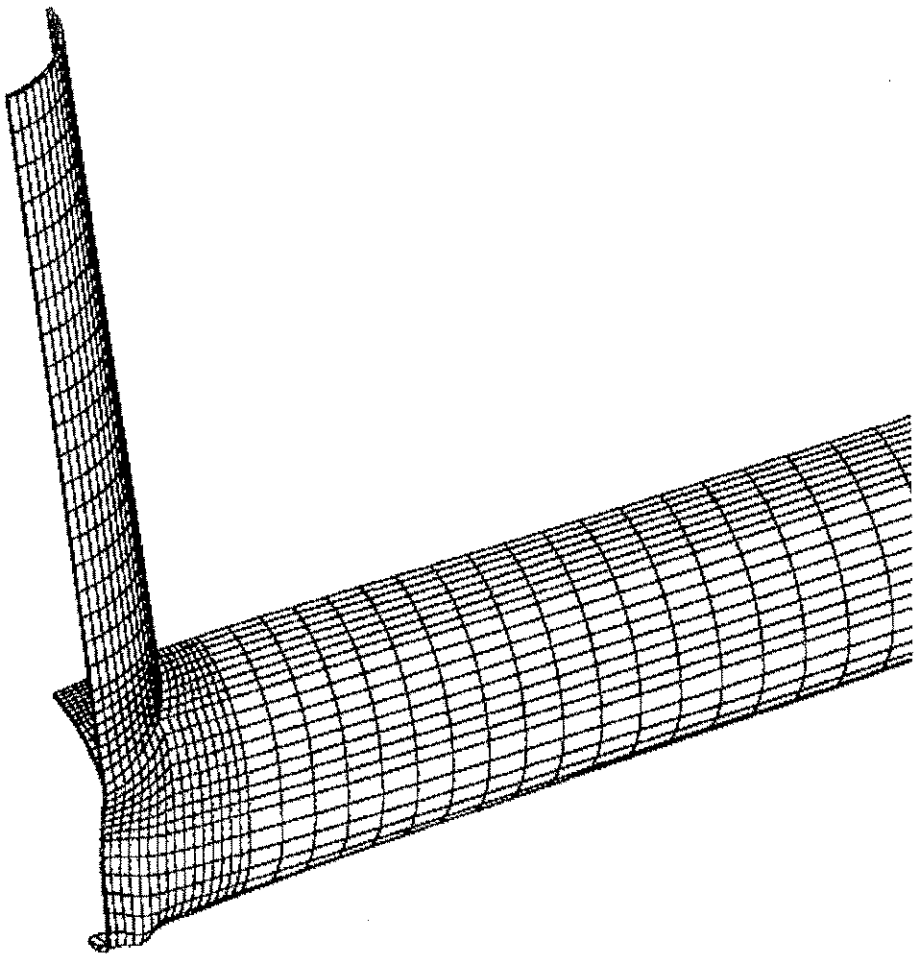

Figure 6.9: Local Chord Buckling of $\beta = 0.8$ T Joint

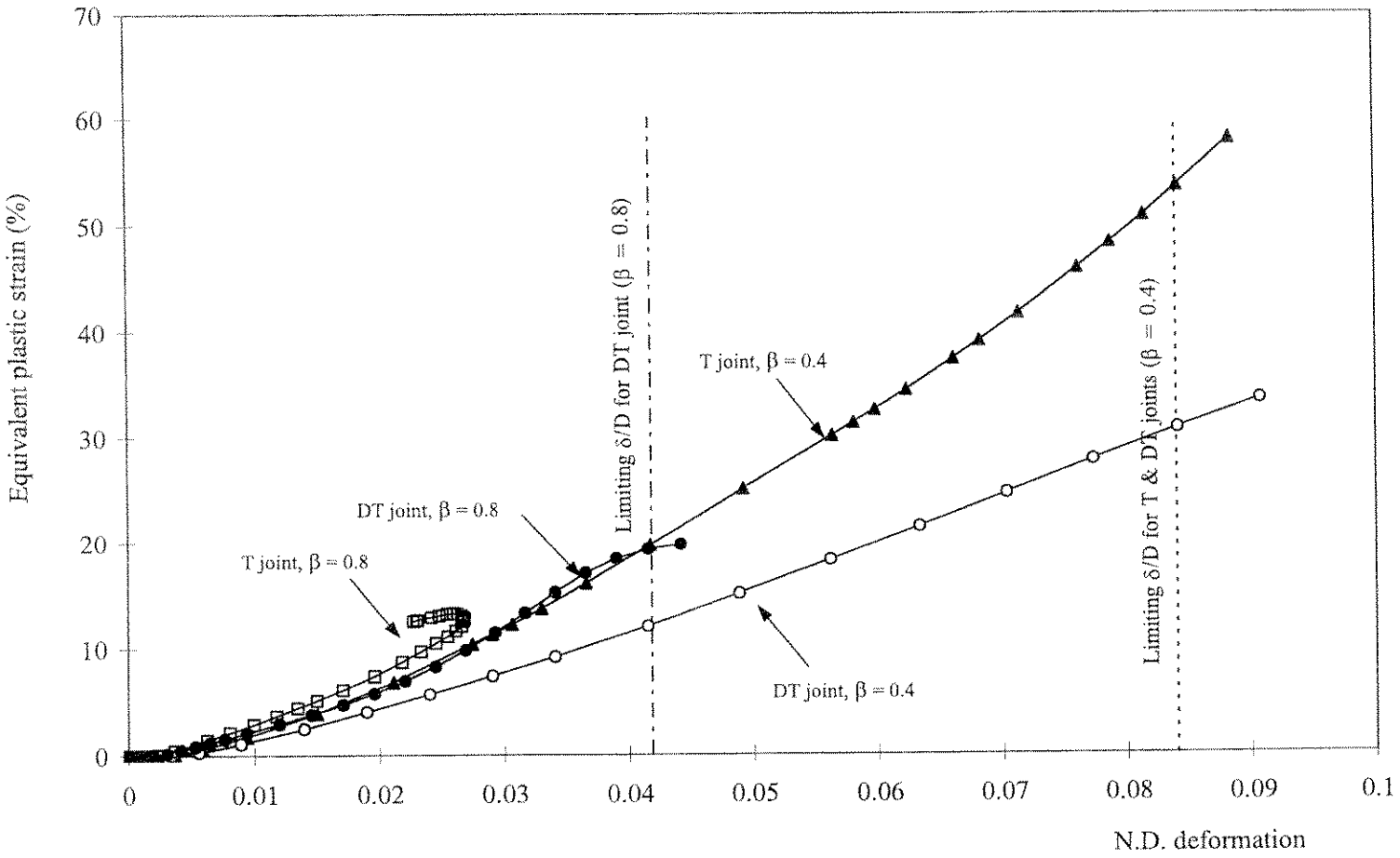

Figure 6.10: Variation of Equivalent Plastic Strain with ND Deformation

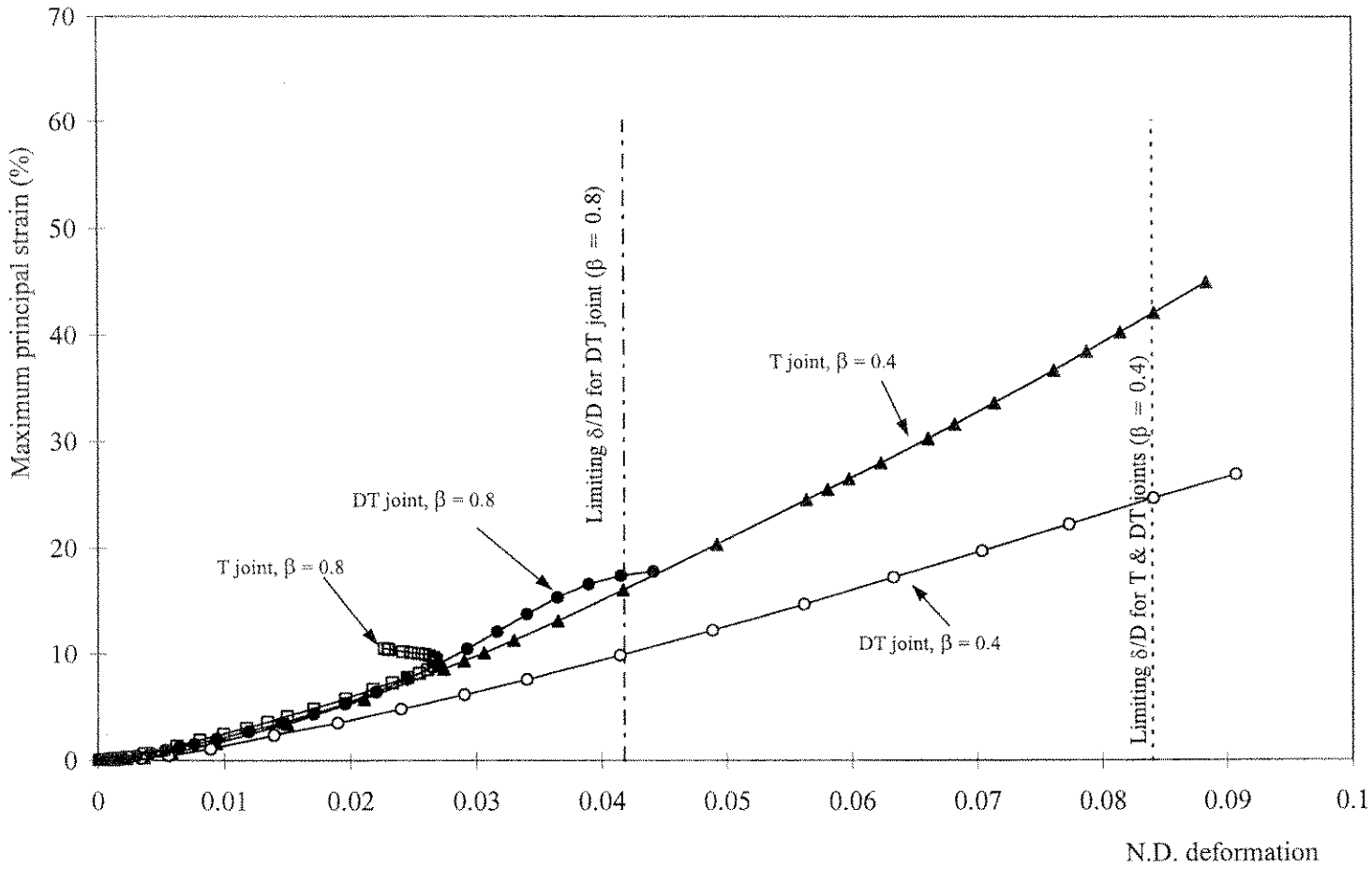

Figure 6.11: Variation of Maximum Principal Strain (Tensile) with N.D. Deformation

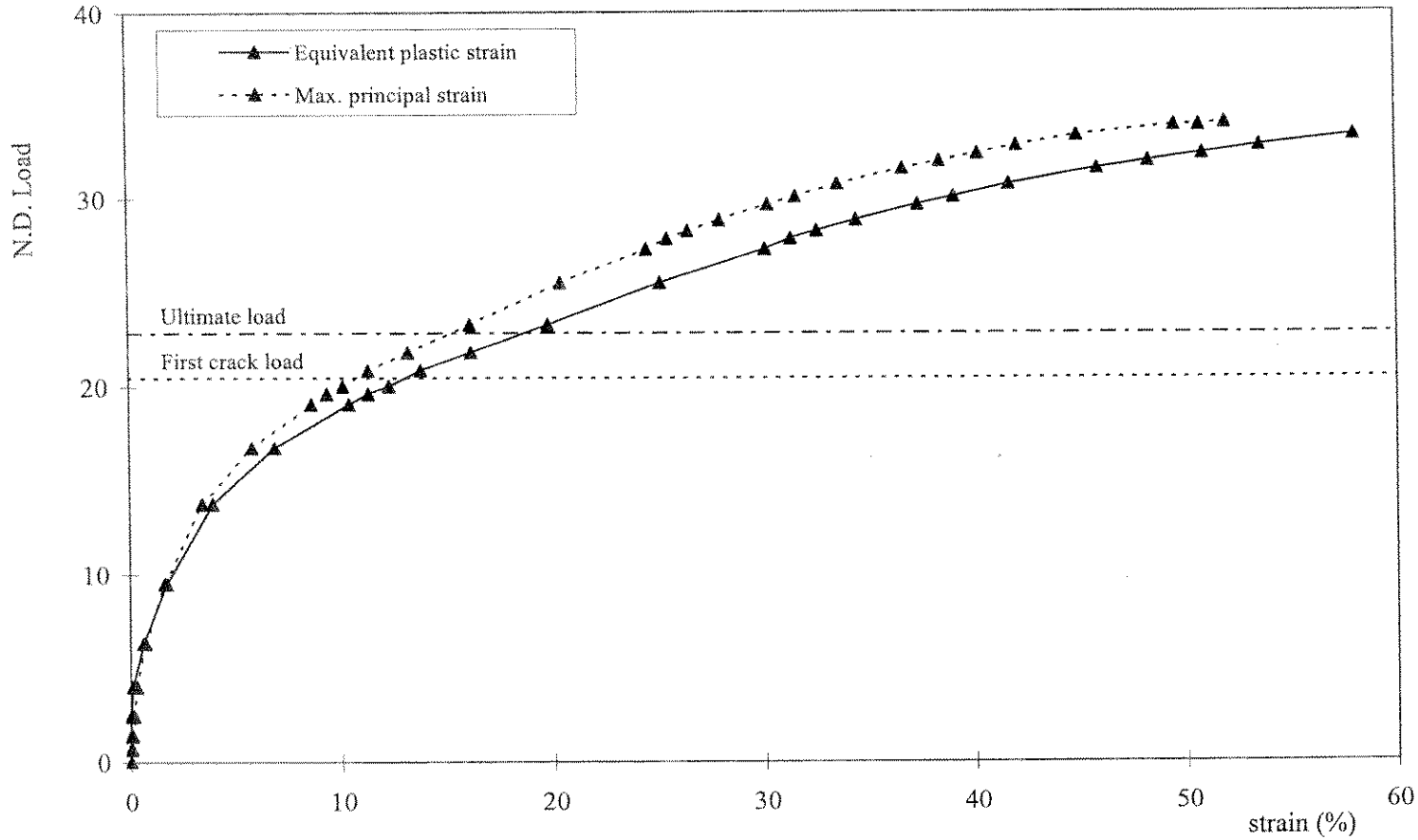

Figure 6.12: Load vs. Strain Plots for T Joint with $\beta = 0.4$, $\gamma = 25$, $\tau = 0.81$

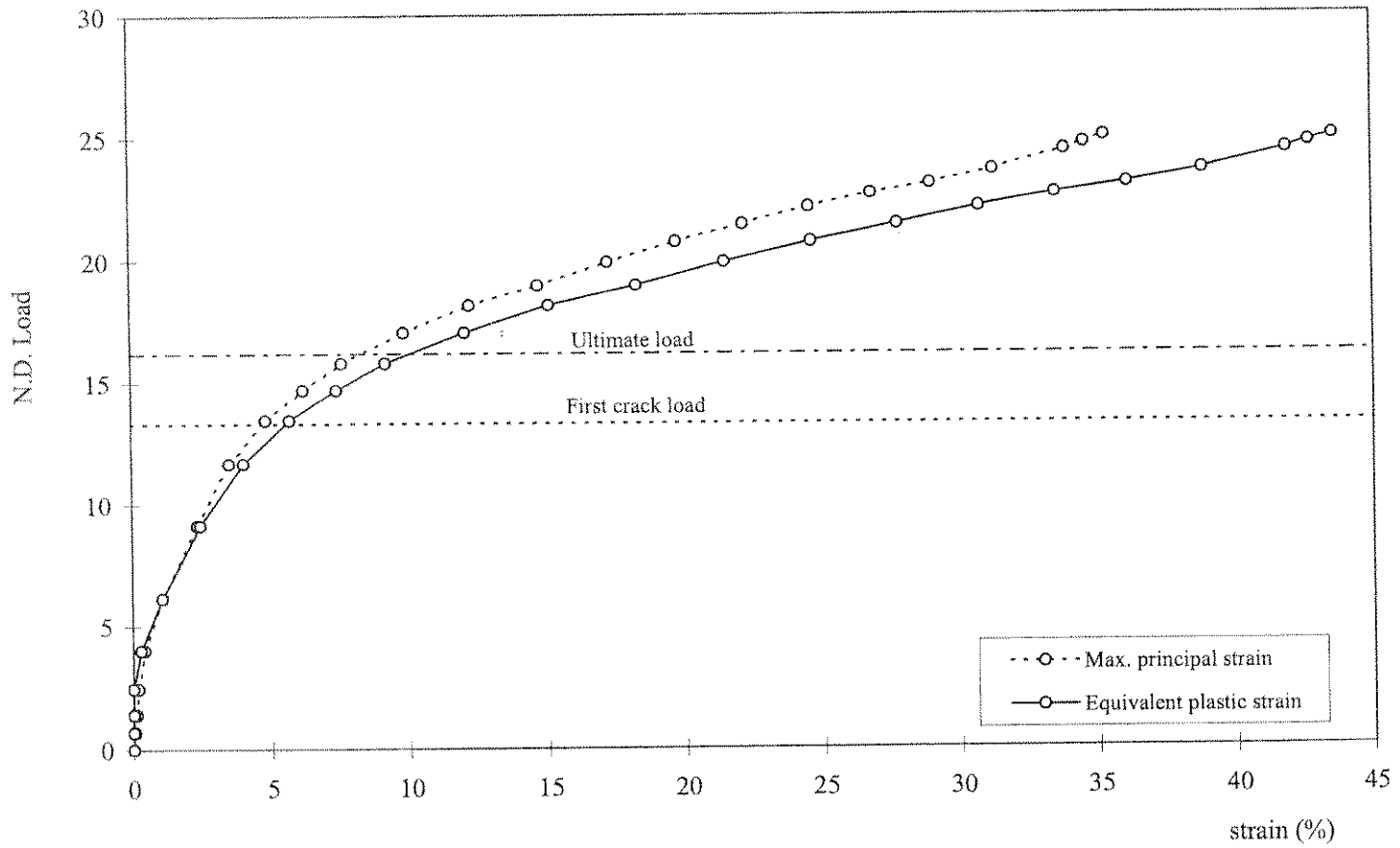

Figure 6.13: Load vs. Strain Plots for DT Joint, $\beta = 0.4$, $\gamma = 25$, $\tau = 0.81$

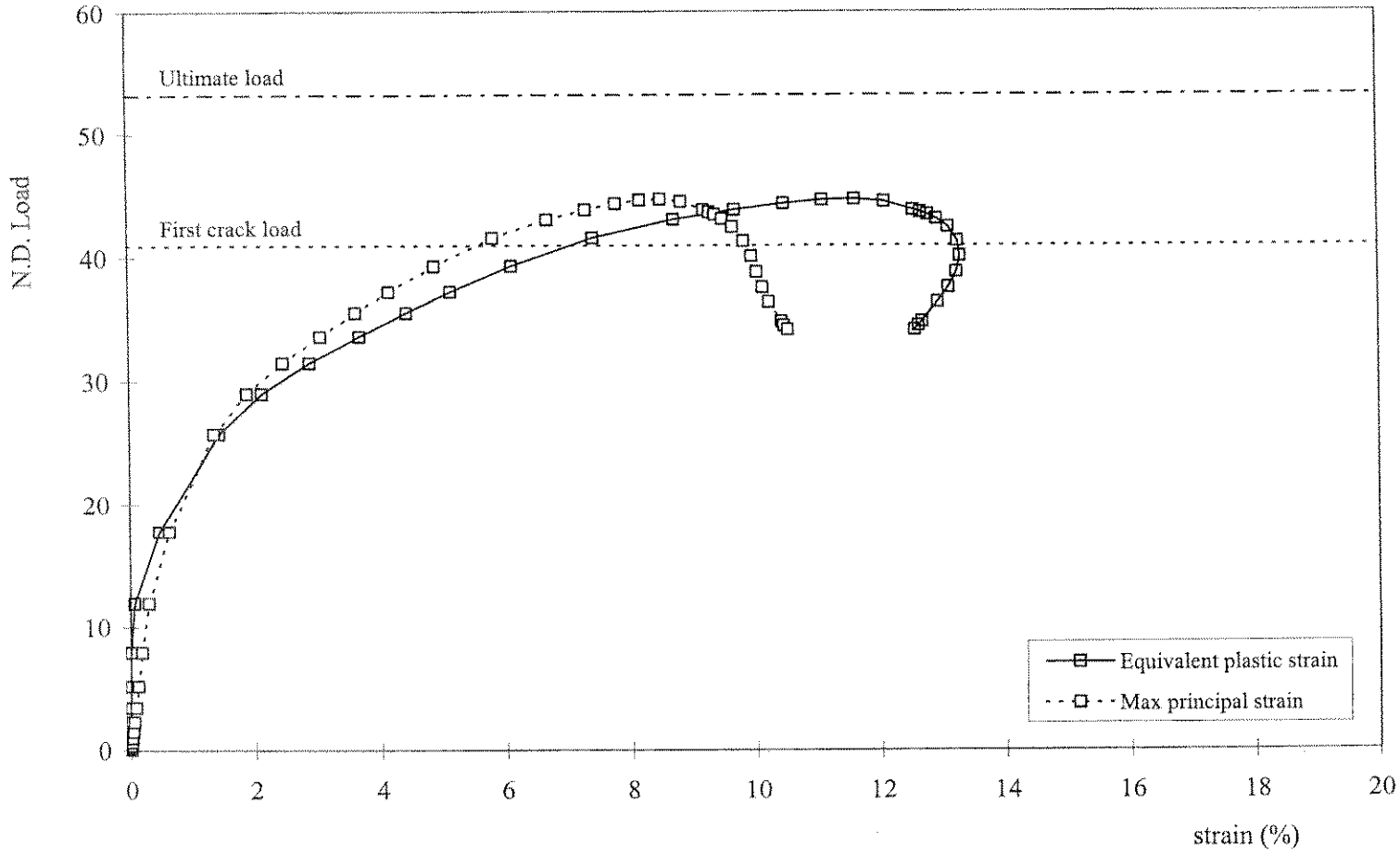

Figure 6.14: Load vs. Strain Plots for T Joint, $\beta = 0.8$, $\gamma = 25$, $\tau = 0.81$

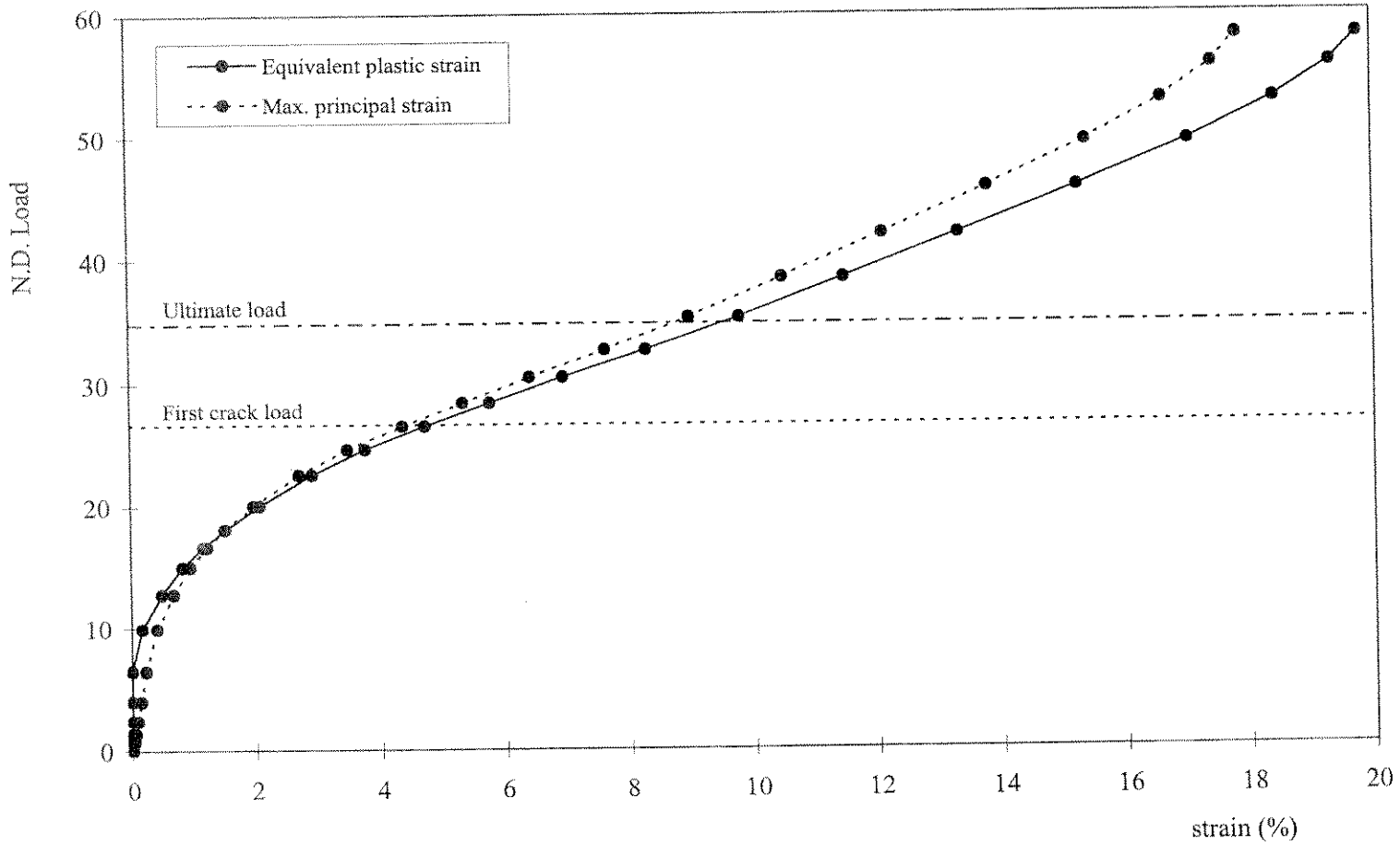

Figure 6.15: Load vs. Strain Plots for DT Joint, $\beta = 0.8$, $\gamma = 25$, $\tau = 0.81$

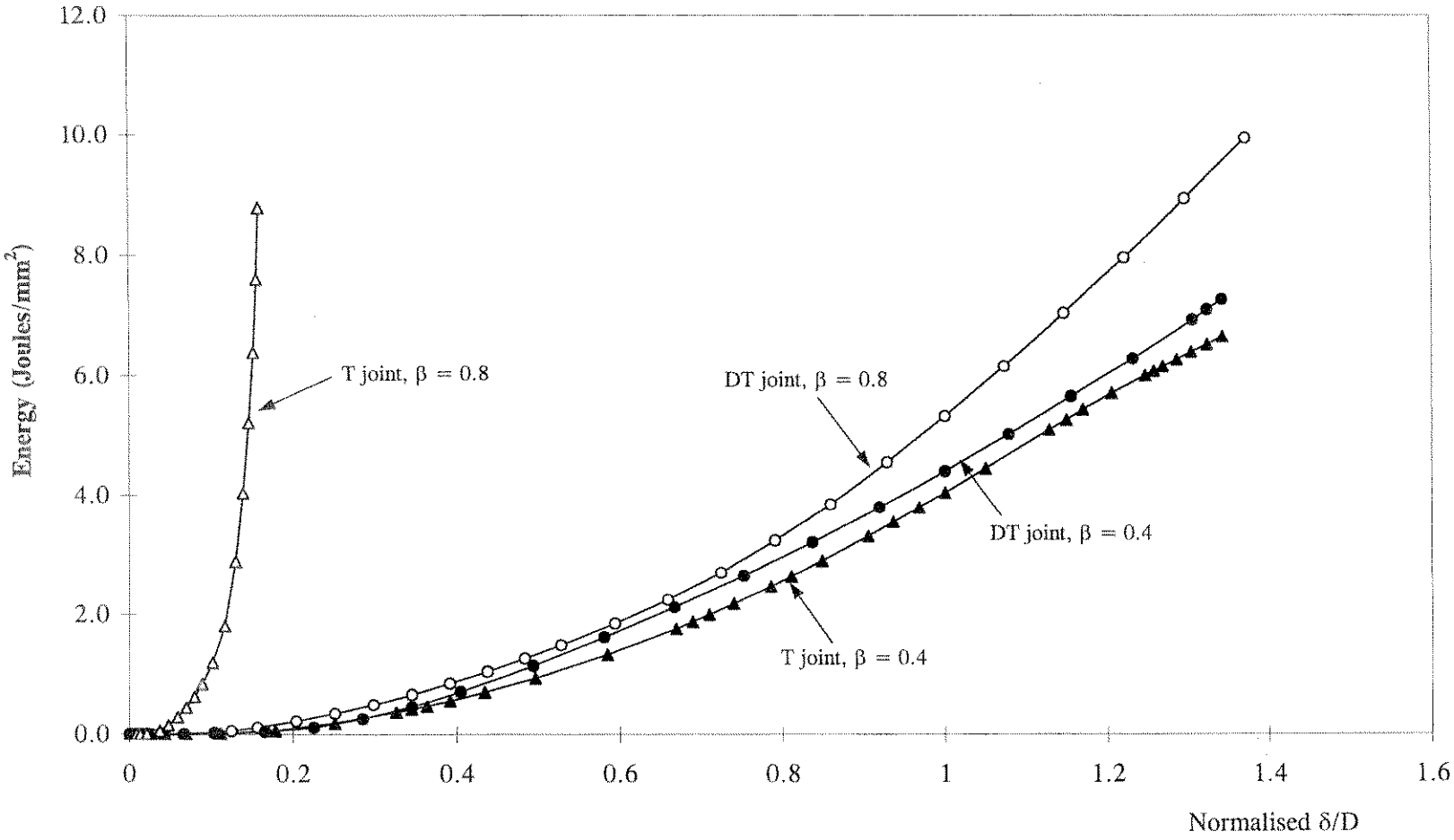

Figure 6.16: Variation of Plastic Work with Normalised ND Deformation

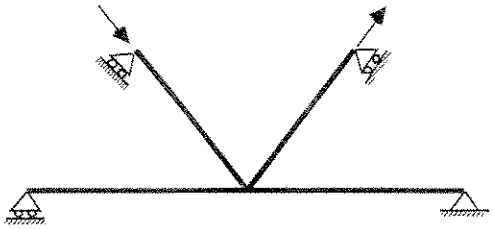

(a) Model

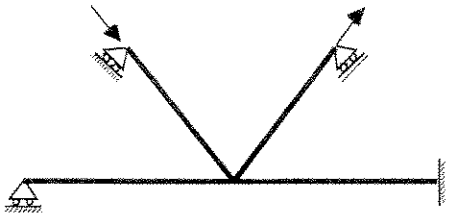

(b) Model

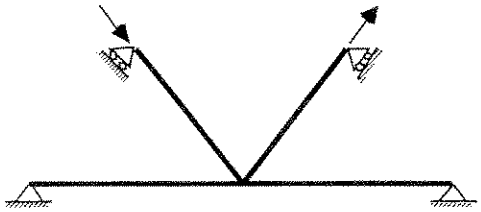

(c) Model

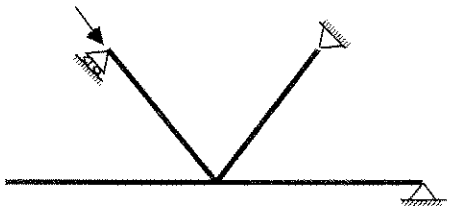

(d) Model

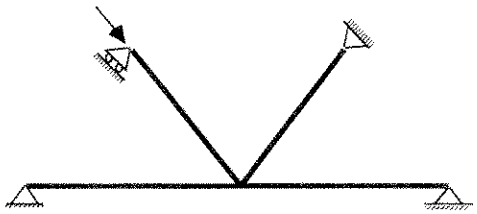

(e) Model

Figure 6.17: Boundary Restraints Used for FE Analysis of K Joints

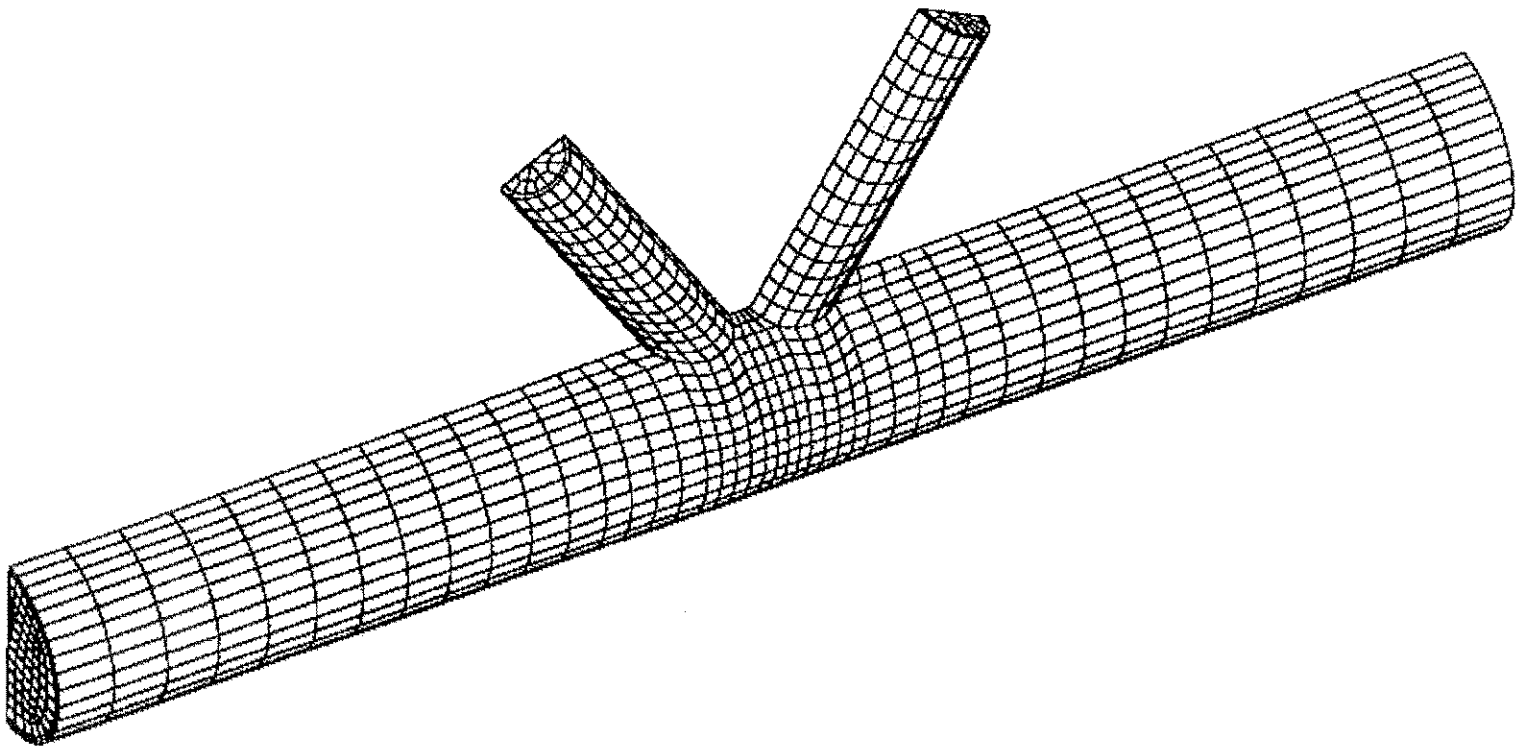

Figure 6.18: FE Mesh of K Joint, $\beta = 0.4$

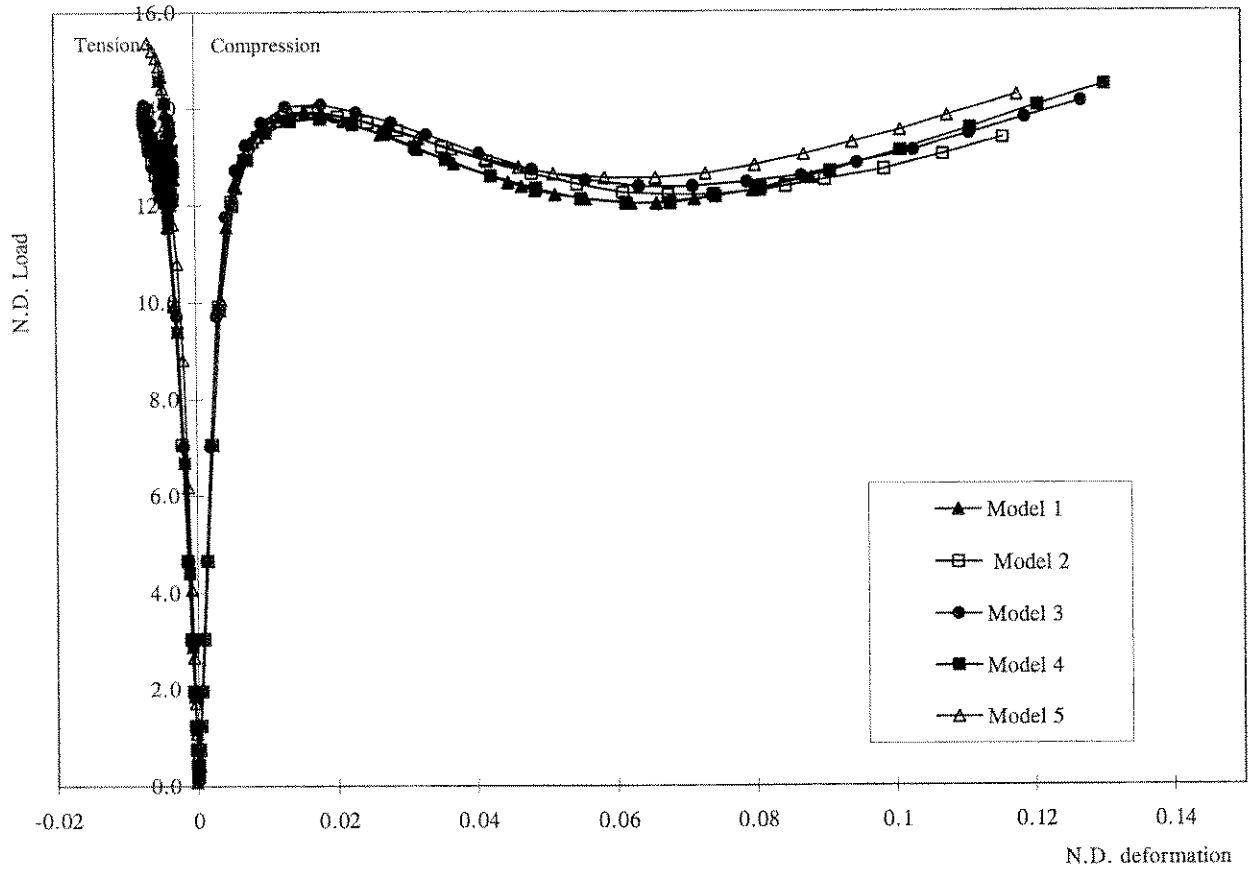

Figure 6.19: Pδ Curves for K Joint, $\beta = 0.4$, $\gamma = 15$, $\tau = 0.81$

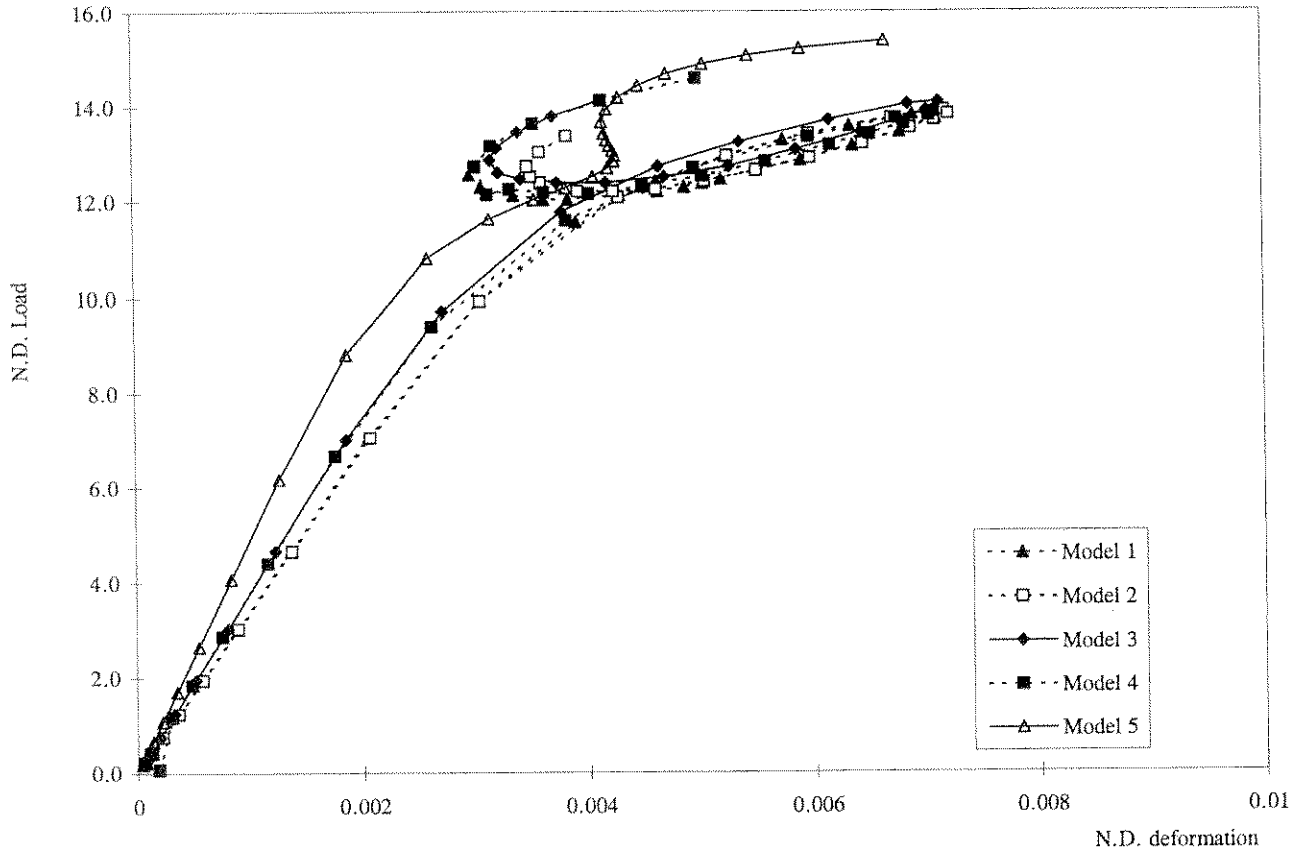

Figure 6.20: Pδ Curve (Tension Brace) for K Joint, $\beta = 0.4$, $\gamma = 15$, $\tau = 0.81$

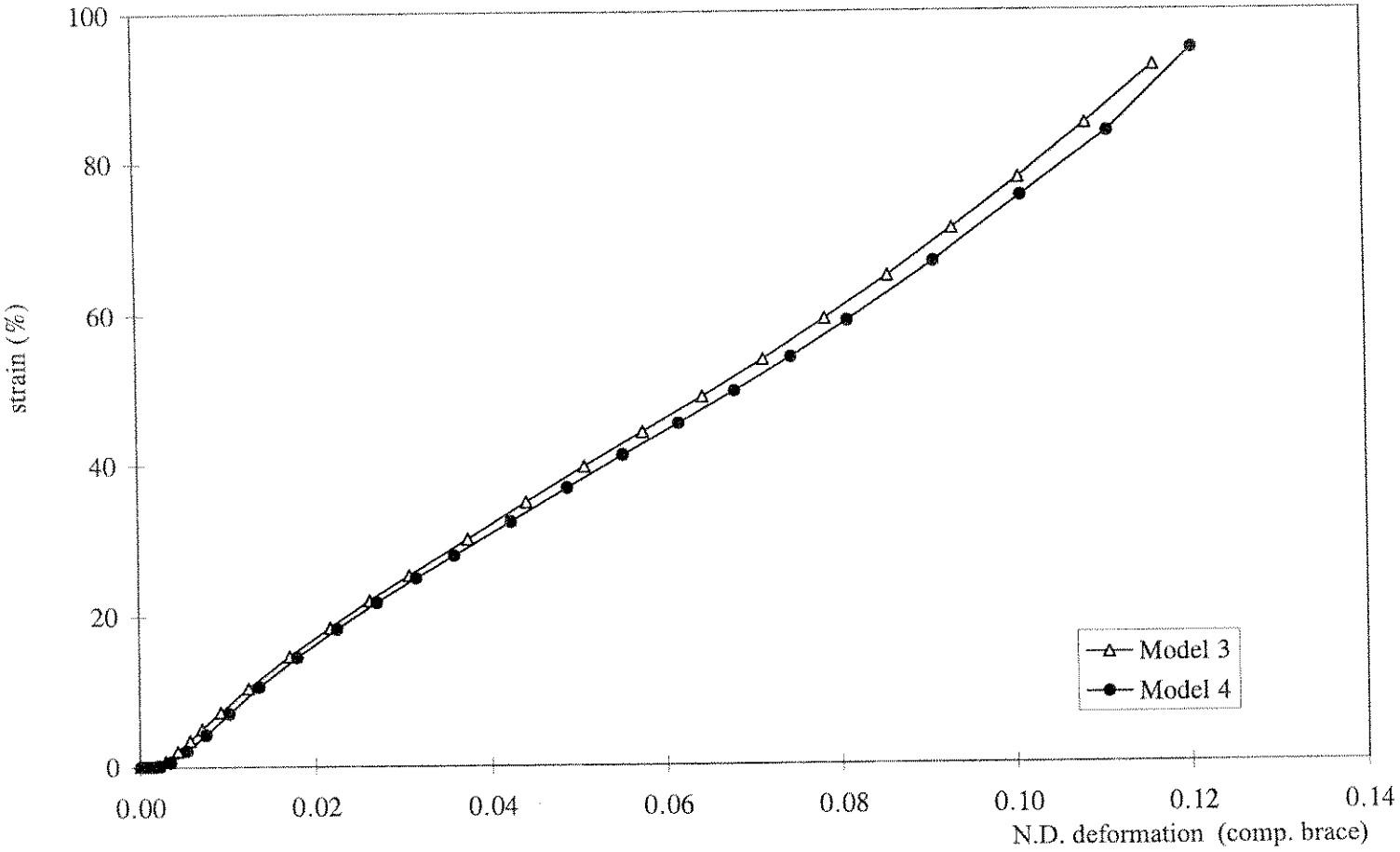

Figure 6.21: Maximum Equivalent Plastic Strain (Gap Region) vs. N.D. Deformation for K Joint, $\beta = 0.4$, $\gamma = 15$, $\tau = 0.81$

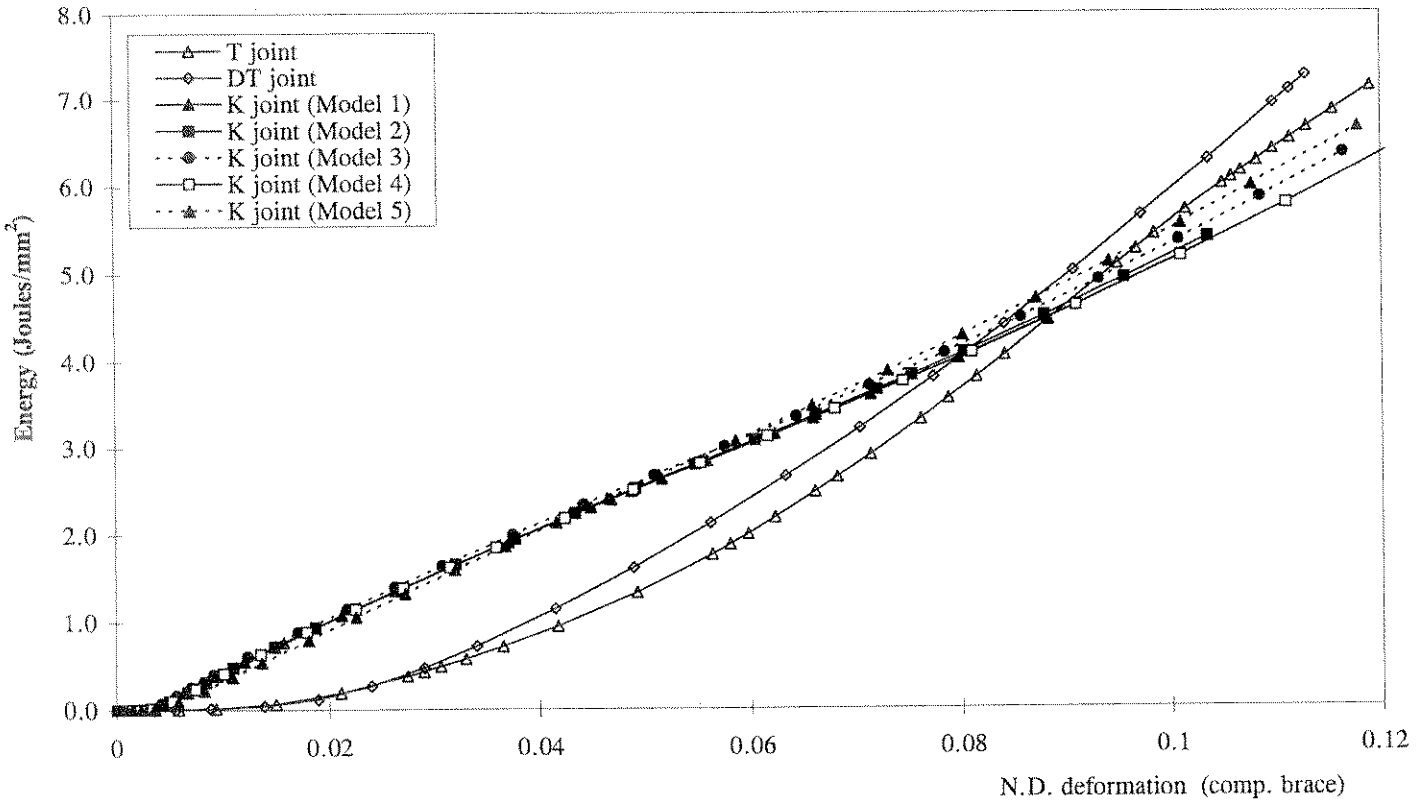

Figure 6.22: Variation of Plastic Work with N.D. Deformation

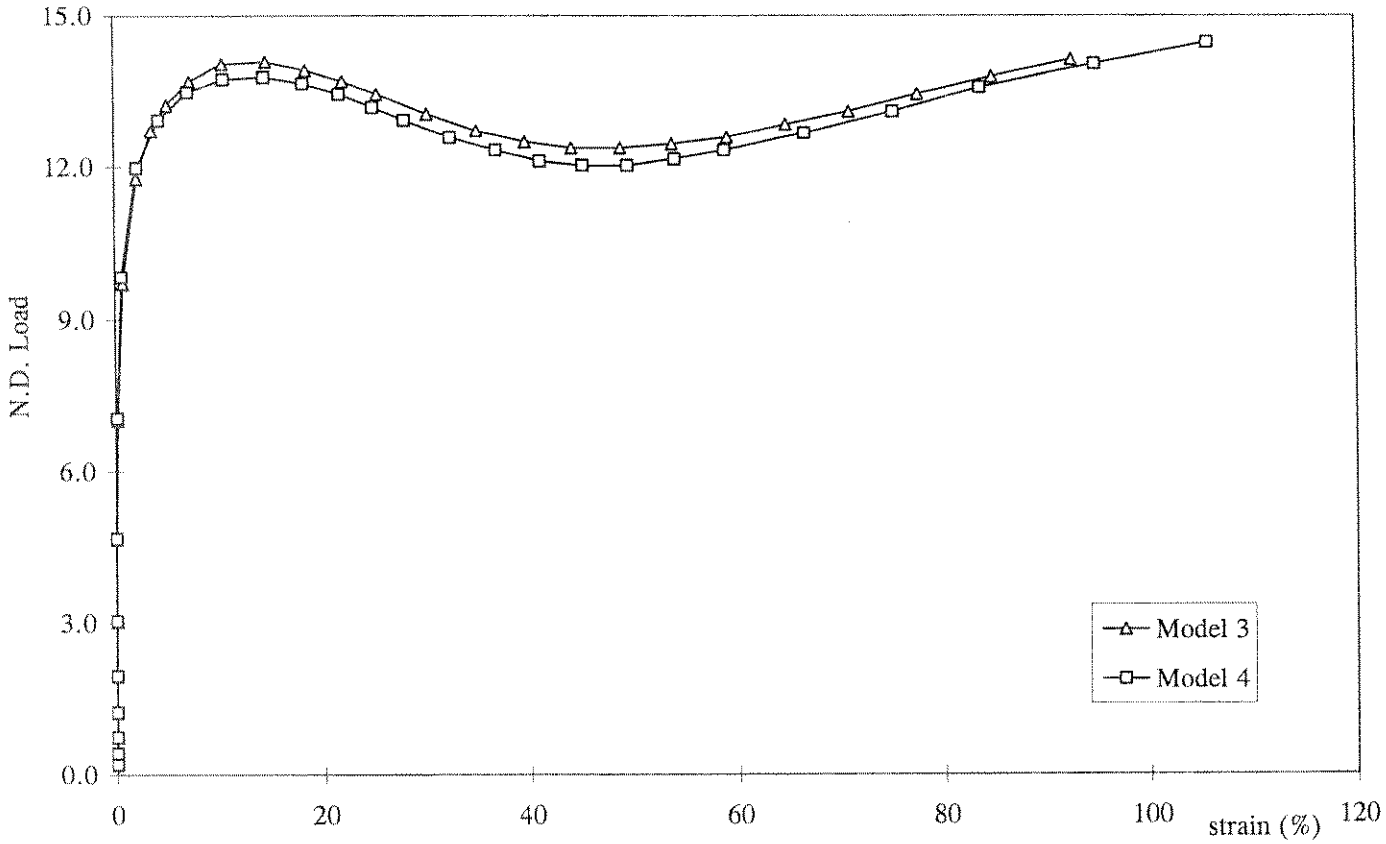

Figure 6.23: Load vs. Maximum Equivalent Plastic Strain in Chord (Gap Region) for K Joint, $\beta = 0.4$, $\gamma = 15$, $\tau = 0.81$

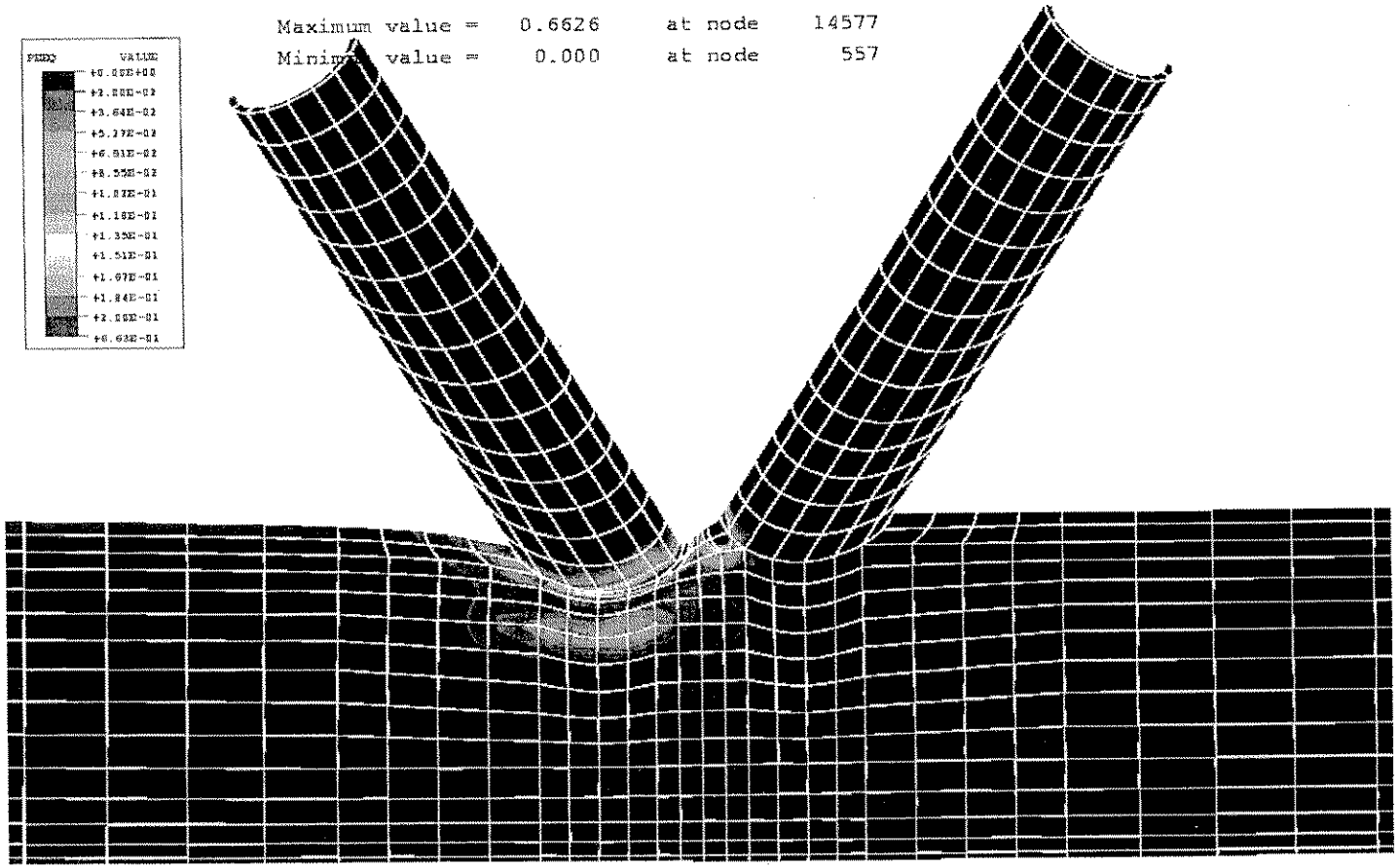

Figure 6.24: Contour Plot of Equivalent Plastic Strain

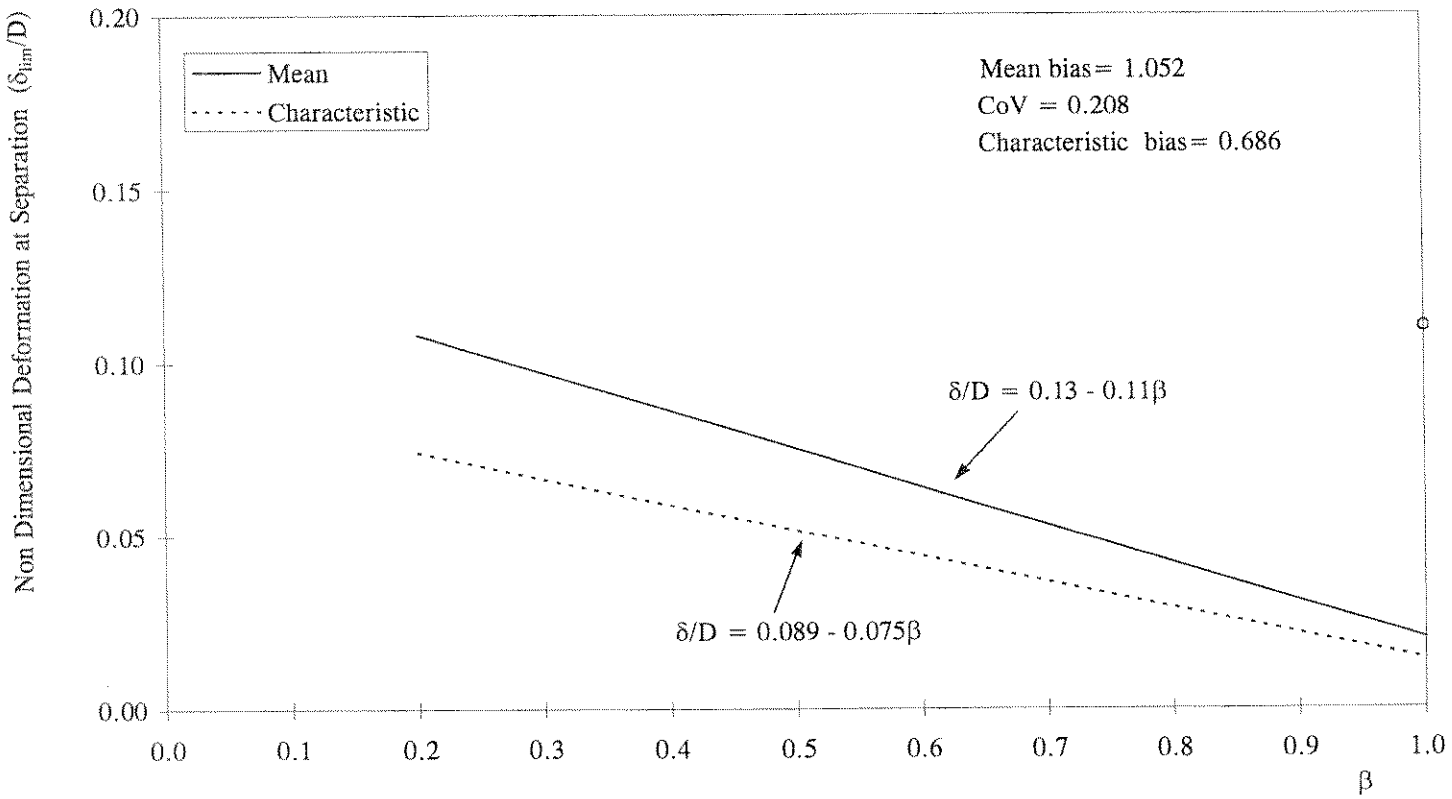

Figure 6.25: Non-Dimensional Deformation at Separation Against β for DT Joints Under Tension Loading

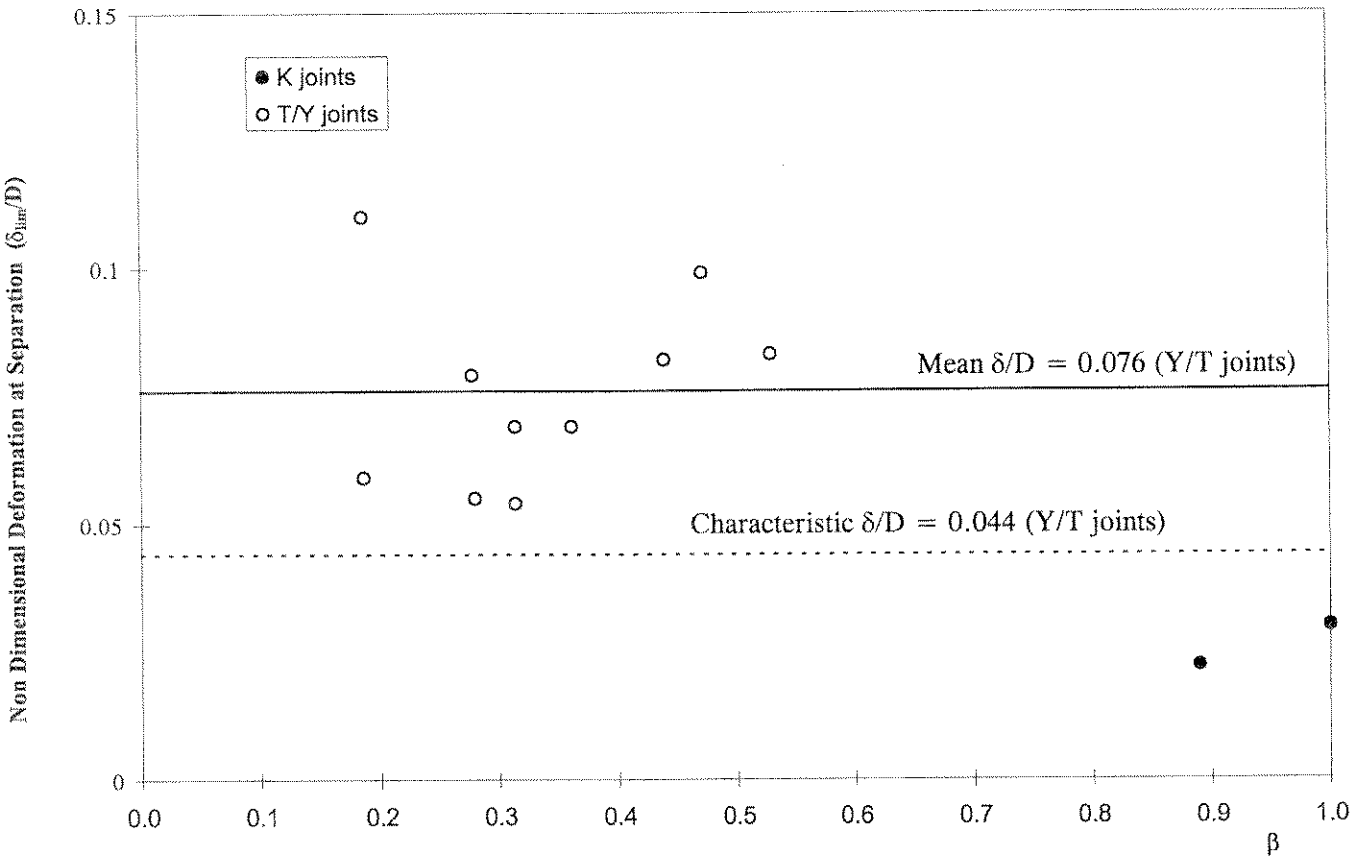

Figure 6.26: Non-Dimensional Deformation at Separation Against β for T/Y Joints Under Tension and K Joints Under Balanced Axial Loading

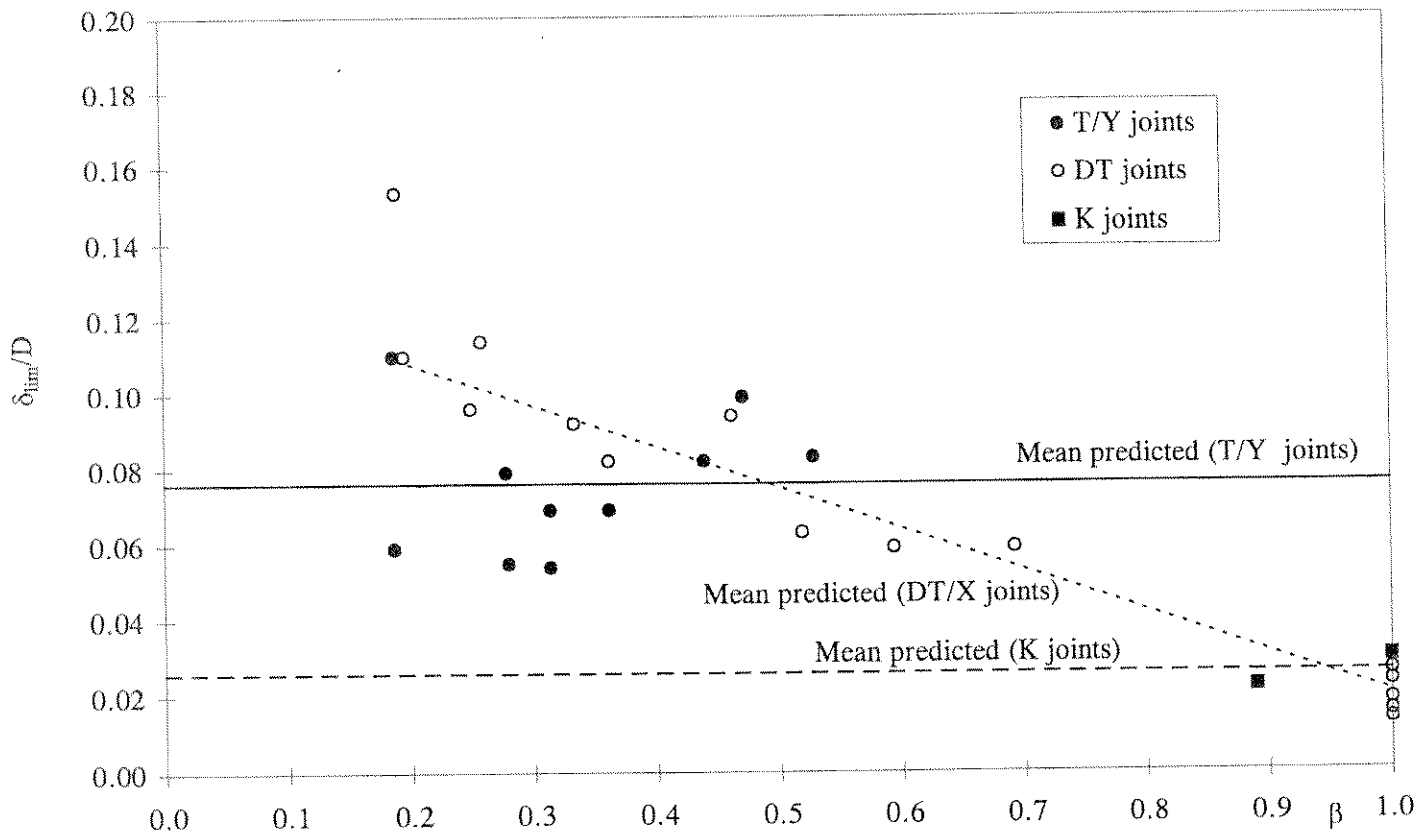

Figure 6.27: δ_{lim}/D for DT, T/Y Joints Under Tension Loading and K Joints Under Balanced Axial Loading

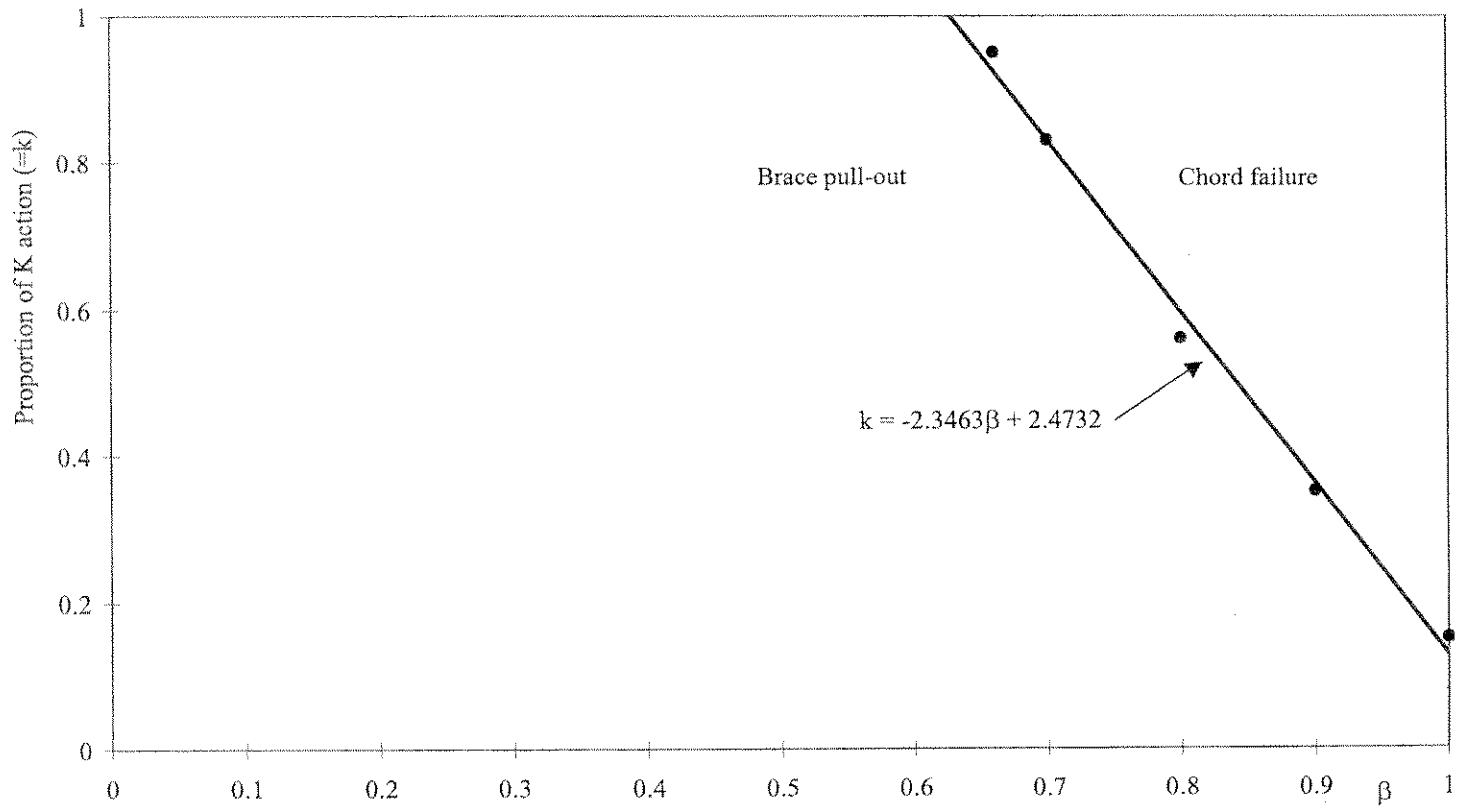

Figure 6.28: Plot of Degree of K Action vs. β at Which Chord Fracture Becomes Critical

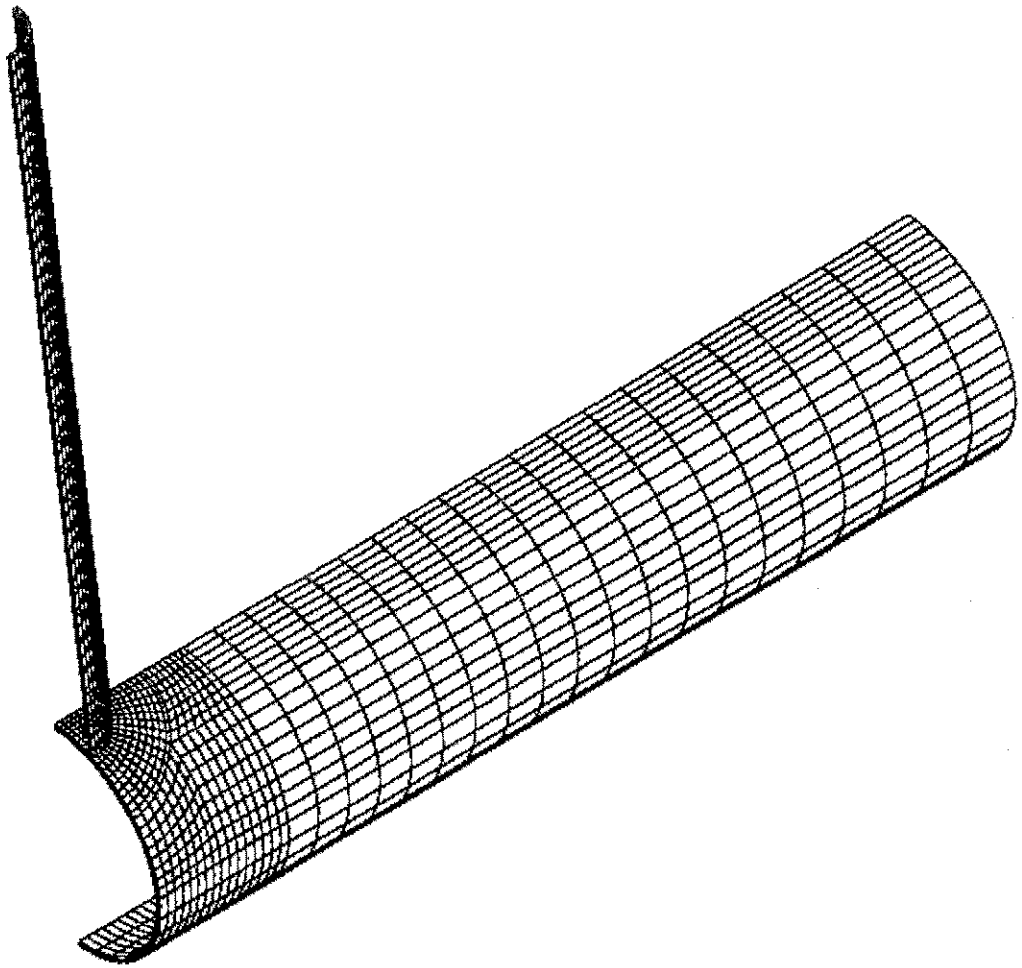

Figure 7.1: FE Mesh for T Joint, $\beta = 0.4$

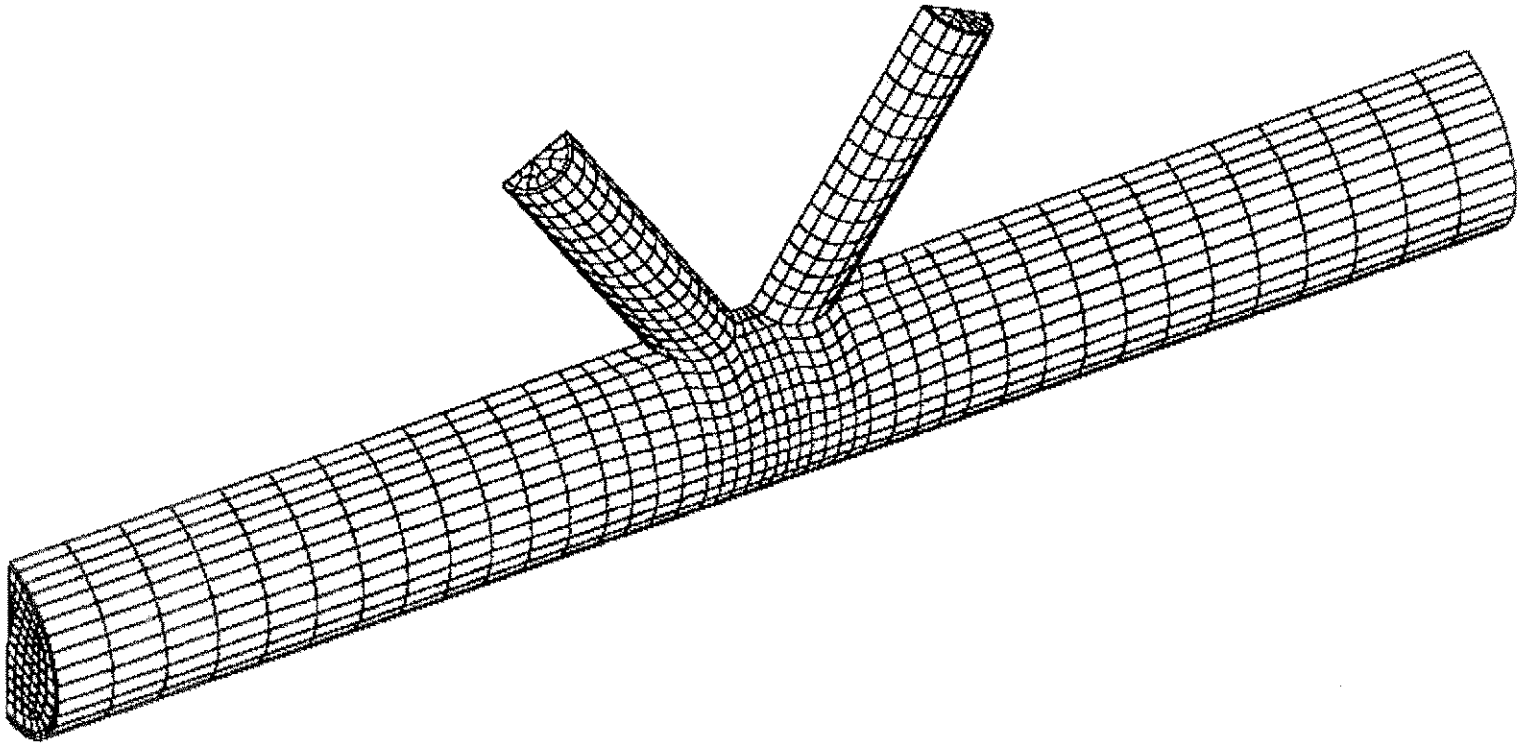

Figure 7.2: FE Mesh for K Joint, $\beta = 0.4$

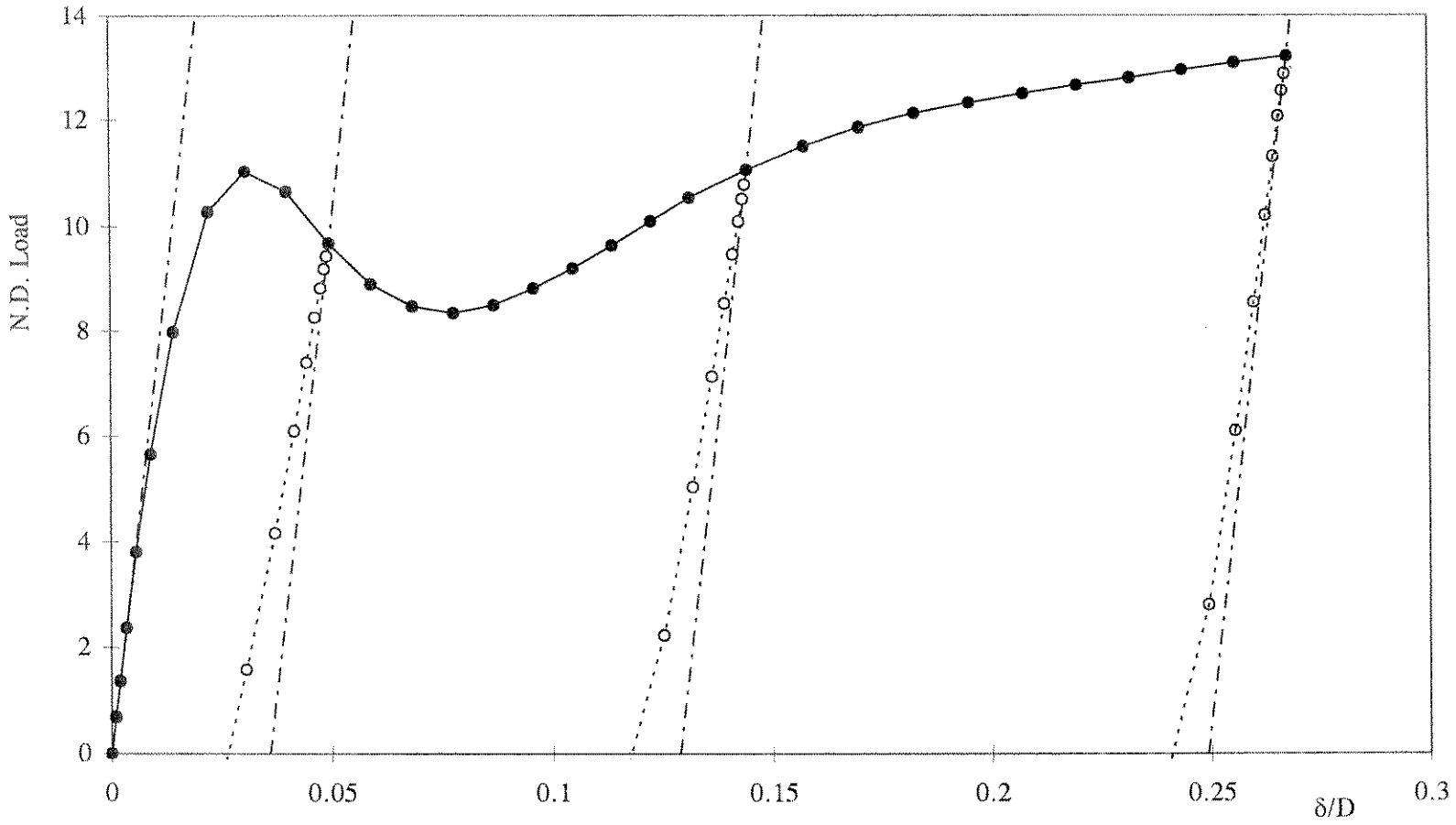

Figure 7.3: P-δ Plot for DT Joint under Compression Loading, β = 0.4, γ =25, τ =0.81

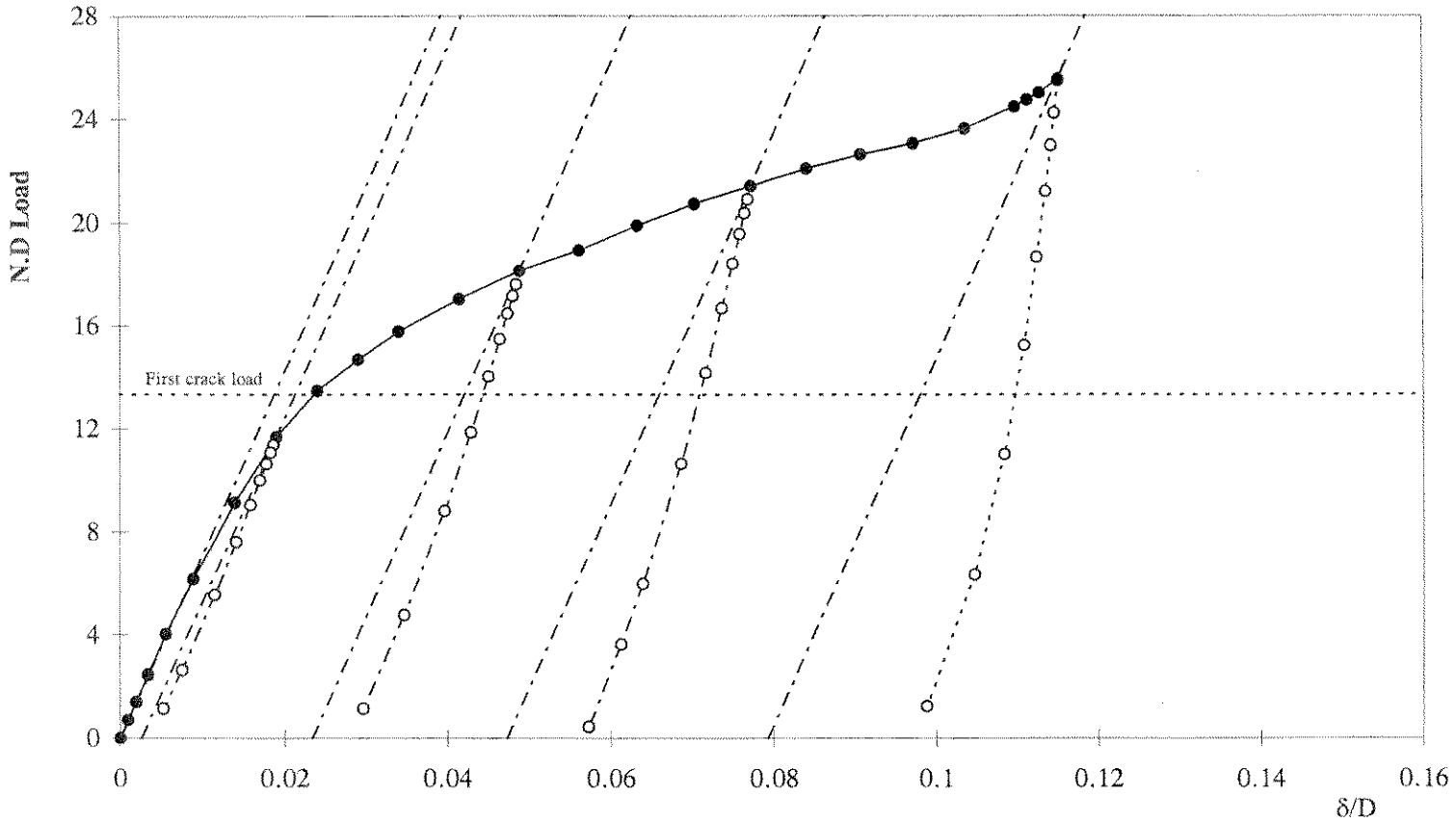

Figure 7.4: P-δ Plot for DT Joint under Tension Loading, $\beta = 0.4$, $\gamma = 25$, $\tau = 0.81$

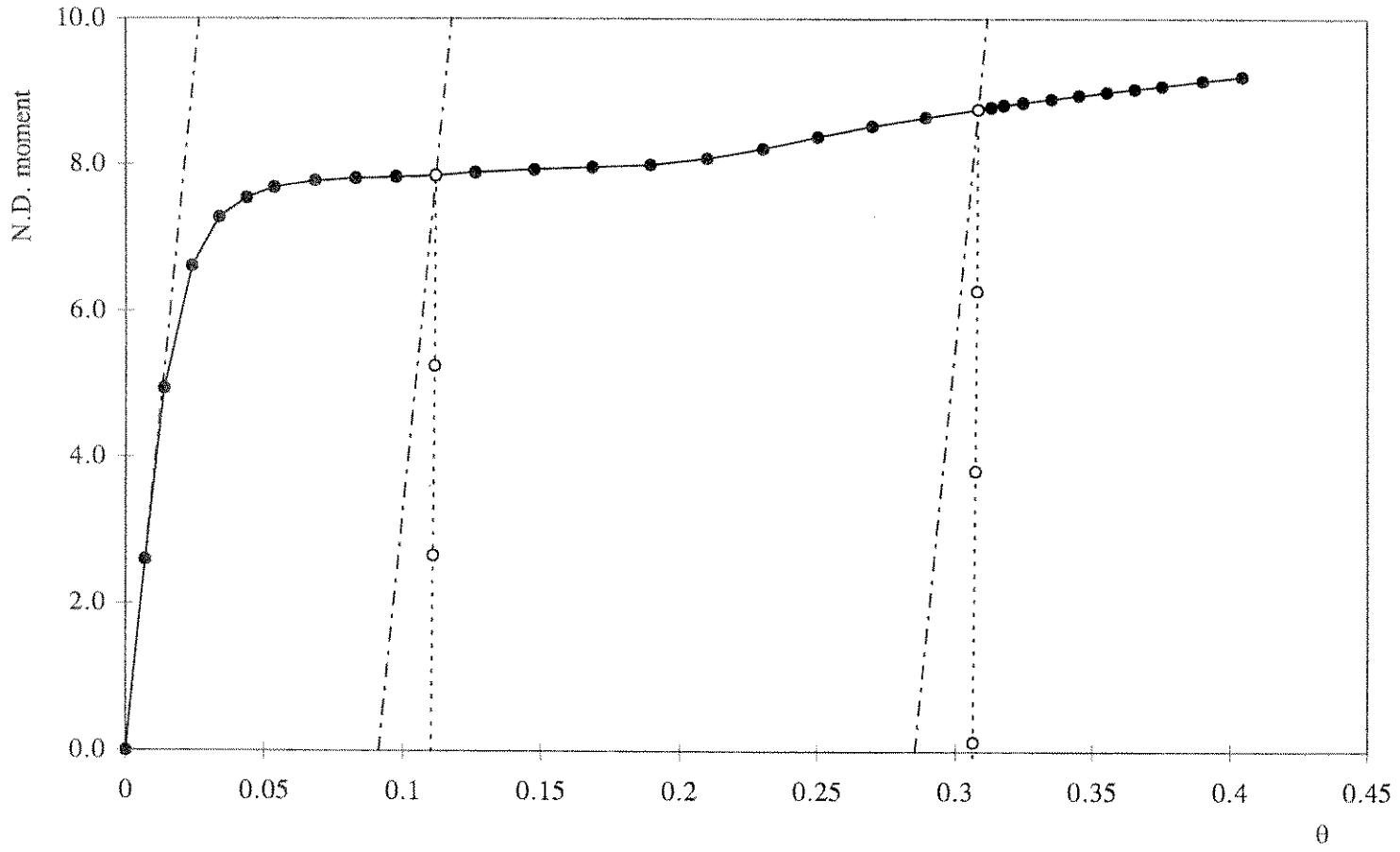

Figure 7.5: M-θ Curve for DT Joint under IPB Loading, β = 0.4, γ =25, τ =0.81

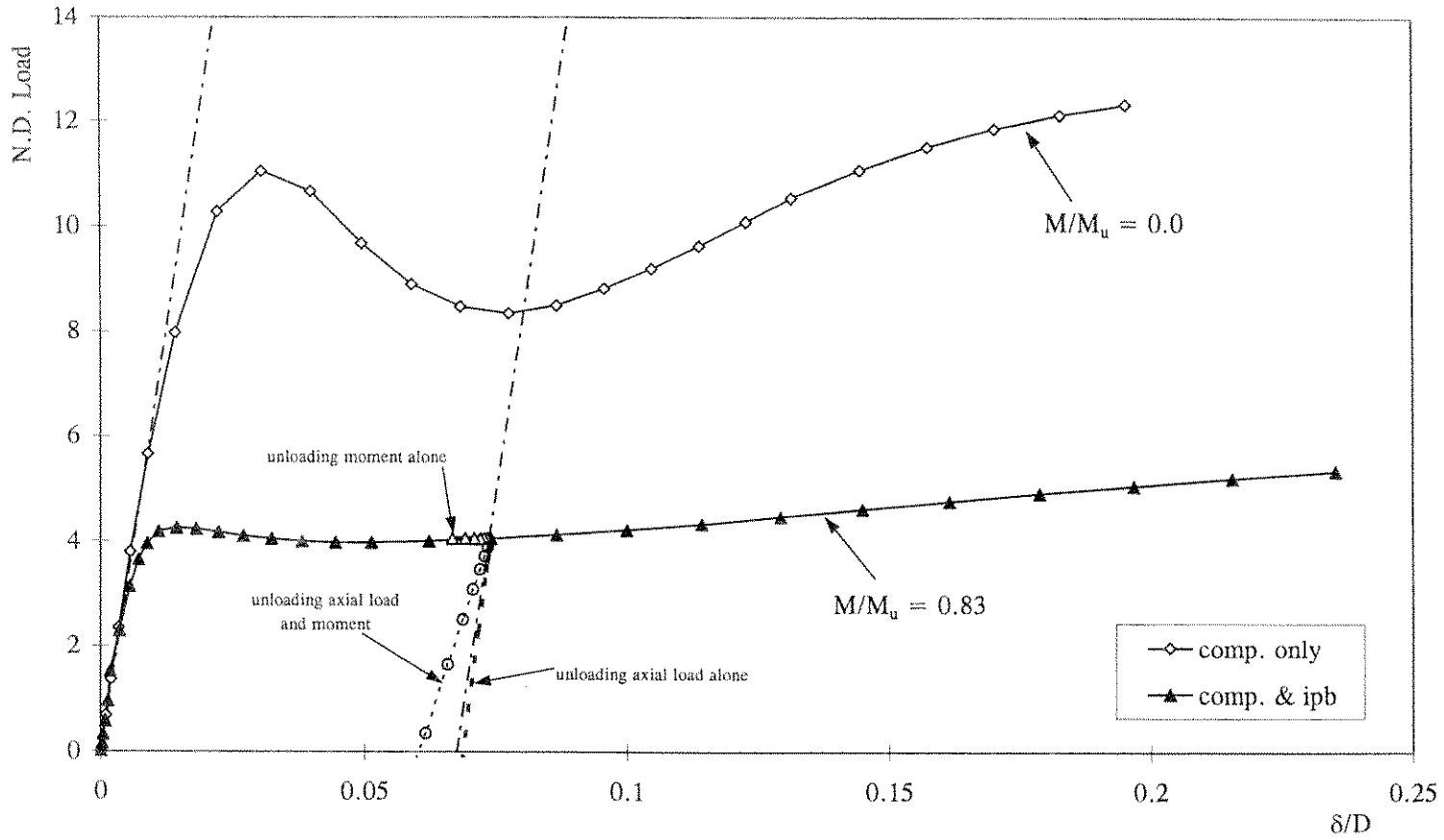

Figure 7.6: P-δ Plot for DT Joint under Proportional Compression and IPB Loading, β = 0.4, γ =25, τ = 0.81

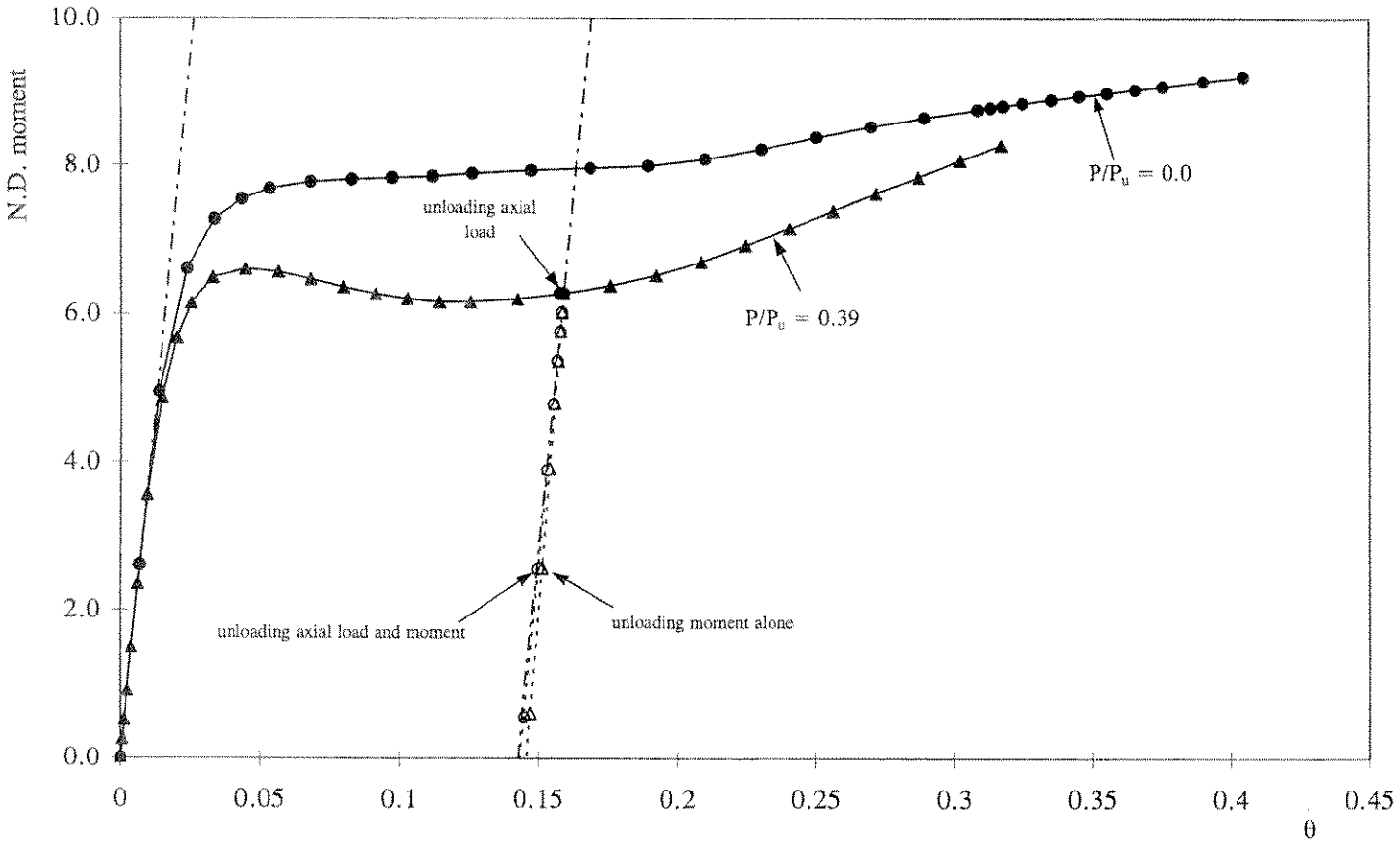

Figure 7.7: M-θ Curve for DT Joint under Axial and IPB Loading (Proportional Loading), β = 0.4, γ =25, τ =0.81

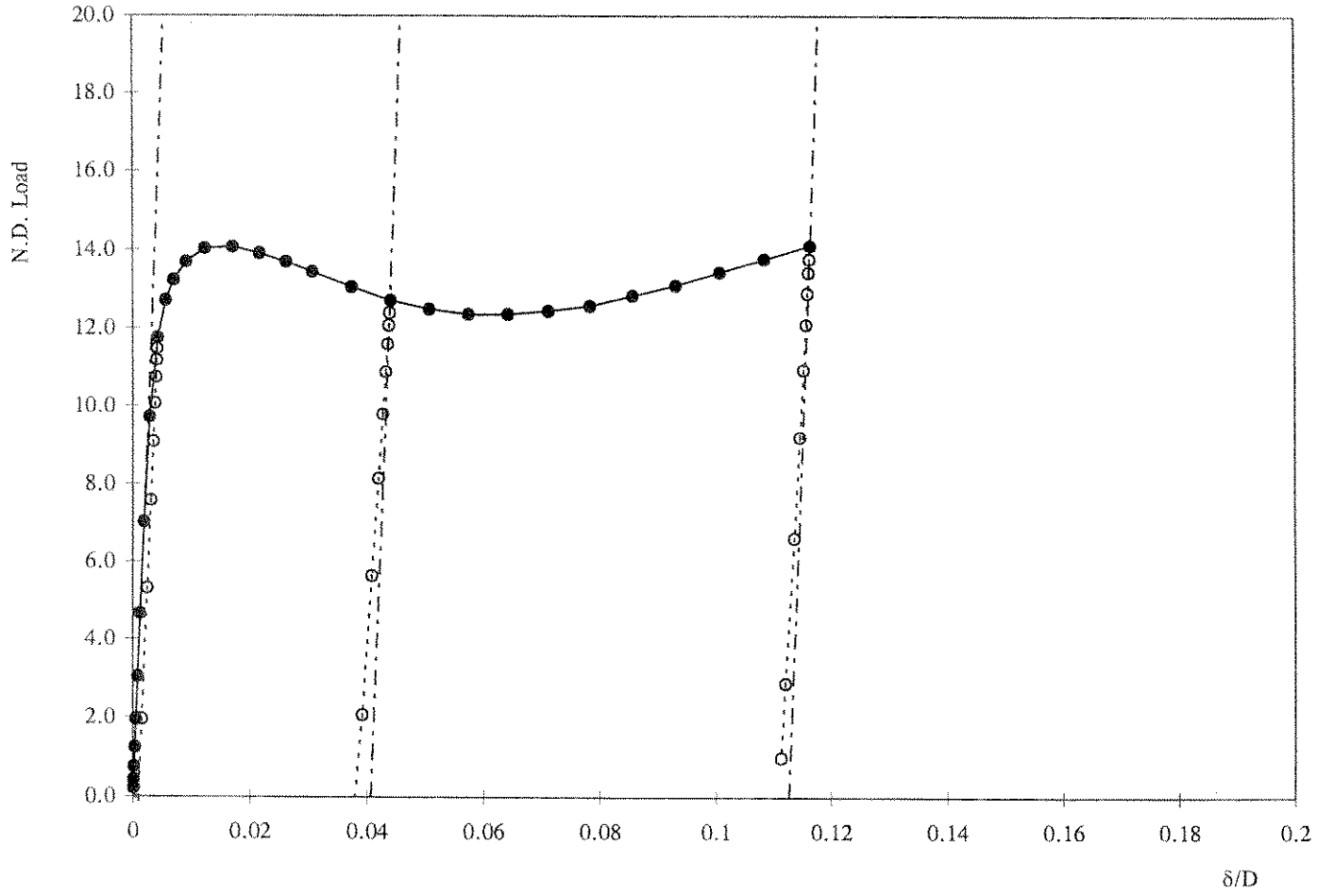

Figure 7.8: P-δ Curve (Compression Brace) for K Joint, β = 0.4, γ =15, τ =0.81

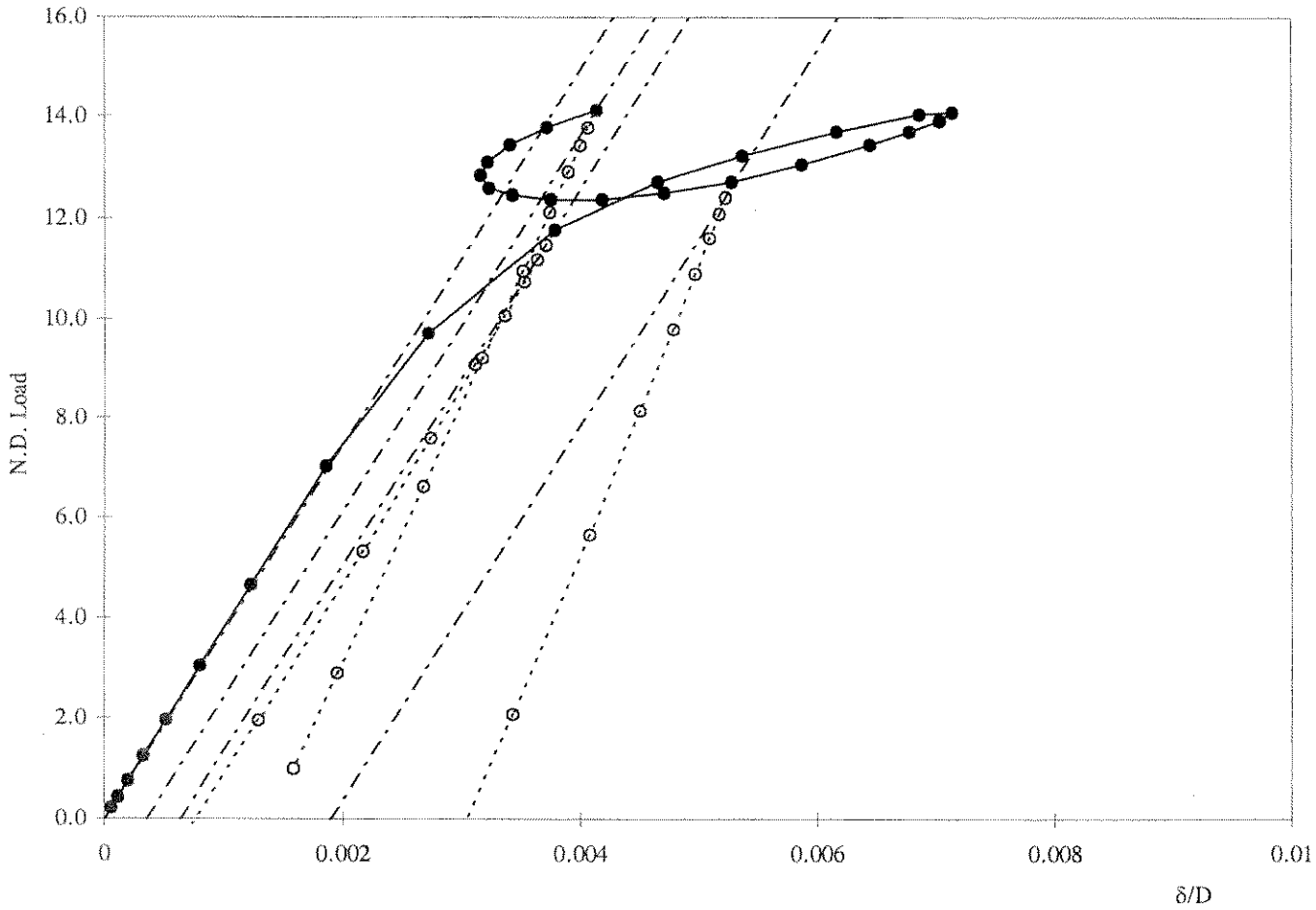

Figure 7.9: P-δ Curve (Tension Brace) for K Joint, β = 0.4, γ =15, τ =0.81

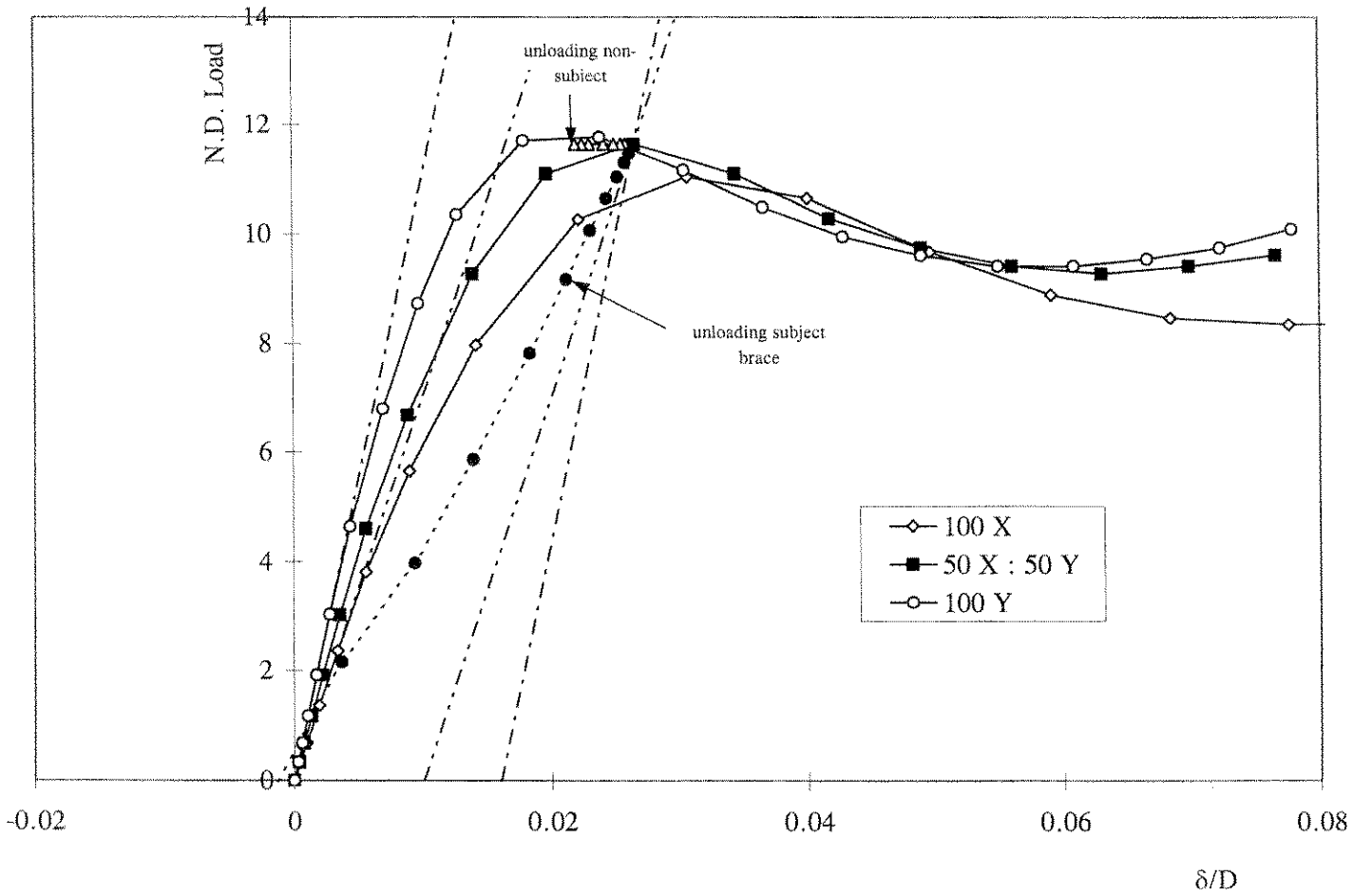

Figure 7.10: P-δ Plot for DT Joint under Compression Loading, β = 0.4, γ =25, τ = 0.81

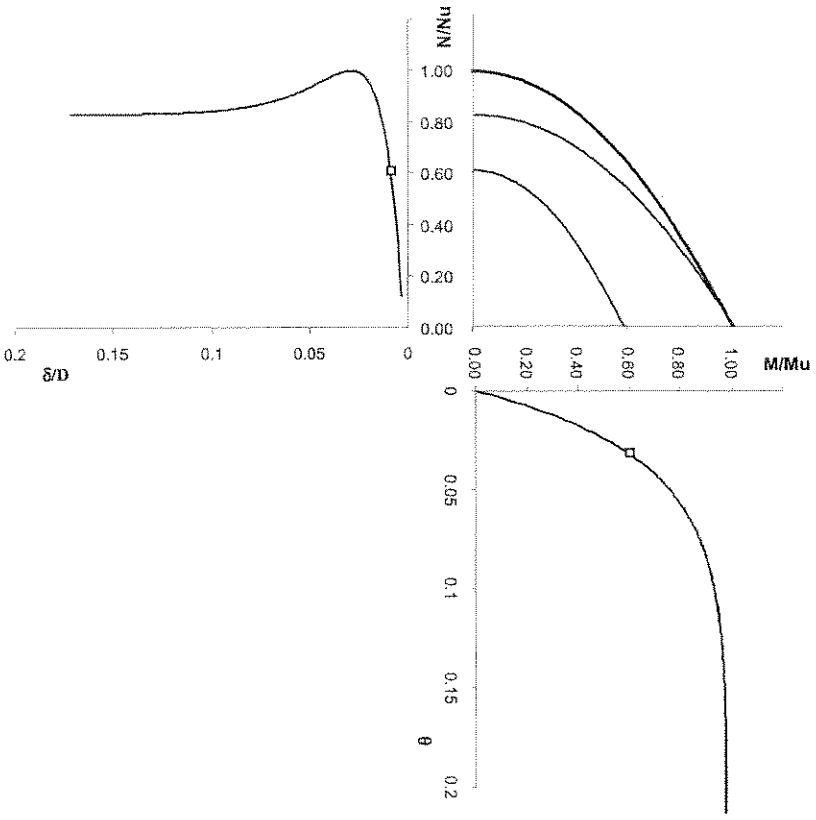

Figure 8.1: Plasticity model for combined loading

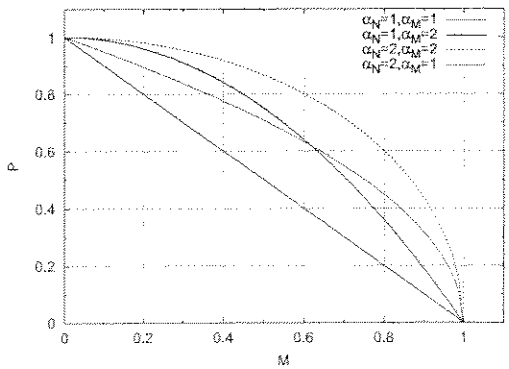

Figure 8.2: Shape of interaction surfaces

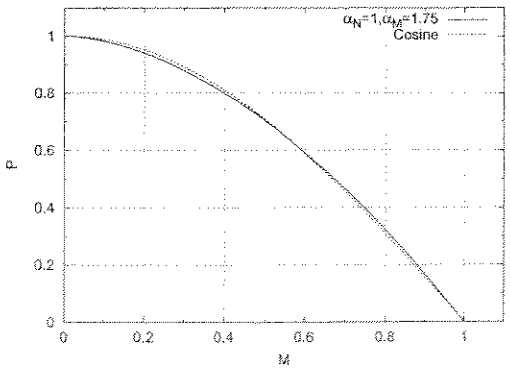

Figure 8.3: Comparison with API joint formula

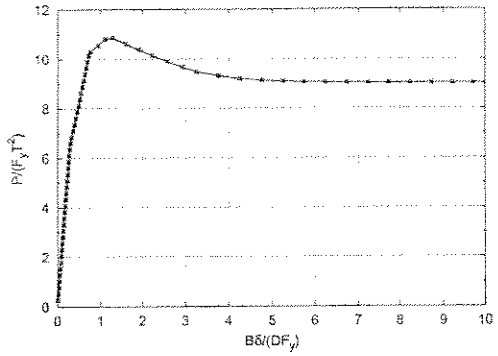

Figure 8.4: Compression loading

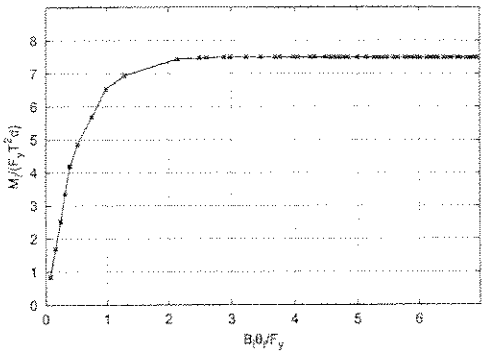

Figure 8.5: In-plane bending

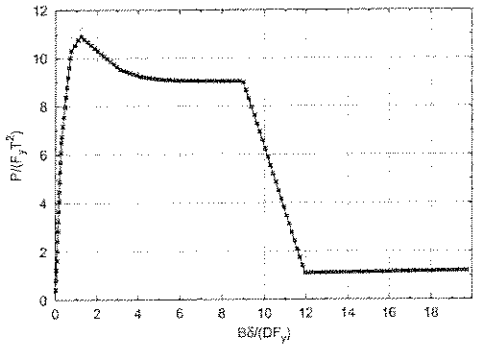

Figure 8.6: Ductility limit and simulation of rupture

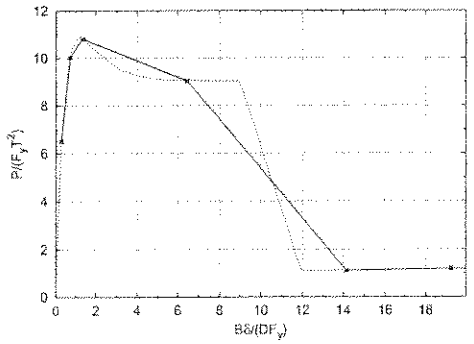

Figure 8.7: Simulation using extremely coarse load steps

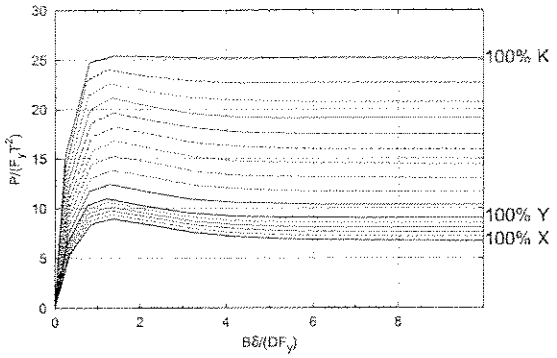

Figure 8.8: Uni-axial Pδ curves for joints of mixed classification. Compression

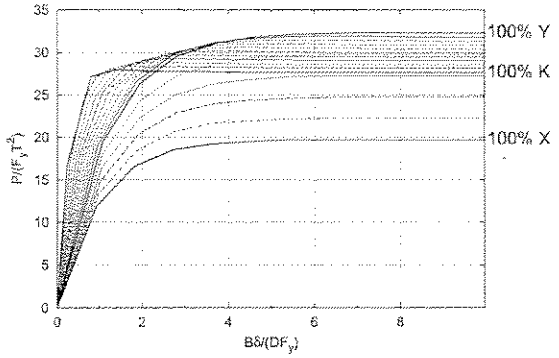

Figure 8.9: Uni-axial Pδ curves for joints of mixed classification. Tension

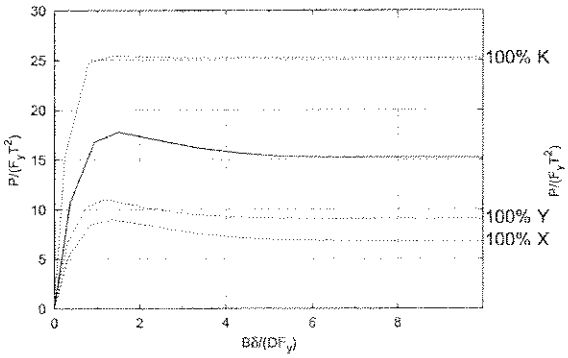

Figure 8.10: Compression Pδ curve for 30% Y, 20% X and 50% K

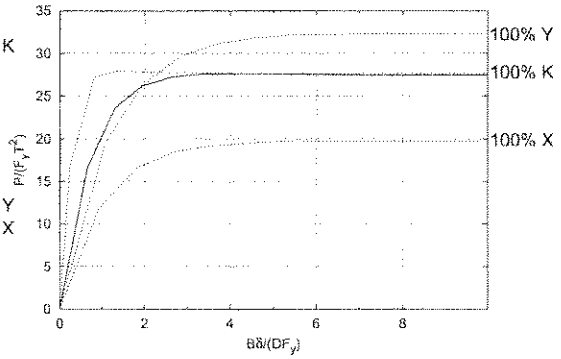

Figure 8.11: Tension Pδ curve for 30% Y, 20% X and 50% K

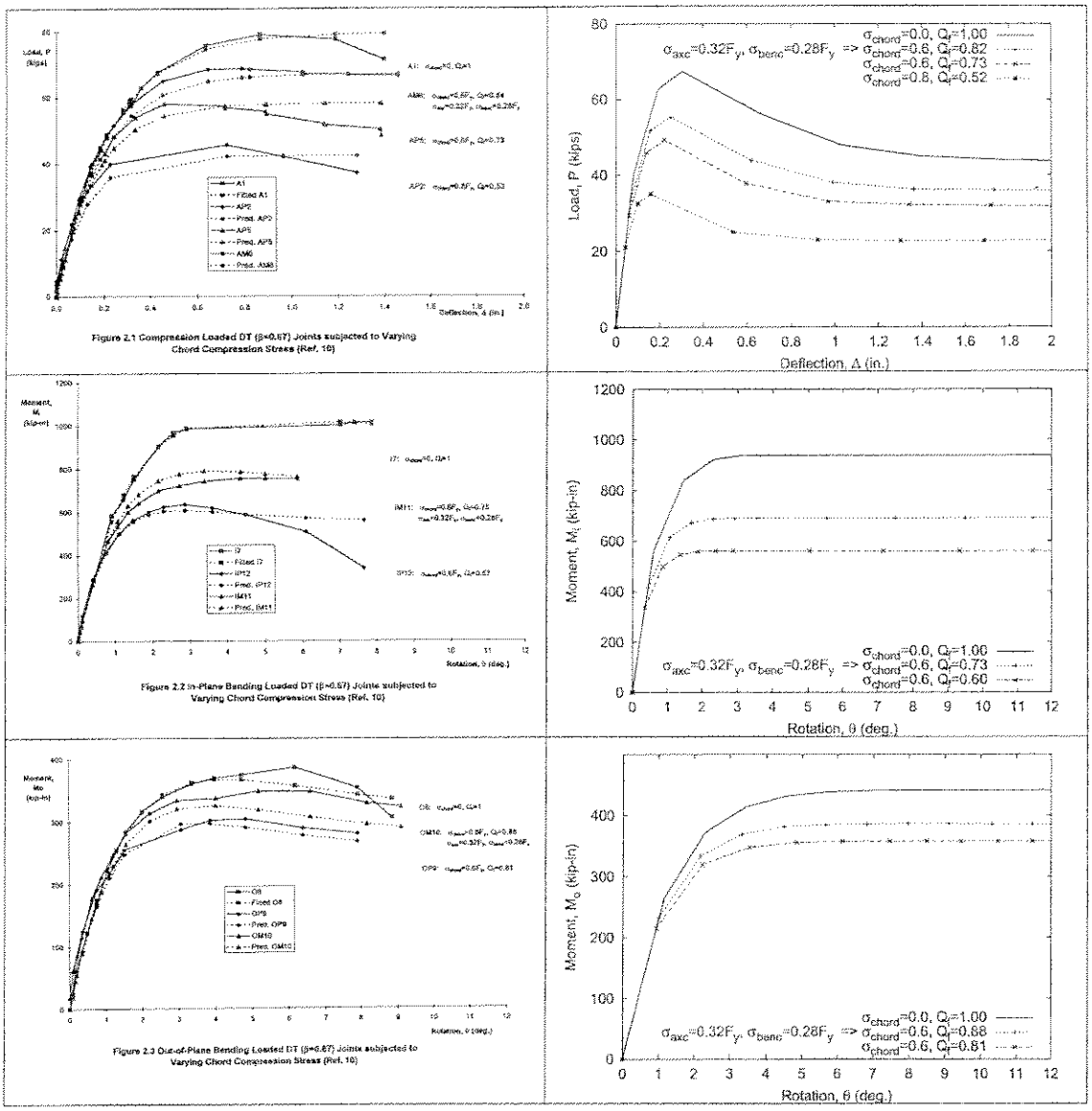

Figure 8.12: Compression loaded DT (β=0.67) joints subjected to varying chord compression stresses. Test results[8.1] and numerical predictions.

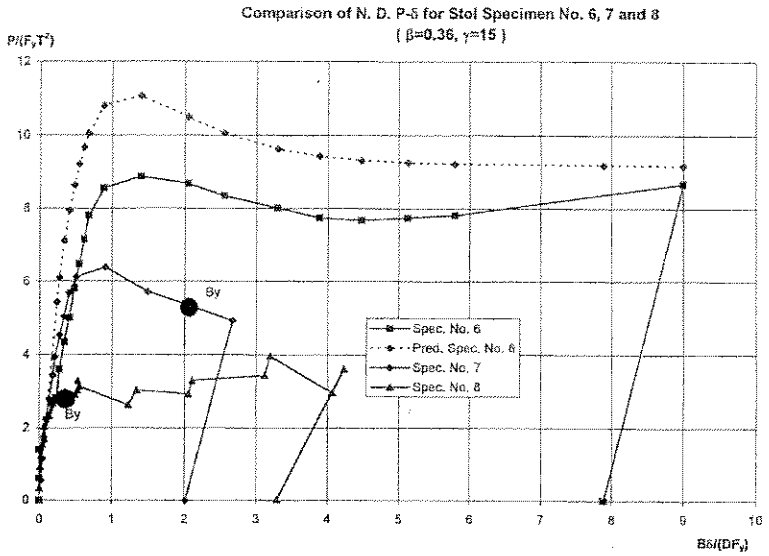

Figure 8.13: Pδ Response

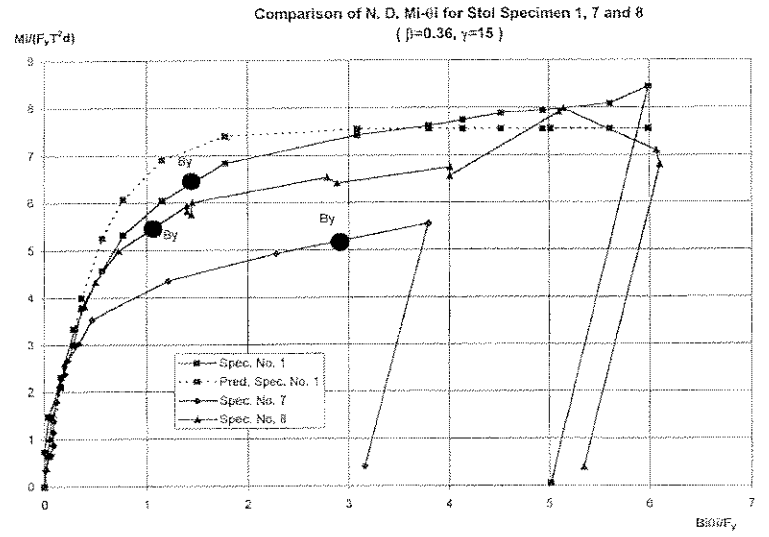

Figure 8.14: Mθi Response

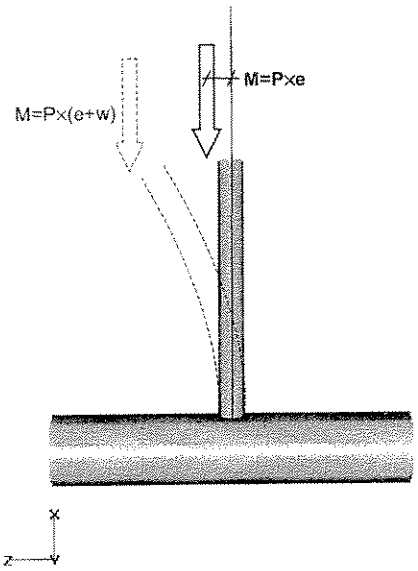

Figure 8.15: Numerical model

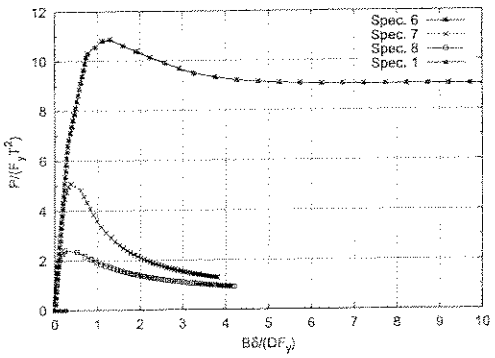

Figure 8.16: Numerical Pδ behaviour with P-Δ effects

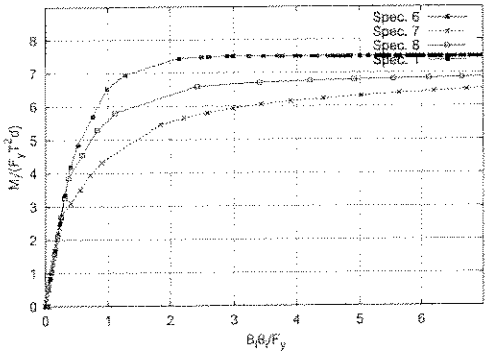

Figure 8.17: Numerical $M\theta_i$ behaviour with P-Δ effects

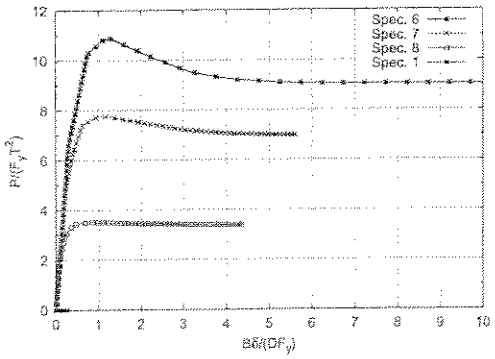

Figure 8.18: Numerical Pδ behaviour excluding P-Δ effects

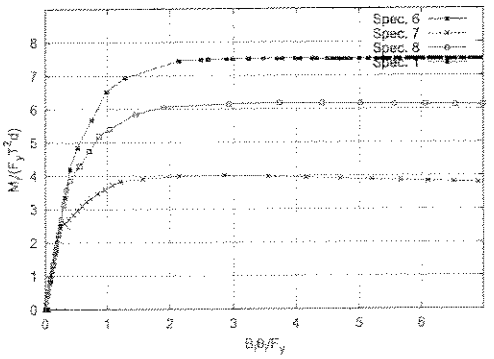

Figure 8.19: Numerical $M\theta_i$ behaviour excluding P-Δ effects

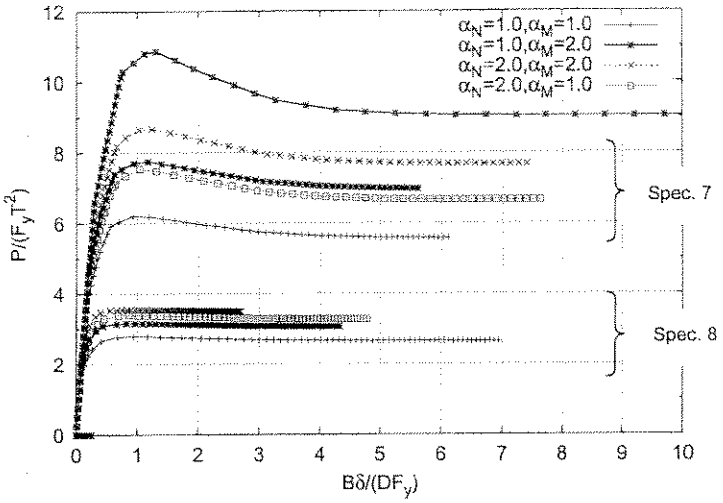

Figure 8.20: Effect of yield surface shape on Pδ

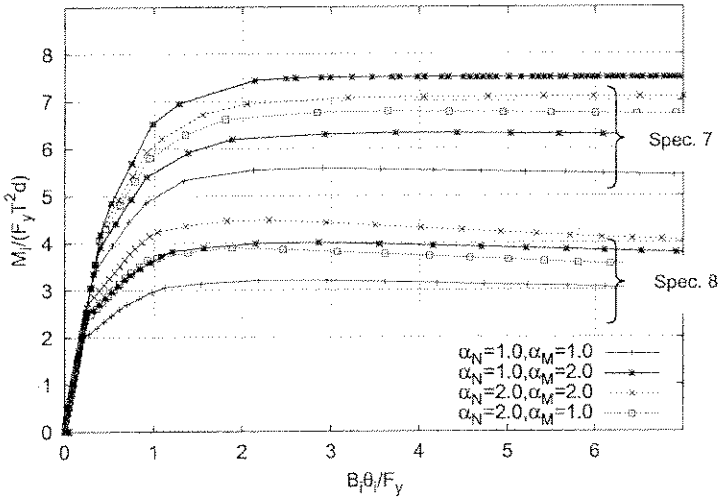

Figure 8.21: Effect of yield surface shape on Mθ characteristics

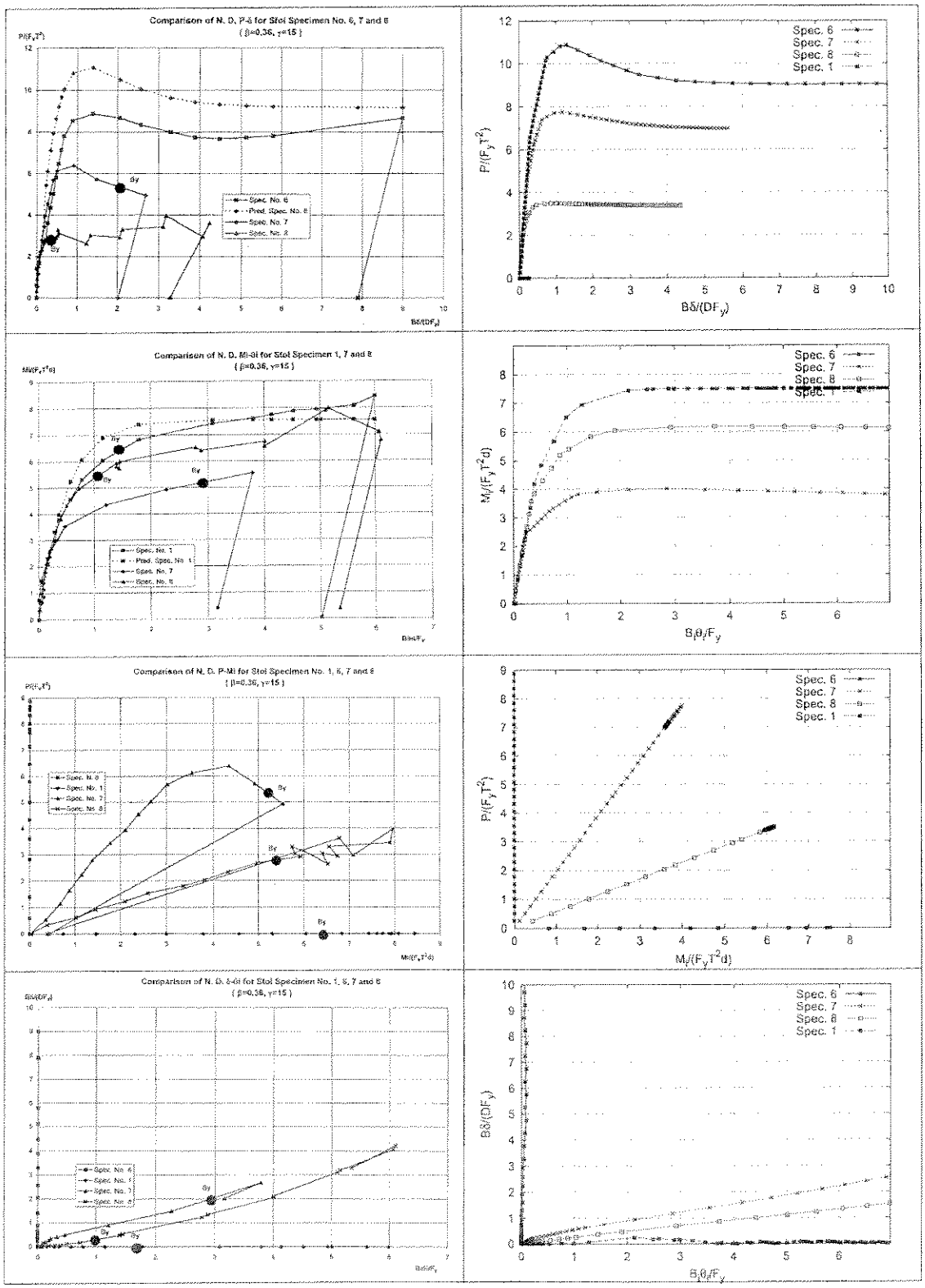

Figure 8.22: Combined Axial and IPB loading. Stol specimens 1, 6, 7 and 8

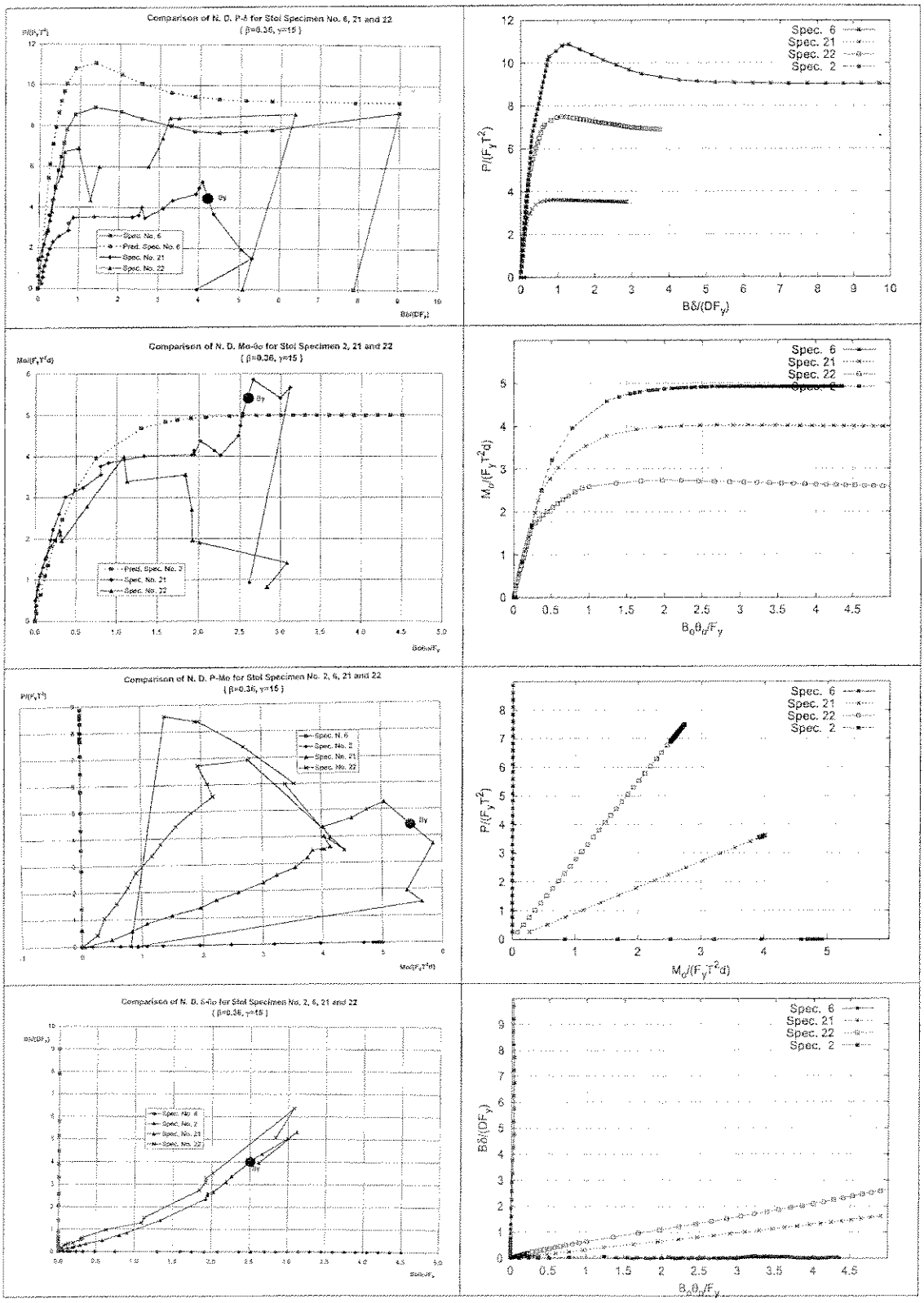

Figure 8.23: Combined Axial and OPB loading. Stol specimens 2, 6, 21 and 22

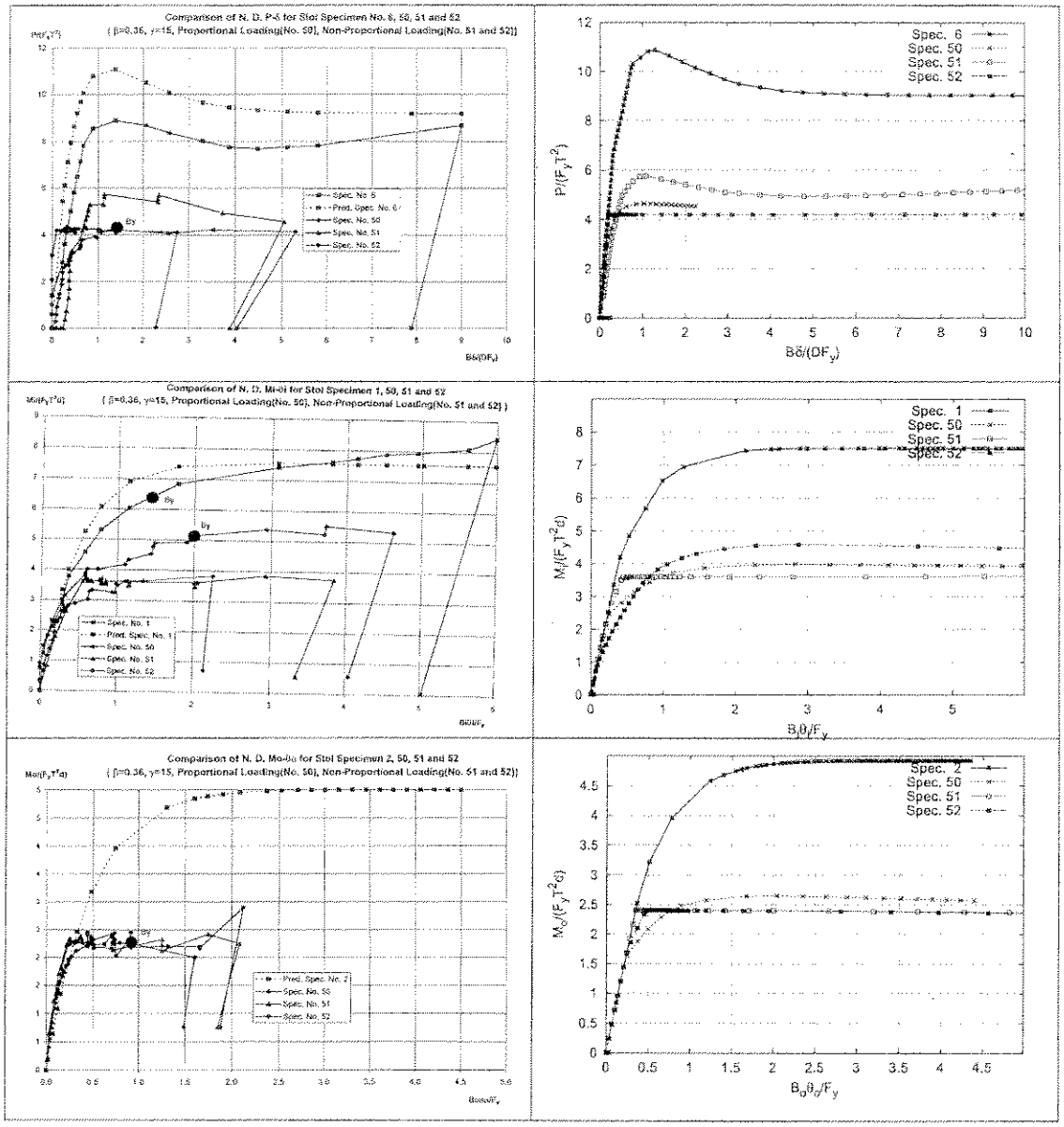

Figure 8.24: Combined Axial, IPB and OPB loading. Stol specimens 1, 2, 6, 50, 51 and 52. Proportional loading (No. 50), Non-proportional loading (Nos. 51 and 52)

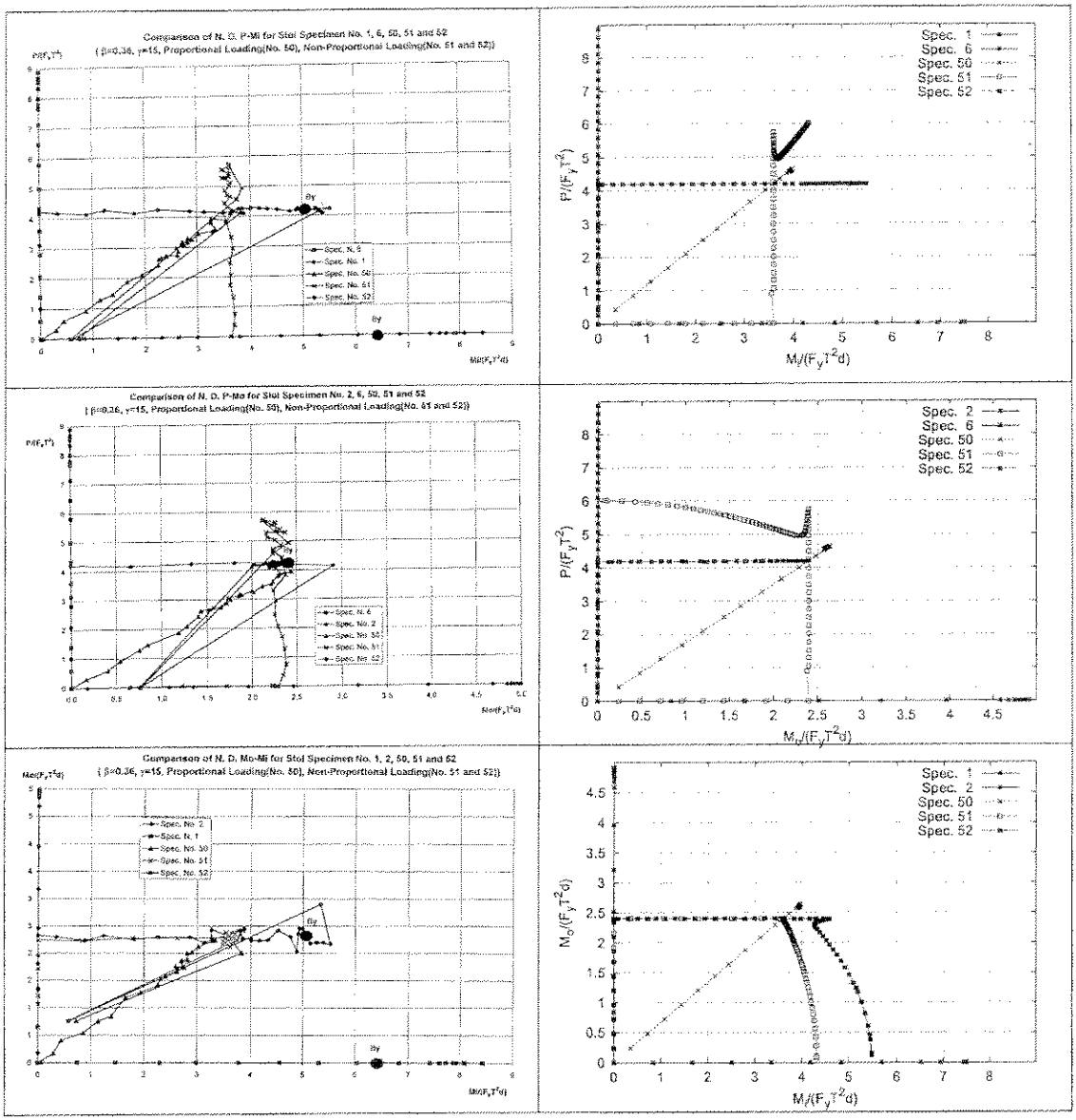

Figure 8.25: Combined Axial, IPB and OPB loading. Stol specimens 1, 2, 6, 50, 51 and 52. Proportional loading (No. 50), Non-proportional loading (Nos. 51 and 52)

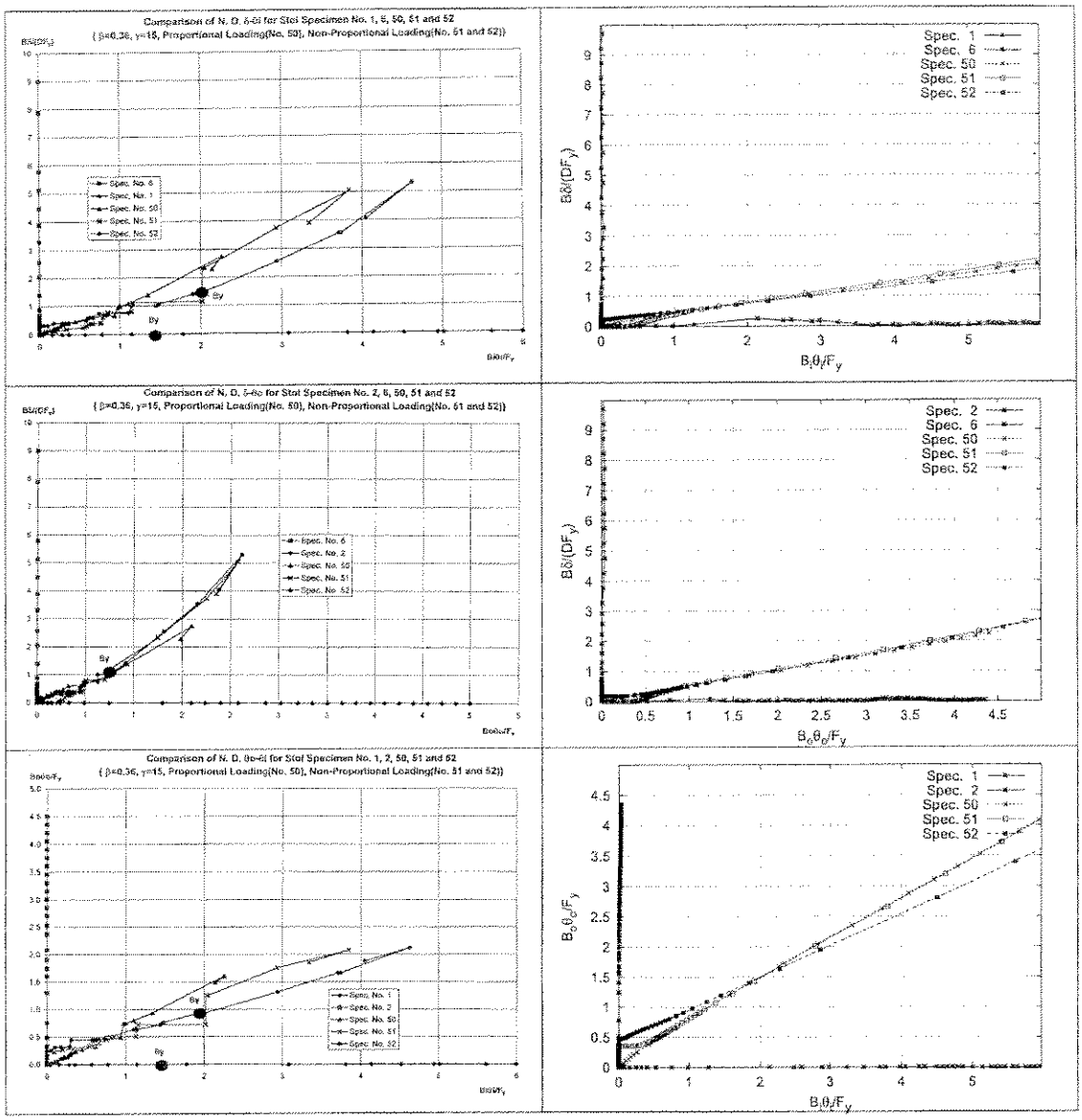

Figure 8.26: Combined Axial, IPB and OPB loading. Stol specimens 1, 2, 6, 50, 51 and 52. Proportional loading (No. 50), Non-proportional loading (Nos. 51 and 52)

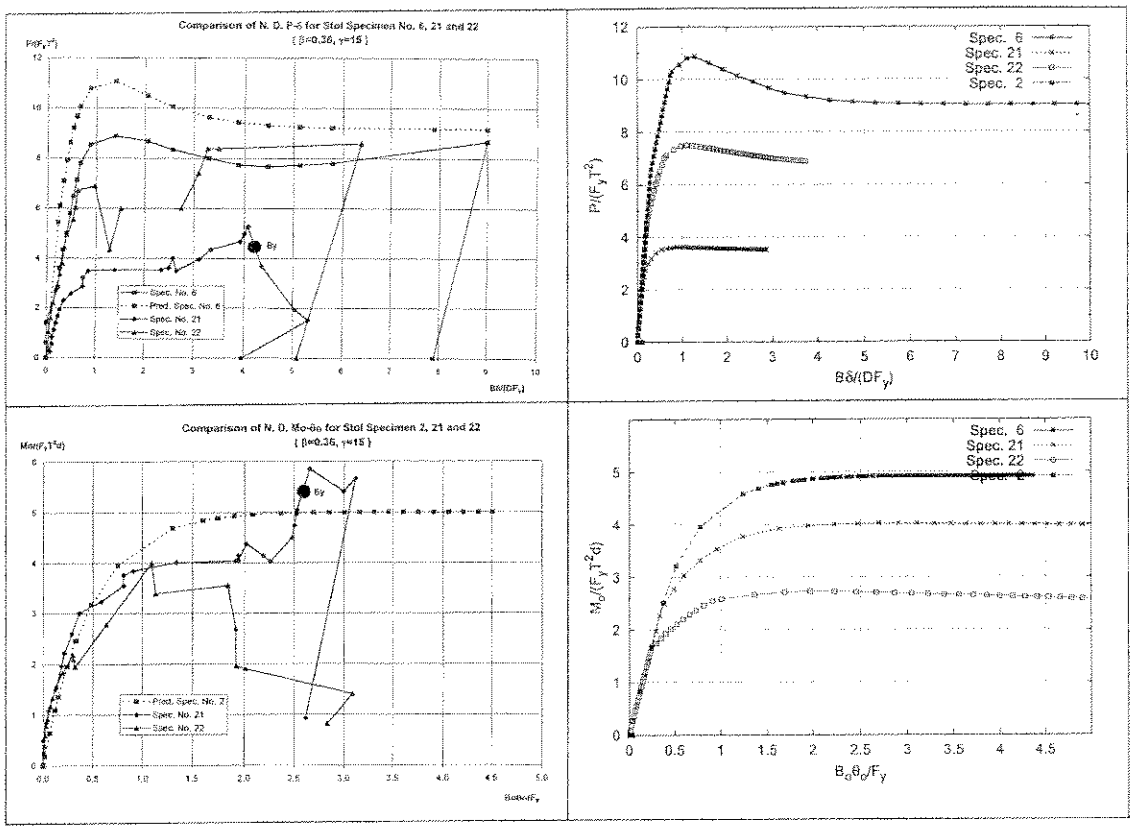

Figure 8.27: Combined Axial and OPB loading. Stol specimens 2, 6, 21 and 22 α_N=1, α_{IPB}=2, α_{OPB}=2

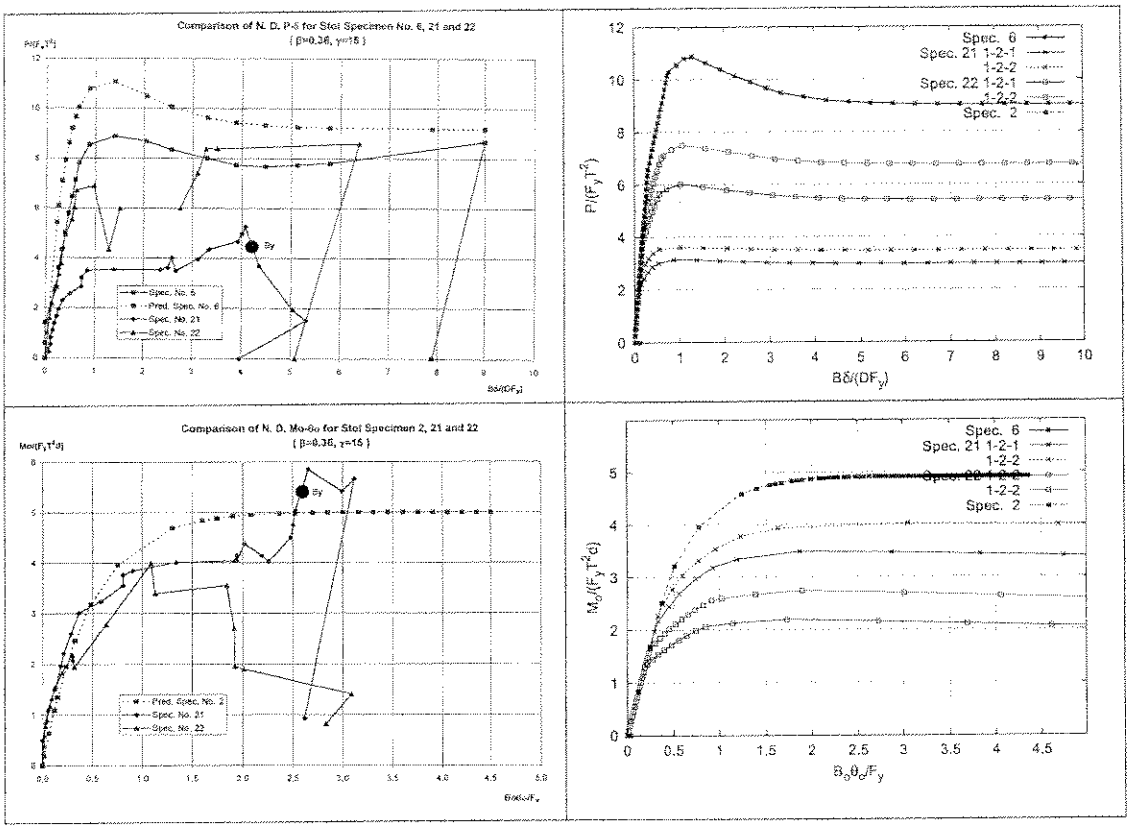

Figure 8.28: Combined Axial and OPB loading. Stol specimens 2, 6, 21 and 22
α_N=1, α_{IPB}=2, α_{OPB}=1

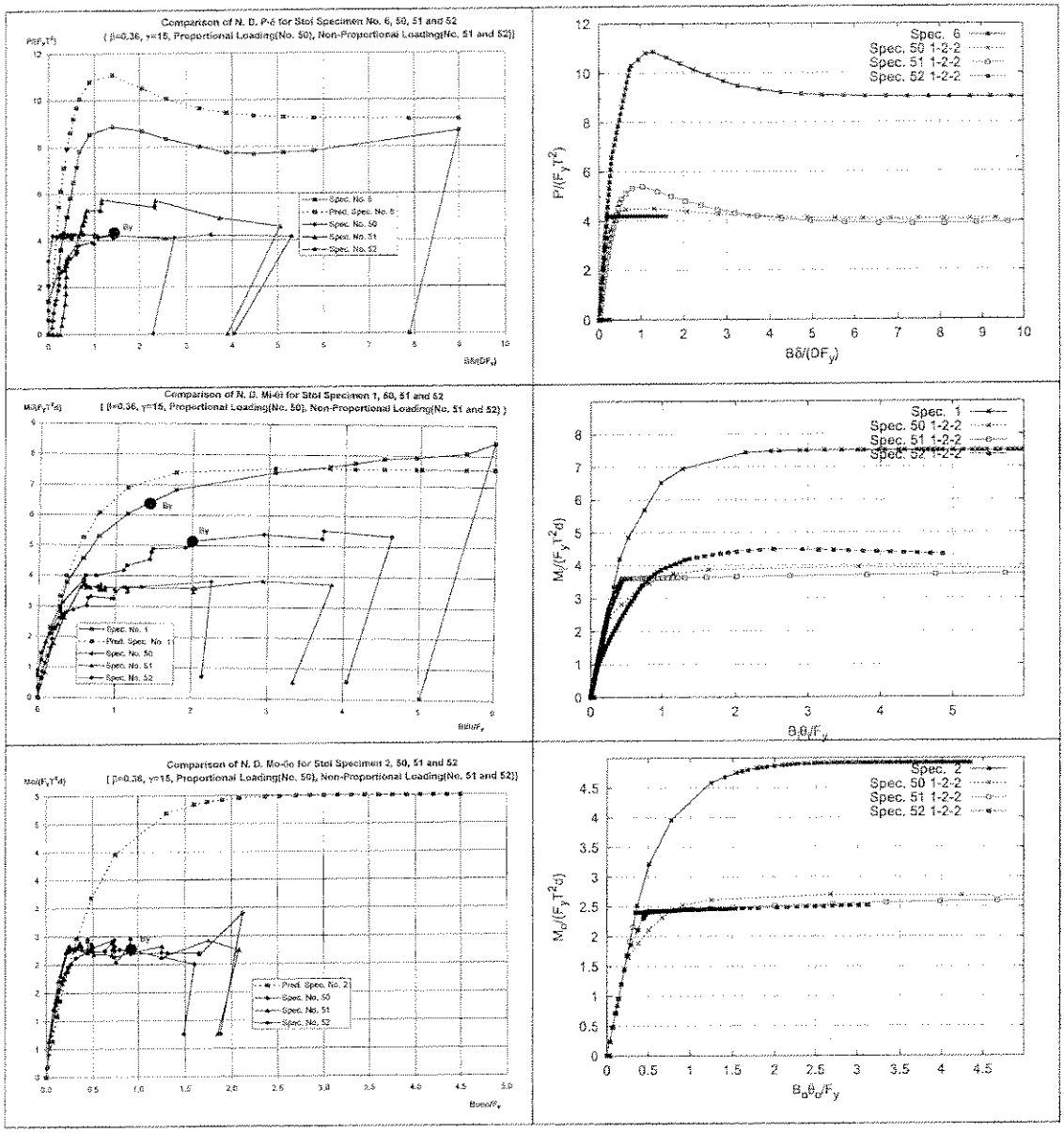

Figure 8.29: Combined Axial, IPB and OPB loading. Stol specimens 1, 2, 6, 50, 51 and 52. Proportional loading (No. 50), Non-proportional loading (Nos. 51 and 52) α_N=1, α_{IPB}=2, α_{OPB}=2

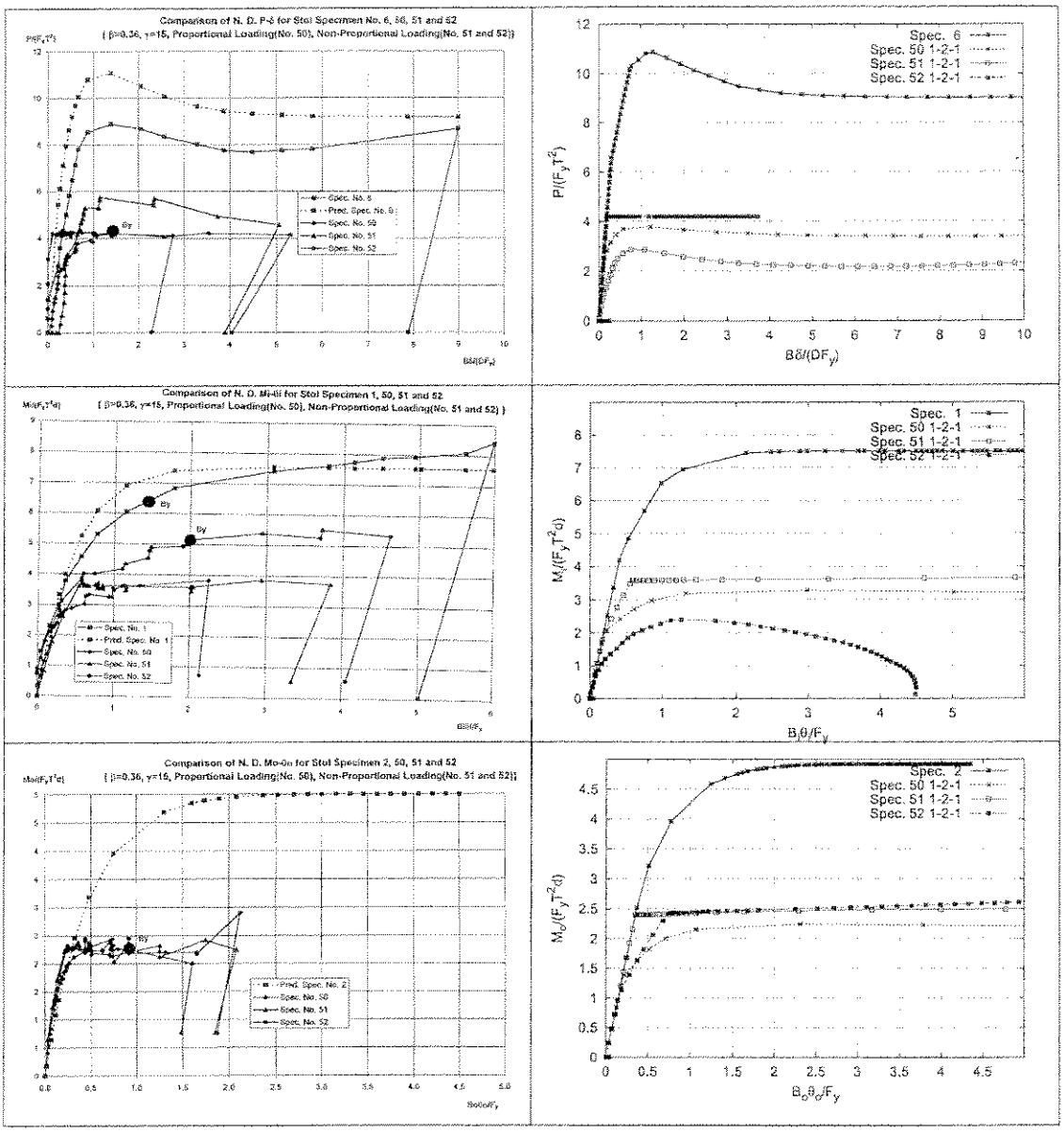

Figure 8.30: Combined Axial, IPB and OPB loading. Stol specimens 1, 2, 6, 50, 51 and 52. Proportional loading (No. 50), Non-proportional loading (Nos. 51 and 52) α_N=1, α_{IPB}=2, α_{OPB}=1

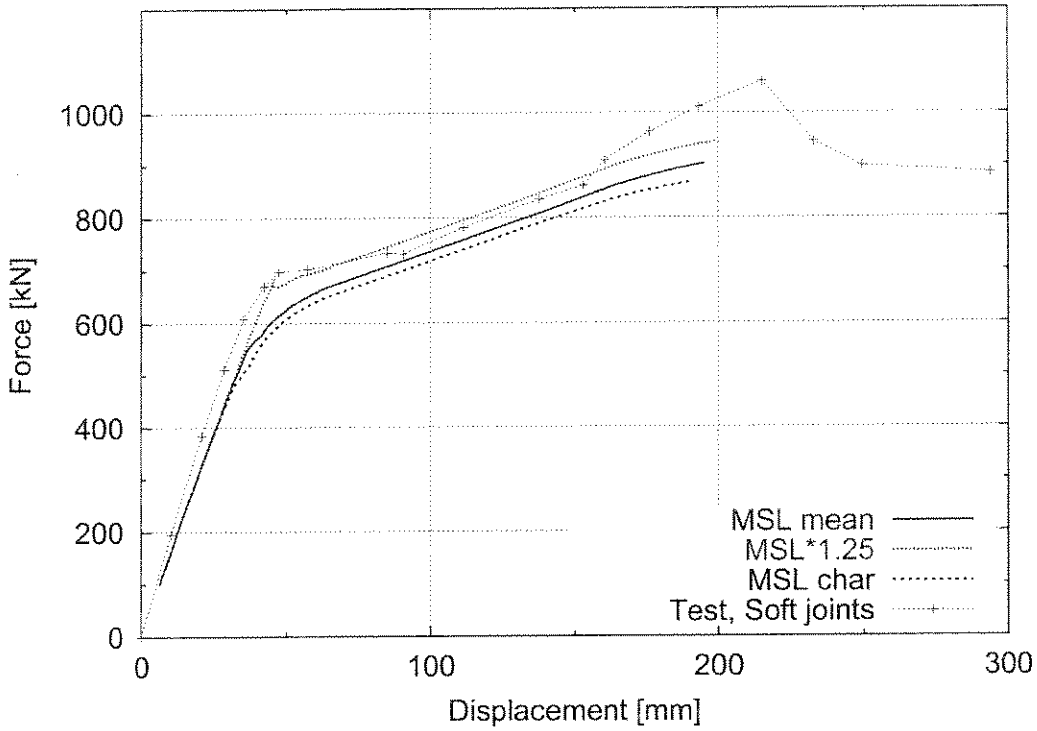

Figure 8.31: Predicted versus measured frame behaviour

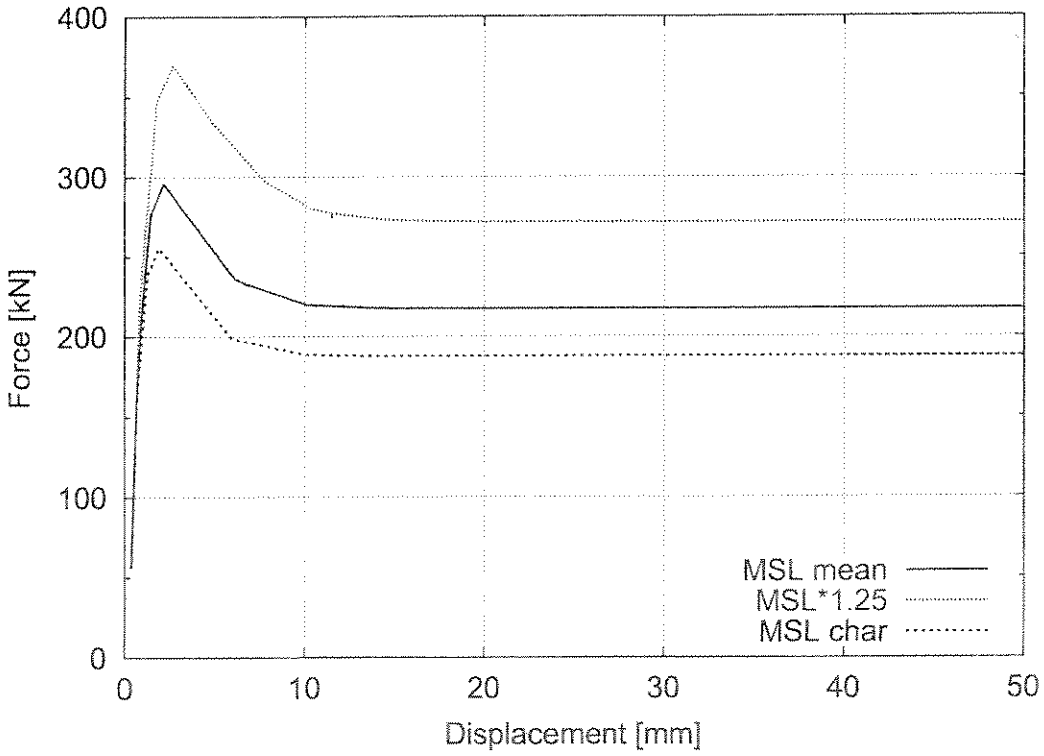

Figure 8.32: Joint models

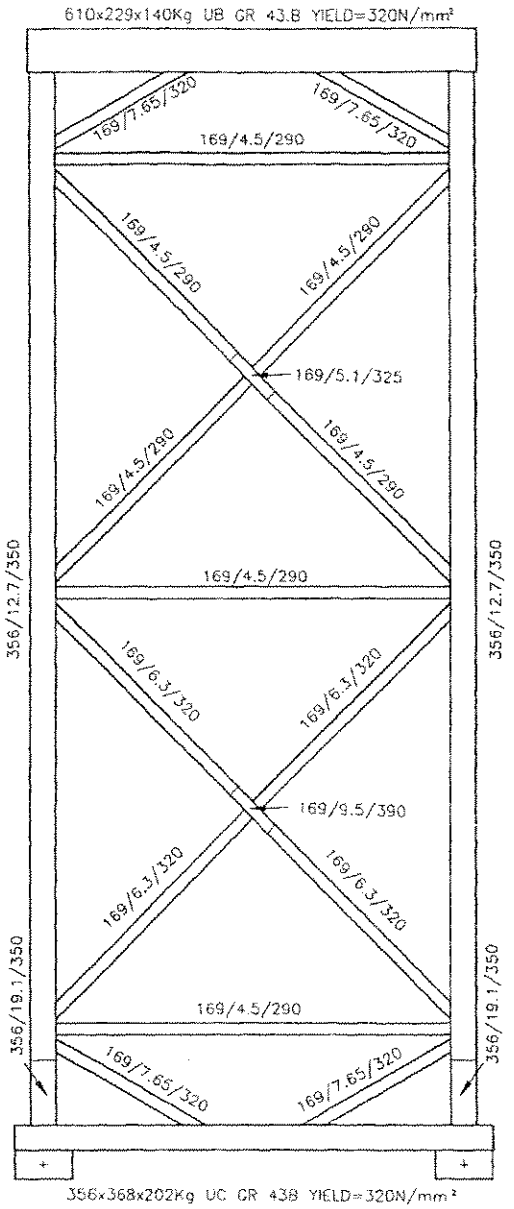

Figure 9.1: Frame II properties

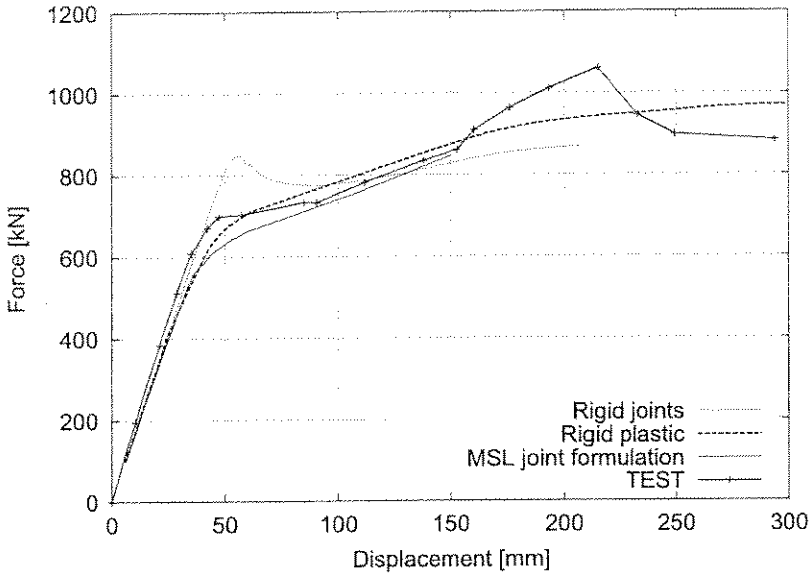

Figure 9.2: Frame II behaviour compared to test measurements

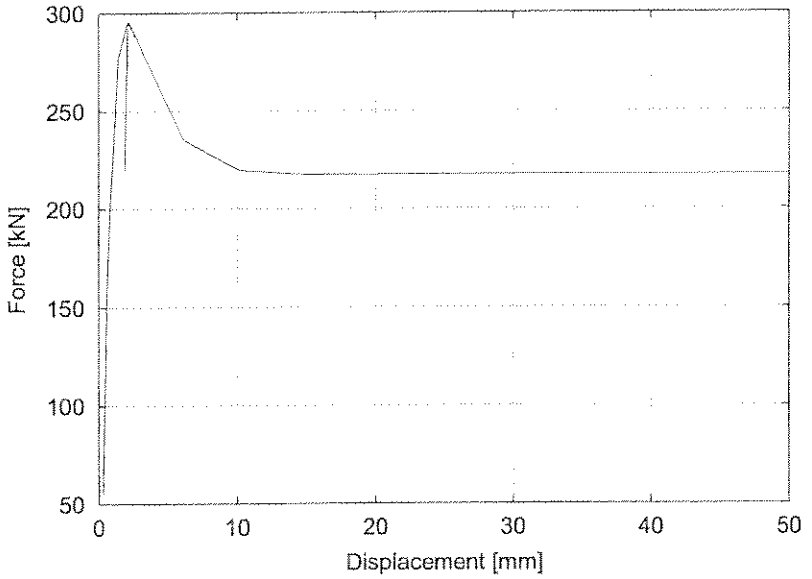

Figure 9.3: Frame II joint behaviour

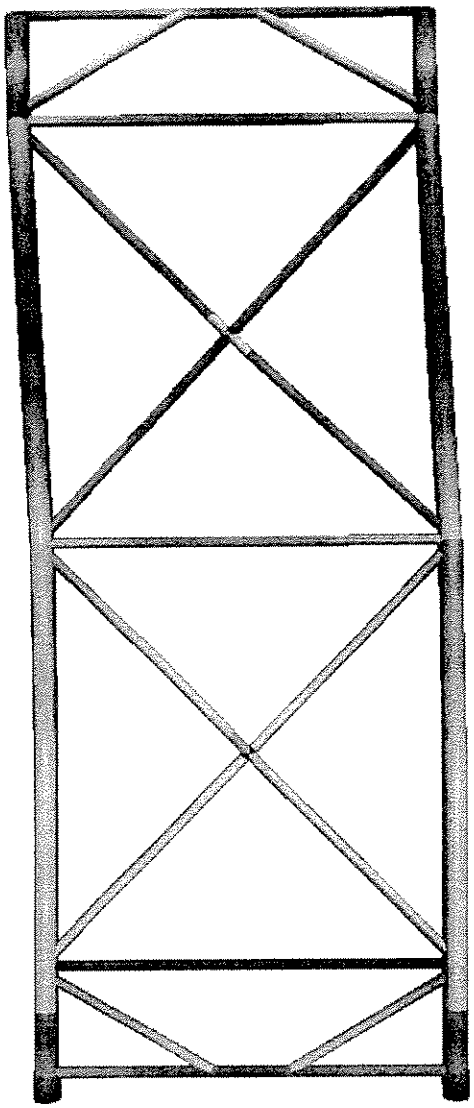

Figure 9.4: Frame II deformations

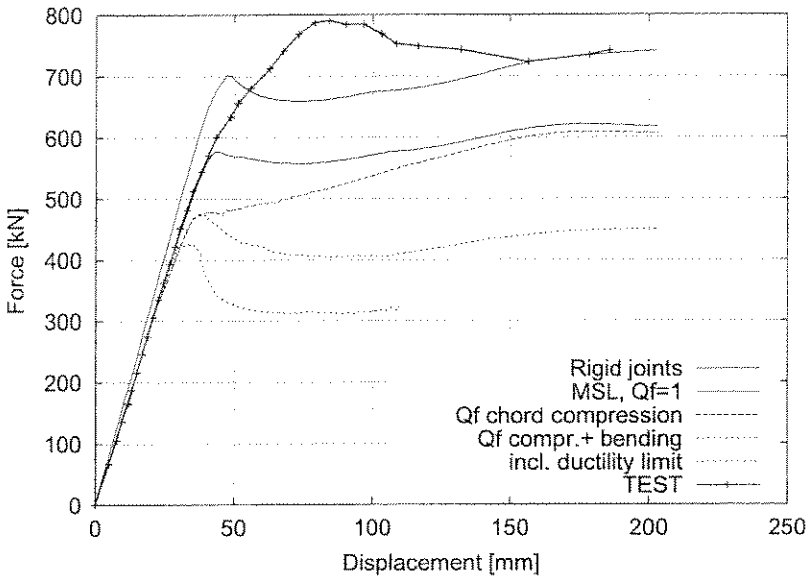

Figure 9.5: Frame VI behaviour compared to test measurements

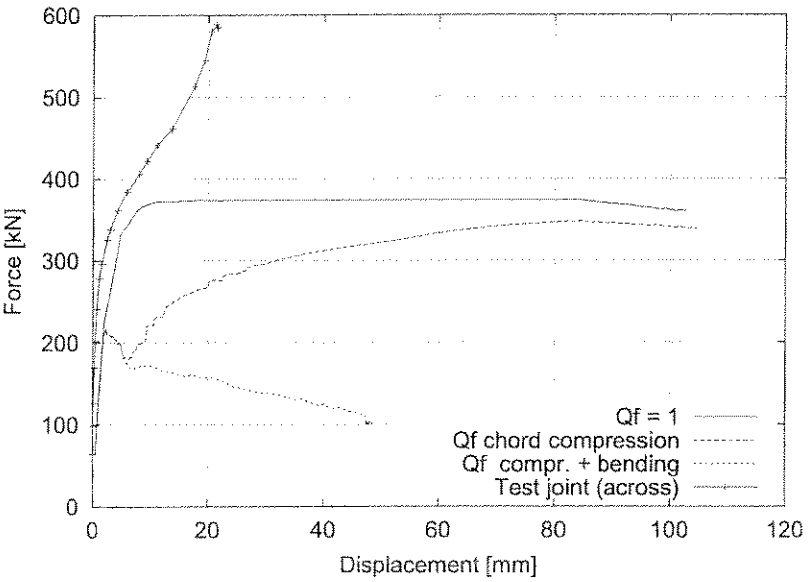

Figure 9.6: Frame VI joint behaviour

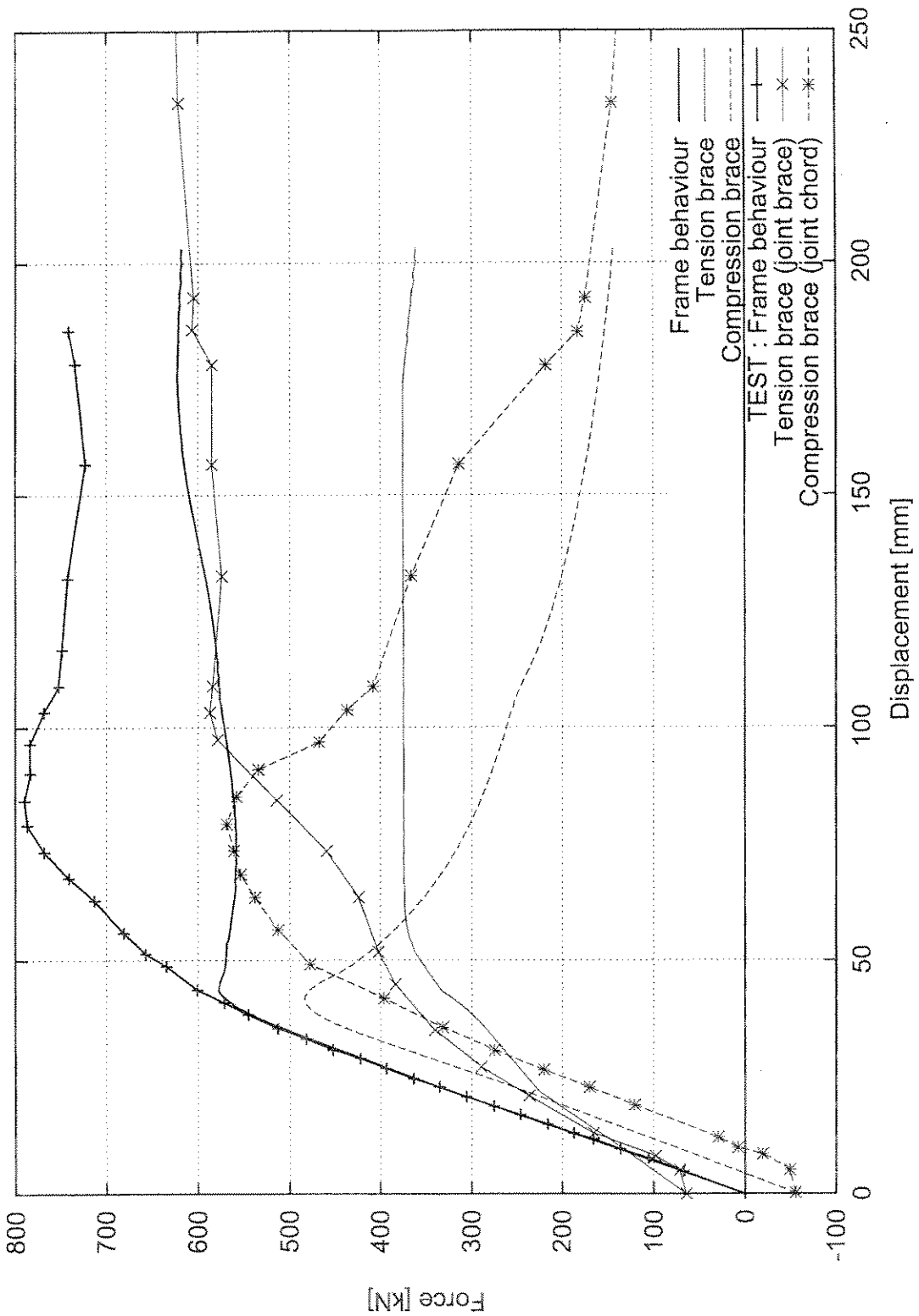

Figure 9.7: Frame VI joint and brace forces

C20400R014

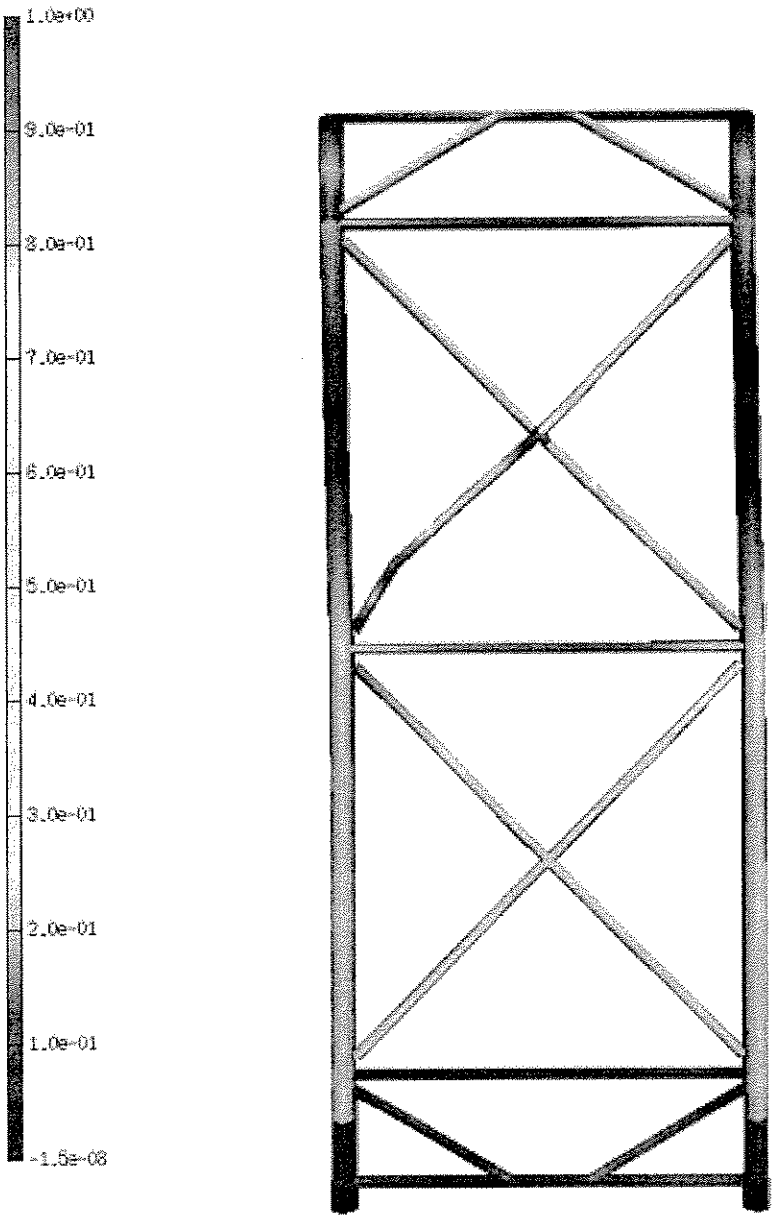

Figure 9.8: Frame VI deformations

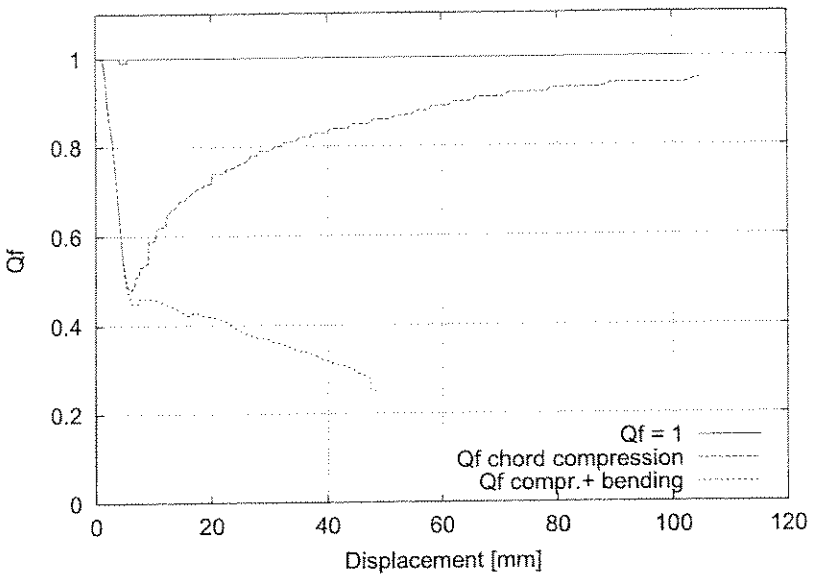

Figure 9.9: Frame VI variations in Q_f during analysis

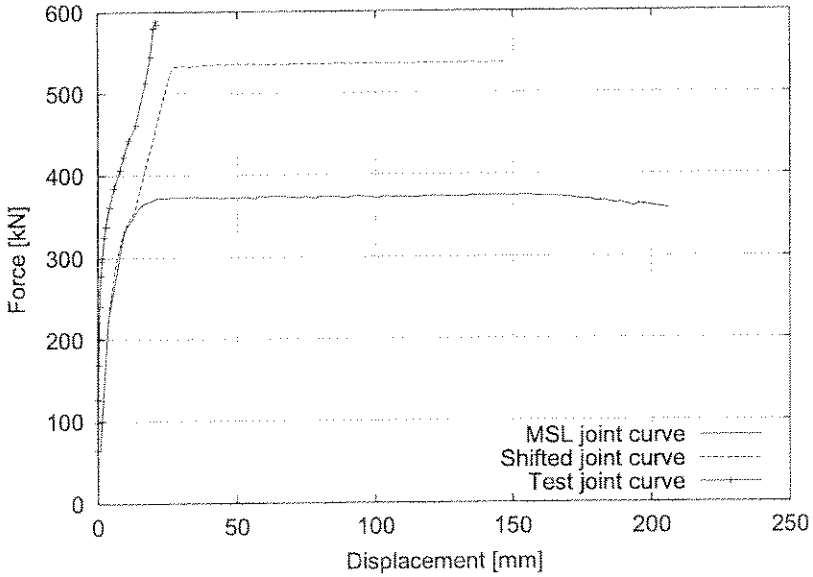

Figure 9.10: Frame VI alternative tension joint behaviour

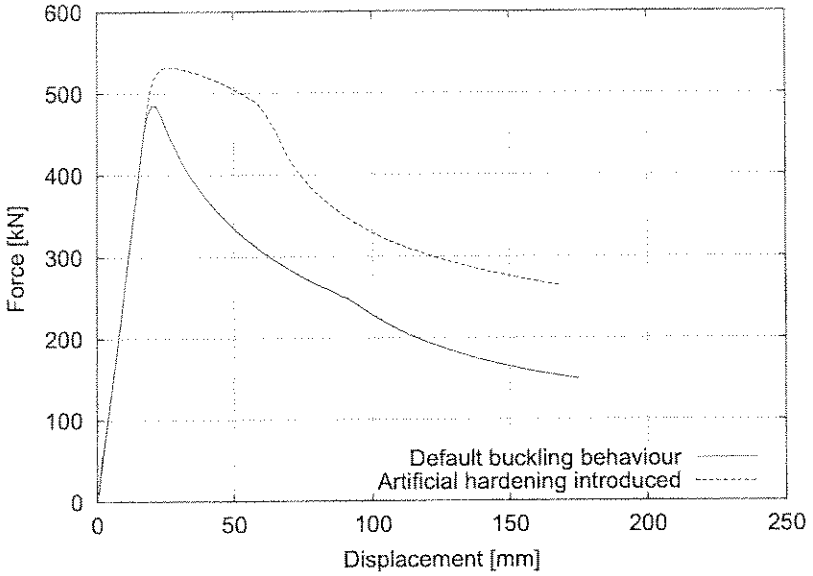

Figure 9.11: Frame VI alternative brace hardening

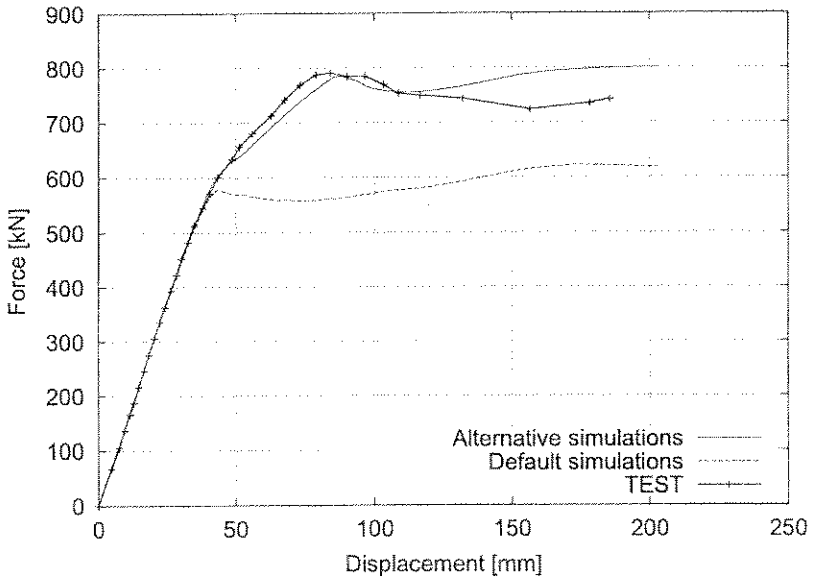

Figure 9.12: Frame VI alternative frame behaviour

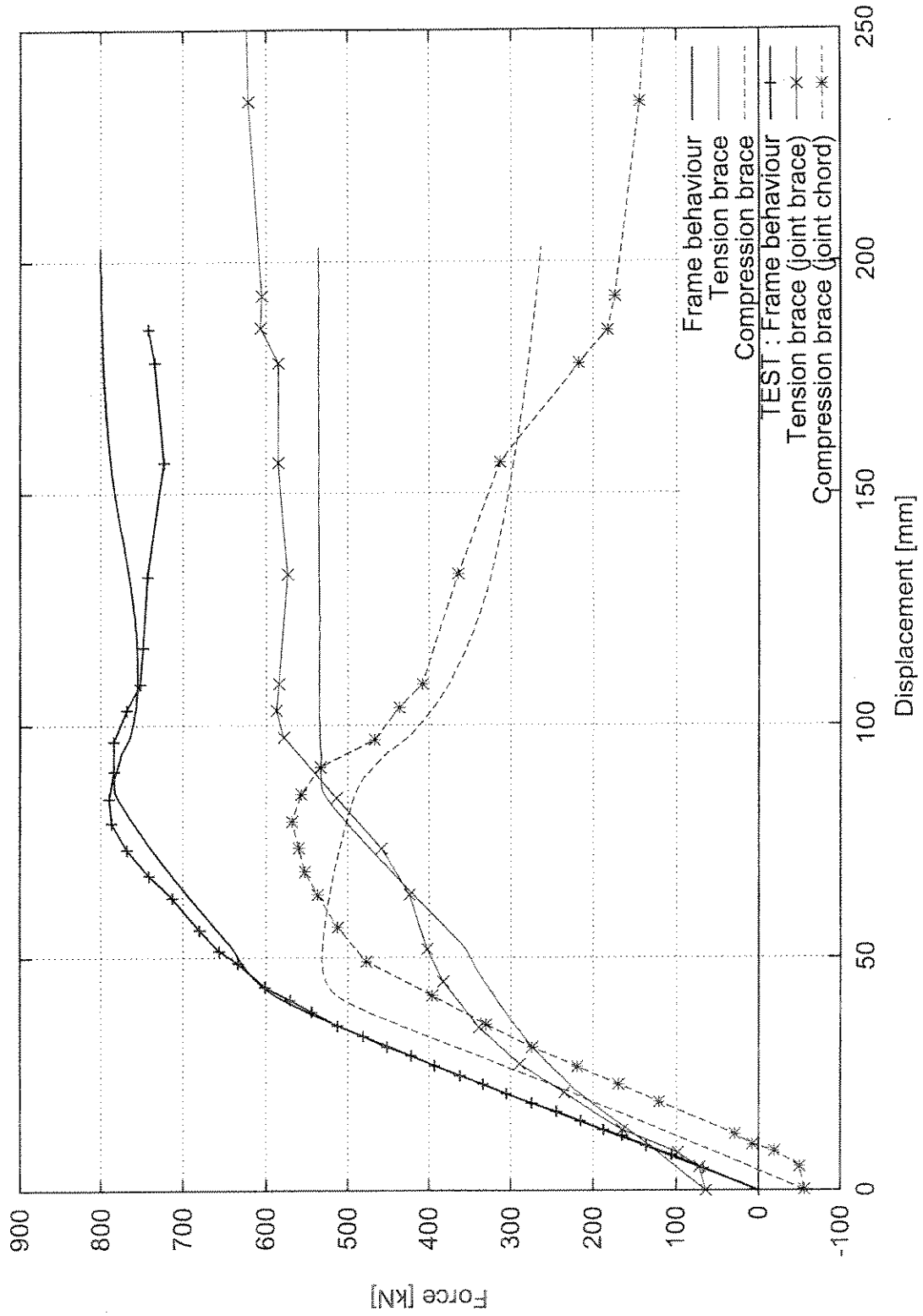

Figure 9.13: Frame VI alternative joint and brace forces

C20400R014

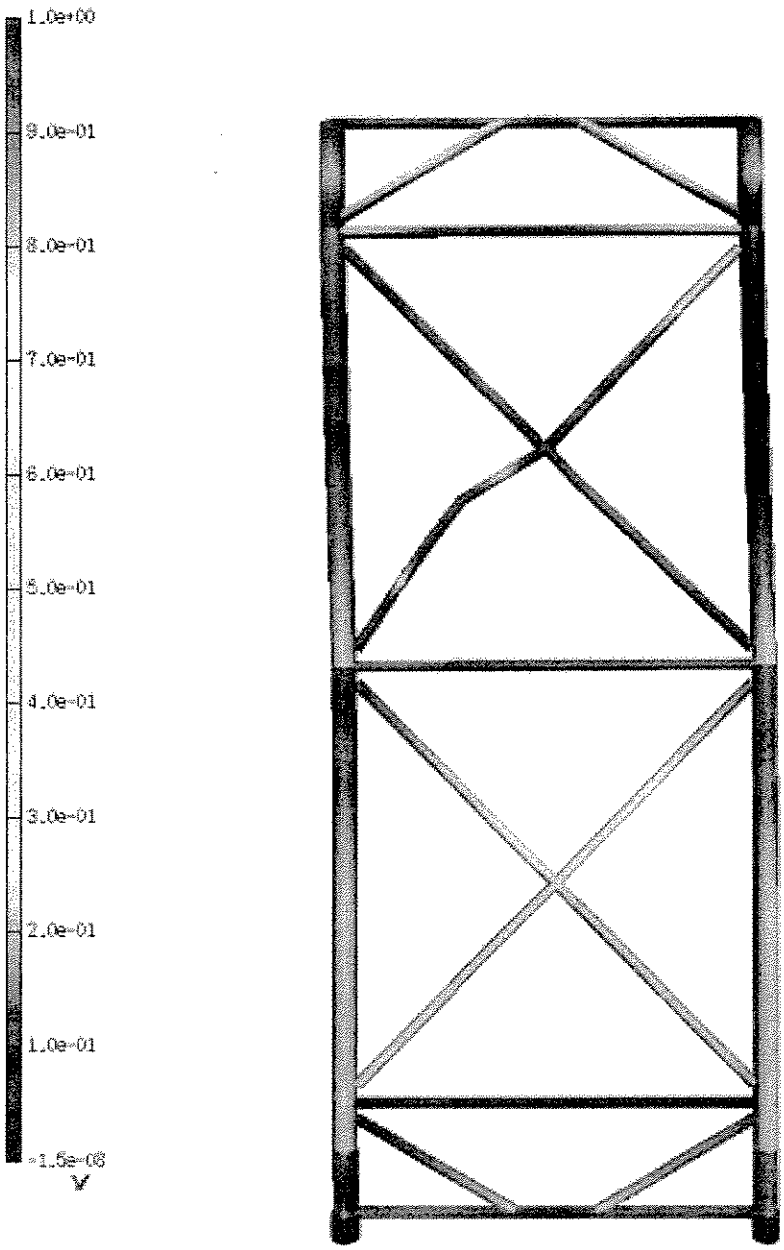

Figure 9.14: Frame VI alternative frame deformations

C20400R014

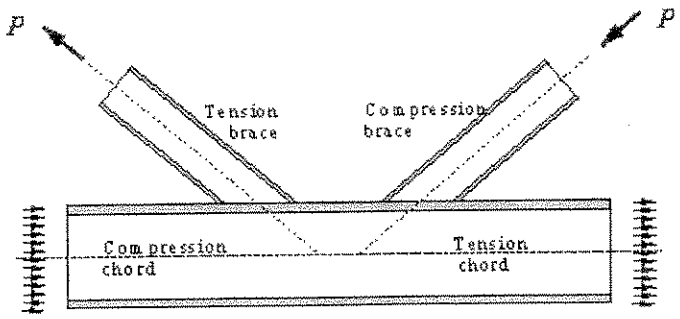

Figure 9.15: K-joint stress distributions

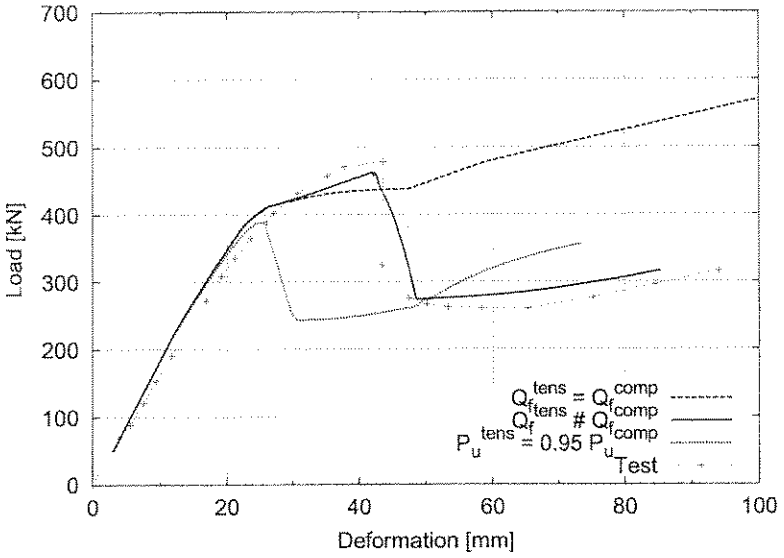

Figure 9.16: Effect of Q_f calculation procedure on frame predictions

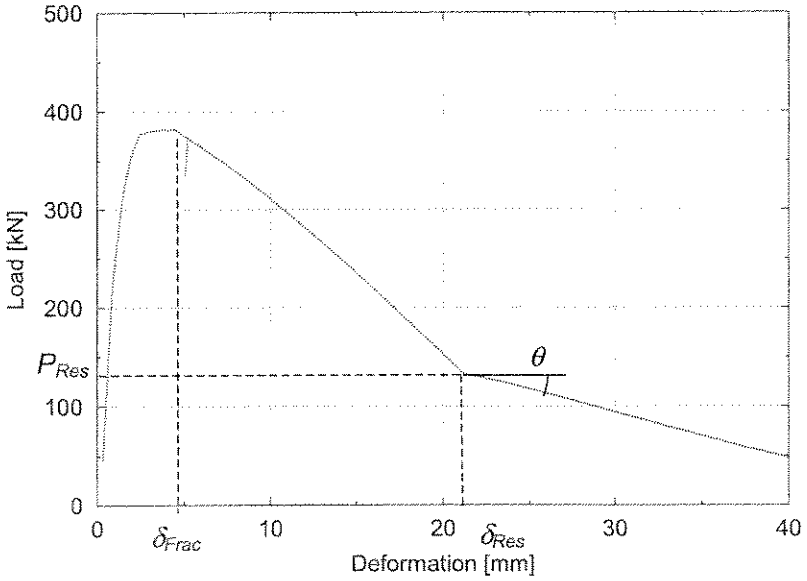

Figure 9.17: "Post rupture" calibration

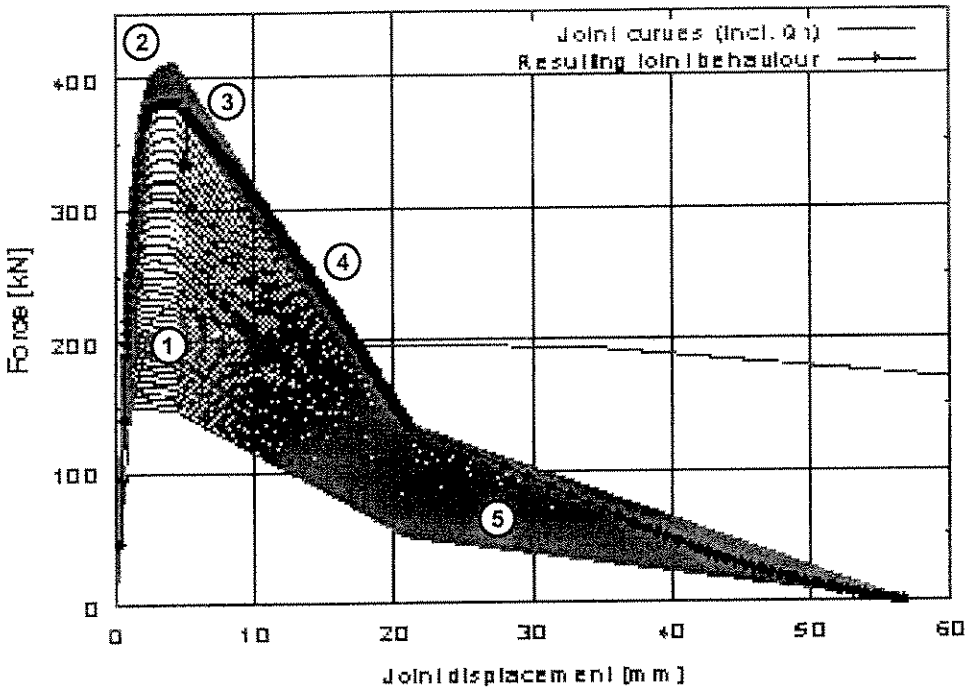

Figure 9.18: Behaviour of tension K joint

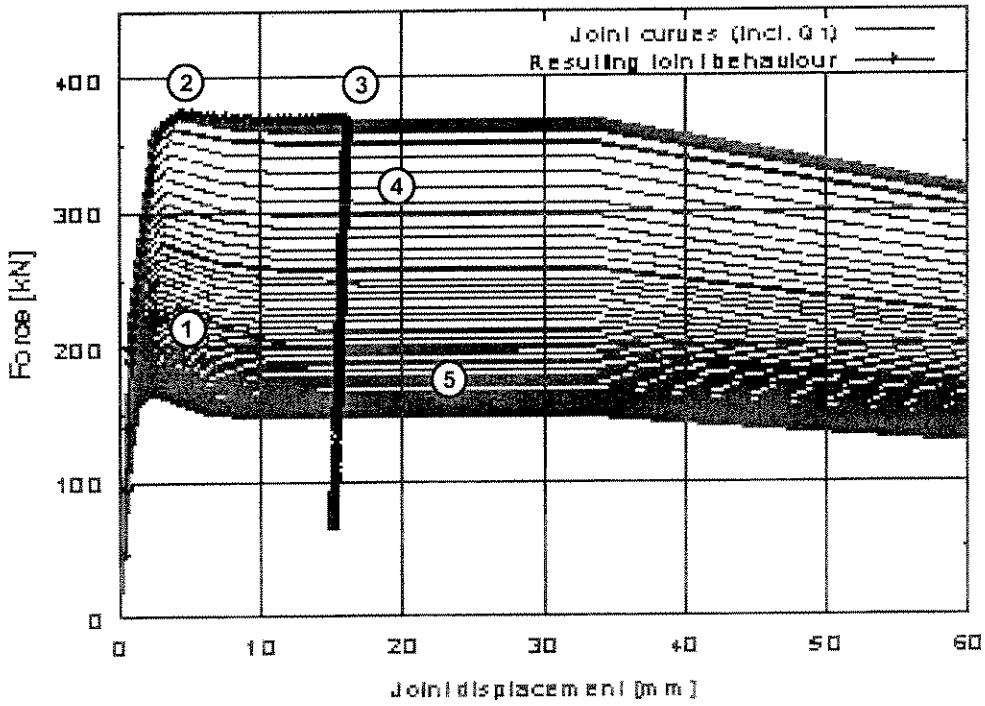

Figure 9.19: Behaviour of compression K-joint

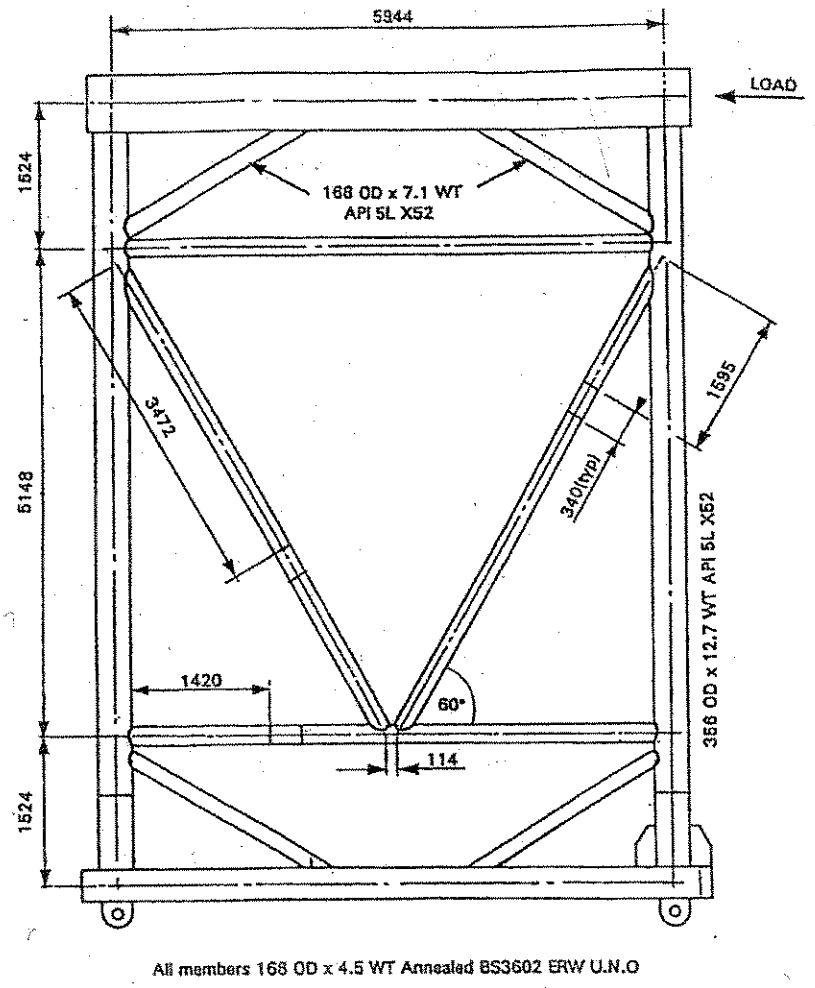

Figure 9.20: Frame VII properties

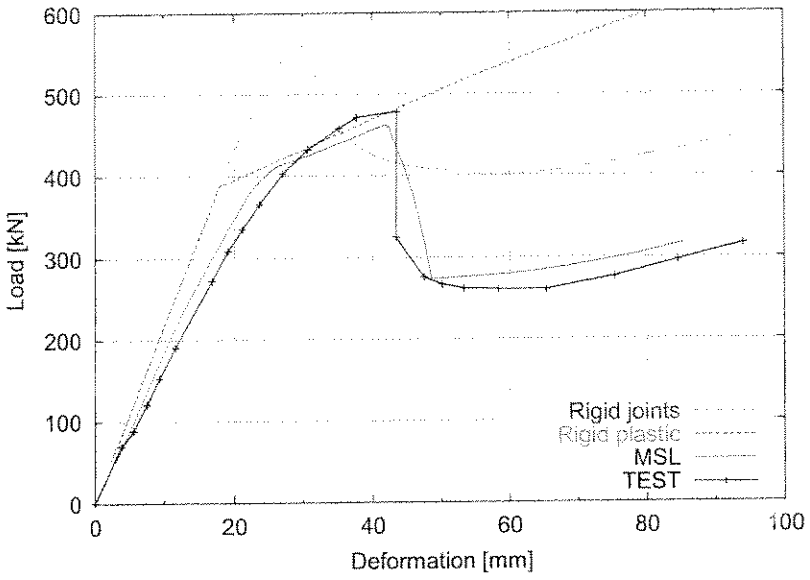

Figure 9.21: Frame VII behaviour compared to test measurements

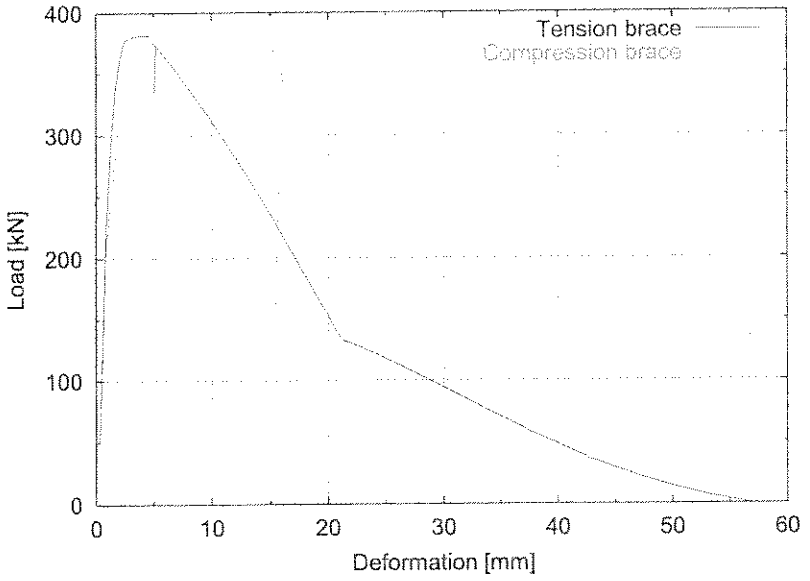

Figure 9.22: Frame VII joint behaviour

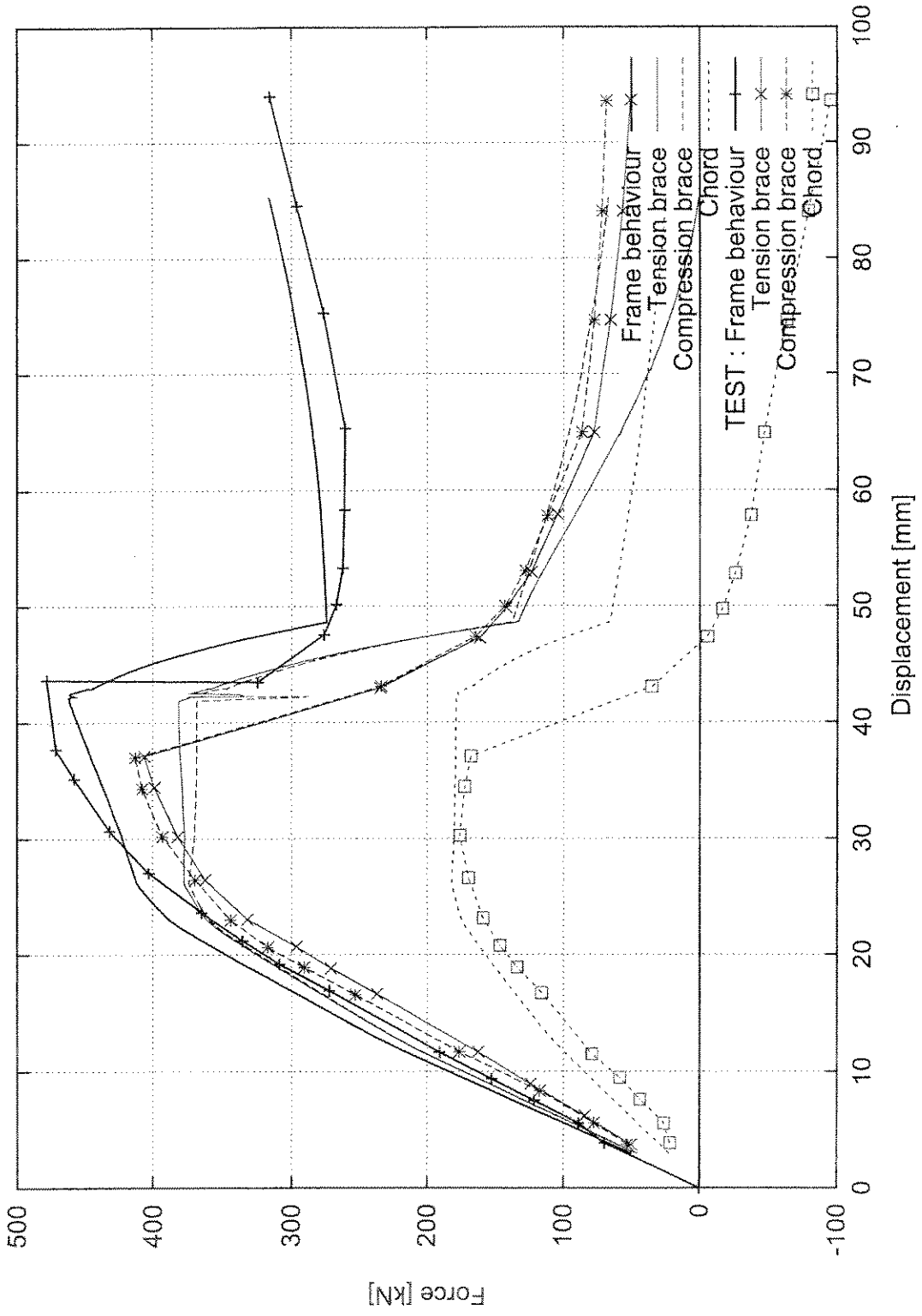

Figure 9.23: Frame VII joint and brace forces

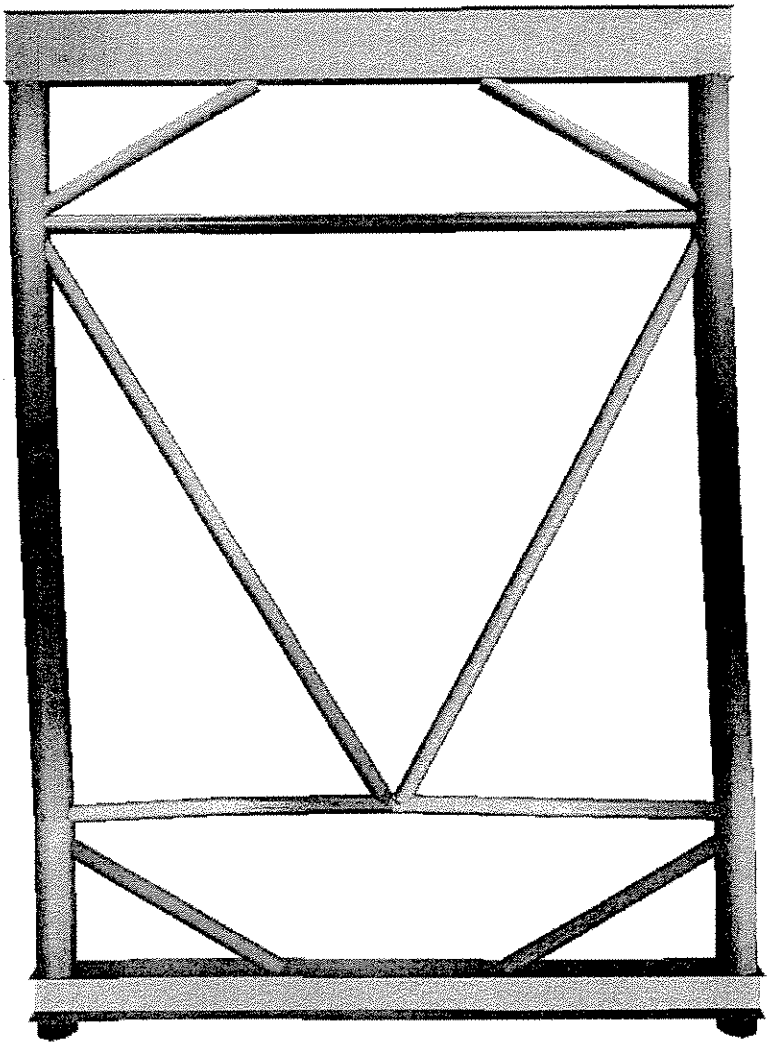

Figure 9.24: Frame VII deformations

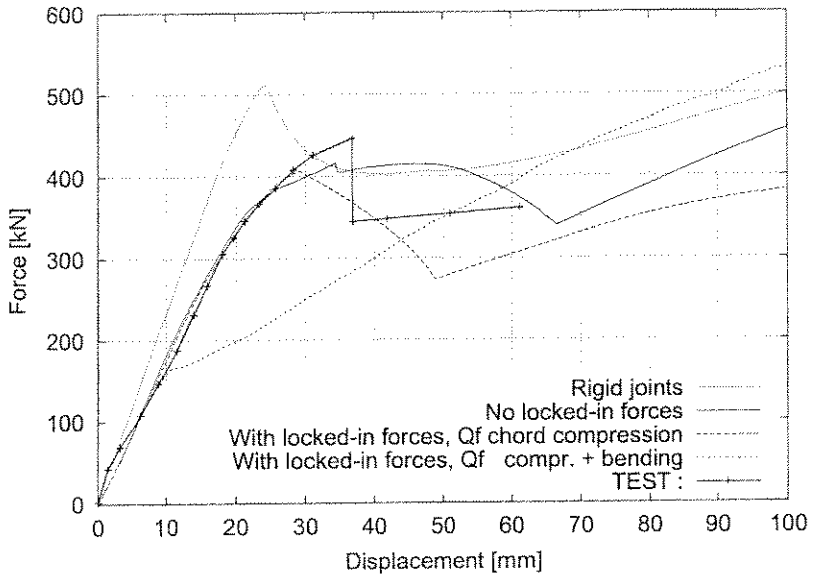

Figure 9.25: Frame VIII behaviour compared to test measurements

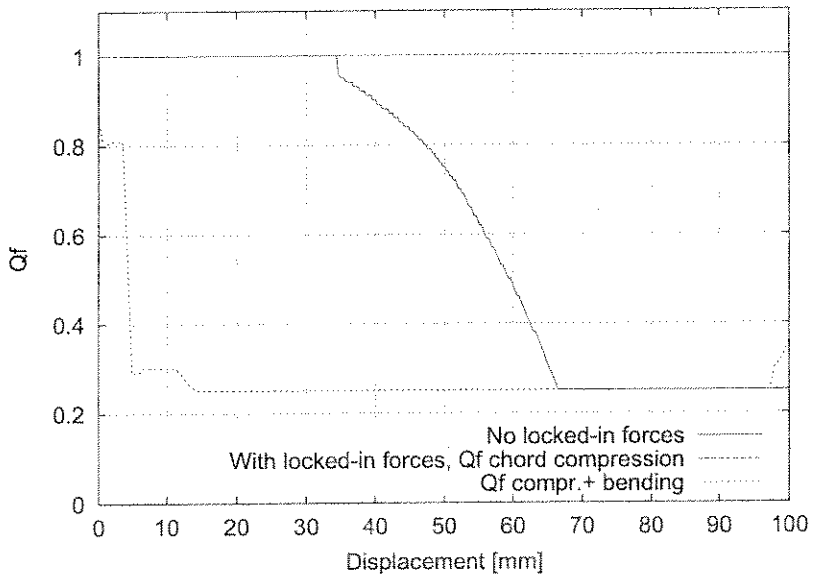

Figure 9.26: Frame VIII variation of Q_f variation during the analysis

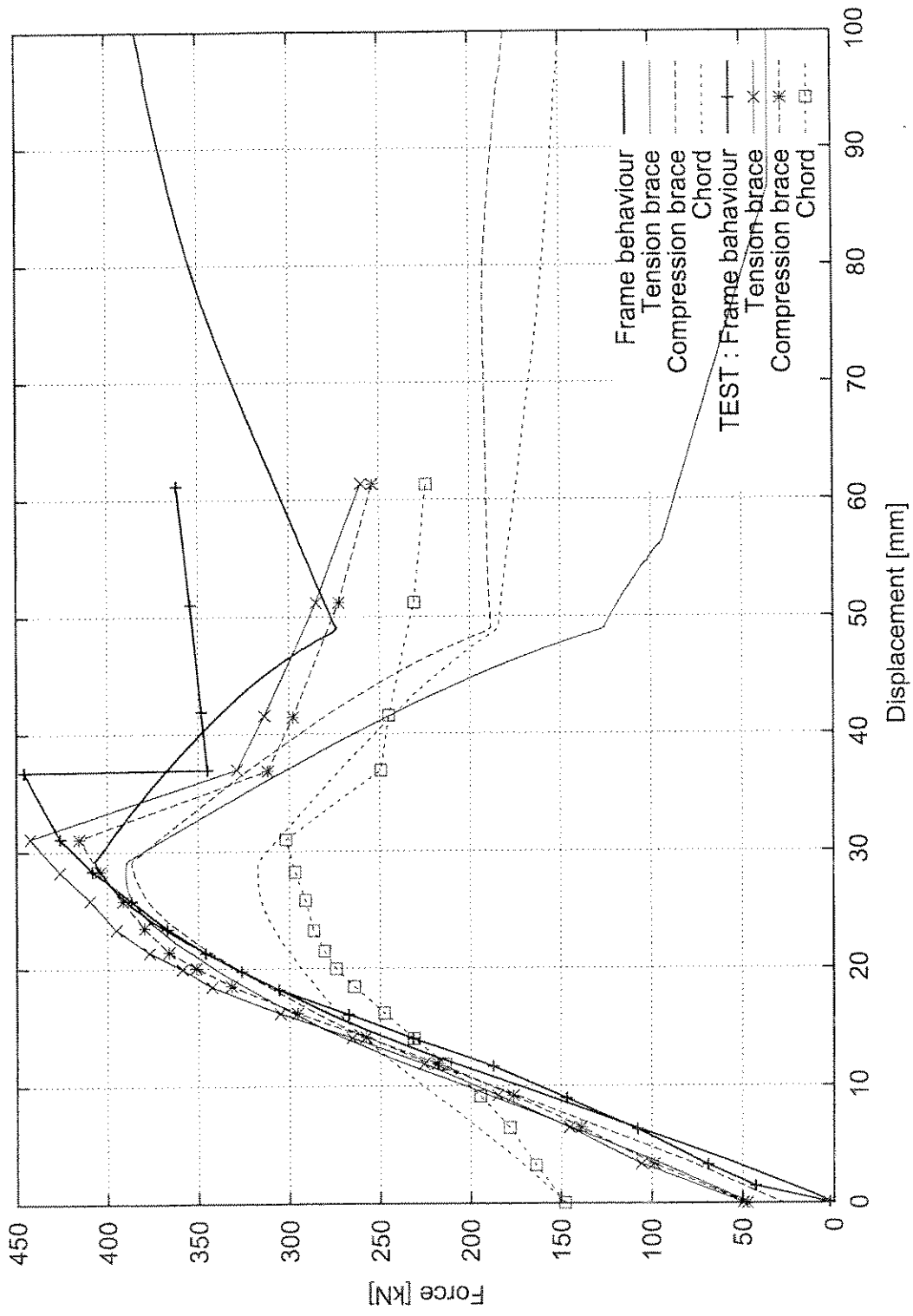

Figure 9.27: Frame VIII joint and brace forces

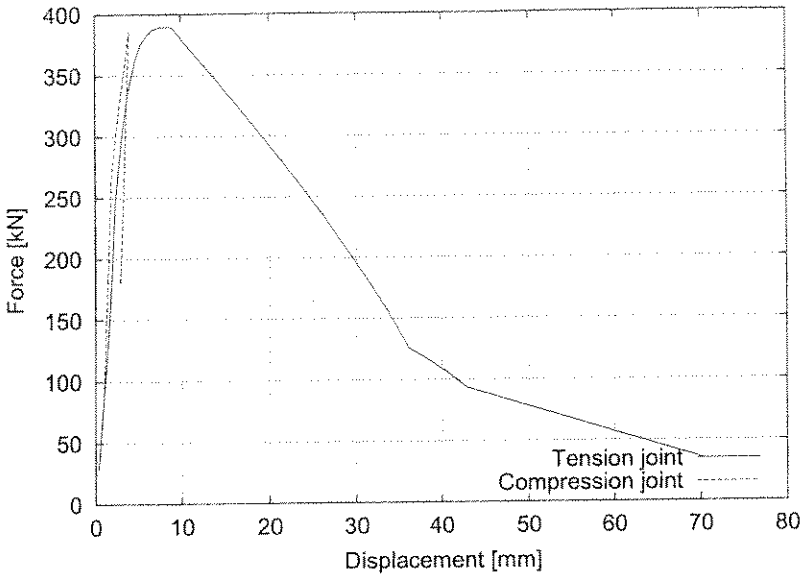

Figure 9.28: Frame VIII joint behaviour

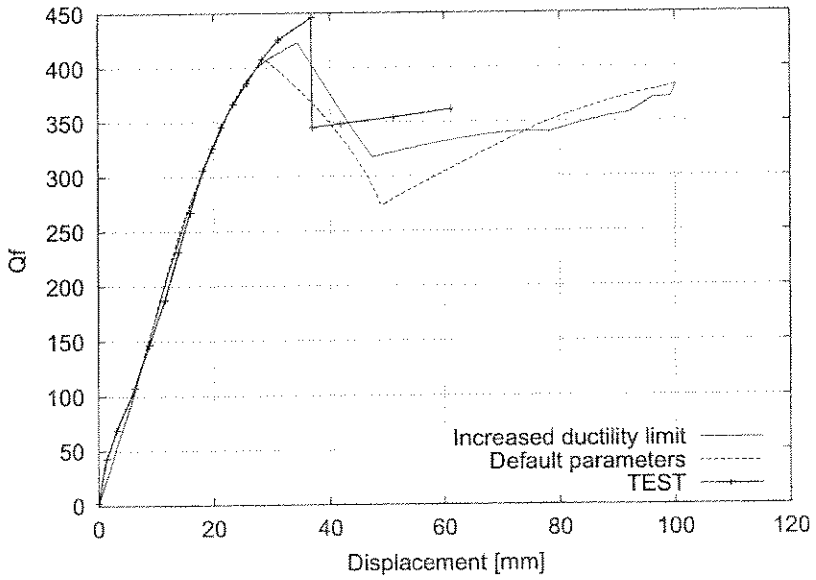

Figure 9.29: Frame VIII behaviour with alternative joint ductility limit

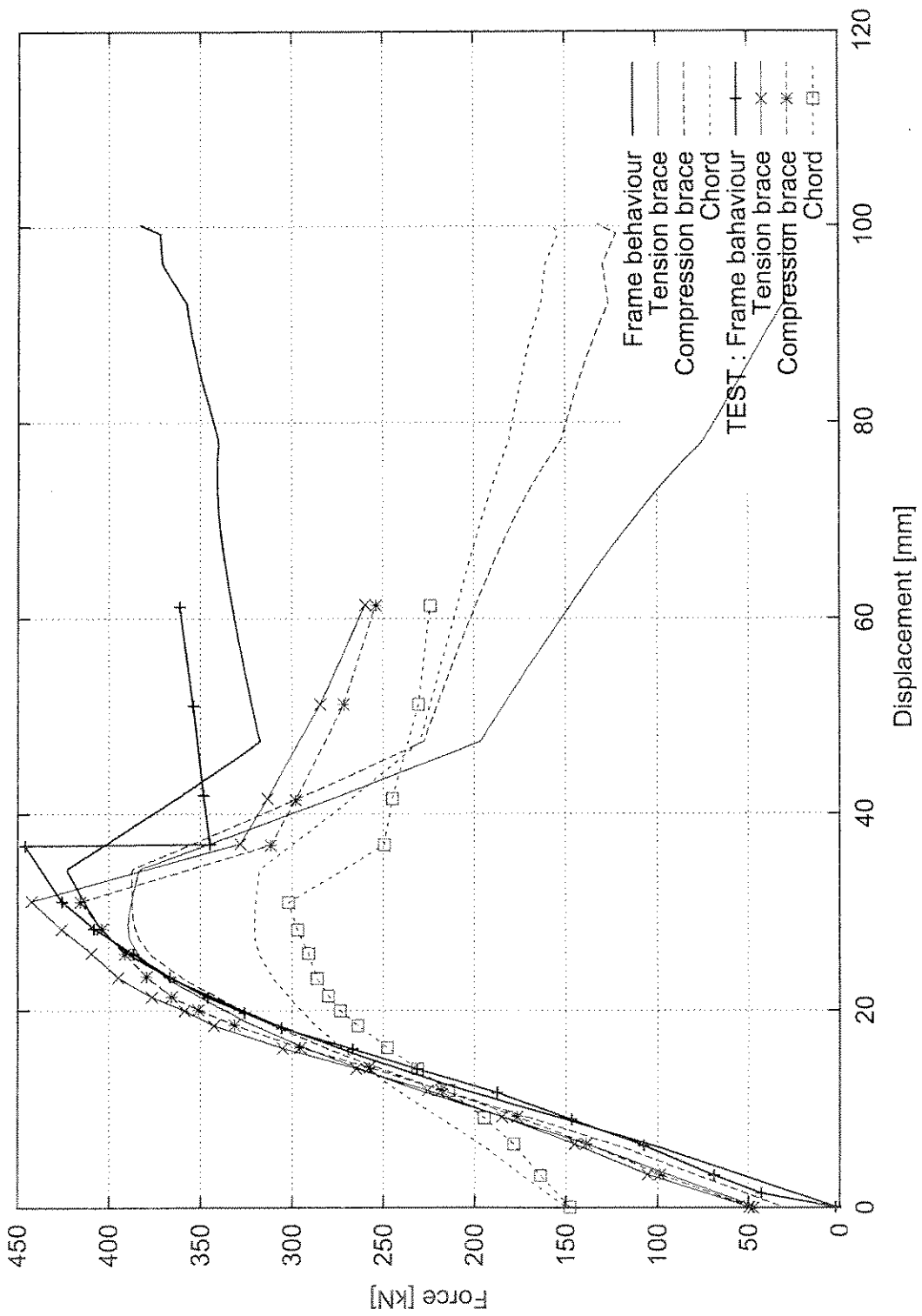

Figure 9.30: Frame VIII joint and brace forces with alternative ductility limit

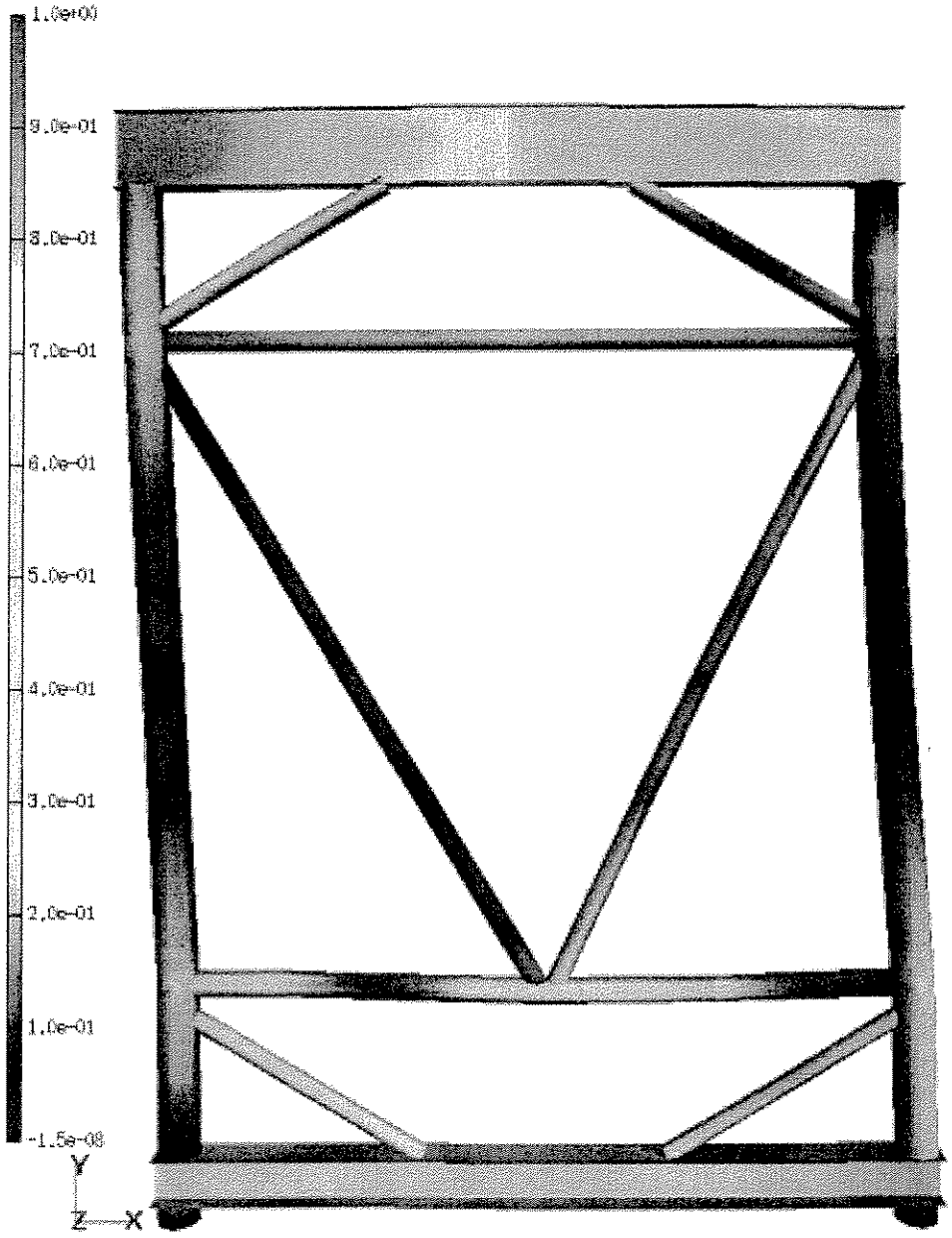

Figure 9.31: Frame VIII deformations

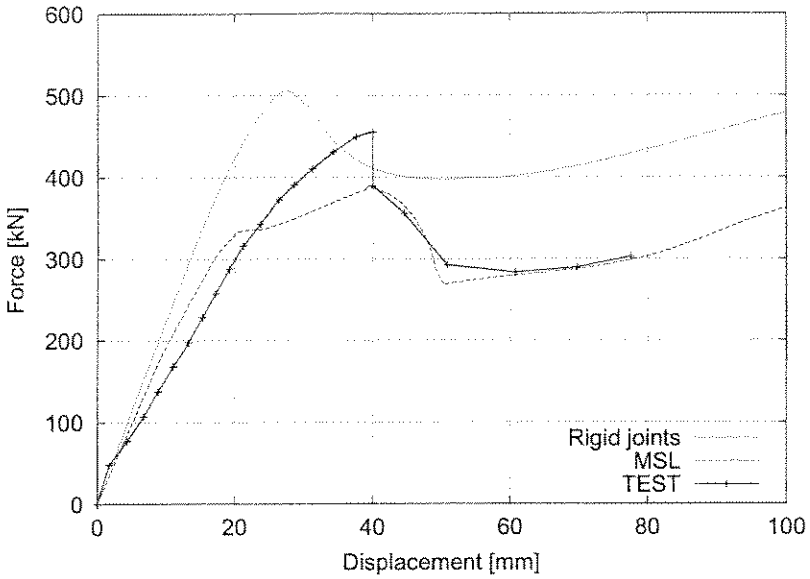

Figure 9.32: Frame X behaviour compared to test measurements

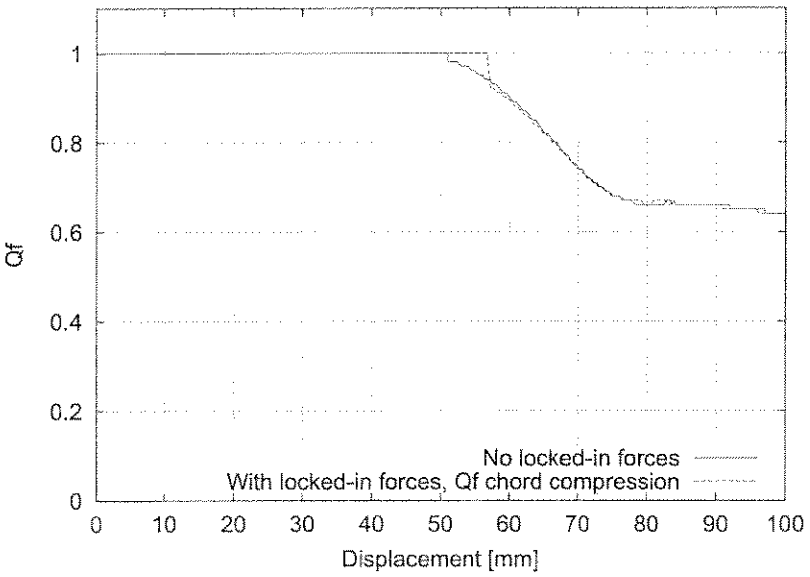

Figure 9.33: Frame X variation of Q_f variation during the analysis

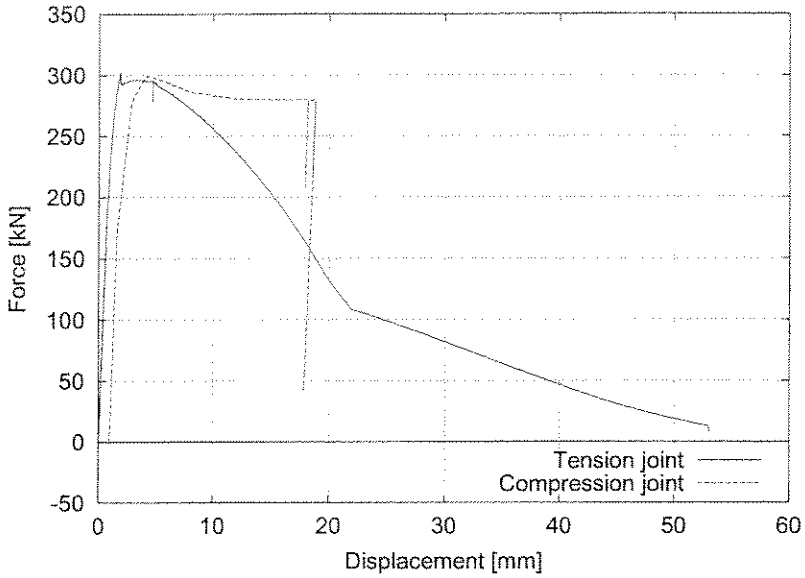

Figure 9.34: Frame X joint behaviour

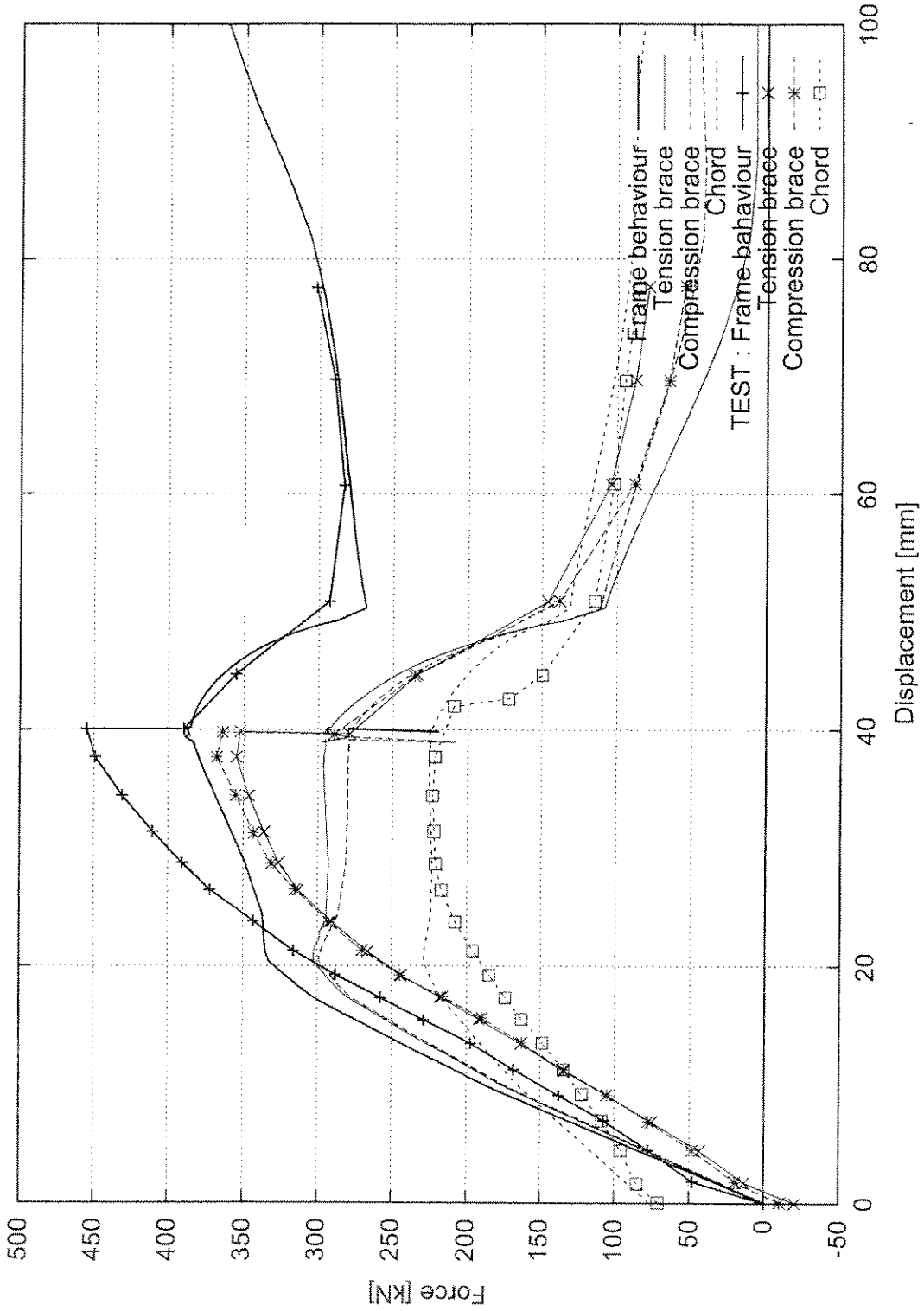

Figure 9.35: Frame X joint and brace forces

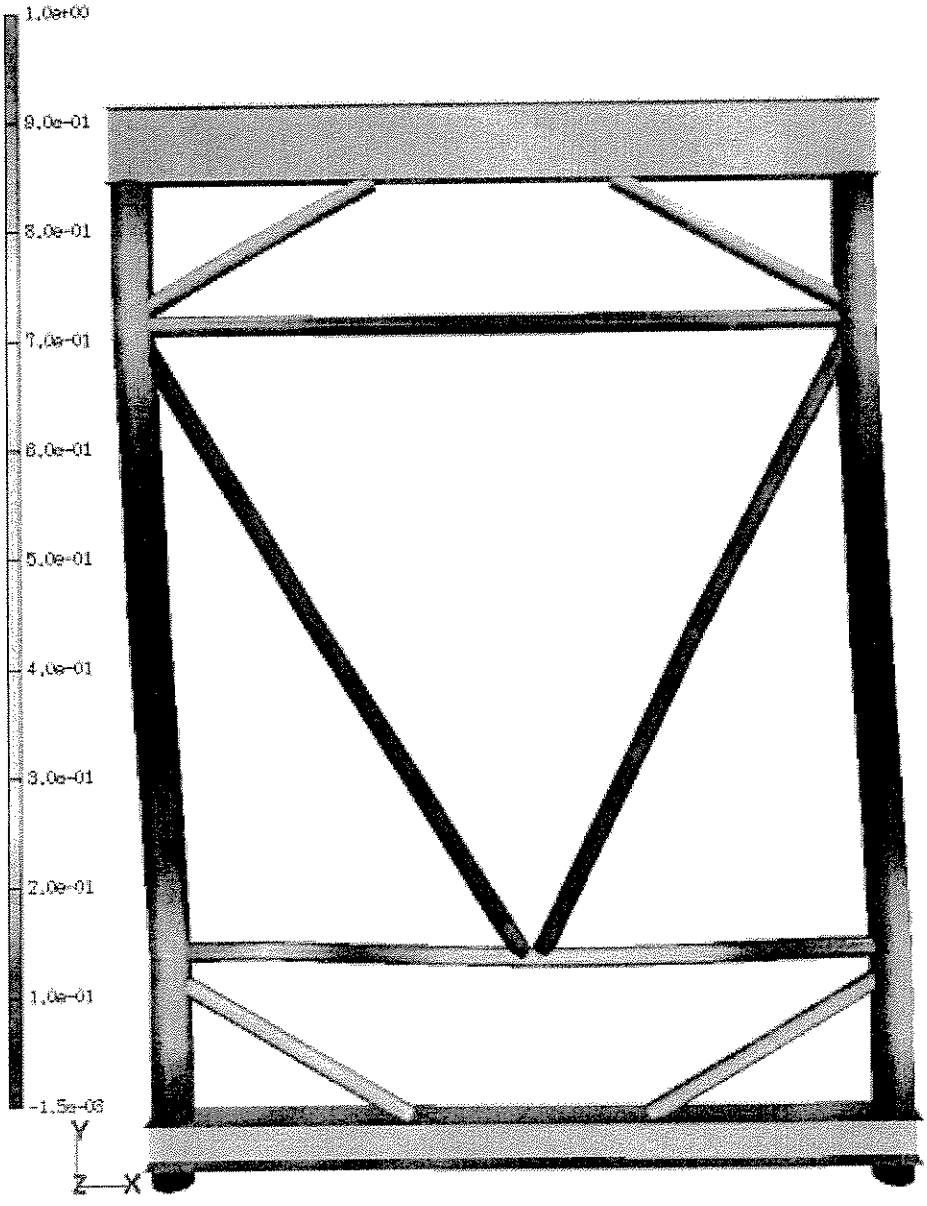

Figure 9.36: Frame X deformations

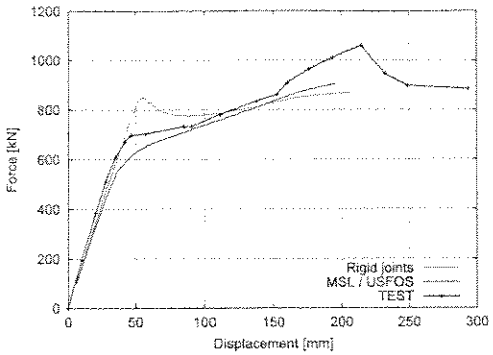

Figure 9.37: Frame II
X joint in compression

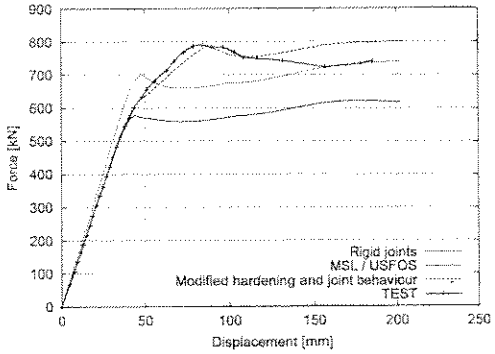

Figure 9.38: Frame VI
X joint in tension

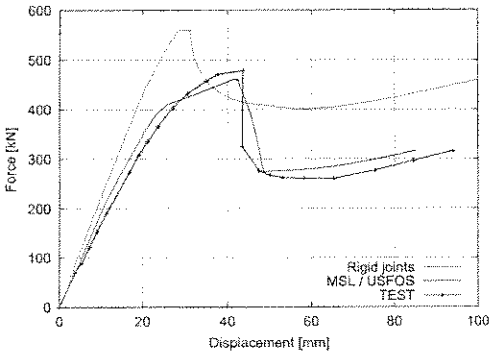

Figure 9.39: Frame VII
Gap K joint, β = 1.0, g/D=0.1

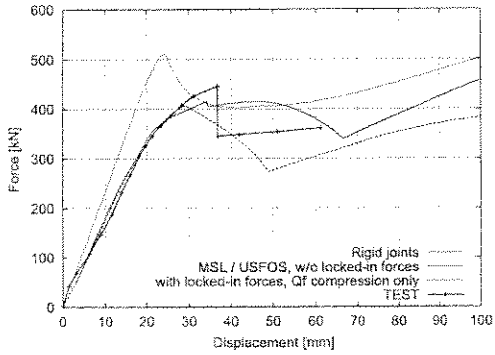

Figure 9.40 Frame VIII
Gap K joint, β = 0.7, g/D=0.1

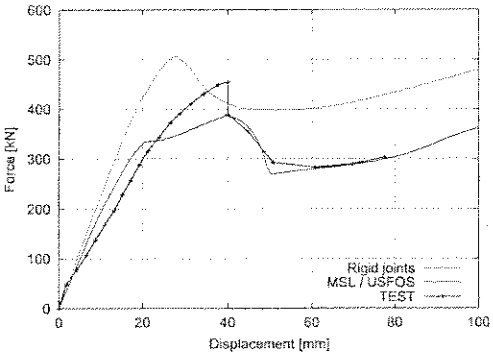

Figure 9.41: Frame X
Gap K joint, β = 1.0, g/D=0.2

APPENDIX A

Non-Dimensional Load-Deformation Formulations for Joints of Mixed Classification

A.1 Axial Loading

The original load-deformation (Pδ) equation selected in phase I of the project for individual joints (K, X or Y) is as follows:

$$P = d - a\left[1 - b\exp(-c\delta)\right]^2 \qquad \ldots \text{A.1}$$

where a, b, c and d are coefficients derived from functions of the joint geometry.

This was developed and non-dimensionalised as follows (see Section 3):

$$P = \phi P_u\left(1 - A\left[1 - \left(1 + 1/\sqrt{A}\right)\exp\left(-B\delta/(\phi Q_f F_y D)\right)\right]^2\right) \qquad \ldots \text{A.2}$$

where Pu is the mean joint capacity, ϕ is the strength level adjustment factor, A and B are coefficients, D is the chord diameter, Fy is the chord yield stress and Q_f is the chord stress factor.

The link between these two equations is as follows:

$$d = \phi P_u \qquad a = \phi P_u A \qquad b = 1 + \frac{1}{\sqrt{A}} \qquad c = \frac{B}{\phi D F_y Q_f}$$

The initial stiffness can be expressed as follows:

$$K_{ini} = 2abc(b-1) = 2\phi P_u A\left(1 + \frac{1}{\sqrt{A}}\right)\frac{B}{\phi D F_y Q_f}\frac{1}{\sqrt{A}} = 2P_u\left(1 + \sqrt{A}\right)\frac{B}{D F_y Q_f} \qquad \ldots \text{A.3}$$

Similarly, the initial stiffness for pure K, X and Y actions can be obtained as follows:

$$K_K = 2\phi_K P_{uK}\left(1 + \sqrt{A_K}\right)\frac{B_K}{\phi_K D F_y Q_{fK}}$$

$$K_X = 2\phi_X P_{uX}\left(1 + \sqrt{A_X}\right)\frac{B_X}{\phi_X D F_y Q_{fX}}$$

$$K_Y = 2\phi_Y P_{uY}\left(1 + \sqrt{A_Y}\right)\frac{B_Y}{\phi_Y D F_y Q_{fY}} \qquad \ldots \text{A.4}$$

Note, the ϕ factors cancel in Equation A.4 but it is helpful to leave them in to understand Equation A.7.

The coefficients of A_K, B_K and Pu_K, A_X, B_X and Pu_X, A_Y, B_Y and Pu_Y and their load proportions, C_K, C_X and C_Y are known for K, X and Y actions respectively. Note that $C_K + C_X + C_Y = 1.0$. The problem is to predict the A, B and Pu and hence whole joint axial load-deformation performance for joints having mixed classifications.

An initial stiffness correction factor ψ is proposed to give a predicted stiffness in agreement with observations on available data:

$$\psi = \frac{K_{K,X,Y}}{K_{inipred}} \qquad \ldots \text{A.5}$$

$$K_{K,X,Y} = \left(\frac{C_K}{K_K} + \frac{C_X}{K_X} + \frac{C_Y}{K_Y} \right)^{-1} \quad \ldots A.6$$

$$K_{inipred} = 2\left(C_K \phi_K P_{uK} + C_X \phi_X P_{uX} + C_Y \phi_Y P_{uY}\right) \times$$

$$\left(1 + \left(C_K A_K^2 + C_X A_X^2 + C_Y A_Y^2\right)^{\frac{1}{4}}\right) \frac{C_K B_K / \phi_K Q_{fK} + C_X B_X / \phi_X Q_{fX} + C_Y B_Y / \phi_Y Q_{fY}}{DF_y} \quad \ldots A.7$$

Finally, A, B and ϕ Pu are obtained as follows to use in equation A.2.

$$A = \sqrt{C_K A_K^2 + C_X A_X^2 + C_Y A_Y^2} \quad \ldots A.8$$

$$B = \psi\left(C_K B_K + C_X B_X + C_Y B_Y\right) \quad \ldots A.9$$

$$\phi P_u = C_K \phi_K P_{uK} + C_X \phi_X P_{uX} + C_Y \phi_Y P_{uY} \quad \ldots A.10$$

A.2 Moment Loading

Classification of joints for moments is a procedure that is not necessary because the moment capacities for K, X and Y joints are normally the same. However, the introduction of ϕ, the strength level adjustment factor, in the Mθ formulation (Equation 3.11b) requires further consideration should different values be assigned to ϕ_K, ϕ_X and ϕ_Y.

In principle, the same procedure given above for the mixed classed Pδ formulation could be used for Mθ, with substantial simplification as now $A_K = A_X = A_Y$, $B_K = B_X = B_Y$ and therefore $K_K = K_X = K_Y$. Working through the algebra, the corresponding equations to A8 to A9 are found to be:

$$A = A \quad \ldots A.11$$

$$B = \psi B \quad \ldots A.12$$

$$\phi M_U = (C_K \phi_K + C_X \phi_X + C_Y \phi_Y) M_U \quad \ldots A.13$$

Where

$$\psi = \left[\left(C_K \phi_K + C_X \phi_X + C_Y \phi_Y\right) \left(\frac{C_K}{\phi_K} + \frac{C_X}{\phi_X} + \frac{C_Y}{\phi_Y} \right) \right]^{-1} \quad \ldots A.14$$

It may be noted that Equations A.13 and A.14 need knowledge of moment classification action factors (C_K, C_X and C_Y) for their evaluation. However, as noted above, moment classification has always been considered unnecessary and there is no established procedure or indeed any obvious way for conducting moment classification. It is recommended, therefore, that the ϕ_K, ϕ_X and ϕ_Y factors for moment loading are set equal to each other (present steel data largely supports this simplification). In this case ψ (Equation A.14) will equal unity and the right hand

side of Equation A.13 defaults directly to the left hand side. In short, classification for moment loading is completely avoided.

APPENDIX B

Plasticity Formulation for
Coupled Pδ - Mθ Response

Plasticity Formulation

This Appendix presents the theoretical basis of a plasticity model derived for joint modelling. Results from preliminary studies with a similar but simpler formulation are shown in Section 5.3. Although the mathematics may seem quite involved, the main message is that it has been possible to derive a theoretically consistent plasticity formulation for the problem at hand, and that the formulation seems to work. It is also worth pointing out that a similar mathematical complexity is required for modelling material yielding/hardening behaviour in nearly all general purpose FE programs.

B.1 General

Material nonlinearities are modelled by yield hinges introduced in the joint elements (see Figure 5.1). The behaviour of the hinges is governed by plastic flow theory, according to an isotropic or a kinematic hardening model. Associated flow is assumed, with plastic potentials defined by interaction formulas for the element cross-section. The model is formulated in force-space, i.e. it relates plastic displacements and rotations to section forces and moments.

The novel aspects in the proposed approach are that:

(i) the hardening behaviour for each force component is directly determined by an input $P\delta$ curve

(ii) each force component follows an independent hardening rule (given by the independent P, M_{ipb} and M_{opb} curves), resulting in a continuously changing shape of the yield surface.

B.2 Plastic interaction function

The plastic interaction function may be given by Equation B.1. Here, the capacity equations of the API and HSE codes are given together with a general, user-defined plastic potential. For the user-defined capacity formulation, the shape of the plastic potential is given by the $\alpha()$-parameters.

$$\Gamma = \begin{cases} \cos\left(\frac{\pi}{2}\frac{N}{N_u}\right) - \sqrt{\left(\frac{M_{ipb}}{M_{ipb,U}}\right)^2 + \left(\frac{M_{opb}}{M_{opb,U}}\right)^2} & \text{(API)} \quad \text{... B.1a} \\ \left|\frac{N}{N_U}\right| + \left(\frac{M_{ipb}}{M_{ipb,U}}\right)^2 + \left|\frac{M_{opb}}{M_{opb,U}}\right| - 1 & \text{(HSE)} \quad \text{... B.1b} \\ \left(\frac{N}{N_U}\right)^{\alpha 1} + \left(\left(\frac{M_{ipb}}{M_{ipb,U}}\right)^{\alpha 3} + \left(\frac{M_{opb}}{M_{opb,U}}\right)^{\alpha 4}\right)^{\alpha 5} - 1 & \text{(user defined)} \quad \text{... B.1c} \end{cases}$$

B.3 Elastic-Perfectly Plastic Model

The yield condition is represented by an interaction function between axial force, in-plane bending and out-of-plane bending.

$$\Gamma = f\left(\frac{N}{N_U}, \frac{M_{ipb}}{M_{ipb,U}}, \frac{M_{opb}}{M_{opb,U}}\right) - 1 = 0 \qquad \ldots B.2$$

N, M_{ipb}, M_{opb} are the joint forces and N_U, $M_{ipb,U}$, $M_{opb,U}$ are the joint capacities for each force component. $\Gamma = 0$ represents full plastification of the cross section. $\Gamma = -1$ is the initial value of a stress-free cross section. In principle, a state of forces characterized by $\Gamma > 0$ is illegal.

The flow rule for associated flow is given by:

$$\Delta v^P = \begin{bmatrix} g_1 & 0 \\ 0 & g_2 \end{bmatrix} \begin{bmatrix} \Delta\lambda_1 \\ \Delta\lambda_2 \end{bmatrix} = G\Delta\lambda \qquad \ldots B.3$$

stating that plastic displacement increments are normal to the cross sectional yield surface, Γ, multiplied by a scalar, $\Delta\lambda$. The surface normal is given by:

$$g_i^T = \frac{\partial\Gamma}{\partial S_i} = \left[\frac{\partial\Gamma}{\partial N}, \frac{\partial\Gamma}{\partial M_{ipb}}, \frac{\partial T}{\partial M_{opb}}\right]_i \qquad \ldots B.4$$

and index i refers to beam end 1 and beam end 2.

The consistency rule is defined such that the state of forces move from one legal plastic state to another plastic state, following the yield surface so that $\Gamma = 0$. For an elastic-perfectly plastic material model, this can be expressed as:

$$\Delta\Gamma = \frac{\partial\Gamma}{\partial N}\Delta N + \frac{\partial\Gamma}{\partial M_{ipb}}\Delta M_y + \frac{\partial\Gamma}{\partial M_{opb}}\Delta M_z \qquad \ldots B.5$$

$$= g^T \Delta S_i$$

$$= 0$$

When both nodes are considered, Equation B.5 takes the form:

$$G^T \Delta S = 0$$

Elasto-plastic Stiffness Matrix

The elastic stiffness expression for the joint element is expressed as:

$$\Delta S = K_E \Delta v^E \qquad \ldots B.6$$

The total displacement increment is separated into elastic and plastic components:

$$\Delta v = \Delta v^E \Delta v^P \qquad \ldots B.7$$

and the stiffness equation is expressed as:

$$\Delta S = K_E (\Delta v - \Delta v^P) \quad \text{... B.8}$$

$$= K_E \Delta v - K_E G \Delta\lambda$$

when the flow rule, Equation B.3, is introduced.

Pre-multiplying with G^T, the right-hand side takes the form of the consistency rule (Equation B.5):

$$G^T \Delta S = G^T K_E \Delta v - G^T K_E G \Delta\lambda \quad \text{... B.9}$$

$$= 0$$

and the plastic increment can be solved:

$$\Delta\lambda = (G^T K_E G)^{-1} (G^T K_E \Delta v) \quad \text{... B.10}$$

Substituting $\Delta\lambda$ back into Equation B.8, the elasto-plastic stiffness of the element becomes:

$$\Delta S = K_E \Delta v - K_E G \Delta\lambda \quad \text{... B.11}$$

$$= K_E \Delta v - K_E G (G^T K_T G)^{-1} G^T K_E \Delta v$$

$$= (K_E - K_E G (G^T K_E G)^{-1} G^T K_E) \Delta v$$

$$= K_{EP} \Delta v$$

B.3 Strain Hardening Model

At each state of plastic deformation at the hinge, there exists a unique capacity surface in force space given by:

$$\Gamma = f\left(\frac{N}{N_0 R_N}, \frac{M_{ipb}}{M_{ipb,0} R_{ipb}}, \frac{M_{opb}}{M_{opb,0} R_{opb}}\right) - 1 = 0 \quad \text{... B.12}$$

where N_0, $M_{ipb,0}$, $M_{opb,0}$ are "elastic" joint capacities and R_k are hardening functions, expressed as a function of the plastic deformations for each force degree of freedom.

$$\Delta R = k_h \Delta\lambda^P = k_h g_s \Delta\lambda \quad \text{... B.13}$$

In the context of joint modelling, the hardening function $R(v^P)$ can be directly derived from the nonlinear $P\delta$ and $M\theta$ curves. The "linear" part of the curves is extracted as v^E; the remaining part of the curve is included as "hardening", where the degree of hardening is directly given by the plastic deformation v^P associated with each degree of freedom.

The consistency rule now takes the form

$$\Delta\Gamma = \frac{\partial\Gamma}{\partial S}\Delta N + \frac{\partial\Gamma}{\partial R}\Delta R$$

$$= \frac{\partial \Gamma}{\partial N}\Delta N + \frac{\partial \Gamma}{\partial M_{ipb}}\Delta M_{ipb} + \frac{\partial \Gamma}{\partial M_{opb}}\Delta M_{opb}$$

$$= \frac{\partial \Gamma}{\partial R_N}\Delta R_N + \frac{\partial \Gamma}{\partial R_{ipb}}\Delta R_{ipb} + \frac{\partial \Gamma}{\partial R_{opb}}\Delta R_{opb}$$

$$= g_S^T \Delta S_i + g_R^T k^h g_s \Delta\lambda \quad \text{... B.14}$$

$$= 0$$

When both nodes in the element are considered, Equation B.14 takes the form:

$$G_S^T \Delta S + G_R^T \Delta K_H G_S \Delta\lambda = 0$$

The stiffness equation is again expressed by Equation B.8:

$$\Delta S = K_E (\Delta v - \Delta v^P) \quad \text{... B.15}$$

$$= K_E \Delta v - K_E G_S \Delta\lambda$$

Pre-multiplying with G^T and combining with Equation B.14, the right-hand side now takes the form:

$$G_S^T \Delta S = G_S^T K_E \Delta v - G_S^T K_E G_S \Delta\lambda \quad \text{... B.16}$$

$$= -G_R^T K_H G_S \Delta\lambda$$

The plastic increment can now be solved as:

$$\Delta\lambda = \left(G_S^T K_E G_S - G_R^T K_H G_S\right)^{-1} G_S^T K_E \Delta v \quad \text{... B.17}$$

Substituting $\Delta\lambda$ the elasto-plastic stiffness of the beam now becomes:

$$\Delta S = K_E \Delta v - K_E G_S \Delta\lambda \quad \text{... B.18}$$

$$= K_E \Delta v - K_E G_S \left(G_S^T E_E G_S - G_R^T K_H G_S\right)^{-1} G_S^T K_E \Delta v$$

$$= \left(K_E - K_E G_S \left(G_S^T K_E G_S - G_R^T K_H G_S\right)^{-1} G_S^T K_E\right)\Delta v$$

$$= k_T^{ep} \Delta v$$

Hardening functions $R(v^P)$

In the context of joint modelling, the hardening function $R(v^P)$ and k^h can be directly derived from the nonlinear Pδ and Mθ curves (Equation B.19a and B.19b), where N_U and M_U are the maximum joint capacities under axial force and bending, respectively.

$$\frac{N}{N_U} = 1 - A\left(1 - \left(1 + \frac{1}{\sqrt{A}}\right) e^{-\frac{B\delta}{Q_y f_y D}}\right)^2 \quad \text{... B.19a}$$

$$\frac{M}{M_U} = 1 - A\left(1 - \left(1 + \frac{1}{\sqrt{A}}\right) e^{-\frac{B\theta}{Q_y f_y}}\right)^2 \quad \text{... B.19b}$$

The plasticity formulation requires that the joint element is assigned an elastic stiffness, a limit to the elastic range, and a plastic stiffness or hardening function. Thus, the plastic interaction function is given by:

$$\Gamma = f\left(\frac{N}{N_0 R_N}, \frac{M_{ipb}}{M_{ipb,0} R_{ipb}}, \frac{M_{opb}}{M_{opb,0} R_{opb}}\right) - 1 = 0 \quad \text{... B.20}$$

where N_0 and M_0 denotes the limits of the elastic range and R_k are the hardening functions. Comparing Equations B.19a and B.20, the hardening functions are given by:

$$R_N = \frac{N_U}{N_0}\left\{1 - A\left(1 - \left(1 + \frac{1}{\sqrt{A}}\right) e^{-\frac{B\delta}{Q_y f_y D}}\right)^2\right\} \quad \text{... B.21}$$

The elasto-plastic stiffness for the individual degrees of freedom are then given by:

$$\frac{1}{k} = \frac{1}{k_e} + \frac{1}{k_h} \quad \text{... B.22}$$

where k_e is the elastic stiffness and k_h is the hardening stiffness. The resulting stiffness k should be equal to the derivatives of the $P\delta$ and $M\theta$ curves (Equation B.23).

$$k_N = \frac{dN}{d\delta} = -2\frac{N_U A}{N_0}\left(1 + \frac{1}{\sqrt{A}}\right)\frac{B\delta}{Q_y f_y D}\left(1 - \left(1 + \frac{1}{\sqrt{A}}\right) e^{-\frac{B\delta}{Q_y f_y D}}\right) e^{-\frac{B\delta}{Q_y f_y D}} \quad \text{... B.23}$$

$$k_M = \frac{dM}{d\theta} = -2\frac{M_U A}{M_0}\left(1 + \frac{1}{\sqrt{A}}\right)\frac{B\theta}{Q_y f_y}\left(1 - \left(1 + \frac{1}{\sqrt{A}}\right) e^{-\frac{B\theta}{Q_y f_y}}\right) e^{-\frac{B\theta}{Q_y f_y}}$$

With the elastic stiffness taken as the secant stiffness from the origin to the limit of the "elastic" region, the hardening stiffness can then be directly calculated from Equation B.22.

Gradients to the yield surface

The change in yield function due to a change in external forces is given by:

$$g_{S,i}^{T} = \frac{\partial \Gamma}{\partial S_i} = \left[\frac{\partial \Gamma}{\partial N}, \frac{\partial \Gamma}{\partial M_{ipb}}, \frac{\partial T}{\partial M_{opb}} \right]_i \quad \ldots \text{B.24}$$

The change in yield function due to changes in surface shape and extension of the yield surface is given by:

$$g_{R,i}^{T} = \frac{\partial \Gamma}{\partial R_i} = \left[\frac{\partial \Gamma}{\partial R_N}, \frac{\partial \Gamma}{\partial R_{ipb}}, \frac{\partial T}{\partial R_{opb}} \right]_i \quad \ldots \text{B.25}$$

Index i refers to beam end 1 and beam end 2.

Using the general, user defined, interaction function from Equation B.1c, the instantaneous yield surface (including hardening) is given by:

$$\Gamma = \left(\frac{N}{N_0 R_N} \right)^{\alpha 1} + \left(\left(\frac{M_{ipb}}{M_{ipb,0} R_{ipb}} \right)^{\alpha 3} + \left(\frac{M_{opb}}{M_{opb,0} R_{opb}} \right)^{\alpha 4} \right)^{\alpha 5} - 1 = 0 \quad \ldots \text{B.26}$$

The derivatives are:

$$\frac{\partial \Gamma}{\partial N} = \frac{\alpha 1}{N_0 R_N} \left(\frac{N}{N_0 R_N} \right)^{(\alpha 1 - 1)} \quad \ldots \text{B.27}$$

$$\frac{\partial \Gamma}{\partial M_{ipb}} = \frac{\alpha 5 \alpha 3}{M_{ipb,0} R_{ipb}} \left(\frac{M_{ipb}}{M_{ipb,0} R_{ipb}} \right)^{(\alpha 3 - 1)} \left(\left(\frac{M_{ipb}}{M_{ipb,0} R_{ipb}} \right)^{\alpha 3} + \left(\frac{M_{opb}}{M_{opb,0} R_{opb}} \right)^{\alpha 4} \right)^{(\alpha 5 - 1)}$$

$$\frac{\partial \Gamma}{\partial M_{opb}} = \frac{\alpha 5 \alpha 4}{M_{opb,0} R_{opb}} \left(\frac{M_{opb}}{M_{opb,0} R_{opb}} \right)^{(\alpha 4 - 1)} \left(\left(\frac{M_{ipb}}{M_{ipb,0} R_{ipb}} \right)^{\alpha 3} + \left(\frac{M_{opb}}{M_{opb,0} R_{opb}} \right)^{\alpha 4} \right)^{(\alpha 5 - 1)}$$

$$\frac{\partial \Gamma}{\partial R_N} = -\alpha 1 \frac{N}{N_0} \left(\frac{1}{R_N} \right)^2 \left(\frac{N}{N_0 R_N} \right)^{(\alpha 1 - 1)} \quad \ldots \text{B.28}$$

$$\frac{\partial \Gamma}{\partial R_{ipb}} = -\alpha 5 \, \alpha 3 \frac{M_{ipb}}{M_{ipb,0}} \left(\frac{1}{R_{ipb}} \right)^2 \left(\frac{M_{ipb}}{M_{ipb,0} R_{ipb}} \right)^{(\alpha 3 - 1)} \cdot \left(\left(\frac{M_{ipb}}{M_{ipb,0} R_{ipb}} \right)^{\alpha 3} + \left(\frac{M_{opb}}{M_{opb,0} R_{opb}} \right)^{\alpha 4} \right)^{(\alpha 5 - 1)}$$

$$\frac{\partial \Gamma}{\partial R_{opb}} = -\alpha 5\,\alpha 4 \frac{M_{opb}}{M_{opb,0}} \left(\frac{1}{R_{opb}}\right)^2 \left(\frac{M_{opb}}{M_{opb,0} R_{opb}}\right)^{(\alpha 4 - 1)}$$

$$\cdot \left(\left(\frac{M_{ipb}}{M_{ipb,0} R_{ipb}}\right)^{\alpha 3} + \left(\frac{M_{opb}}{M_{opb,0} R_{opb}}\right)^{\alpha 4} \right)^{(\alpha 5 - 1)}$$

Integration of constituitive equations

The global load increment determines the total deformation for each element in the structure. To speed up the analysis procedure, a simple cutting plane algorithm is introduced to integrate the constituitive equations, i.e. to determine the distribution between elastic and plastic displacement for each member (Ortiz and Simo[B.1]).

An initial trial step is executed for each member, assuming that the element remains elastic for the full increment in displacements

$$\Delta S^E_{n+1} = k^E_T \, \Delta v^{tot} \qquad \text{... B.29}$$

$$S_{n+1} = S_n + \Delta S^E_{n+1}$$

Subscript n refers to the previous, converged load step and subscript n+1 refers to the current step.

The resulting internal forces are then checked against the current yield condition to see if the assumption holds. If the yield condition is violated, i.e. $\Gamma\left(S_{n+1}\right) = 0$, some of the element deformations will have to be taken as plastic deformations. The plastic deformations are determined by an iterative procedure, repeated until

(a) the state of forces satisfy the yield criterion $\Gamma\left(S_{n+1}\right) = 0$

(b) the plastic deformations satisfy the hardening rule

(c) the elastic and plastic deformations equals the total incremental deformations

This is expressed by the following steps:

1. The plastic increment is calculated from the consistency condition. The consistency condition during local force iterations is formulated as:

$$\Gamma^{k+1}_{n+1} = \Gamma^k_{n+1} + d\Gamma \qquad \text{... B.30}$$

$$= \Gamma^k_{n+1} + \frac{\partial \Gamma}{\partial S} dS^k_{n+1} + \frac{\partial \Gamma}{\partial R} dR^k_{n+1}$$

$$= \Gamma^k_{n+1} + \left(g^k_{S,n+1}\right)^T dS^k_{n+1} + \left(g^k_{R,n+1}\right)^T k^k_{n+1} \, g^k_{S,n+1} \, d\Delta\lambda$$

$$= 0$$

where prefix d() denotes iterative changes in S, R and $\Delta\lambda$. External, total deformations remain fixed during these iterations. Thus, $dv^{tot} = 0$ and

$$dS = k_E \left(dv^{tot} - dv^P \right) \quad \ldots B.31$$

$$= -k_E \, dv^P$$

$$= -k_E \, g \, d\Delta\lambda$$

The consistency condition can now be re-written as:

$$\Gamma^{k+1}_{n+1} = \Gamma^{k}_{n+1} + \left(g^k_{S,n+1}\right)^T dS^k_{n+1} + \left(g^k_{R,n+1}\right)^T H^k_{R,n+1} \, g^k_{S,n+1} \, d\Delta\lambda \quad \ldots B.32$$

$$= \Gamma^{k}_{n+1} - \left(g^k_{S,n+1}\right)^T k^E_{n+1} \, g^k_{S,n+1} \, d\Delta\lambda + \left(g^k_{R,n+1}\right)^T k^k_{R,n+1} \, g^k_{S,n+1} \, d\Delta\lambda$$

$$= 0$$

and $d\Delta\lambda$ can be solved as

$$d\Delta\lambda = \left(-\left(g^k_{S,n+1}\right)^T k^E \, g^k_{S,n+1} + \left(g^k_{R,n+1}\right)^T k^h_{R,n+1} \, g^k_{S,n+1} \right)^{-1} \Gamma^k_{n+1} \quad \ldots B.33$$

2. The accumulated plastic increment is calculated

$$\Delta\lambda^{k+1}_{n+1} = \Delta\lambda^{k}_{n+1} + d\Delta\lambda \quad \ldots B.34$$

3. Accumulated plastic deformations are calculated

$$\Delta v^{P(k+1)}_{n+1} = \Delta v^{P(k)}_{n+1} + g^k_{n+1} \, d\Delta\lambda \quad \ldots B.35$$

4. Internal forces are calculated as the accumulated forces up to the last increment, minus the relaxation in forces due to plasticity

$$S^{k+1}_{n+1} = S^0_{n+1} - k^E \Delta v^{P(k+1)}_{n+1} \quad \ldots B.36$$

$$= S^k_{n+1} - k^E \, g^k_{n+1} \, d\Delta\lambda$$

5. The hardening corresponding to the plastic deformations are calculated as

$$R^{k+1}_{n+1} = R^k_{n+1} + k^h_{R,n+1} \, g^k_{S,n+1} \, d\Delta\lambda \quad \ldots B.37$$

6. The internal forces are checked against to see if the current yield condition is satisfied

$$\Gamma\left(S_{n+1}\right) > 0 \quad \ldots B.38$$

Repeat from step 1 until the yield condition is satisfied.

REFERENCES

B.1 Ortiz, M. and Simo, J. (1986). An analysis of a new class of integration algorithms for elastoplastic constitutive relations. *Int.J.Numer.Meth. Engng, vol.23,353-366.*

APPENDIX C

User Manual Documentation for
Joint Module (as Implemented in USFOS)

MSL JOINT FORMULATION

GENERAL

This is a short presentation of the user input and –output for the implementation of the MSL joint formulation in USFOS.

CONTENTS

APPENDIX C MSL JOINT FORMULATION

C.1 Sample input

C.2 Result print-out

C.3 Input description

SAMPLE INPUT

The following shows the input required to include MSL joint characteristics in the analysis of a 2D K-frame. The input is described in more detail below.

```
'
' ---------------------------------------------------------------
' Joint properties defined by MSL curves and plasticity formulation:
' ---------------------------------------------------------------
'
 JNT_FORM     3         ! 0=beam stub  1=P-delta spring  3=plasticity model
 JNTCLASS     1         ! 0=OFF        i>0 : interval for (re)classification
'
'
'          nodex    chord1    chord2     Can    Rule   CapLevel GammaQf
 CHJOINT      7         6         7       0     MSL      mean      1.0
'
'
```

RESULT PRINT-OUT

Each time joint (re)classification is performed, the following information is printed to the .out file.

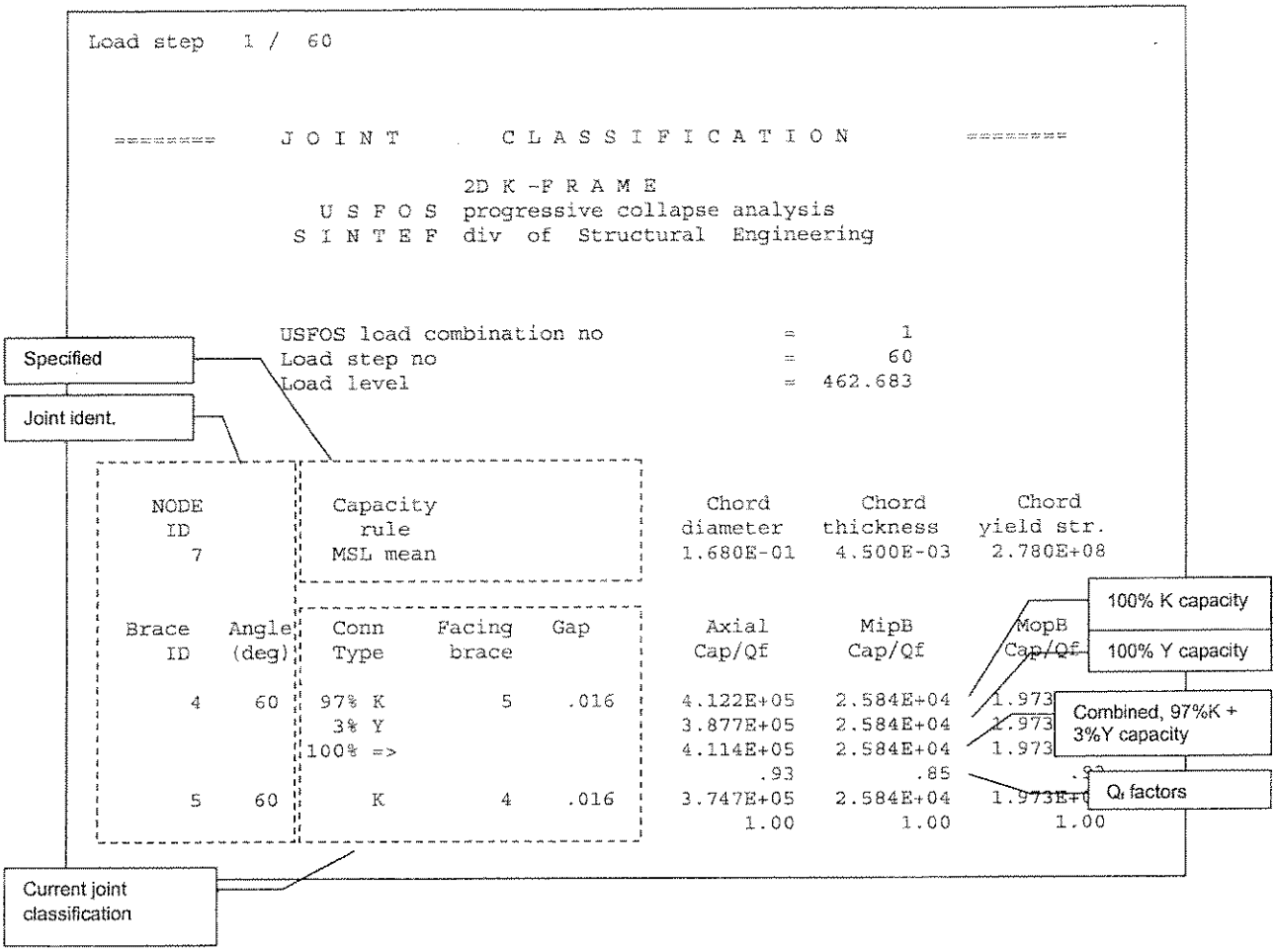

Input description

CHJOINT nodex elnox1 elnox2 geono CapRule CapLevel Q_f_SafetyCoeff		
Parameter	*Description*	*Default*
nodex	External node number referring to the joint where joint capacity and non-linear joint behaviour should be considered	
elnox1	External element number defining one of the two **CHORD** elements connected to the node	
elnox2	External element number defining the second **CHORD** element	
geono	Geometry reference number defining the diameter and thickness of the chord at the joint (canned joint). If omitted or equal to 0, the data for *elnox1* is used.	
CapRule	Capacity rule: -1 or "API" : API (no more data required) -2 or "DOE" : DoE (no more data required) -3 or "user" : User defined capacity and surface definition, additional data required (see next pages). -4 or "MSL" : MSL non-linear joint characteristics -101 : User defined *P-δ* Joint Springs, additional data required (see next pages).	
CapLevel	Capacity level or capacity multiplier. "mean" : use mean value joint capacities "char" : use characteristic joint capacities `scalfact` : joint capacities are set to mean value capacities multiplied by `scalfact`, (where "`scalfact`" is a positive real number). This option is only available with the MSL joint formulation.	mean
Q_f_Safety Coeff	The Q_f factor for joint capacities includes a safety factor (or partial safety coefficient) in the chord stress utilisation factor. $0 \leq \gamma_{Qf} \leq 1$: MSL Q_f formulation, using γ_{Qf} as safety coefficient $\gamma_{Qf} >> 1$: Cancels out the chord load effects and gives Q_f=1	1.0

CHJOINT nodex elnox1 elnox2 geono CapRule CapLevel Q_f_SafetyCoeff

With this record, the capacity of each brace/chord connection at the tubular joint will be checked according to a selected joint capacity equation

This check will impose restrictions on the load transfer through each brace/chord connection at the specified joint, and the non-linear joint characteristics will be included in the USFOS analysis.

Extra elements will be introduced in the FE model, and the behaviour of these elements assigned according to the selected joint capacity rule or specified joint capacity, and the FE formulation selected for the "joint elements".

The joint capacity rule or joint capacity is specified by the **CHJOINT** record(s).
The FE formulation for the "joint elements" is selected by the **JNT_FORM** record.

Note that use of the MSL formulation is confidential under the contract of the MSL JIP project "Non-linear joint modelling for ….". Access to this formulation is limited to

- participants of the MSL JIP project
- their affiliated companies
- other parties acting under authorisation from the above
- MSL and SINTEF

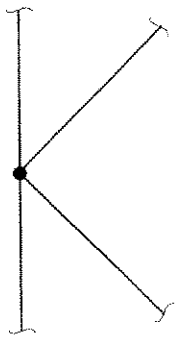

Conventional joint model

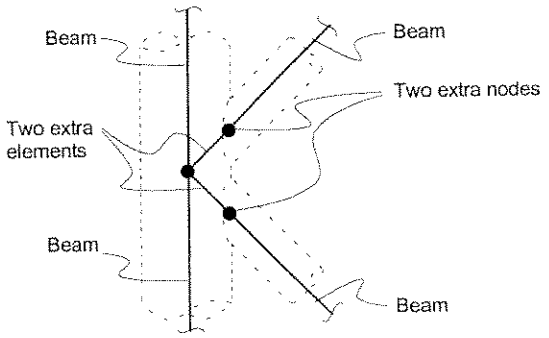

Joint with capacity check included

JNT_FORM form		
Parameter	*Description*	*Default*
Form	FE formulation for the "joint elements" introduced by the CHJOINT option. Capacity level or capacity multiplier. 0 : Beam-column representation. Default on old versions of USFOS, but no longer recommended. The three-hinge mechanism in the beam-column element may introduce numeric instabilities for the small "joint elements". 1 : P-δ spring representation. Un-coupled P-d curves with ductility limits will be generated automatically for each joint degree of freedom, based on the capacities specified under the **CHJOINT** record(s). 3 : Plasticity formulation including brace load interaction and joint (re)classification as specified by the **JNT_CLASS** record. JNT_FORM 3 is required for the MSL joint formulation.	0

Use of the **CHJOINT** option will introduce extra elements in the FE model. The behaviour of these elements will be assigned according to the selected joint capacity rule or specified joint capacity. The FE formulation for the "joint elements" is selected by the **JNT_FORM** record.

P-δ curves (option 1) are derived from the actual capacities as follows:

Displacement = 0.1% of Chord diameter defines 'yielding' (confer JSURFSIZ)

Displacement = 1.0% of Chord diameter defines maximum force/moment

Displacement = 5.0% of Chord diameter defines end of maximum capacity

Displacement = 10 % of Chord diameter defines fracture of joint

The generated curves are printed in the '.out' - file, and the **peak capacities** will be printed using the **Verify/Element/Information** option in **xfos**.

This record is given once

JNT_CLASS interval		
Parameter	*Description*	*Default*
interval	Joints will be (re)classified according to geometry and force state at specified intervals during the analysis. The joint capacities will be updated according to the revised classification, P-δ curves for each joint degree of freedom and the Q_f factor will be updated. 0 : No joint classification. 1 : Continuous joint (re)classification. Joint capacities, non-linear joint characteristics and the Q_f factor will be updated at every step in the USFOS analysis. n >1 : Joints will be (re)classified at every n'th step. Joint capacities, non-linear joint characteristics and the Q_f factor will be updated at every n'th step in the USFOS analysis.	0
This record is only valid in combination with "**JNT_FORM 3**", i.e. when the "joint elements" are represented by the plasticity formulation. Ref. the **JNT_FORM** record. This record is given once		